Book of Abstracts
CAHMDA-II International Workshop on

The Terrestrial Water Cycle: Modeling and Data Assimilation across Catchment Scales

Adriaan J. Teuling
Hidde Leijnse
Peter A. Troch
Justin Sheffield
Eric F. Wood

Workshop held 25–27 October 2004
at Princeton University, New Jersey, USA

Report 122

Sub-department Water Resources
Nieuwe Kanaal 11
6709 PA Wageningen
http://www.dow.wau.nl/whh

ISSN 0926-230X

This book was created with the text formatting system LaTeX 2ε and reproduced by Grafisch Service Centrum, Wageningen, The Netherlands, from camera-ready copy supplied by the editors.
1st Printing
October 2004

Contents

Program

Day 1 - Monday 25th October

8:30 Welcome address and opening workshop - Eric Wood

Session 1 - The water budget and the acceleration of the hydrological cycle (Chair: Eric Wood)

9:00 Key-note: J. Roads - Closing continental-scale water and energy budgets (Page 40)

9:45 Key-note: K.E. Trenberth - Manifestations of global climate change on accelerating the hydrological cycle: prospects for increases in extremes (Page 37)

10:30 Poster introduction

10:45 Coffee break & Poster viewing

11:45 Plenary discussion: "Are we making progress in addressing large scale water cycle problems?" (Moderator: Eric Wood)

12:45 Lunch

Session 2 - Scaling in time and space: methodological approaches (Chair: Guido Salvucci)

14:00 Key-note: John D. Albertson - Temporal dynamics of soil moisture variability: from theoretical basis to modeling implications (Page 60)

14:45 Key-note: Dongryeol Ryu and James S. Famiglietti - Geostatistical aspects of scaling behavior observed in regional scale surface soil moisture fields (Page 66)

15:30 Poster introduction

15:45 Coffee break and Poster viewing

16:45 Plenary discussion: "Have we made progress with current methodological approaches, and if so which ones?" (Moderator: Guido Salvucci)

17:45 End day 1

18:45 Reception and Dinner

Day 2 - Tuesday 26th October

Session 3 - Hydrological modeling across scales (Chair: Peter Troch)

9:00 Key-note: Dennis P. Lettenmaier - From catchment to continental scale: Issues in dealing with hydrological modeling across spatial and temporal scales (Page 90)

9:45 Key-note: R. Rigon, G. Bertoldi, T.M. Over, and D. Tamanini - GEO_{TOP}: a distributed model of the hydrological cycle in the remote sensing era (Page 102)

10:30 Poster introduction

10:45 Coffee break and Poster viewing

11:45 Plenary discussion: "Are we learning anything from distributed modeling regarding water cycle variability and its scaling?" (Moderator: Peter Troch)

12:45 Lunch

Session 4 - Data assimilation: potential for advancement (Chair: Wade Crow)

14:00 Key-note: Pedro Viterbo - Soil moisture assimilation for meteorological purposes: Observation synergy and data assimilation needs (Page 134)

14:45 Key-note: Dara Entekhabi - Land data assimilation: surface states and flux estimation based on multiscale and multispectral measurements (Page 154)

15:30 Poster introduction

15:45 Coffee break and Poster viewing

16:45 Plenary discussion: "What are the limitations with current assimilation approaches, and how can they be overcome?" (Moderator: Wade Crow)

17:45 End day 2 and Reception

Day 3 - Wednesday 27th October

Session 5 - Computational approaches for large-scale hydrologic problems (Chair: Thorsten Wagener)

9:00 Key-note: Dennis McLaughlin - Computational approaches for large-scale hydrologic problems (Page 182)

9:45 Key-note: C.D. Peters-Lidard, S.V. Kumar, Y. Tian, J. Geiger, P.R. Houser, J. Sheffield, E.F. Wood, K. Mitchell, and P. Dirmeyer - The GSFC Land Information System as a multiscale ensemble hydrological modeling testbed (Page 189)

10:30 Poster introduction

10:45 Coffee break and Poster viewing

11:45 Plenary discussion: "How do we expand into larger scale, distributed systems, including multi-flux systems" (Moderator: Thorsten Wagener)

12:45 Closing of workshop: Eric Wood and Peter Troch

Preface

This is the Book of Abstracts of the CAHMDA-II workshop "The Terrestrial Water Cycle: Modeling and Data Assimilation Across Catchment Scales", held from October 25th to 27th, 2004, at Princeton University, Princeton, NJ. The CAHMDA* workshops are organized to bring together experts in hydrological modeling to discuss new modeling strategies, and the potential of using advanced data assimilation methods to improve parameterization and predictability of distributed and semi-distributed catchment-scale hydrological models useful for water cycle research. CAHMDA-I was held from September 3rd to 5th 2001, at De Wageningse Berg conference center in Wageningen, the Netherlands.

The motivation behind CAHMDA-II is to assess the state-of-the-art in observing, explaining and modeling the terrestrial water cycle and to identify research needs to make progress in these areas. Progress is urgently needed in order to be able to quantify climate-induced changes in the large-scale hydrological cycle. A potential consequence of climate change is the acceleration of the terrestrial hydrological cycle, which may manifest itself in the form of increased precipitation and evapotranspiration. The effects on the environment and society in terms of changes to hydrological extremes (floods or droughts) is unknown but potentially large and damaging.

The workshop opens with a session on the water budget and the acceleration of the hydrological cycle (**Session 1**). Currently, there is a scientific debate and controversy over whether potential evaporation rates are increasing or decreasing, and over trends in actual evaporation [*Walter et al.*, 2004]. The decreasing trend in pan evaporation observed in several countries seems contrary to concurrent increasing trend in water budget-derived actual evapotransiration, GCM-based estimates of evapotranspiration, temperature, precipiatation and cloudiness [*Hobbins et al.*, 2004]. Several studies indicate that incident shortwave radiation at land surfaces has significantly decreased between 1960 and 1990, and land temperature has increased by 0.4°C over the same period. From a surface energy balance perspective, this counterintuitive behavior can be resolved through a decrease of surface evaporation and associated reduced evaporative surface cooling [*Wild et al.*, 2004]. The inferred decrease of evaporation by *Wild et al.* [2004] implies that the observed intensification of the hydrological cycle over extratropical land is more likely due to increased moisture advection from the oceans than due to increased local moisture release through evaporation. Several papers in this session shed new light on closing the water and energy budget at continental scales and manifestations of global climate change on acceleration of the hydrological cycle. The central theme during the discussion is "Are we making progress in addressing large scale water cycle problems?"

The second session of the workshop focusses on methodological approaches in understanding scaling of hydrological stores and fluxes in time and space (**Session 2**). Although the quantitative contribution of soil moisture to the global water budget is negligible, it plays a central role

*CAHMDA: CAtchment-scale Hydrological Modeling and Data Assimilation

in the global water cycle by controlling the partitioning of water and energy fluxes at the earth's surface, and can control the continental water distribution through land-surface atmosphere feedback mechanisms [*Koster et al.*, 2003]. Improved understanding of near-surface soil moisture variability is needed for the transformation of point-scale measurements and parameterizations to scales required for climate studies, operational weather forecasting, and large scale hydrological modeling. Methodological approaches discussed are soil moisture variance budgets derived from statistical fluid mechanics and geostatistical methods to investigate scaling behavior of soil moisture fields. The issue whether these and other methodological approaches help in understanding scaling behavior of surface soil moisture are further discussed.

Session 3 is about hydrological modeling across scales. Currently, the role of lateral flow and its effect on structured spatial variability is underestimated within land surface schemes [*Wood*, 1999]. New modeling strategies that explicitely account for the 3D geomorphological structure of landscapes are needed for land surface parameterizations of the climate system. Recent progress in our modeling capacities of subsurface flow processes [*Troch et al.*, 2003] enables a parsimonious representation of the dominant landscape controls on root zone soil moisture spatio-temporal variability. For example, *Kumar* [2004] derived explicit expressions for near-surface layer averaged lateral transport contribution (diffusion, gravity, dispersion, and convergence) to soil moisture variability due to land-surface curvature. These and other issues in dealing with hydrological modeling across spatial and temporal scales and distributed modeling approaches are presented. What can we learn from distributed modeling regarding water cycle variability and its scaling?

Data assimilation can improve our ability to predict hydrological extremes such as floods and droughts, it can play an important role in increasing the accuracy of water and energy balance computations and in assessing the errors related to such computations. *Walker and Houser* [2004], by means of a numerical twin data assimilation study, found that near-surface soil moisture observations must have an accuracy better than 5% vol. to positively impact soil moisture forecasts, and that daily near-surface soil moisture observations achieve the best soil moisture and evapotranspiration forecasts. Observation with spatial resolution finer than the land surface model resolution produce the best results, but spatial resolutions coarser than the model resolution yields only a slight degradation. They also found that satisfying the spatial resolution and accuracy requirements is much more important than repeat time. **Session 4** discusses potential of advancement in water cycle studies through data assimilation procedures. The discussion focusses on the limitations with current assimilation methods, and on how these limitations can be overcome.

Session 5 addresses computational approaches for large-scale hydrological problems. Computational efficient techniques for dealing with large nonlinear hydrologic data assimilation problems are presented. A particular interesting recent development is the Land Information System (LIS) of NASA Goddard Space Flight Center. LIS is based on the Land Data Assimilation System (LDAS) and is capable of global, distributed hydrometeorological modeling at spatial resolutions down to 1 km. The question of how we expand into larger scale, distributed systems, including multi-flux systems, is further discussed.

The organizing committee would like to express its gratitude to Ms. Shawn Strouss for helping them with the organization of the workshop, and to Dennis McLaughlin (H.M. King Bhumibol Professor of Water Resources Management, MIT) for his financial contribution.

Peter A. Troch
Eric F. Wood
Adriaan J. Teuling
Hidde Leijnse
Justin Sheffield

1 The water budget and the acceleration of the hydrological cycle

Terrestrial water storage variations using GRACE: Implications for water budget closure at multiple scales

J. Famiglietti[1], J. Chen[2], S. Holl[1], M. Rodell[3], K. Seo[4], T. Syed[1], and C. Wilson[4]

[1]*Department of Earth System Science, University of California, Irvine, California, USA*
[2]*Center for Space Research, University of Texas, Austin, Texas, USA*
[3]*Hydrological Sciences Branch, NASA Goddard Space Flight Center, Greenbelt, Maryland, USA*
[4]*Department of Geological Sciences, University of Texas, Austin, Texas, USA*

First results from GRACE observations show great promise for monitoring water storage changes on land. In this poster we show our latest GRACE-derived water storage change estimates, including global fields, global terrestrial time series, and basin scale extractions. Uncertainties are quantified, and comparisons to global models and available observations are presented. Implications for water cycle closure are discussed, as are new applications that the GRACE estimates will enable, at the large basin scale, the global ocean scale, and the global water cycle scale.

Water balance estimates of seasonal changes in terrestrial water storage for major river basins of the northern mid-latitudes

M. Hirschi[1], **S.I. Seneviratne**[2], **P. Viterbo**[3], **and C. Schär**[1]

[1]*Institute for Atmospheric and Climate Science, ETH Zürich, Switzerland*
[2]*NASA Goddard Space Flight Center, Greenbelt, Maryland, USA*
[3]*European Centre for Medium-Range Weather Forecasts, Reading, UK*

Terrestrial water storage plays an important role in the hydrological cycle, but is an unknown in most parts of the world. There are very few measurements of its main components (mainly soil moisture, groundwater, and snow), and therefore model results can not be validated in most regions. In this study, we compute and analyse monthly changes in terrestrial water storage for medium- to large-scale river basins derived from water-balance computations using a combination of observations and reanalysis data.

Method By combining the terrestrial and atmospheric water balances, the monthly changes in terrestrial water storage $\left\{\frac{\overline{\partial S}}{\partial t}\right\}$ can be expressed as:

$$\left\{\frac{\overline{\partial S}}{\partial t}\right\} = -\left\{\frac{\overline{\partial W}}{\partial t}\right\} - \left\{\overline{\nabla_H \cdot \vec{Q}}\right\} - \left\{\overline{R}\right\}, \tag{1.1}$$

where $\left\{\overline{\nabla_H \cdot \vec{Q}}\right\}$ is the atmospheric water vapor flux divergence, $\left\{\frac{\overline{\partial W}}{\partial t}\right\}$ is the change in atmospheric water vapor content (both from ERA-40 reanalysis data), and $\left\{\overline{R}\right\}$ is the measured runoff. The overbar denotes the temporal average (i.e., monthly means) and $\{\}$ the space average over the catchment. The approach is applied to many major river basins in Europe, Asia and North America (see Figure 1.1). The analysis covers the full 45-year time period (1958–2002) of the ERA-40 reanalysis from ECMWF (European Centre for Medium-Range Weather Forecasts) but is temporally limited in some river basins depending on the availability of runoff data from the Global Runoff Data Center or the U.S. Geological Survey.

The method has been developed over the Mississippi region [*Seneviratne et al.*, 2004]. Validation has shown excellent agreement between diagnosed estimates and observations of terrestrial water storage (soil moisture, groundwater, snow) in Illinois (domain size of 2×10^5 km^2) for a 10-year period 1987–1996, both in terms of the mean seasonal cycle and its interannual variations.

Validation and Results Some additional validation of the method with soil moisture observations from the Global Soil Moisture Data Bank* [*Robock et al.*, 2000] is performed in Asia and Western Russia. Despite the fact that only one observational component of the terrestrial water storage is available, the correlations between estimated changes and observations are encouraging in some basins (see e.g., Figure 1.2 for the Volga basin). The amplitudes of soil moisture observations often seem to be smaller than the estimates. Especially in basins of higher latitudes, the seasonal changes in snow cover play obviously an important role for the overall terrestrial water storage changes and could explain in part the larger amplitudes of the computed estimates.

The long-term mean of the diagnosed water storage estimates in the different river basins is well balanced in Asia and Western Russia, whereas for many basins in Europe and North America a

*http://climate.envsci.rutgers.edu/soil_moisture/

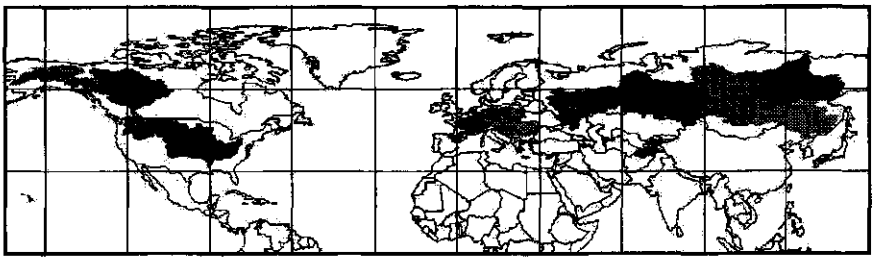

Figure 1.1: Investigated river basins.

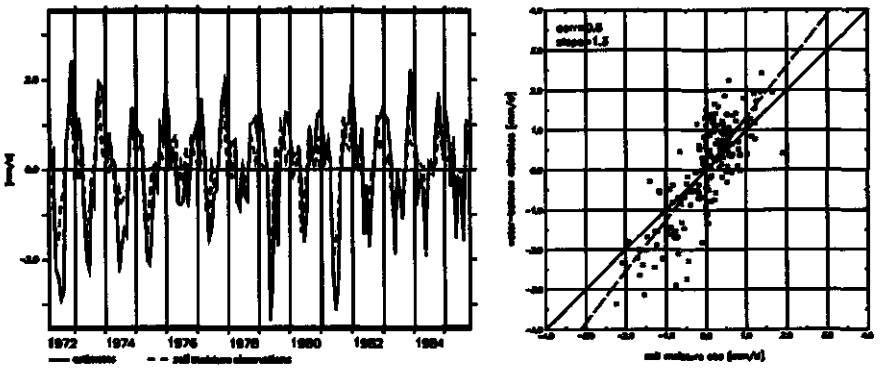

Figure 1.2: Computed water-balance estimates vs. soil moisture observations (both in mm d^{-1}) in the Volga basin (1,333,747 km^2) for the period 1972–1985 (time series and scatter plot of monthly data).

drift is observed (see Figure 1.3). The analysis suggests that the magnitude of the imbalances is not only dependent on the size of the river basins (as even small basins in Western Russia and Asia appear to have almost no drifts) but also on the geographical region under consideration. The complex topography of the European region could have negative effects on the quality of the ERA-40 reanalysis data. Validation of ERA-40 atmospheric water vapor flux divergence has shown smaller values of moisture convergence in Central Europe compared to older studies presented in *Alestalo* [1983], which could explain the observed negative trends in the river basins of this region.

Diagnosed estimates of terrestrial water storage variations over European catchments are then used for comparison with regional climate models involved in the EU-project PRUDENCE (see Figure 1.4). Results show that there are substantial differences between models. Several of them as well as ERA-40 appear to underestimate the decrease in terrestrial water storage during summer compared to the water-balance estimates. Note, however, that the diagnosed estimates might not be as accurate for this region, due to the imbalances discussed above.

Conclusions and Outlook These results suggest that the investigated method has the potential to provide reasonable data of terrestrial water storage variations for the validation of regional and global climate models in regions with large-scale river basins where observational data is not available. Further computations over the last 45 years in other regions of the world could provide a global data set of this climate variable. Results show that the ERA-40 water vapor convergence

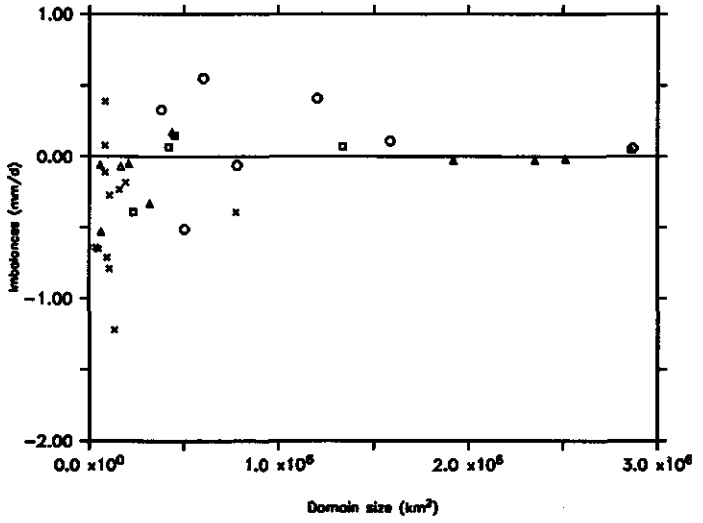

Figure 1.3: Long-term mean of water storage (mm d^{-1}) vs. basin area (km^2) for the European (×), the West Russian (□), the Northern and Central Asian (△), and the North American (○) domains.

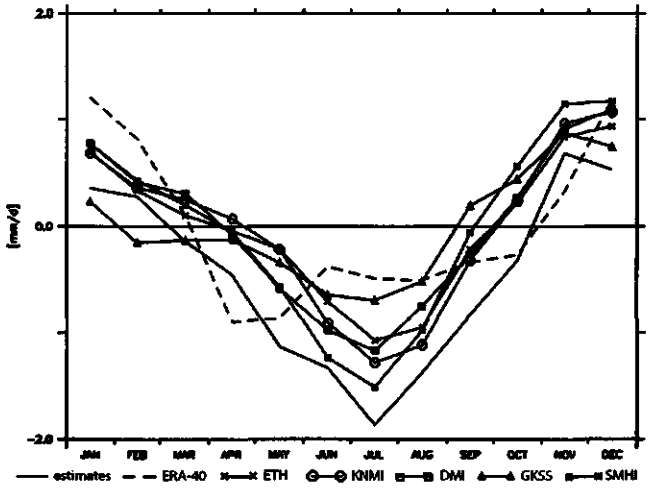

Figure 1.4: Comparison of estimates with PRUDENCE model runs and ERA-40 terrestrial water storage variations (mm d^{-1}) for the Danube basin (772,220 km^2) and the period 1961–1990.

data is of sufficient quality to provide useful constraints for land-surface data assimilation in large-scale catchments. However, the quality of ERA-40 water vapor convergence in some regions and its temporal homogeneity are the subject of further analysis and may help to improve the quality of the generated data set in Europe.

An evaluation of a 52-year land surface model simulation using observational forcing

H. Sharif[1], N.L. Miller[1], W. Crow[2], and E.F. Wood[3]

[1]*Berkeley National Lab, USA*
[2]*USDA-ARS, USA*
[3]*Princeton University, Princeton, New Jersey, USA*

Long-term basin-scale hydrologic response is related to physiographic descriptors and climate data. Multi-year land surface and subsurface processes are coupled to topography as well as large-scale atmospheric processes, soil memory, and vegetation change. The Red/Arkansas River basin has been the focus of investigations to study the interaction of atmosphere with the land surface, subsurface, and vegetation. For this reason, this basin was the first large scale areas studied under the GEWEX Continental Scale International Project (GCIP). Portions of the basin were the site of the latest International H2O Project (IHOP-2002) and the Department of Energy IOP 2002 experiments. A 52-year simulation using the fully distributed version of TOPLATS at 1 km resolution for the Red/Arkansas River basin is preformed. Forcing data (precipitation, incoming radiation and surface meteorology) interpolated from meteorological and rain gauge observations are used. TOPLATS is particularly well suited for such an analysis since it combines a detailed representation of surface water and energy balance processes while capturing the topographically induced horizontal redistribution of subsurface water. Analysis of mean-monthly, seasonal, and annual changes in soil moisture, latent heat, sensible, as correlated to large-scale patterns was performed. The correlation between mean-monthly, seasonal, and annual variations in surface energy fluxes, soil moisture, and stream flow and large-scale atmospheric patterns was examined. Results help to clarify the source of long-term hydrologic variability within the basin. In addition, the potential of TOPLATS enhancements - like the addition of a dynamic vegetation module to improve the model's representation of this variability were explored.

Basin-scale water-balance estimates of terrestrial water-storage variations: Potential for data assimilation

Sonia I. Seneviratne[1,2], Rolf Reichle[1,2], Randal D. Koster[2], Sarith P.P. Mahanama[1,2], M. Hirschi[3], and Christoph Schär[3]

[1]*Goddard Earth Sciences and Technology Center, University of Maryland, Baltimore, Maryland, USA*
[2]*Global Modeling and Assimilation Office, NASA/GSFC, Greenbelt, Maryland, USA*
[3]*Atmospheric and Climate Science ETH, ETH Zürich, Switzerland*

Terrestrial water storage (mostly encompassing soil moisture, groundwater and snow) is a key climatic variable, which is relevant both for short-term and seasonal forecasting, as well as for long-term climate modeling. Despite its importance, it is not routinely measured and observations of its individual components are scarce. A possible approach for deriving estimates of this quantity is the use of water-balance computations based on the following three variables: moisture flux convergence, changes in atmospheric moisture content, and river runoff [*Seneviratne et al.*, 2004, hereafter referred to as S04]. This methodology was shown to give reliable results for various river basins of the northern mid-latitudes and to compare well with available ground observations [S04, *Hirschi et al.*, 2004, hereafter referred to as H04]. Here we compare estimates derived with this approach with offline simulations performed with the National Aeronautics and Space Administration (NASA) Catchment Land Surface Model (hereafter "Catchment model" or CLSM; *Koster et al.*, 2000; *Ducharne et al.*, 2000). These results are used to assess the potential gain in using water-balance estimates of terrestrial water-storage variations in a data assimilation framework.

Employed data The present study makes use of estimates of basin-scale terrestrial water-storage variations (S04, H04), derived with the following equation [e.g., *Peixoto and Oort*, 1992]:

$$\left\{\frac{\overline{\partial S}}{\partial t}\right\} = -\left\{\overline{\nabla_H \cdot \mathbf{Q}}\right\} - \left\{\frac{\overline{\partial W}}{\partial t}\right\} - \left\{\overline{R}\right\} \tag{1.2}$$

where $\left\{\overline{\nabla_H \cdot \mathbf{Q}}\right\}$ is the moisture flux divergence, $\left\{\frac{\overline{\partial W}}{\partial t}\right\}$ is the change in atmospheric moisture content in the column above the considered area, and $\{\overline{R}\}$ is the measured runoff. All quantities are temporal and areal averages for a given time frame (monthly variations) and region. Note that the area of the considered domain is a critical factor for the accuracy of such computations and should be of the order of 10^5 to 10^6 km^2 at least [e.g., *Rasmusson*, 1968; *Yeh et al.*, 1998]. S04 tested this approach in a 10-year (1987–1996) case study for the Mississippi River basin using European Centre for Medium-Range Weather Forecasts (ECMWF) ERA-40 reanalysis data and streamflow measurements. The derived estimates were found to be reasonable for all Mississippi subbasins and to agree well with available observations of soil moisture, groundwater and snow in Illinois. The dataset used here was derived for several river basins of the northern mid-latitudes and covers the whole ERA-40 period (1958–2002, see H04). For the present study, we only use data from river basins with soil moisture observations (Amur, Dnepr, Don, Lena, Neva, Ob, Volga, Yenisei, see Figure 1.5a). The comparisons also include the Illinois domain (Figure 1.5b) investigated in S04.

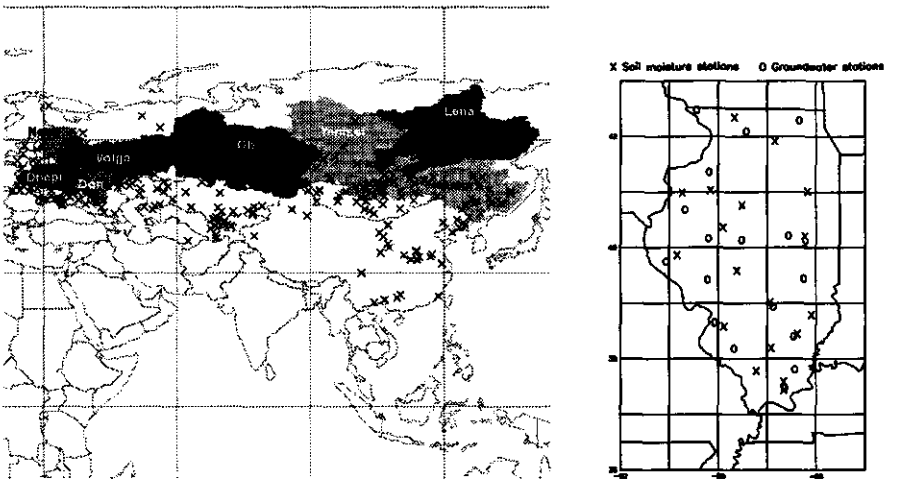

Figure 1.5: (a) Basins investigated in Asia and soil moisture stations available (×); (b) Soil moisture (×) and groundwater (o) measurements sites available in Illinois.

The land surface integrations analyzed here were performed with the Catchment model [*Koster et al.*, 2000; *Ducharne et al.*, 2000], a recently developed land surface scheme, which uses the hydrological catchment (or watershed) as basic computational unit. In each catchment, the vertical profile of soil moisture is determined by the equilibrium soil moisture profile from the surface to the water table, and the deviations from the equilibrium soil moisture profile in a 1-m root zone layer and a 2-cm surface layer. Unlike traditional, layer-based models, the Catchment model includes horizontal redistribution of soil water within each hydrological catchment based on the statistics of the catchment topography [*Koster et al.*, 2000]. The present simulations, covering a 15-year period (1979–1993), are forced with a dataset combining ERA-15 reanalysis data with observations-based corrections for precipitation, radiation, temperature, and humidity [*Berg et al.*, 2003]. These integrations were conducted and analyzed by *Reichle et al.* [2004] in a recent study comparing satellite and model soil moisture with ground observations.

Soil moisture measurements from the Global Soil Moisture Data Bank [*Robock et al.*, 2000] are available for various basins in Russia and Asia (Amur, Dnepr, Don, Lena, Neva, Ob, Volga, Yenisei; Figure 1.5a) as well as for 19 sites in the state of Illinois (*Hollinger and Isard*, 1994, Figure 1.5b). For Illinois, concomitant groundwater (Figure 1.5b) and snow measurements (not shown) are also available from the Illinois State Water Survey and the Midwest Climate Center, respectively [e.g., *Yeh et al.*, 1998, , S04]. For the present comparisons, areal estimates for the investigated domains are obtained through an averaging of the available observations for the respective basins or domains. Note that in some regions this procedure can lead to some biases if the observations are not well distributed throughout the considered domain.

Results First, we compare the respective correlations of the water-balance estimates and the model integrations with the ground observations. Figure 1.6 displays the coefficients of correlation (r^2) of the two datasets in each investigated domain for the years with available observations witin the time period 1979–1993, both for the absolute values (top) and the anomalies (bottom). Note that in the case of the Catchment model, we use the total terrestrial water storage of the model (i.e., including soil water down to the water table, as well as snow and interception) for consistency with the water-balance estimates. One should keep in mind that the observations, with the exception of

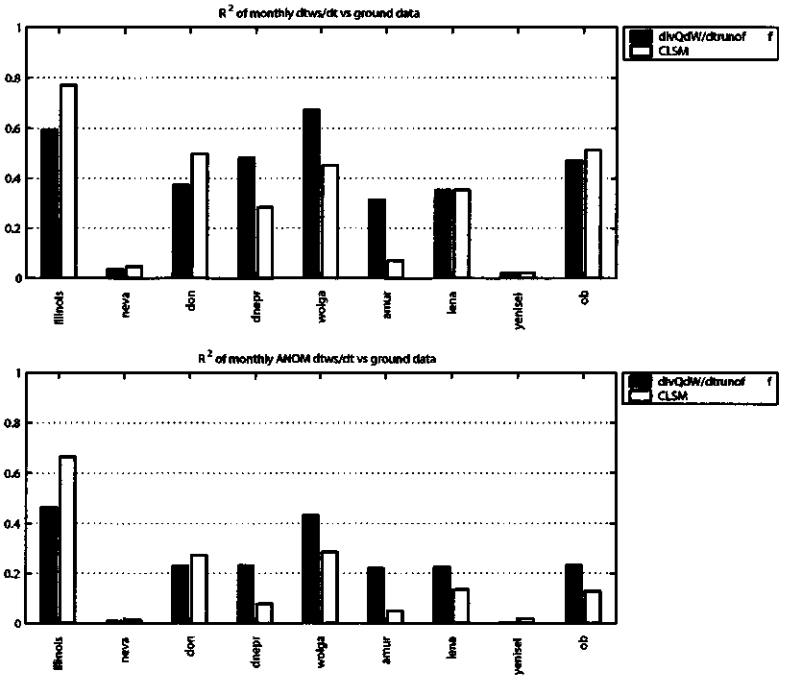

Figure 1.6: Histograms of r^2 values between the ground observations and the water-balance estimates (black), respectively the Catchment model (white): (top) Absolute values; (bottom) anomalies.

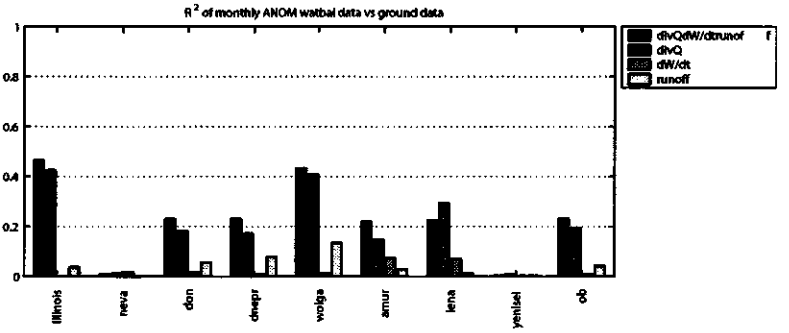

Figure 1.7: Histogram of r^2 values between ground observations and individual components of water-balance estimates: sum of components (black), moisture flux divergence (dark gray), changes in atmospheric moisture content (medium gray), and runoff (light gray): Anomalies.

Illinois, correspond for their part to variations in soil moisture only.

The agreement between the two datasets and the observations varies from region to region, but the two approaches perform worst in the same domains (Yenisei, Neva). Note that this might be due in part to poor representability (Neva) or uneven distribution (Yenisei) of the available observations in these two basins. In the other domains, the water-balance estimates and the land surface model appear similarly skillful on average, though significant differences are found in some domains (Illinois, Dnepr, Volga, Amur). In Illinois, the Catchment model is closer to the observations, possibly due to a high quality of the forcing data in this region. In the Amur basin, on the contrary, the model performs comparatively poorly, either due to poorer forcing or to model biases in this region. Note that rain gauge density is known to be a critical factor for the accurate forcing of a land surface model [*Oki et al.*, 1999], and is likely to be only sufficient in North America and Europe [*Koster et al.*, 2004; *Reichle et al.*, 2004].

Interestingly, the water-balance estimates appear comparatively skillful at capturing the interannual variability of the observations (Figure 1.6, bottom plot). This can be mostly linked to the contribution of the moisture flux convergence, as this component correlates best with the anomalies of the observed variations in terrestrial water storage and soil moisture (Figure 1.7).

Conclusions Preliminary results suggest that both the water-balance estimates and the land surface model driven with optimized forcing are similarly skillful on average, but that their performances can significantly differ in some regions, possibly dependant on the quality of the precipitation forcing used to drive the land surface model. Their skill appears in part complementary: They perform best in different regions (Illinois for the land surface model and Northern Russia for the water-balance estimates), and also capture different features from the observations, the water-balance estimates being more skillful at capturing the interannual variability of the observations. This suggests that quantities such as atmospheric moisture convergence or runoff could possibly be used with success in a data assimilation framework aiming at the creation of a terrestrial water-storage dataset. The potential of such an approach is expected to be highest in regions with poor forcing data.

Closing the terrestrial water balance using a combination of modeling, remote sensing and data assimilation

Venkat Lakshmi[1]

[1]*Department of Geological Sciences, University of South Carolina, Columbia, South Carolina, USA*

Numerous satellite missions have been launched and continue to be approved and progress that measure various parameters of the hydrological cycle. These include, atmospheric water vapor, cloud height and fraction, surface and air temperature, vegetation, soil moisture, precipitation and surface humidity. It will be the purpose of this presentation to (1) outline the outstanding problems in hydrology with respect to water budgets and (2) list and describe the satellite sensors capable of hydrological studies and lastly, (3) present initial results on use of satellite data for hydrological modeling and data assimilation.

Simulation of water sources for GEWEX CSEs: MAGS, GCIP and LBA

Michael G. Bosilovich[1] **and Jiundar Chern**[1]

[1]*NASA/GSFC, USA*

In the discussion of water cycle intensity, regional variations can be significantly different from the global background [e.g., *Bosilovich et al.*, 2004]. Better understand the regional water cycle, we have run a 50-year AGCM simulation, including diagnostics for the geographical sources of water vapor and precipitation recycling. In this paper, we focus on the water sources and precipitation recycling for the GEWEX Continental-scale Experiments (CSEs) in the Americas (Figure 1.8). The numerical simulation contains variables of all the sources of water for many of the GEWEX CSEs and for all seasons. Here, we will focus on what drives precipitation recycling during the maximum recycling season for each of the Americas CSEs.

Model The primary atmospheric numerical model used in this study is the Finite Volume General Circulation Model [fvGCM; *Lin*, 2003]. The finite-volume dynamical core uses a terrain-following Lagrangian control-volume vertical coordinate system [*Lin*, 2003; *Collins et al.*, 2003]. The FVGCM dynamical core formulation includes a conservative Flux-Form Semi-Lagrangian (FFSL) transport algorithm with Gibbs oscillation-free monotonicity constraint on sub-grid distribution. The FFSL has consistent and conservative transport of air mass and absolute vorticity [*Lin and Rood*, 1997]. This feature of the system makes the FFSL particularly useful for water vapor and passive tracer simulations.

The physical parameterizations of the fvGCM are based on NCAR Community Climate Model version 3.0 (CCM3) physics. The NCAR CCM3 parameterizations are a collection of physical processes with a long history of development and documentation [*Kiehl et al.*, 1998]. The moist physics package includes the *Zhang and McFarlane* [1995] deep convective scheme, which handles updrafts and downdrafts and operates in conjunction with the *Hack* [1994] mid- and shallow convection scheme. This version of the fvGCM uses the Common Land Model [versions 2, described by *Dai et al.*, 2003]. The validation of regional aspects of the simulated hydrological cycle are discussed by *Bosilovich et al.* [2003].

Recycling Methodology The model also includes water vapor tracers (WVT) to quantify the geographical source of water for global precipitation [*Bosilovich and Schubert*, 2002; *Bosilovich*, 2002; *Bosilovich et al.*, 2003]. In this configuration, the source of water for a tracer is the evaporation from a prescribed region. This humidity is then predicted as a passive tracer (separate and distinct from the model's specific humidity prognostic variable) including tracer transport and precipitation and turbulent tendencies, using

$$\frac{\partial q_T}{\partial t} = -\nabla_3 \cdot (q_T V) + \frac{\partial q_T}{\partial t}_{turb} + \frac{\partial q_T}{\partial t}_{Prec} \tag{1.3}$$

where q_T is the three-dimensional water vapor tracer, V is the three-dimensional wind, *turb* denotes the turbulent tendency not including surface evaporation (vertically integrates to zero) and *Prec* denotes the sum of all tracer precipitation tendencies (including condensation, rain evaporation, and convective vertical movement; vertically integrates to P_T). The tracer precipitation tendencies are computed proportional to the total precipitation tendency, where the proportionality is based on the ratio of tracer water to total water [*Bosilovich and Schubert*, 2002].

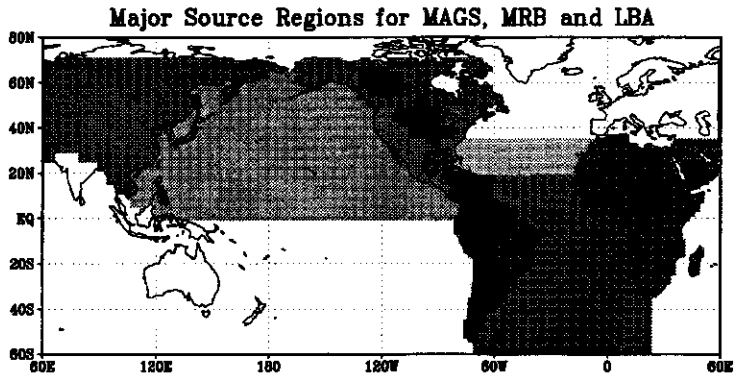

Figure 1.8: Geographical source regions that play a major role in the water cycle for MAGS, MRB and LBA CSEs.

The WVT methodology requires an investment in developing the code and also computing additional atmospheric prognostic variables. Precipitation recycling (but not specific external sources) can also be determined by simpler bulk diagnostic methods [e.g., *Brubaker et al.*, 1993]. The bulk diagnostic methods use monthly data and solve a simplified water budget. This can be compared to the value determined from the WVT method (but will evaluated in the near future).

Global climate The atmospheric general circulation model (AGCM) simulation runs at $2° \times 2.5°$ resolution for 50 years (1948–1997). The SST is prescribed following Hadley Centre data product [see *Bosilovich et al.*, 2004, for details]. Since there is a trend in the SST forcing there is also a trend in the response of the AGCM. The response of the global precipitation depends on land/sea regions and also latitude (Figure 1.9).

Figure 1.9 suggests opposed trends over land and ocean, it is not an absolute delineation. Land, especially tropical land, shows a decreasing trend of precipitation (somewhat comparable to the GHCN observed data base), while oceans generally have increasing trends of precipitation. This relationship is also apparent in other AGCM simulations [*Bosilovich et al.*, 2004]. Global, continental and oceanic trends are summarized in Table 1.1. While continental temperatures are increasing, evaporation is decreasing. This is leading to continental total precipitable water (TPW) that has no statistically significant trend (but relative humidity may be then decreasing).

In this paper, we are investigating the processes of precipitation recycling in the GEWEX CSEs in the Americas (MAGS, MRB and LBA). Initially, we may neglect the trends in the background climate. This may be acceptable for MAGS and MRB, but analysis of LBA will certainly required better understanding of the trends.

CSE Water budgets In our analysis of the CSE water budgets, we first analyze the mean annual cycle to identify the major sources of water, and the time of maximum precipitation recycling (figure not shown). The time of maximum recycling is June and July for MAGS and MRB, and October and November for LBA. Figure 1.10 shows the mean water budgets during the time of maximum precipitation recycling. The MAGS basin is dominated by zonal moisture transport. While recycling is a significant contribution, Pacific ocean provides the primary source, and external continental sources are also very important (including Asia). The Mississippi River Basin relies on the "conveyor belt" of water vapor, where the easterly flow across the tropics turns northward toward the central US, then exits the eastern boundary. The tropical Atlantic Ocean sources

Table 1.1: FVGCM trends for global, continental and oceanic variables. Bold indicates statistical significance at 1%, while normal is not significant at 10% (only Land TPW).

Unit per 50 year	Global	Land	Ocean	GHCN
P (mm d^{-1} y)	0.024	−0.127	0.081	−0.076
TPW (mm)	0.631	0.085	0.837	
T (K)	0.311	0.265	0.331	
E (mm d^{-1} y)	0.024	−0.038	0.047	

Table 1.2: Correlations between different water vapor variable area averaged time series of the maximum recycling season for each basin.

MAGS	P	E	P-E	TQ	MAGS	NPO	Asia	QV_W	QV_E	QV_S
E	0.50	1.00								
P−E	**0.81**	−0.10	1.00							
TQ	0.46	0.45	0.22	1.00						
MAGS	**0.53**	0.31	0.40	0.29	1.00					
NPO	**−0.55**	−0.18	**−0.50**	−0.34	**−0.58**	1.00				
Asia	**−0.69**	−0.33	**−0.57**	−0.32	**−0.63**	0.41	1.00			
QV_W	**−0.51**	−0.04	**−0.56**	−0.42	**−0.67**	**0.61**	**0.65**	1.00		
QV_E	**0.59**	0.01	**0.67**	0.49	**0.61**	**−0.52**	**−0.60**	**−0.83**	1.00	
QV_S	0.01	0.34	−0.21	0.07	−0.03	−0.01	0.07	0.04	−0.25	1.00
QV_N	−0.17	−0.27	−0.01	−0.31	−0.02	−0.04	−0.04	−0.10	−0.26	−0.48
MRB	P	E	P-E	TQ	MRB	NPO	Trop Atl	QV_W	QV_E	QV_S
E	**0.96**	1.00								
P−E	**0.83**	**0.64**	1.00							
TQ	**0.57**	**0.55**	0.46	1.00						
MRB	**0.87**	**0.88**	**0.61**	0.41	1.00					
NPO	**−0.54**	**−0.54**	−0.41	−0.43	**−0.58**	1.00				
Trop Atl	−0.36	−0.36	−0.27	0.25	−0.48	−0.03	1.00			
QV_W	0.31	0.31	0.22	−0.13	0.19	0.32	−0.41	1.00		
QV_E	−0.17	−0.12	−0.21	−0.03	0.04	−0.29	−0.01	**−0.69**	1.00	
QV_S	0.40	0.32	0.45	**0.64**	0.05	−0.19	0.40	0.09	**−0.54**	1.00
QV_N	−0.16	−0.21	−0.03	**−0.54**	−0.04	0.35	−0.34	0.39	**−0.51**	−0.35

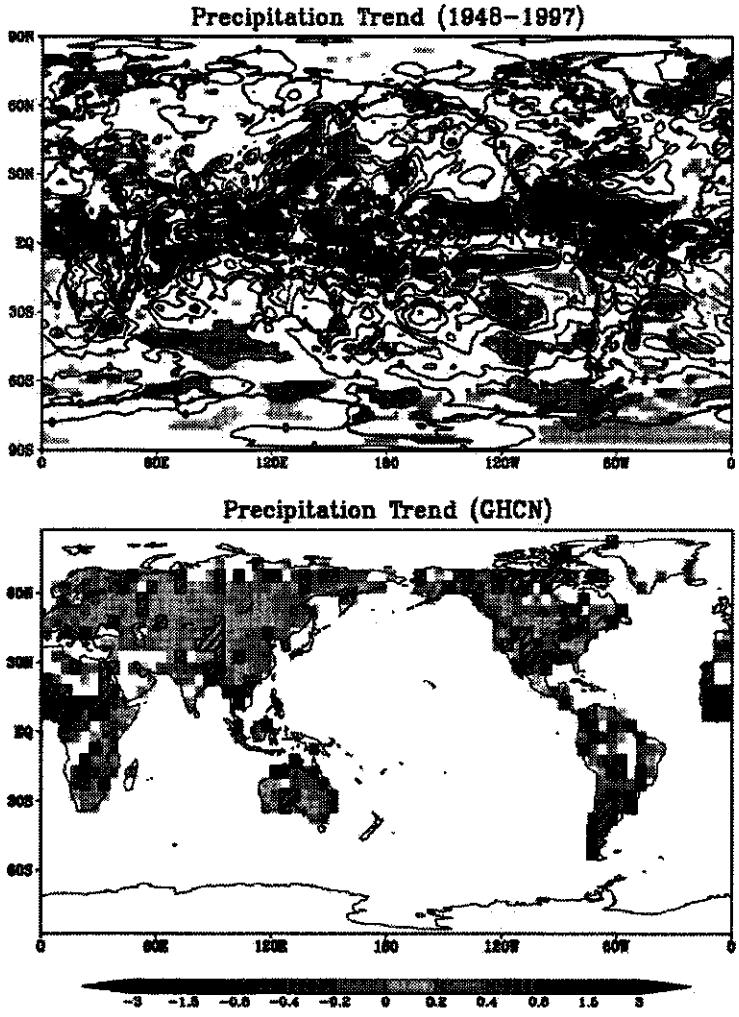

Figure 1.9: Trends of annual Precipitation anomalies from the FVGCM 50-year simulation (colors are statistically significant at 5%) and the GHCN precipitation observation data set (crosshatch indicates statistically significant at 5%). Units are mm d^{-1} per 50 years.

dominate the water budget, but the relatively small area of the Gulf of Mexico, is still an important contributor.

The LBA budget has a similarity to the northern basins, in that there is a significant oceanic source of water (South Atlantic, instead of Pacific). However, there is a clear difference in monthly moisture convergence. LBA Precipitation nearly doubles the evaporation, so that there must be outside sources of water. Nonetheless, 27% of the precipitation has a local source. However, considering the evaporation, 52% of evaporation stays within the basin, compared to 18% and 23% of evaporation for MAGS and MRB respectively. Note here that the precipitation recycling

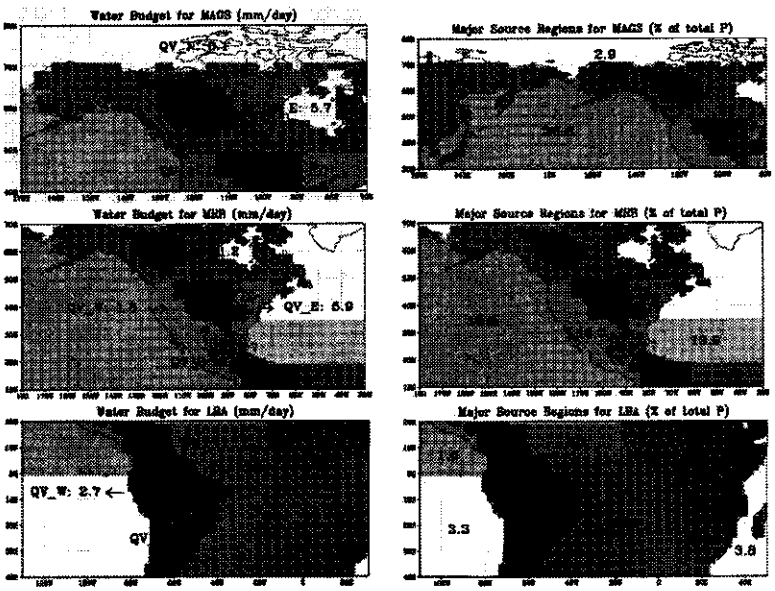

Figure 1.10: Moisture budgets and primary precipitation sources (percent of total precipitation) for each of the CSEs, MAGS (top), MRB (middle) and LBA (bottom). Budget units are mm d^{-1}

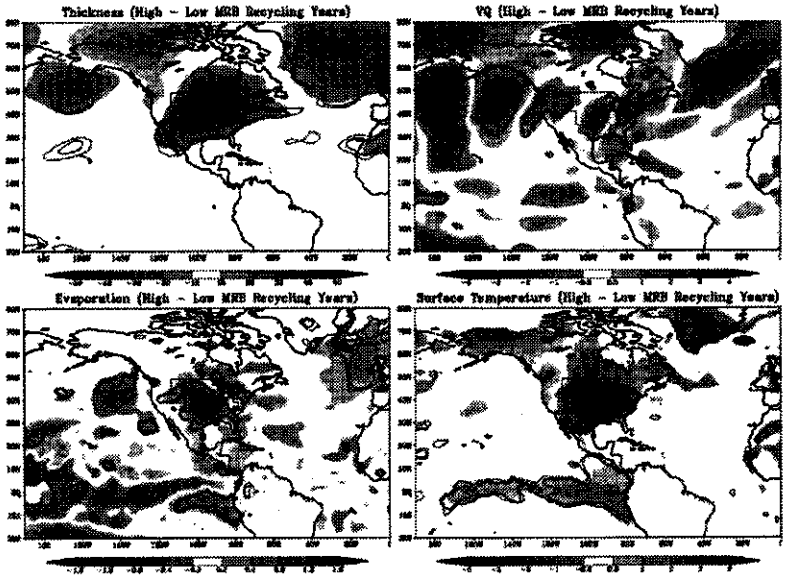

Figure 1.11: Differences between the five highest and lowest recycling ratio season. Statistically significant differences are indicated by the solid contour intervals (at 5 and 10% levels). The units are m, m s^{-1}, g kg^{-1}, mm d^{-1}, and K.

is a function of area, and the intercomparison of different basins should be qualitative.

Precipitation Recycling Composites The purpose of this paper is to better define the conditions that lead to precipitation recycling on basin scales. With 50 years of simulation data, we can identify the highest and lowest recycling seasons, and define the large-scale conditions associated with each. In general, the five highest and lowest recycling seasons (as determined by the recycling ratio) in each basin was outside of ± 1 standard deviation of the mean. Therefore, we define the high recycling as the mean of the five highest seasons, and low recycling as the five lowest seasons.

Figure 1.11 shows the difference between the high and low recycling seasons for the Mississippi River Basin. There are significant large-scale features associated with the precipitation recycling. Low 500 mb thickness anomalies with higher recycling likely reduce the intensity of the Great Plains low-level jet. Also, temperatures are colder concurrent with increased evaporation. This is also related to a concurrent increase in total precipitation (not shown). There may be some teleconnections with the tropical easter Pacific SSTs, but this needs further investigation. It makes sense that the high recycling is associated with increased evaporation. However this is not the case for MAGS. There is a much weaker correlation between precipitation and evaporation in MAGS than MRB, along with weaker correlation between the local source and evaporation. MAGS recycling appears related to whether the large-scale moisture transport intensity (weak transport leads to more recycling).

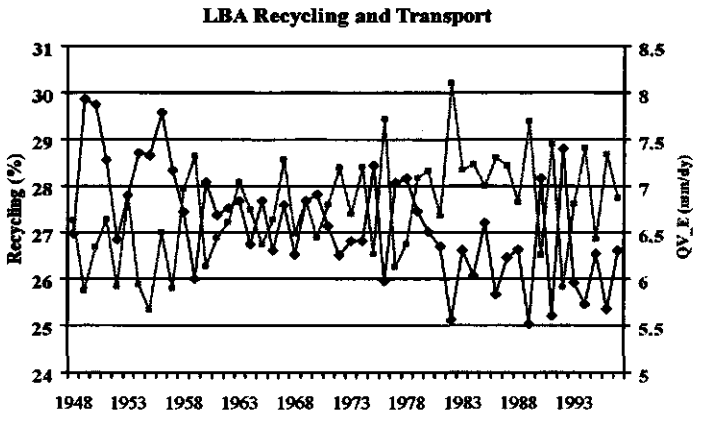

Figure 1.12: Time series of the maximum recycling season averaged LBA recycling ratio and easterly moisture transport into LBA.

In LBA, high recycling is also related more to the weaker zonal flow (from the Atlantic) than variations in evaporation. The high recycling is related to cold temperatures in the tropical eastern Pacific Ocean (figures not shown). The trend in SST forcing also leads to trends in both the moisture transport into LBA and the LBA recycling (Figure 1.12). It is important to note that deforestation is not included in this numerical simulation

In the near term, we will investigate the potential teleconnections between MRB and the tropical SSTs, continue analyzing the trends in LBA, and evaluate bulk recycling methods.

Collateral damage - the unpleasant side-effects of ignoring observation errors in water balance calculations

E.E. van Loon[1], J. Brown[1], and W. Bouten[2]

[1]*Institute for Biodiversity and Ecosystem Dynamics, University of Amsterdam, Amsterdam, The Netherlands*

Well-defined observation uncertainty is a prerequisite to successfully apply parameter or state estimation. However, in most hydrological studies the particular structure of this uncertainty is neglected. We show the type and magnitude of errors that arise from this neglect in 1D (vertical column) as well as in 2D (a field of columns, with lateral routing) water balance calculations. In our system, we deal with observations of rainfall, evapo-transpiration (indirectly via meteo-observations), soil moisture in the unsaturated zone, depth to the saturated zone, recharge and discharge via ground and surface water. Typical observations errors for each of these variables are specified and the effects are evaluated. We generate our data rather than relying on field observations, in order to control both model and observation errors. However,the properties of our system are chosen such that these resemble real systems as close as possible.

The results show that, in both 1D and 2D systems, the errors generally do not average out, but rather enforce each other. In addition, we show that with a correct system description and (partial) incorrect observation uncertainty, it is not possible to identify the correct source of error on the basis of full input and state-observations using classical system identification tools. The incorrect representation of system behaviour would be diagnosed as either a wrong model structure, parameter set, observation uncertainty or a combination of these.

If there is redundancy in the observations, there are different ways to identify observation uncertainty: (1) independent of a model; (2) by hierarchical modeling, and (3) by resampling. If there are enough data, any identification of observation error can be done independent of a dynamic model. This is the simplest and also the most robust one, as it prevents model structural errors to be incorrectly labelled as observation errors. Hierarchical modeling is a technique where coarse scale models and observations constrain fine-scale equivalents and vice versa. This technique is applicable if for instance radar rainfall and discharge data is available at a coarse scale, and meteo-observations together with in-situ soil moisture observations at a fine scale. Resampling techniques esimate model error structures by evaluating the impact of omitting observations on nearby predictions, while correcting for spatial and temporal correlations in the observations. Low impacts imply in this context a large observation error. All three methods rely on independence of the observation errors between the redundant data. In addition, hierarchical modeling and space-time resampling assume an approximately correct model structure. The degree to which the methods are able to withstand violations of these assumptions is illustrated in our study.

Global mapping of water sources using water vapor tracer diagnostics

Jiundar Chern[1] and Michael G. Bosilovich[1]

[1]*NASA/GSFC, USA*

Recently, we have implemented the water vapor tracer (WVT) diagnostics in the NASA finite volume General Circulation Model (fvGCM). In the WVT approach, atmospheric water is "tagged" at its surface source as a constituent tracer and followed through atmospheric processes until it precipitated from the atmosphere. This technique permits quantitative study of the local and remote sources of precipitation at any point or area within the model's simulation. The most detailed diagnostic could be attained by using one WVT for each model grid point. Since each WVT is treated as a three-dimensional prognostic variable in the model, the number of WVTs in one simulation is limited due to the computing resource.

In this study, the global water sources are divided into 4° × 5° boxes from 60°S to 70°N. To differentiate the contributions from land and ocean near the costal region, two WVTs are used in each 4° × 5° box based on the model's land sea mask. The total number of WVTs is about 2500. Eleven simulations have been performed, each with more than 200 tracers, at 2.0° × 2.5° resolution for the period 1948–1997. The first 20-year (1948–1967) runs has been done, we will present the detailed mean atmospheric water cycle (surface evaporation source, WVT moisture transport, and WVT precipitation) for some major cities and river basins in the world. The temporal and spatial climate variabilities of the regional and local water budgets will be evaluated using the principle analysis of the WVT diagnostics. In addition,the global map of local precipitation recycling based on 4° × 5° grid box will be examined.

Use of small reservoirs in West Africa as remotely-sensed cumulative runoff gauges

Nick van de Giesen[4,1], **Jens Liebe**[2,1], **Marc Andreini**[1,3], **and Tammo Steenhuis**[2]

[1]*Center for Development Research, Bonn University, Germany*
[2]*Biological and Environmental Engineering, Cornell University, USA*
[3]*International Water Management Institute, Ghana*
[4]*Technical University, Delft, The Netherlands*

Throughout the semi-arid to sub-humid tropics, people have built thousands of small reservoirs to overcome dry periods. The social value of water in such regions as West and Southern Africa, South and South-East Asia, and central Brazil, is very high. Small reservoirs, with volumes from 10^4 to 10^7 m^3, provide the rural population of these areas with water for households, cattle, fisheries, and small-scale irrigation. Besides positive socio-economic impacts, small reservoirs may also have negative impacts on human health and aquatic ecology. The general thinking is that construction of reservoirs at village level has less negative impact than the construction of large dams. As such, many governmental and non-governmental development programs promote further construction of small reservoirs.

One obvious question with respect to this development is if an optimal density exists, beyond which further construction of reservoirs shows diminishing returns due to limited total water availability, market saturation, or negative health and environmental impacts. Within the CGIAR's Challenge Program on Water for Food, the Small Reservoirs Project[†] addresses these research questions concerning the overall behavior of reservoir ensembles in the Volta, Limpopo, and Sao Francisco basins. The work presented here also builds on field work done within the framework of the GLOWA Volta Project[‡].

Hydrological knowledge of the semi-arid and sub-humid tropics is very limited and the observation network in these parts of the world has been declining rapidly since the hydrological decade. Remote sensing still holds great promise to fill gaps in ground-based observation networks but scientific progress has been slower than anticipated. One added problem is that the regions considered here are under almost permanent cloud cover during the rainy season. This makes microwave-based (radar) remote sensing the main source of data with respect to the hydrological state of the land surface, whereby, unfortunately, the luscious vegetation tends to obscure any soil moisture signal during the wet season. There is, however, one well-established application of radar satellite imagery and that is the mapping of open water. Clearly, (changes in) volumes stored in the thousands of small reservoirs contain imperfect but hydrologically relevant information. The question now is to what extent we can use reservoir states, as derived from radar images, to calibrate and validate hydrological models.

In the remainder, we first briefly sketch the different components of the water balance of the reservoirs, and how different parts of the balance can be observed or modeled. This sketch includes a simple accounting scheme that allows keeping track of remotely-sensed runoff estimates, consisting of most likely runoff, and, under specific conditions, minimum and maximum discharges that constrain possible model output. Finally, the limitations and potential of using remote sensing of

[†]http://www.smallreservoirs.org
[‡]http://www.glowa-volta.de

reservoirs for model calibration is demonstrated by a simulation, showing the effects of model and measurement errors and of the use of constraints.

Reservoir Water Balance The basic reason why we want to examine the usefulness of satellite-observed reservoirs for runoff estimation and model calibration is that a survey showed a very good correlation between surface area and storage volume in the Upper East Region of Ghana. According to a bathymetric survey of sixty reservoirs, 97.5% of the observed variability in volume could be explained on the basis of surface area. This was especially remarkable because the basic shapes of the reservoir surfaces were extremely diverse. The relation found, and used here, was $\text{Vol} = 8.52 \cdot \text{Area}^{1.437}$ ($10^{-3}\,\text{m}^3$). The surface area of reservoirs that are larger than one hectare can be observed with good accuracy with ERS-PRI images, as shown in Figure 1.13.

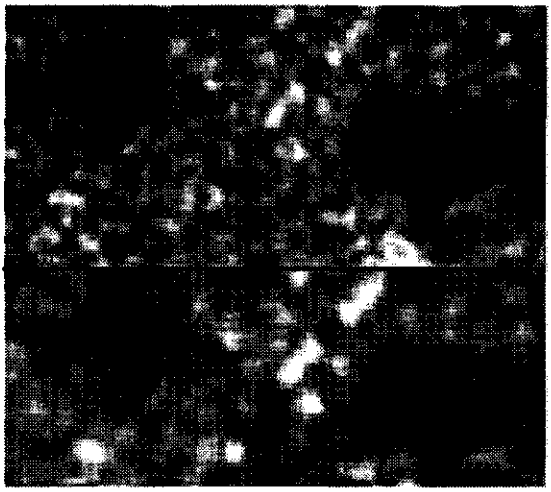

Figure 1.13: Two small reservoirs in the Upper East Region of Ghana as observed by ESA's ERS2. The classification was based on density slicing of the mean band from the co-occurrence measure analysis.

On the basis of satellite images, we can calculate surfaces and thus volumes. ERS2 covers the area of interest on a monthly basis. By subtracting the volumes from two subsequent overpasses, we obtain a measure of how much water has run off into the reservoir during that particular month. The accuracy of this volume estimate is about 95%. One still needs to account for losses through evaporation, seepage through dam and bottom, and water use for irrigation and other purposes. All these elements of the water balance are subject of an on-going intensive field measurement campaign. It is expected that evaporation can eventually be modeled with standard meteorological observations with an error of 10% on a monthly time scale. Seepage and water use will be much more error prone and can probably not be modeled within less than a 30% error.

In addition to errors in the water balance, one also has to deal with the facts that reservoirs may spill unknown amounts during months with large runoff, and that such spills may cascade into a reservoir below. Cascades with a length of up to five reservoirs are known to occur in neighboring Burkina Faso. To keep track of possible spills, a matrix-based accounting scheme was developed that keeps track of the connectivity under spilling conditions. When a reservoir is close to being full during an ERS2 overpass, this reservoir is marked as such and no runoff estimate will be available for that month. When a reservoir is observed to be almost full, a constraint is used

instead that simply states that the actual runoff must exceed the runoff based on the observed area differences. When such a reservoir cascades into a downstream reservoir, this information can be taken into account. In the remainder of this extended abstract, it is, for the sake of simplicity, assumed that no cascading takes place.

Calibration of hydrological model In order to assess how useful satellite observed reservoir areas can be, we developed a simple hydrological model that was first run in forward mode to predict observable reservoir areas. Subsequently, model parameters were fitted on the basis of the information that would be available from satellite images. The fitting was repeated for four error levels, 0%, 10%, 20%, 30%. For each level, a uniformly distributed random error within the range of plus/minus the given percentage of the error-free observation was imposed. Runoff into each reservoir was derived from the difference in storage in two successive months, plus modeled evaporation and water-use. When observable reservoir areas were close to maximum capacity, no discharge estimate for that month was used. For those months, only minimum runoff could be used to constrain the model.

The hydrological model used is simple but covers the main hydrological processes at work in small watersheds in West Africa, as observed through detailed field work over the past decade. The model consists of a Thornthwaithe-Mather (TM) module, which simulates regional recharge, and a watershed-specific runoff coefficient (RO). The TM module uses only one regional parameter, S_{max}, which represents the maximum storage in the soil that needs to be filled before recharge takes place. All recharge is assumed to runoff via the groundwater. In addition, direct runoff occurs from built-up, degraded, and saturated areas. RO represents the fraction, varying between 0.5% and 3%, of each watershed that is covered by such runoff generating areas. The forward model is run on a daily time step. Runoff then accumulates in the reservoirs from which evaporation and water-use are extracted. The predicted areas are, after addition of errors, used as input for inverse runoff calculation and parameter fitting. It is recognized that such simulated observations are somewhat removed from the often unforeseeably more complicated reality, but this is the only way in which effects of error in otherwise non-observable variables can be assessed. In this case we are particularly interested in three aspects:

- To what extent does the fact that only cumulative monthly observations are available limit the fitting accuracy?
- For months in which reservoirs may have spilled, only constraints on the minimum discharge can be used. How does this affect the fitting?
- What is the effect of the large errors in, especially, the modeled water-use?

The setting is that of the Upper East Region of Ghana, where 154 reservoirs have been identified on the basis of remote sensing and for which monthly ERS coverage is available since October 2003. For the purpose of this extended abstract, the built-in solver of Excel was used to estimate model parameters through (constrained) error minimization. With the given model complexity, only up to eleven parameters (S_{max} and ten individual RO's) could be calibrated reliably with this solver. The intention is to do a more advanced optimization for all 154 reservoirs for the final article and presentation. The results are shown in Table 1.3, which compares original and fitted parameter values for different input error levels.

Two things become clear from the table with fitted model parameters. First, even with relatively high errors in estimated water-use, the fitted parameters are close to the original model values. This close fit bodes well for using small reservoirs as runoff gauges as observed by satellites. Clearly, the proper processes still need to be captured in the models, so hydrological field work in

Table 1.3: Effect of input errors (0%, 10%, 20%, 30%) and those of the use of constraints on the ability to retrieve the original model values using the observable changes in storage and modeled evaporation and water-use.

		Constraints used				No use of constraints			
	Original	0%	10%	20%	30%	0%	10%	20%	30%
S_{max}	350.0	347.9	347.4	347.8	342.7	360.5	360.6	360.4	360.9
RO_1	2.40	2.42	2.51	2.85	3.06	2.42	2.51	2.31	3.06
RO_2	1.40	1.40	1.47	1.33	1.60	1.41	1.47	1.47	1.60
RO_3	1.70	1.69	1.60	1.95	2.09	1.69	1.60	1.86	2.09
RO_4	1.30	1.30	1.27	1.12	1.72	1.30	1.27	1.37	1.72
RO_5	2.00	1.99	2.01	2.03	2.01	1.99	2.01	2.03	2.01
RO_6	0.50	0.51	0.53	0.29	0.55	0.51	0.53	0.51	0.55
RO_7	1.20	1.20	1.25	1.46	1.33	1.20	1.25	1.46	1.33
RO_8	1.80	1.80	1.86	1.80	2.19	1.80	1.86	1.83	2.19
RO_9	0.70	0.67	0.69	0.87	0.75	0.67	0.69	0.76	0.75
RO_{10}	0.50	0.48	0.45	0.80	0.56	0.48	0.45	0.55	0.56
Avg Error		0.01	0.05	0.19	0.24	0.01	0.05	0.08	0.24

the region of interest remains very important. Second, using reservoirs that spilled as constraints on the minimum flow amount only improved the fit of the regional variable, S_{max}. The reason for this is simply that reservoirs spilled during months with high flows when the rainfall to be stored in the soils exceeded S_{max}. By using the minimum flow constraint, the model was "forced" to spill at the right time by adjusting S_{max}.

In general, the proposed method of runoff observation and model calibration is promising. Observing water stored in small dams with radar satellites can contribute to the on-going hydrological research on Prediction in Ungauged Basins (PUB), especially in parts of the world where the value of water is high and hydrological observations scarce.

A bold, innovative future for measuring the dynamics of global surface fresh waters

Doug Alsdorf[1]

[1]*Department of Geography, University of California, Los Angeles, California, USA*

River discharge as well as lake and wetland storage of water are critical elements of land surface hydrology, yet they are poorly observed globally and the prospects for improvement from in-situ networks are bleak. Considering this, a NASA Surface Water working group[§] is focused on answering the following science and applications questions: (1) What are the observational and data assimilation requirements for measuring natural and manmade surface storage and river discharge that will allow us to (a) understand the land surface branch of the global hydrologic cycle, (b) predict the consequences of global change, and (c) make assessments for water resources management? (2) What are the roles of wetlands, lakes, and rivers (a) as regulators of biogeochemical and constituent cycles (e.g., carbon, nutrients, and sediments) and (b) in creating or ameliorating water-related hazards of relevance to society? Global models of weather and climate could be constrained spatially and temporally by stream discharge and surface storage measurements. Yet this constraint is rarely applied, despite weather and climate modeling results showing that predicted precipitation is often inconsistent with observed discharge. Thus, as satellite missions are developed for global observations of critical hydrologic parameters such as soil moisture (i.e., HYDROS) and precipitation (i.e., GPM), the lack of concomitant measurements of runoff and surface water storage at compatible spatial and temporal scales may well result in inconsistent parameterizations of global hydrologic, weather, and climate models. Fortunately, several spaceborne methods have provided potential avenues toward answering these hydrologic questions. Among the most promising are active radar and lidar methods that measure inundation area, water heights, and changes. For example, radar altimetry is well known for its ability to measure ocean surface topography and such methods should be easily adaptable to inland waters. The global observations possible from such platforms will have important implications for global water cycle research.

[§]http://www.swa.com/hydrawg

Manifestations of global climate change on accelerating the hydrological cycle: prospects for increases in extremes

K.E. Trenberth[1]

[1]*Climate Analysis Section, NCAR, USA*

The issue of how the hydrological cycle will change as the climate changes is complicated considerably by somewhat independent changes in pollution (aerosol), whereby increases typically act to short-circuit the hydrological cycle. However with warming, the main prospect is for increased water holding capacity and associated increased water vapor in the atmosphere. The rate of increase of 7% K^{-1} is much greater than projected rates of increase in overall evaporation and precipitation, which are more like 1–2% K^{-1} and are governed by the surface heat budget. Hence the prospects are for increases in precipitation intensity but decreases in duration or frequency of precipitation. In addition increased rain at expense of snowfall is likely, with major impacts on snow pack (storage) and soil moisture. The changes directly impact partitioning into soil moisture and runoff, and make prospects of both droughts and floods more likely. On top of these general tendencies are changes in storm tracks and large regional changes associated with teleconnections, such as from El Niño. More attention is needed to hourly precipitation in both the real world and models to determine how the precipitation characteristics are changing in both. Water management will be a major issue in the future.

How should precipitation change as the climate changes? This is a key question that could have a substantial impact on society and the natural environment, as it can directly affect availability of fresh water, the quality of potable water, drought and floods. Usually the only measure of precipitation cited is amount. Yet most of the time it does not rain or snow. So just a little thought makes us realize that we need to be concerned also with how often it rains: the frequency; and how hard it rains when it does rain: the intensity or rainfall rate, as well as the amounts. We also need to be concerned about whether the precipitation switches from snow to rain or vice versa. Also, it turns out that making these distinctions allows us to make more sensible statements about the likely changes and how to best examine the data on precipitation.

The term "global warming" is often taken to refer to global increases in temperature accompanying the increases in greenhouse gases in the atmosphere. In fact it should refer to the additional global heating (sometimes referred to as radiative forcing) arising from the increased concentrations of greenhouse gases, such as carbon dioxide, in the atmosphere. Increases in greenhouse gases in the atmosphere produce global warming through an increase in downward infrared radiation. This increase in surface heating can indeed increase surface temperatures but it also increases evaporation. In fact it is more likely to do the latter as long as adequate moisture is around and over the oceans, which encompass 71% of the globe, water is everywhere. For example, after a rain storm, when the sun comes out, the first thing that happens is that the puddles dry up and the surface of the ground dries before the sun's heat goes into raising temperature.

When the temperature increases, so does the water-holding capacity of the atmosphere. This is why we tend to use relative humidity as a measure of moisture as it signifies the percentage of moisture the atmosphere can hold rather than the absolute amount. At very cold temperatures, the atmosphere can hardly hold any moisture, in effect it gets "freeze dried", and so liquid water amounts from snow at temperatures below freezing are quite small.

Of course, enhanced evaporation depends upon the availability of sufficient surface moisture and, over land, this depends on the existing climate. In fact surface moisture comes directly from evaporation as well as through transpiration in plants, together called evapotranspiration. However, it follows that naturally occurring droughts are likely to be exacerbated by enhanced potential evapotranspiration (drying).

Thus if the water carrying capacity of the atmosphere increases and there is enhanced evaporation, the actual atmospheric moisture should increase, as is observed to be happening in many places. Over the United States and Gulf of Mexico, for example, moisture amounts in the lowest 20,000 feet of the atmosphere increased about 10% from 1973–1994.

Further, globally there must be an increase in precipitation to balance the enhanced evaporation but the processes by which precipitation is altered locally are not well understood. Precipitating systems of all kinds (rain clouds, thunderstorms, extratropical cyclones, hurricanes, etc) feed mostly on the moisture already in the atmosphere at the time the system develops, and precipitation occurs through convergence of available moisture on the scale of the system. Hence, the atmospheric moisture content directly affects rainfall and snowfall rates, but not so clearly the total precipitation, at least locally. Thus, it is argued that global warming leads to increased moisture content of the atmosphere, which in turn favors stronger rainfall events. In other words, when it rains it should rain harder than it used to under similar circumstances. This is exactly what is observed to be happening in many parts of the world, thus increasing risk of flooding. It is further argued that one reason why increases in rainfall should be spotty is because of mismatches in the rates of rainfall versus evaporation. Evaporation occurs typically at about 3 mm per day but moderate or heavy rain can easily be 25 mm or more per day. Thus rain dries out the bulk atmosphere unless the winds bring in more moisture from remote areas, and the weather system runs out of moisture. Moreover, heavier rains are apt to runoff at the expense of soil moisture, increasing risk of drought unless compensated for by precipitation increases.

Because of constraints in the surface energy budget, there are also implications for the frequency and/or efficiency of precipitation. The global increase in evaporation is determined by the increase in surface heating and this controls the global increase in precipitation. Moisture amounts are not limited by this but instead are limited by the moisture carrying capacity, and so precipitation rates that depend on the latter are apt to increase more rapidly than amounts, implying that the frequency of precipitation or duration of events must decrease, raising the likelihood of fewer but more intense events.

There are many potential complications. An increase in atmospheric moisture may lead to increases in relative humidity and increased clouds, which could cut down on solar radiation and reduce the energy available at the surface for evaporation. Those feedbacks are included in the climate models and alter the magnitude of the surface heat available for evaporation in different models but not its sign. The accumulations depend greatly on the frequency, size and duration of individual storms, as well as the rate, and these depend on atmospheric static stability (vertical structure) and other factors as well. In particular, the need to vertically transport heat absorbed at the surface is a factor in convection and extratropical weather systems, both of which act to stabilize the atmosphere. Increased greenhouse gases also stabilize the atmosphere. Those are additional considerations in interpreting model responses to increased greenhouse gas simulations.

Other major complications occur through changes in aerosols, which have multiple effects. A direct influence is to reflect solar radiation, as occurs with the milky white sulfate particles. However carbonaceous aerosols, such as soot, absorb solar radiation. Both lead to cooling at the surface, but the second also heats the region where the aerosol is located. Hence this short circuits the hydrological cycle which otherwise would take the surface heat as evaporation and release it in the lower atmosphere as latent heat during precipitation. Other indirect influences also occur on cloud.

Typically aerosol increases the number of cloud droplets, making the cloud brighter for the same cloud liquid water, and the droplets are smaller and hence less likely to fall, leading to longer-lived clouds. But absorption in clouds heats the region and can help burn off the cloud. Cloud in turn leads to cooling at the surface, less evaporation and thus less cloud. The net effect depends on the climate regime, the type of aerosols, and is poorly known and poorly done in models.

It is argued that increased moisture content of the atmosphere favors stronger rainfall and snowfall events, thus increasing risk of flooding. Although there is a pattern of heavier rainfalls observed in many parts of the world where the analysis has been done, another factor is increasing settlement of flood plains, which changes vulnerability to flooding. Flooding records are confounded by changes in land use, construction of culverts and dams, and other means designed to control flooding.

With higher average temperatures expected, more precipitation is likely to fall in the form of rain rather than snow, especially in the spring and autumn, which will increase run off. In addition, faster snow melt is likely to aggravate springtime flooding. A major consequence is decreased snow pack as the spring occurs, leading to diminished water storage and soil moisture in the summer. This also means less recycling of moisture, whereby local evaporation helps feed clouds and local rains, that is more important in summer compared with winter, and enhances risk of summertime drought. This mechanism is especially likely in mountain regions and mid to high latitude continents.

The above arguments suggest that there is not such a clear expectation on how local total precipitation amounts should change, except as an overall global average. Complicated patterns of precipitation change should occur where storm tracks shift; where the storms previously tracked gets drier and where they shift to becomes wetter. Beyond this, it is suggested that examining moisture content, rates and frequency of precipitation, and phase (rain or snow), and how they change with climate change may be more important and fruitful than just examining precipitation amounts in understanding what is happening, both in the real world and in climate models. But many data analyses are not done to illuminate these aspects. To be compatible with life times of significant rain events, yet still deal with whole storms rather than individual rain cells, examination of hourly precipitation data is recommended. Such data are also retrievable from climate models, but such data are seldom archived. It is strongly recommended that a new focus should occur on hourly precipitation amounts.

For further reading see *Dai et al.* [submitted], *Trenberth* [1998], *Trenberth* [1999] and *Trenberth et al.* [2003].

Closing continental-scale water and energy budgets

J. Roads[1]

[1]*Scripps ECPC, UCSD, La Jolla, California, USA*

One of the goals of the Global Energy and Water-Cycle (GEWEX) Continental Scale Experiments (CSEs) is to accurately estimate or "close" the water budget on continental scales. The GEWEX Hydrometeorology Panel (GHP) coordinates the CSEs and affiliated experiments, which now include eight representative world climate regions. The CSE regions over the Americas include the Mackenzie (MAGS), Amazon (LBA) and La Plata (LPB) river basins as well as the coterminous US (GAPP). In Europe, there is the Baltic river and sea basin (BALTEX) and in Asia (GAME) there are 4 sites over the Lena river basin as well as other Asian regions (HUBEX, Tibet, GAME tropics). In Australia, there is a site over the Murray Darling Basin (MDB). An affiliated experiment has begun over western equatorial Africa (AMMA). Most of the CSEs include major river basins and one has an inland sea (BALTEX). In general all include large continental scale regions. This talk will provide an overview of past, present and future GHP efforts to develop an atmospheric and surface water and energy budget global and regional synthesis over the individual CSEs.

Mixtures of Gaussians for uncertainty description in latent heat flux estimates from remotely sensed information

R. Wójcik[1], P.A. Troch[1], H. Stricker[1], P.J.J.F. Torfs[1], E.F. Wood[2], H. Su[3], and Z. Su[3]

[1]*Hydrology and Quantitative Water Management Group, Wageningen University, Wageningen, The Netherlands*
[2]*Princeton University, Princeton, New Jersey, USA*
[3]*Alterra Green World Research, Wageningen, The Netherlands*

Latent heat flux (LE) is the key variable that provides a link between energy and water budgets at the land surface. The conventional methods to estimate LE are based on point measurements of energy balance components and are representative only for very local scales. Recently a new class of techniques based on remotely sensed (RS) information has been developed to compute LE at scales from a point to a continent. Despite their potential, especially for regional and global hydrological applications, "satellite-derived" LE_{sat} usually does not compare well with "in-situ measured" LE_{is}. Both proxies of LE, however, contain the information about the true value of this quantity. The difficulty in inferring this information from data is due to different sources of uncertainty involved (e.g., measurement errors, scale problems, inadequacies in physical models that transform satellite observations into LE estimates). In this work we seek to investigate the use of non-parametric Gaussian mixture density models (GMDM's) to describe the conditional uncertainty of LE_{sat} given LE_{is}. This approach does not require any a priori assumptions on the form of the conditional density i.e. the algorithms we use in this study are completely data driven. An extra benefit from having the conditionals described by GMDM's is that they can further be applied to identify the recently developed non-linear Kalman filter for ensemble data assimilation [see *Anderson and Anderson*, 1999; *Torfs et al.*, 2002]. This is the long run objective of this research.

Data and methods LE_{is} estimates used in this study come from seven Energy Balance Bowen Ratio (EBBR) ARM/CART stations (E15, E4, E9, E20, E7, E25, E8) distributed across the Southern Great Planes (SGP) region of the United States. These estimates are based on 30-min averaged observations. The LE_{sat} estimates were obtained using SEBS (Surface Energy Balance System) developed by *Su* [2002] and are based on instantaneous observations. The both types of LE proxies were obtained at 1 hourly resolution in the period of 1 July 2001–30 September 2001.

To describe the conditional uncertainty of LE_{is} given LE_{sat} a joint probability density function (pdf) f needs first to be fitted to bivariate sample $\{LE_{sat,k}; LE_{is,k}\}_{k=1}^{K}$. In this work the focus is on the use of GMDM's [see e.g. *McLachlan and Peel*, 2000] which are defined as linear combinations of Gaussian densities (see Figure 1.14), called components:

$$f(\mathbf{x}) = \sum_{n=1}^{N_c} w_n g_{(\mathbf{m}_n, \mathbf{C}_n)}(\mathbf{x}) \tag{1.4}$$

where $\mathbf{x}$ is a vector of variables, N_c the number of components, $g_{(\mathbf{m}_n, \mathbf{C}_n)}$ stands for the Gaussian density with mean $\mathbf{m}_n$ and covariance $\mathbf{C}_n$. Here $\mathbf{x} = [LE_{sat}\, LE_{is}]^T$. The w_n's are the component weights and satisfy $w_n \geq 0$ and $\sum w_n = 1$. Note that the conditional density $f(LE_{is}|LE_{sat})$ that is

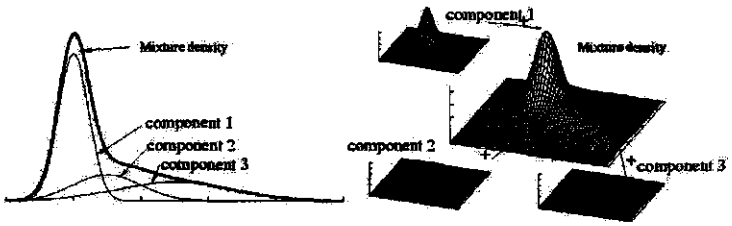

Figure 1.14: 1D and 2D example of GMDM (in both cases as a linear combination of 3 components).

calculated from (1.4) is also a GMDM. To fit (1.4) to the data the procedure of *Figueiredo and Jain* [2002] was applied.

First attempt To apply the above described methodology we derived the estimates of LE_{sat} by forcing SEBS with the following instantaneous RS inputs: short wave radiation derived from a 50 km GOES product and 1/8 degree GOES surface temperature. The rest of the input variables that were needed to run SEBS [see *Su*, 2002] was either measured or taken from LDAS database. Next we grouped LE_{sat} and LE_{is} data according to landuse. Our hypothesis here is that at regional scale the bivariate dependency structure should be invariant within a particular landuse class. Moreover, this step is intended to tackle the dimensionality reduction issue in non-linear ensemble Kalman filters as described by *Anderson and Anderson* [1999] and *Torfs et al.* [2002]. Figure 1.15 shows the result of this operation. It can be seen in the figure that the dependency *pattern* between LE_{is} and LE_{sat} is not really visible. Thus, the data in Figure 1.15 would be of little use for data assimilation purpose. The blurring effect might be due to undersampling which stems from the fact that data availability of GOES temperature is greatly affected by the cloud cover and the algorithm that is used to retrieve the surface temperature. Moreover, there is a spatial and temporal scaling problem involved (we compare point values with 1/8 decimal degree values), there is a measurement error in LE_{is} values and there is an error in LE_{sat} values. The latter might be a combination of errors in RS inputs to SEBS and limitations of SEBS itself to reflect the complicated physical situation in the near-surface layer of air. In what follows we address this issue by performing Monte-Carlo sensitivity analysis of SEBS to two RS inputs that in our view greatly influence the quality of LE_{sat} estimates: net radiation and surface temperature.

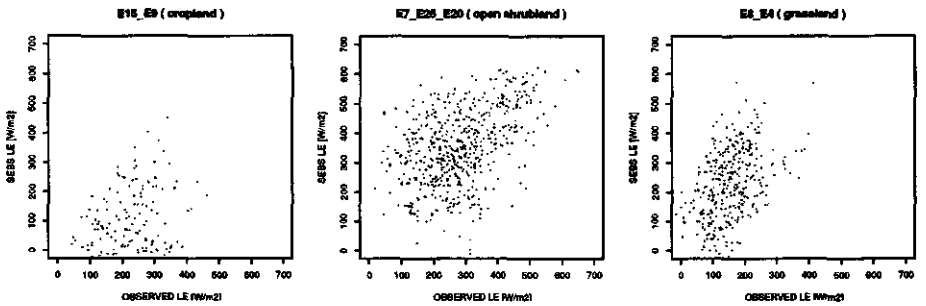

Figure 1.15: Bivariate 1-hourly *LE* data grouped according to landuse for the period 1 July 2001–30 September 2001. LE_{sat} estimates are derived from GOES products.

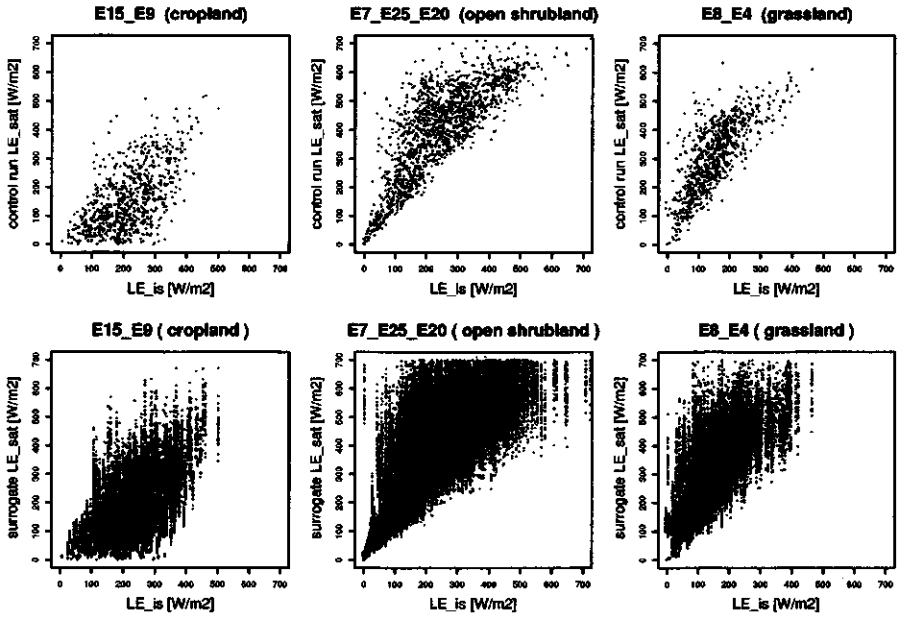

Figure 1.16: Bivariate 1-hourly *LE* data grouped according to landuse for the period 1 July 2001–30 September 2001. Upper panel: control run. Lower panel: surrogates.

Control run and surrogate RS data Accordingly, SEBS was forced with net radiation calculated from measured radiation components. Surface temperature was derived from outgoing long wave radiation. The rest of the inputs remained the same as mentioned in the previous section. In this way we obtained somewhat idealized LE_{sat} data (read: no RS error involved) which is reffered to as the control run (see upper panel of Figure 1.16). Note the transparent non-Gaussian dependency structure of bivariate *LE* data. Next, surrogate LE_{sat} data was created by perturbing the control run with percentual error in the net radiation (by comparing RS derived net radiation with measured net radiation we estimated this error as 15%). Technically, each net radiation measurement in the control run was treated as a mode of log-normal distribution and the 15% error as its coefficient of variation. From each distribution 30 points were drawn at random and propagated through SEBS to obtain LE_{sat} surrogates. Those are shown in lower panel of Figure 1.16.

Then, bivariate GMDM's were fitted to both control run and surrogate data from Figure 1.16 (for an example of fitted pdf's see upper panel of Figure 1.17). To determine to which extent the bivariate structure in control run was deteriorated due to sattelite error in net radiation we compared the fitted pdf's in terms of probabilistic similarity measure introduced by *Scott and Szewczyk* [2001]:

$$sim(f_1; f_2) = \frac{\int f_1(x) f_2(x) dx}{(\int f_1(x)^2 dx \int f_2(x)^2 dx)^{\frac{1}{2}}} \tag{1.5}$$

This measure is 0 if two pdf's show no similarity and 1 if two pdf's are just the same. For cropland, open shrubland and grassland $sim(f_1; f_2)$ was 0.96, 0.96 and 0.98 respectively. This implies that

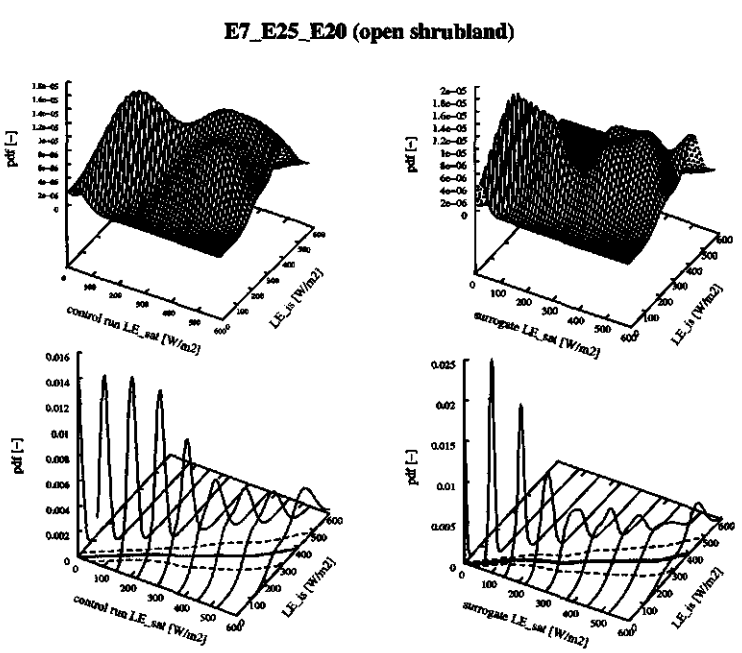

Figure 1.17: An example of MDGM's fitted to open shrubland LE data. Upper panel: joint pdf's $f(LE_{is}, LE_{sat})$ for control run and surrogates respectively (the similarity between the two pdf's is 0.96). Lower panel: conditional pdf's $f(LE_{is}|LE_{sat})$ for control run and surrogates. The solid line in X-Y plane represents conditional expectation and dashed lines represent standard deviation bands.

the error in net radiation has negligible effect on probability structure in control run data.

Continuation The same analysis will be performed for the surface temperature. The results will be shown during the poster session. In parallel we work on an uncertainty analysis of LE measurements from EBBR ARM/CART stations.

Evaluation of satellite soil moisture retrieval algorithms using AMSR-E data

Ruud Hurkmans[1], Bob Su[2], and Thomas J. Jackson[3]

[1]*Hydrology and Quantitative Water Management Group, Department of Environmental Sciences, Wageningen University and Research Center, Wageningen, the Netherlands*
[2]*Centre for Geo-Information, Alterra, Wageningen University and Research Center, Wageningen, the Netherlands*
[3]*Hydrology and Remote Sensing Laboratory, Agricultural Research Service, US Department of Agriculture, Beltsville, Maryland, USA*

Since soil moisture is a key variable in interactions between land surface and atmosphere it is important to create large-scale, long-term soil moisture datasets. Microwave remote sensing can be an important tool to do this. In this study, three soil moisture retrieval algorithms designed to retrieve soil moisture from AMSR-E are evaluated using two validation datasets. Two of these algorithms only use AMSR-E brightness temperature as input, the third one uses an additional vegetation dataset. The amount of parameters needed for validation differed strongly between the algorithms. Results indicated that all algorithms yielded reasonable results, but the use of extra vegetation data proved to be an essential advantage and significantly improved the overall estimations. However, additional datasets and validation parameters make it hard to apply an algorithm at large scales.

Introduction Soil moisture is a key variable in the interaction of land surface and atmosphere. Therefore, to monitor environmental changes like climate change, soil moisture needs to be monitored over extensive areas and periods of time. Spaceborne passive microwave remote sensing can be a powerful tool to achieve this and therefore various sensors of this type and algorithms to retrieve soil moisture from them have been proposed [*Njoku et al.*, 2003; *Koike et al.*, 2000]. In this work three retrieval algorithms using brightness temperature data of the Advanced Microwave Scanning Radiometer (AMSR) [*Kawanishi et al.*, 2003] are evaluated and tested on two different validation datasets.

Microwave remote sensing and soil moisture Microwave remote sensing is suitable for large-scale soil moisture remote sensing because it is independent of cloud cover and solar illumination. Due to the higher sensitivity to soil moisture and larger penetration depth, sensors operating at low frequencies are the most suitable for soil moisture remote sensing. Also, there is less influence of atmosphere and vegetation. Soil moisture retrieval is based on the Radiative Transfer Equation [*Jackson*, 1993]:

$$T_B = \Gamma \cdot e_r \cdot T_S + (1-\omega)T_C(1-\Gamma) + (1-e_r)(1-\omega)T_C(1-\Gamma)\Gamma \tag{1.6}$$

where T_B is the brightness temperature, T_S and T_C are temperatures of soil and canopy respectively (all in K), ω is the single scattering albedo [-], e_r is the surface emissivity [-] and Γ is the canopy transmissivity [-] that can be described by:

$$\Gamma = \exp\left(\frac{-\tau}{\cos(\theta)}\right) \tag{1.7}$$

where τ is the optical depth of the vegetation and θ is the viewing angle of the satellite. ω is very small at microwave wavelenghts and can be neglected. e_r depends on surface roughness and soil moisture content. The first is corrected for by means of the approach of [*Choudhurry et al.*, 1979] and soil moisture can be derived from the corrected emissivity by the Fresnel equation and a dielectric mixing model such as *Wang and Schmugge* [1980]. Three retrieval algorithms are evaluated in this work:

- the Jackson algorithm [*Jackson*, 1993] solves the inverted version of (1.6) and needs extra vegetation information (e.g. a vegetation index) to estimate τ. Temperatures of surface and canopy are assumed equal and derived empirically from a high frequency AMSR-E channel [*de Jeu*, 2003].
- the de Jeu algorithm [*de Jeu*, 2003] solves (1.6) iteratively using two T_B channels for vegetation optical depth and surface emissivity simultaneously. Temperatures are derived similar to the Jackson algorithm.
- the Wen algorithm [*Wen et al.*, 2003] also solves (1.6) iteratively, however the solved quantities in this case are surface temperature and surface emissivity.

Validation datasets The first validation dataset that was used was the Mongolia Match-up dataset [*Kaihatsu*, 2003]. The dataset covered an $2.5° \times 2.5°$ area in central Mongolia and ran from 1 July 2002 to 21 September 2002. Ground observations were available on a daily base at 12 locations at a depth of 3 cm and for the Jackson algorithm vegetation information was derived from MODIS EVI[1].

The second dataset, from SMEX02 [*HRSL*, 2002], took place in a study area around Ames, Iowa, USA between 25 June 2002 and 12 July 2002. In this case daily groundobservations at 47 locations for the upper 6 cm of the soil profile were available. For the Jackson algorithm observations of the Vegetation Water Content were used to derive the transmissivity. Since Iowa is relatively densely populated the C-band of AMSR-E interfered with radio traffic [*Li et al.*, 2004]. Therefore for this dataset the X-band channel of AMSR-E was used.

Results As far as the Mongolian dataset is concerned, from Table 1.4 it appears that observations were mostly overestimated. As can be seen in Figure 1.18, this was mainly due to peaks in the estimations that corresponded to rainfall events. The reaction to these events was different; the effects of rainfall were longer visible in the observations than in the estimations. A possible explanation for this is the fact that observations took place at a depth of 3 cm, while the observing depth at C-band is only in the order of ± 1 cm. The rainfall peaks also explain the low errors of the Wen algorithm: the values at the peaks were lower than for the other algorithms. To the end of the simulation the estimations of the de Jeu and Wen algorithms increased compared to the Jackson algorithm and the observations: this is due to a decrease in T_B values. However, also the vegetation density dropped steeply. This explains the lower values of the Jackson algorithm which reacted also to changes in vegetation, while the other algorithms merely responded to T_B input.

For the SMEX02 dataset, there was a large difference in performance between daytime and nighttime (Table 1.4). Especially the de Jeu and Wen algorithms performed better at night, which is surprising because observations took place at daytime. However, from Figure 1.19 it appears that most of the error in the daytime overpasses came from days at the end of the period. Again, this was due to the high vegetation density; the Jackson algorithm used vegetation information, therefore its bias and SEE were lower. The fact that the algorithms performed better at night can be

[1] `http://tbrs.arizona.edu/project/MODIS/evi.php`

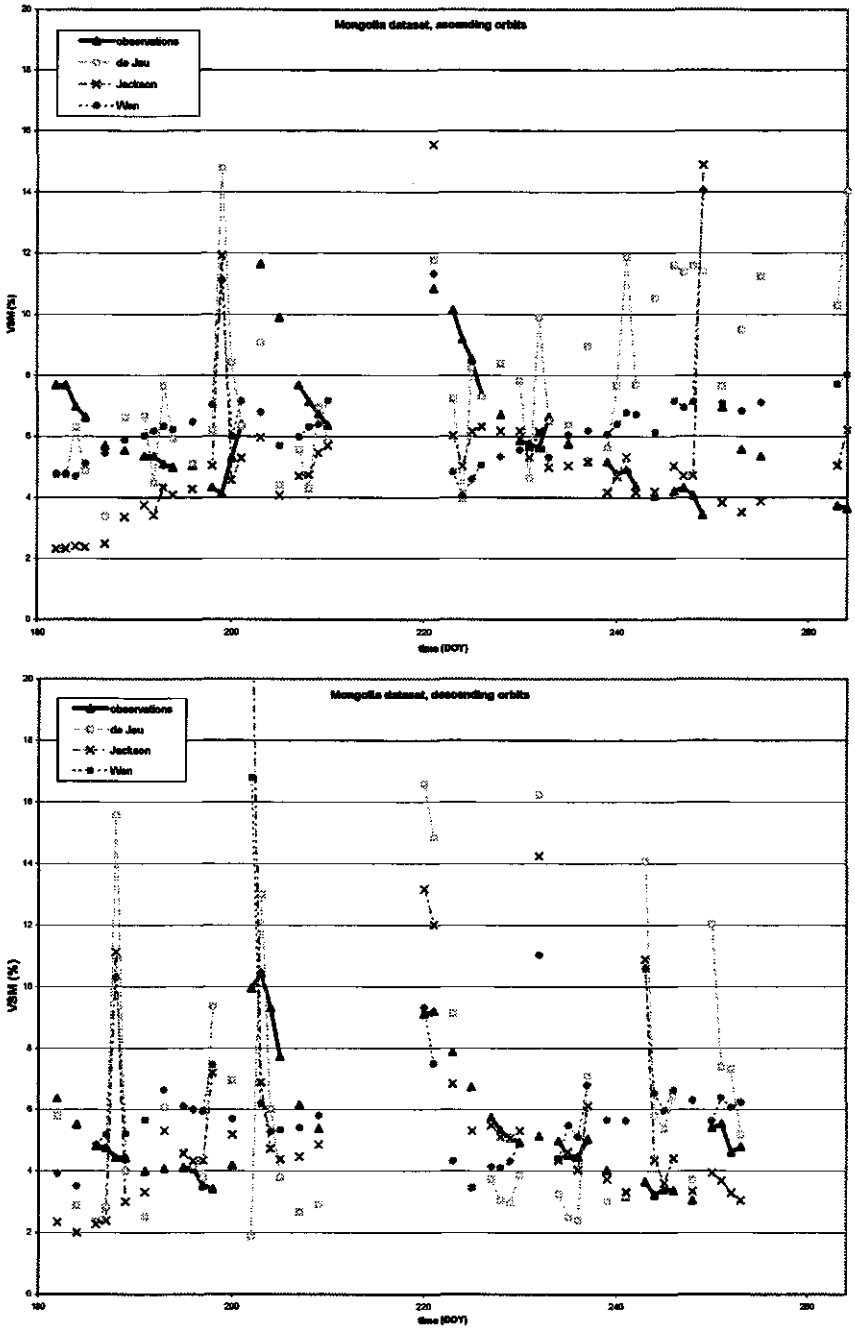

Figure 1.18: Observed and estimated soil moisture content for the Mongolian data. The upper plot shows daytime (ascending) overpasses, the lower plot nighttime (descending) overpasses.

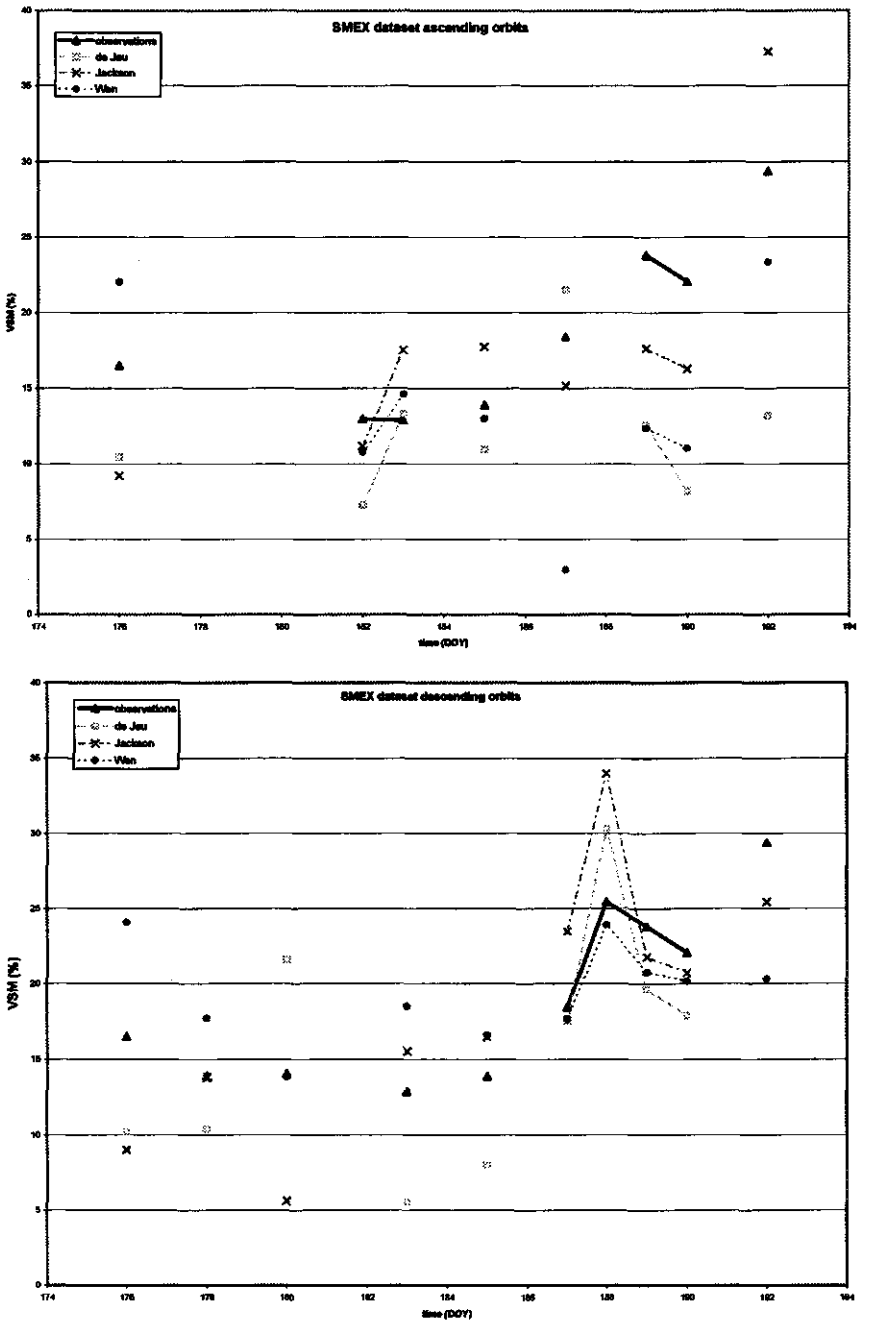

Figure 1.19: Observed and estimated soil moisture content for the SMEX02 data. The upper plot shows daytime (ascending) overpasses, the lower plot nighttime (descending) overpasses.

Table 1.4: Standard Error of Estimation (SEE) and Bias of estimated soil moisture content (estimation minus observation) for the three algorithms, for both daytime and nighttime observations and both datasets.

Mongolia	Daytime overpasses		Nighttime overpasses	
	Bias	SEE	Bias	SEE
Jackson	-0.9144	3.2350	0.3605	3.3799
de Jeu	1.6498	4.1958	0.8072	4.1643
Wen	0.3803	2.9482	0.8995	2.8369
SMEX02	Daytime overpasses		Nighttime overpasses	
	Bias	SEE	Bias	SEE
Jackson	-0.9989	5.4405	-0.4636	5.0948
de Jeu	-6.5661	9.1403	-2.2169	5.1203
Wen	-4.9727	8.4073	0.3156	4.5683

explained by the shallow viewing depth at the frequency used to determine the surface temperature (Ka-band): considering the dense vegetation the canopy temperature was measured rather than the surface temperature. In daytime the surface temperature was higher than the canopy temperature, at night the difference was smaller and the estimates were therefore more accurate.

Conclusions Overall it can be concluded that all algorithms gave reasonable results after validation to each dataset, but the additional vegetation infomation appeared to be an essential input to a retrieval algorithm. The Jackson algorithm yielded better overall results (considering both datasets at day- and nighttime) because of this advantage. The amount of validation to obtain good results differed strongly per algorithm, especially the Wen algorithm required many frequency and area specific parameters, while the de Jeu algorithm required hardly any validation at all. Also the Jackson algorithm made use of several parameters in addition to the vegetation data. This makes the de Jeu algorithm the most applicable for large-scale (global) applications. Finally, the datasets that were used were not ideal for soil moisture retrieval, but they were very different in terms of vegetation density which made them suitable testcases.

Detectability of changes in the global terrestrial water cycle

Justin Sheffield[1] **and Eric F. Wood**[1]

[1]*Dept. Civil and Environmental Engineering, Princeton University, Princeton, New Jersey, USA*

A potential consequence of climate change is the intensification of the global and continental scale water cycle. This intensification may manifest itself in the form of, for example, increased precipitation and faster evaporation, with consequences for human activities in terms of changes to the availability or absence of water, e.g. flooding or drought. Detection of change in the terrestrial water cycle requires monitoring for long periods of time so as to determine whether significant trends can be identified against the background of natural variability. Quantifying the uncertainty in detecting change in the terrestrial water cycle using current observational data and monitoring networks is central to our ability to detect change. By identifying the characteristics of the detection process that limit and constrain our ability to detect climate change, we can identify the best strategies for detection. In this study we estimate the time required to detect significant trends in the components of the terrestrial water cycle and use this as a base to explore the characteristics of detectability.

Using estimates of natural variability from land surface modeling and GCM predicted trends in water cycle components, statistical methods are applied to estimate the length of records required to detect significant trends. The results indicate that decades to centuries of monitoring are required, when given the ideal situation of error-free, long-term datasets of water cycle components over large scales. However, there is considerable uncertainty in the current level of variability of the water cycle at any spatial or temporal scale and the spread of future predictions of change by climate models is large and regionally dependent.

Detectability depends on a variety of factors that include the statistical methodology, the characteristics of the data sets (e.g. its variability, trend magnitude, correlation, etc.), confidence limits used in the statistical tests, and so forth. This study explores some of these issues as a step towards characterizing detectability and quantifying our ability to detect changes in the large scale terrestrial water cycle. We do this through assessments of sensitivity of detection to the above factors, as well as investigations of the most appropriate data attributes, such as temporal scale and measurement error, that result in rapid detection times.

Detection of hydrological effect on local gravity anomalies

Shaakeel Hasan[1], **P.A. Troch**[1], **J. Boll**[2], **and C. Kroner**[3]

[1]*Hydrology and Quantitative Water Management Group, Wageningen University, Wageningen, The Netherlands*
[2]*Department of Biological and Agricultural Engineering, University of Idaho, USA*
[3]*Institute of GeoSciences, Friedrich-Schiller-University, Jena, Germany*

Detecting change in water storage from related temporal variation in gravity has become an important issue for many studies and research related to the Earth and environmental science, oceanography and climatology, and in particular hydrology and geophysics. Finding the relation between water storage and gravity change is promising for hydrologists, in closing the water balance, as well as for geophysicists, in detecting the real long-term gravity change. The Global Geodynamics Project (GGP) began in 1997 with the purpose to record the Earth's gravity field with high accuracy at a number of worldwide stations using superconducting gravimeters (SG). The Gravity Recovery and Climate Experiment (GRACE), jointly implemented by NASA and DLR, is a dedicated twin satellite mission (launched in March 2002) whose objective is to map the Earth's gravity field to high accuracy at monthly intervals. Both GGP and GRACE recognise that tracking the movement of water on and beneath the earth surface is one of the main goals, and thus promise a significant development in hydrological studies. This paper examines the local hydrological effect on gravity at the Geodynamic Observatory Moxa, Germany, by means of time series analysis and distributed hydrological modeling.

Data The data used are from Moxa Geodynamic Observatory (Figure 1.20a). The hydro-meteorological data are collected in the vicinity of the observatory and include hourly precipitation, groundwater, air pressure, temperature, wind speed, humidity, and illuminance and daily surfacewater levels at a V-notch installed in the Silberleite, the small creek in which drainage area the observatory is located. The hourly gravity residuals, hereafter refered to as observed gravity residuals, are obtained after corrections for the Earth tides, polar motion, barometric pressure, and instrumental drift.

Time series analysis From visualization it is clear (Figure 1.20b) that precipitation has a direct and short term effect on gravity, while the effect of long term groundwater change is not always very clear. By means of time series analysis we construct transfer function models [*Box and Jenkins*, 1976] that allow to convert the precipitation and/or groundwater signal to gravity changes. For building the model, we considered two situations: short term response of gravity due to rainfall impulses and long term response of gravity due to slow groundwater changes. The first accounts for high-frequency components, while the latter accounts for low-frequency components in the dynamic behaviour of the total gravity signal.

Distributed hydrological model We used the Soil Moisture Routing (SMR) model to track temporal changes in water storage in the catchment around the gravimeter (Figure 1.20a). The SMR model, originally developed at Cornell University, USA, provides distributed prediction of surface runoff and soil moisture [*Brooks and Boll*, 2004]. The model tracks the flow in and out of grid cells using a basic mass balance:

$$D_i \frac{d\theta_i}{dt} = P - ET_i + \sum Q_{in,i} - \sum Q_{out,i} - L_i - R_i \tag{1.8}$$

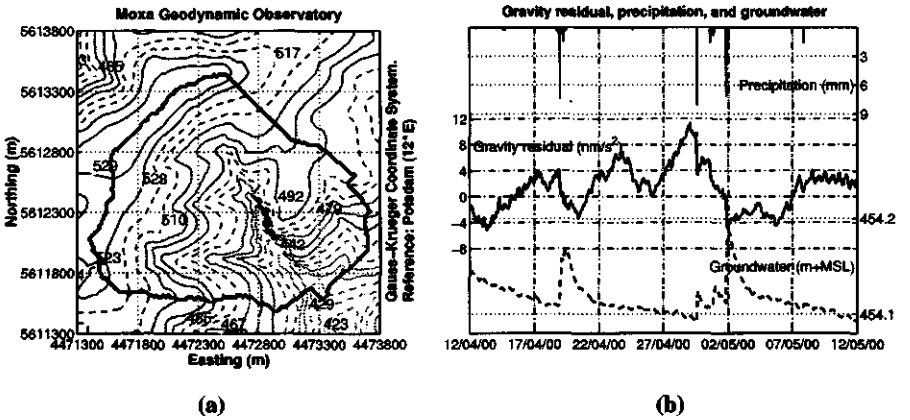

(a) (b)

Figure 1.20: (a) Surrounding topography of Moxa Geodynamic Observatory [lighter and broken lines are contour lines in m+MSL, thick line shows the catchment boundary, the dot indicates the gravimeter location]. (b) Exploring gravity residuals as function of precipitation and groundwater [thick line in the middle is for gravity residuals, lower line for groundwater and upper bars for precipitation].

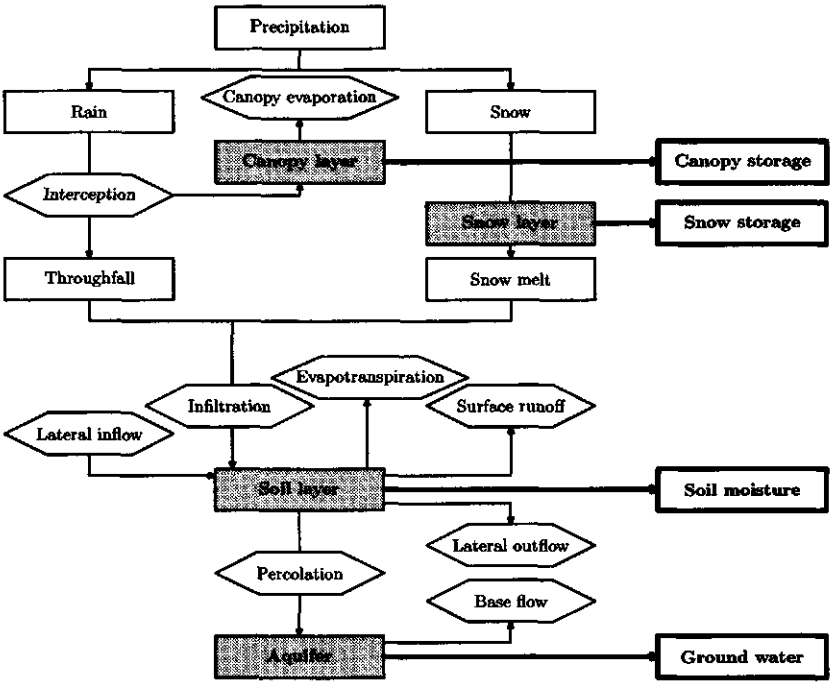

Figure 1.21: Schematic illustrating relevant hydrological processes in the Soil Moisture Routing (SMR) model.

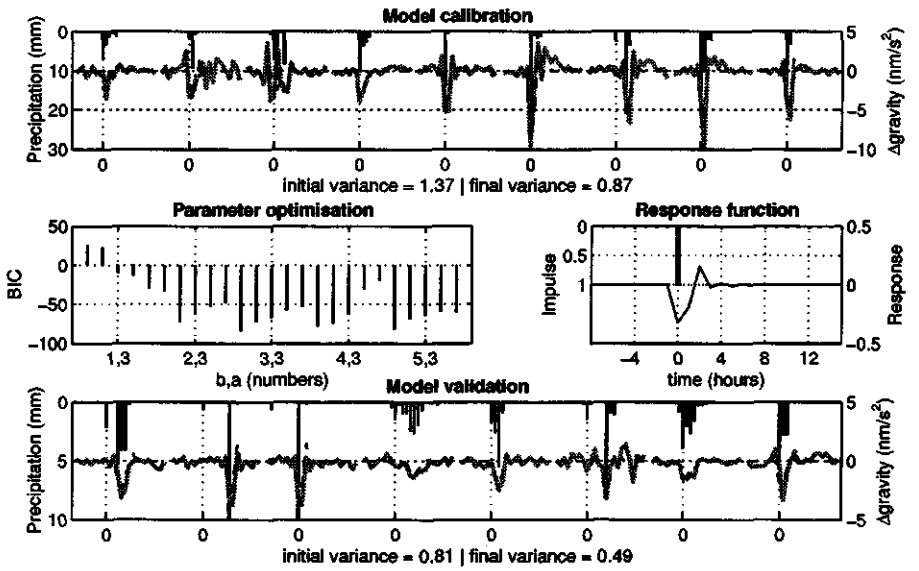

Figure 1.22: Short term gravity response to rainfall impulses [Model calibration showing selected precipitation events (vertical bars) along with observed (gray line) and modeled (dashed line) changes in gravity residuals (top), Model structure characterization (middle-left; a and b represent number of parameters in autoregressive and moving average polynomials of the transfer function (1.10)), Optimized unit impulse response function (middle-right), Model validation showing selected precipitation events (vertical bars) along with observed (gray line) and modeled (dashed line) changes in gravity residuals (bottom)]. Zeros in the calibration and validation plots indicate the starting of the events.

where, i is cell address, D_i is depth to restrictive layer of the cell (cm), θ_i is average moisture content of the cell ($m^3\ m^{-3}$), P is precipitation (rain and snow) (cm), ET_i is actual evapotranspiration (cm), $Q_{in,i}$ is lateral inflow from neighbouring upslope cells (cm), $Q_{out,i}$ is lateral outflow to neighbouring downslope cells (cm), L_i is downward leakage to bedrock (percolation) (cm), and R_i is surface runoff (cm). Note that all the volumetric quantities are presented per area of a grid cell.

Figure 1.21 illustrates the processes in SMR. Calculation of the water balance is facilitated by a GIS, which keeps track of catchment characteristics such as elevation, soil properties, slope, land use and flow direction as well as the moisture stored in each cell at each time step. In this study, the time step was one hour. A detailed description of the model is available in *Boll et al.* [1998] and *Frankenberger et al.* [1999]. Modifications to the SMR model include the addition of a canopy layer to simulate interception, and calculation of gravity residuals based on moisture storage in the canopy, snow and soil.

Based on Newton's law of gravitation in a local cartesian coordinate system, the vertical component of gravitation (gravity anomaly) is given by:

$$\Delta g(r) = G \iiint_{v} \frac{\Delta\rho(r')(z'-z)}{|r'-r|^3} dv \tag{1.9}$$

with the density difference $\Delta\rho$ of the disturbing mass relative to its surrounding, and the volume element $dv = dx'dy'dz'$ [*Torge*, 1989].

Closed-form solutions of (1.9) are available for a multitude of simple bodies with constant density [*Torge*, 1989]. We used rectangular prisms with horizontal limits defined by the pixel size in the DEM and vertical limits of soil depth for soil moisture, snow depth for the snow layer, and canopy interception storage depth for the canopy layer.

Results Considering precipitation events isolated by dry spells, impulse response functions were computed for both gravity and groundwater changes to precipitation. We used a Bayesian Information Criterion (BIC) [*Priestley*, 1981] to optimize the number of parameters in the response functions. We present here the results for gravity response to precipitation impulse (Figure 1.22). During calibration, our impulse response function explains 64% of the variation of the observed gravity change and during validation the explained variance is 61%. If $u_{(z)}$ and $y_{(z)}$ denote the input (precipitation in mm) and output (gravity changes in $\mathrm{nm\,s^{-2}}$), the transfer function in the z-transform domain can be represented as:

$$y_{(z)} = \frac{-0.32 - 0.40z^{-1} + 0.03z^{-2} + 0.08z^{-3}}{1.00 + 0.66z^{-1}} u_{(z)} \tag{1.10}$$

Unlike precipitation effect on gravity, effect of groundwater change is not that straightforward. Gravity, being an integrated signal, contains information related to all kinds of simultaneous mass (re-)distributions. In order to build a transfer function model for long term response of gravity due to slow groundwater changes, we looked at windowed cross correlation between groundwater and gravity for different windows of varying length of 1 day to 1 month at 0 to 5 hours lag. Looking at the histograms of cross correlation coefficient, we find both positive and negative high correlation, as well as no correlation (Figure 1.23). However, from 4 years of data, we find that in more than 50% cases there exists a high negative correlation, while for the rest there is either no correlation or no data or positive high correlation. More investigation is required before we build transfer function models.

The SMR model for the Silberleite catchment was setup using available data sets (DEM, land use, and soil depths). Proper model calibration was hampered because of lack of good quality runoff data. We checked the SMR model results for consistency in computed water balance components and estimated monthly runoff. In general, the model water balance (see Figure 1.24a) is in agreement, for example, with estimates of evaporation/precipitation ratio of $\sim 50\%$ [*Peixoto and Oort*, 1992]. Monthly runoff was estimated from available surface water level data and compared to modeled monthly runoff (see Figure 1.24b). While judging this verification, we have to keep in mind that no data were collected during high discharge and the fact that our model does not have a deep groundwater component, therefore, regional base flow contribution to total runoff at the weir is not simulated. However, the simulated runoff pattern is more or less in agreement with the observed flow pattern.

Figure 1.25-top compares the observed gravity residuals for a 4-year period (2000–2003) with the modeled gravity changes based on spatio-temporal simulations of the water balance components in the catchment and using (1.9). In general, we can reproduce the observed patterns quite well, although the dynamic range of modeled gravity is about 50% of observed gravity. At this moment, it is not clear what causes this. One possible reason could be that the modeled influence zone of mass distribution around the gravimeter underestimates the true influence zone, due to the fact that deep groundwater dynamics are poorly represented in the hydrological model. The effect of horizontal domain size around the gravimeter is shown in Figure 1.25-bottom to illustrate this point.

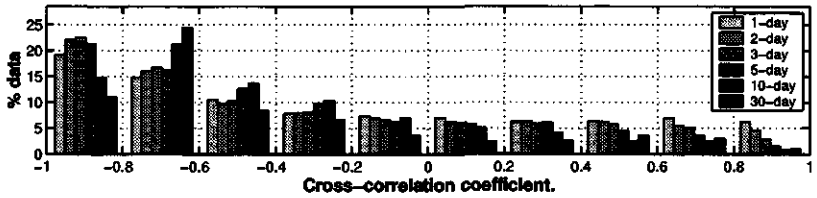

Figure 1.23: Windowed correlation between groundwater and gravity for windows of different time length at lag-0.

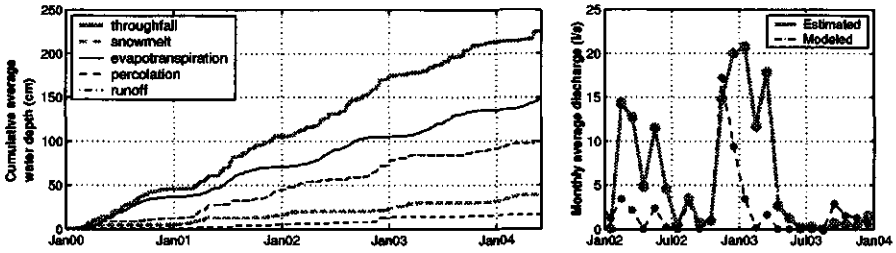

(a) (b)

Figure 1.24: (a) SMR model water balance [gray lines are for input (throughfall-solid and snowmelt-dashed) and black lines are for output (evapotranspiration-solid, percolation-dashed, and runoff-dotted)]. (b) Model verification: estimated and modeled discharge through V-Notch.

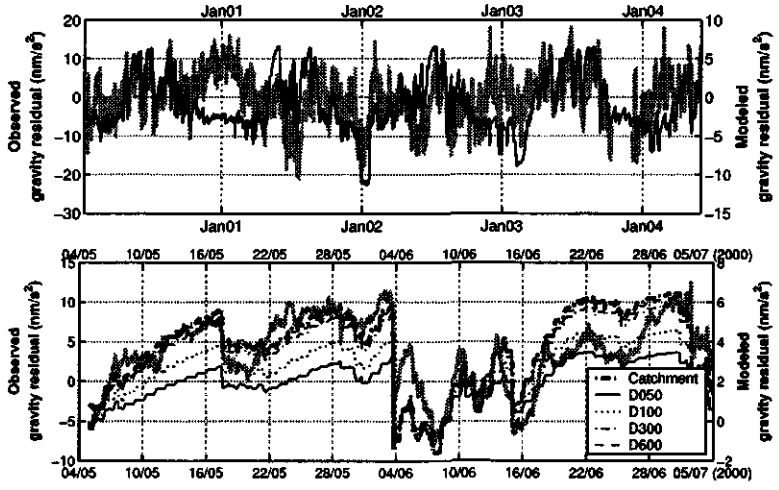

Figure 1.25: Gravity residual: observed (gray) and modeled (black). Modeled residuals containing all storage changes for the entire catchment (top). Effects of different domains in a small time window (bottom).

Conclusion In this paper, both time series analysis and distributed hydrological modeling techniques are explored to explain local gravity anomalies as observed by a superconducting gravimeter at Moxa Geodynamics Observatory, Germany. Both approaches yield encouraging results, and serve complementary objectives. Time series modeling provides us with a simple yet effective technique to correct for precipitation effects on short term gravity residuals. Distributed water balance modeling explains much of the long term behaviour of the gravity signal. From a hydrological persective, in-situ gravity measurements of the kind used in our study offer an intriguing new look at hydrological processes.

Estimation of path-averaged rainfall and evapotranspiration using a single instrument

H. Leijnse[1], **R. Uijlenhoet**[1], **and J.N.M. Stricker**[1]

[1]*Hydrology and Quantitative Water Management Group, Wageningen University, Wageningen, The Netherlands*

The water flux at the land-atmosphere interface is extremely important in both hydrology and meteorology, and many instruments have been developed to measure either precipitation or evapotranspiration at a point in space. It would be useful if a single instrument could be used to measure both fluxes in a path averaged fashion. A microwave link could potentially be used for this purpose.

A microwave link consists of a transmitter and a receiver, between which an electromagnetic wave ($\lambda \sim 1$ cm) propagates through the atmosphere. In the case of rainfall, this propagation is hampered by raindrops in the signal path. The attenuation of the microwave signal (dB km^{-1}) is nearly proportional to the rainfall intensity (mm h^{-1}). In the case of evapotranspiration the propagation is affected by turbulence in the atmospheric boundary layer, from which the evapotranspiration can be estimated.

A microwave link signal was analyzed for several rainfall events and dry periods, and compared to measurements made by other instruments. Several rain gauges were used to measure the rainfall, and the evapotranspiration was estimated using an energy balance method. The results are optimistic, but more research and testing is needed before the instrument can be used operationally to measure both components of the water flux.

2 Scaling in time and space: methodological approaches

Temporal dynamics of soil moisture variability: from theoretical basis to modeling implications

John D. Albertson[1]

[1]*Department of Civil and Environmental Engineering, Duke University, USA*

The combination of inadequately resolved soil moisture fields and nonlinear relationships between fluxes and soil moisture leads to errors in both diagnostic and predictive estimates of large scale mass and energy fluxes. Efforts to empirically define the dynamics of sub-grid spatial variance of soil moisture have led to contradictory results. Moreover, most reports of soil moisture variability range from qualitative to descriptively quantitative. In this paper we present a dynamic conservation equation for the spatial variance of sub-grid root-zone soil moisture, based on first principles of statistical fluid mechanics. We arrive at a variance budget in which explicit covariances between moisture fields and land surface flux fields act to produce or destroy sub-grid moisture variance through time (according to the sign of the correlation between the flux and state fields). A series of examples are reviewed to explore how simple forms of variability in soil, vegetation, precipitation, topography, and initial moisture content lead to evolving covariances between spatial fields of soil moisture and particular land surface fluxes, and how these covariances relate to the temporal trajectory of the spatial variance of soil moisture. We isolate one set of processes and conditions that demonstrates variance *production* through time and another set that demonstrates variance *destruction*. Of particular interest is the tendency for transpiration and infiltration-runoff processes to either produce or destroy variance, depending on the background wetness regime. Field data are also presented and shown to demonstrate a temporal behavior of the spatial variance that is predictable through the proposed approach. Finally, a closure model is presented for the variance budget and its use is shown to lead to improved land surface flux estimates over coarse grids.

Exploiting equilibrium tendencies of soil moisture dynamics for parameter estimation

Guido D. Salvucci[1] **and Marisa Gioiso**[1]

[1]*Boston University, USA*

Two aspects of soil moisture dynamics that can be exploited to parameterize the relation between hydrologic fluxes and soil moisture (s) at both the point-scale and large-scale are explored. They are: (1) the expectation of soil moisture change ($\frac{ds}{dt}$) conditioned on moisture level is equal to zero. Applying this principle to the water balance equations allows direct, empirical estimation of the relation between soil moisture and total water loss (the sum of drainage d, evapotranspiration et, and runoff ro) from precipitation measurements conditionally averaged according to soil moisture level; and (2) the variance of the sum of model-estimated soil moisture changes (i.e., var $\sum(p - et(s) - d(s) - ro(s))$) will contain a term that saturates to the actual soil moisture variance and a term that grows with time. The first term saturates because of the strong negative correlation between increments: i.e., days with positive perturbations in accumulation physically cause days with negative perturbations to occur in the future. The second term grows as a consequence of summing errors due (in part) to poor parameter specification. Thus by minimizing the total variance, we can estimate model parameters, and thereby partition the total water loss term estimated from principle (1) into the evapotranspiration and drainage/runoff components. Most critically, this methodology requires only intermittently sampled forcing data (e.g., p and s), no calibration data (e.g., continuous measurements et, d, or $\frac{ds}{dt}$), and no computationally expensive simulations. The requirements are more parsimonious than alternative methods because the objective function that we minimize is not a measure of actual prediction error, but rather a measure of how nonstationary (and thus error prone) the associated modeled soil moisture process would be for a given set of parameters and forcings. Furthermore, the dependence of the fluxes on soil moisture are expressed using piece-wise continuous polynomials in such a way that the minimization of the objective function can be done with quadratic programming techniques (i.e., the parameters of the model appear in the objective function as quadratic terms). Tests of the method using benchmark numerical simulations, Ameriflux data sets, and remote sensing estimates of soil moisture will be discussed.

Quantitative measures for the local similarity of hydrological spatial patterns

Stephen R. Wealands[1,2], Rodger B. Grayson[2], Jeffrey P. Walker[1], and Günter Blöschl[3]

[1]*Department of Civil and Environmental Engineering, The University of Melbourne, Victoria, Australia*
[2]*Cooperative Research Centre for Catchment Hydrology, Australia*
[3]*Institute of Hydraulics, Hydrology and Water Resources Management, Vienna University of Technology, Vienna, Austria*

The task of assessing similarity between data sets is common in hydrological modelling. While this has been widely researched for temporal data sets, the similarity between spatial patterns has been largely ignored. This has been due to a lack of spatial pattern data. Today there is widespread use of distributed hydrological models and increasing availability of observed spatial patterns. These observed spatial patterns are useful for model calibration and optimisation, though at present there is limited use of the spatial information contained in them. This is mostly due to a lack of understanding in how to make optimal use of this information rich data. The work in this paper investigates some quantitative measures for judging the similarity between observed and simulated spatial patterns, with a particular emphasis on local similarity techniques. The different measures allow the user to assess different aspects of similarity, which can then be used together for automated model calibration and/or evaluation.

Introduction In hydrological modelling, assessing the similarity between data sets is an everyday task, regardless of whether the data is temporal or spatial. Many methods exist for doing this, but most were not developed specifically for hydrological data sets. As such, it is necessary to understand the methods and what their resulting measures actually represent. *Legates and McCabe* [1999] evaluate many methods used for assessing similarity between temporal data sets. Some methods are sensitive to matching extreme values, while others provide a test of fit but ignore absolute differences. It is concluded that relative, absolute, local and global measures should all be stated when assessing the similarity between data sets. Additionally, the use of specialised methods for particular types of hydrological data can provide more informative similarity measures. *Boyle et al.* [2000] present a method in which the hydrograph is divided into "process-related" components. Each component is then compared, providing a measure of similarity that can be directly related to the process. This requires prior knowledge about the phenomenon being compared and is more difficult for spatial data sets (herein referred to as spatial patterns).

There are many methods available for assessing similarity between spatial patterns. Together, these global and local methods can describe the similarity between the values in the spatial patterns. But as with most temporal measures, they mostly ignore the specific arrangement of the values (especially the global methods). As a result of this, most hydrologists rely on visual comparison for assessing similarity [*Grayson et al.*, 2002]. Visual comparison can be thought of as a specialised method, as it incorporates knowledge about the hydrological phenomenon and other ancillary information. However, its weaknesses are that it is neither automated, objective, repeatable nor quantitative - all things that are important when assessing similarity between many data sets. This research aims to address some of these weaknesses by emulating parts of the visual com-

parison process computationally. There is no expectation that a computer algorithm will be able to emulate what the human brain does. However, the steps undertaken during visual comparison suggest many new avenues to pursue for developing specialised methods for assessing similarity. This paper discusses the background to similarity assessment and describes three different methods for assessing local similarity, including an example of their use.

Background A review of the literature on computer vision, image processing and pattern recognition has identified the major processes undertaken during visual comparison and methods that try to emulate them [*Wealands et al.*, 2004]. A visual comparison involves both global and local similarity assessment [*Hagen*, 2003; *Hay et al.*, 2003]. During local comparison, the image is viewed as a set of homogeneous regions, rather than individual pixels [*Hay et al.*, 2003]. The visual comparison also focuses on particular features or parts of the spatial pattern, rather than treating every location equally [*Tompa et al.*, 2000]. During this process, observations such as the similarity of shape, location and intensity are noted. Finally, the observed similarities and differences observed are explained and/or interpreted using extensive background knowledge [*Grayson et al.*, 2002]. Thus, the procedure used during visual comparison can be described as "global similarity assessment, followed by local similarity assessment of regions in the spatial pattern using various measures, with a tolerance for minor differences and additional focus on more important parts of the spatial pattern".

Global methods for assessing similarity of spatial patterns are plentiful [see *Scheibe*, 1993]. Basic statistics, geostatistics and landscape indices can all characterise certain features of the spatial pattern. These numerical summaries can then be compared to measure the similarity between spatial patterns. For local similarity, the most common method used is root mean squared error (RMSE), which provides a summary of the squared residuals. Local similarity methods are far more sensitive to differences between the spatial patterns than global methods, as they evaluate every location and use the spatial data in its complete form. At each location, a measure is calculated (e.g., the squared residual) to represent the similarity and this is stored in an intermediate spatial pattern. The intermediate spatial pattern is useful for closer inspection of the differences and is summarised to produce the resultant local similarity measure.

More specialized methods involve additional processing both before and during the calculation of similarity measures. For example, preprocessing can involve smoothing or aggregation to change the scale of the spatial patterns. These adjusted spatial patterns are then used for computing the similarity measure. Alternatively, each location can be compared against neighbouring locations in the other spatial pattern, with the most similar measure from the whole neighbourhood used to represent the similarity for that location. Both these examples illustrate how a minor modification can alter a standard method, thus making it more specialised.

Local comparison methods The aim of local comparison methods is to emulate the major features of detailed visual comparison, so that these can be quantified and automated. Three methods used to produce local similarity measures are (1) fuzzy comparison, (2) importance maps and (3) image segmentation.

Fuzzy comparison is a method used for tolerating shifts and differences during the calculation of the similarity measure. This allows the user to specify weights for locational matching (i.e., what amount of displacement is acceptable) and value matching (i.e., what amount of error is considered acceptable). The method processes each location in the spatial pattern, computing a similarity value between the respective location and its neighbouring locations in the second spatial pattern [more details in *Hagen*, 2003; *Wealands et al.*, 2004]. From the nine similarity values (range of 0 to 1) computed, the highest level of similarity is retained. Figure 2.1i) shows two different sets of residual and location weights that have been used to calculate the fuzzy similarity between observed and simulated soil moisture data. The more tolerant residual weights

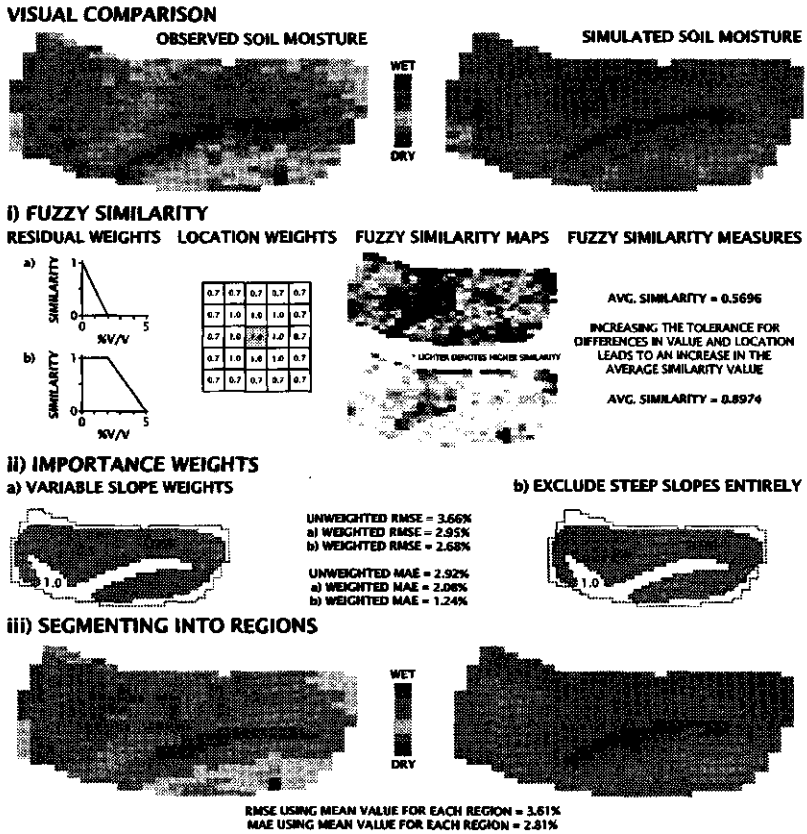

Figure 2.1: Example illustrating three specialized methods for assessing local similarity. The methods aim to emulate some aspects of visual comparison, including i) tolerance for differences in values and locations; ii) focus on certain parts of the spatial pattern more than others; and iii) comparison of regions rather than pixels.

(b) produce a higher overall similarity value than the more limiting weights (a). When multiple sets of observed and simulated spatial patterns are compared, this method can help reveal similar spatial patterns that are not detected by standard local similarity methods due to shifts or minor differences.

Weighting spatial patterns before computing similarity measures is a way of focusing on the "important areas". Visual comparison does this automatically as a result of both visual cues (e.g., bright spots) and background knowledge (e.g., focusing only on areas the user knows are gullies). While there is literature on what draws visual attention in an image, these findings are often related to the type of image. However, it has been recognised that features occurring infrequently in images (e.g., extreme values) are of high perceptual importance [*Tompa et al.*, 2000]. This can be used to produce perceptually weighted spatial patterns, in which the infrequent values are given higher weights than those that are common. Due to the weightings, calculation of the standard RMSE measure will lead to a larger residual where the infrequent values do not match [see

Wealands et al., 2004, for examples]. Weighting can also be applied to limit the areas in which the similarity measure is computed. If the user is only interested in the similarity of certain areas (e.g., north facing slopes), then a weighting that either enhances or separates these areas will focus the meaning of the similarity measure accordingly. Figure 2.1ii) shows the differences between standard RMSE calculations when using different slope weights to focus the comparison. By using the weights to limit the influence of slopes greater than 10 degrees (a), the similarity measure is focused more on similarity in flatter areas. If the weights exclude the steeper areas entirely (b), then a measure that is only related to flat areas is produced.

Segmentation is the process of breaking up an image into regions using a set of rules. The simplest approach to segmentation is thresholding, where a value is chosen to separate an image into two regions. During visual comparison, spatial patterns are viewed as regions rather than pixels [*Hay et al.*, 2003], with the regions detected at varying scales. Emulating this computationally is a difficult task. Using a multiresolution segmentation technique from image processing [*Baatz and Schäpe*, 2000], the spatial patterns of soil moisture have been segmented into homogeneous regions in Figure 2.1iii). Using the mean values for each region, an RMSE measure has been calculated between the segmented spatial patterns. This value is less than the RMSE calculated between the original spatial patterns due to the removal of "noise" via averaging within regions. This method seeks to emulate the region detection process that is done visually, by simplifying the spatial pattern prior to comparison. It may be particularly useful for detecting similarity between noisy data sets, in which the noise precludes the use of standard methods like RMSE.

Discussion This research has investigated multiple methods for assessing different aspects of local similarity between spatial patterns. Methods have been sourced from other disciplines and adapted to work with spatial patterns common in hydrology. These methods focus on emulating aspects of visual comparison. It is widely recognised that no single method for assessing similarity can capture everything, but by using multiple methods together a strong test of spatial pattern similarity can be made. Further work with the methods described above will identify their particular benefit for assessing similarity in different contexts.

Acknowledgments We would like to acknowledge the provision of data by Andrew Western and financial support from the Cooperative Research Centre for Catchment Hydrology, an Australian Postgraduate Award (APA) scholarship, and a Postgraduate Overseas Research Experience Scholarship (PORES) from The University of Melbourne.

Geostatistical aspects of scaling behavior observed in regional scale surface soil moisture fields

Dongryeol Ryu[1] **and James S. Famiglietti**[1]

[1]*Department of Earth System Science, University of California, Irvine, California, USA*

Spatial correlation patterns of surface soil moisture contents in regional scale fields are influenced by the combined effects of atmospheric forcing and land surface features. While small scale spatial variations of land surface features dominate soil moisture fields during dry periods, large scale variations from the atmospheric forcing become more significant during wet period, which has been shown using 2D spectra or semivariograms. Here, the effects of the changes in the spatial correlation on the scaling behavior of surface soil moisture are studied using Monte Carlo simulations. Spatial statistics from recent soil moisture experiments were used to reproduce scaling in the second order statistical moments of soil moisture observed in the SGP97 and SGP99 data. The effects of various semivariogram models, nugget, scale, and relative dominance of small or large scale spatial patterns were assessed through the simulations. Our results imply that, under specific conditions, e.g., in very dry soil moisture fields, using a power-law decay of statistical moments with respect to spatial scale for the statistical downscaling of soil moisture can result in erroneous downscaled prediction of surface energy and water fluxes.

Downscaling of low resolution passive microwave soil moisture observations

Manju Hemakumara[1], Jetse Kalma[1], Jeffrey Walker[2], and Garry Willgoose[3]

[1]*School of Engineering, University of Newcastle, Australia*
[2]*Department of Civil and Environmental Engineering, University of Melbourne, Australia*
[3]*School of Geography, University of Leeds, Leeds UK*

This paper addresses the validation and subsequent downscaling of low resolution (25 km × 25 km) passive microwave near-surface soil moisture data from the Advanced Microwave Scanning Radiometer for the Earth observing system (AMSR-E) on board the Aqua satellite. The paper first reports on large-scale validation experiments which have been undertaken in south eastern Australia, under a range of soil moisture conditions and in different seasons. On each occasion approximately 220 sites were monitored for soil and vegetation properties and soil moisture across a 40 km × 50 km area, with a range of vegetation, soil and topographic attributes. Second, the paper reports on downscaling of the low resolution AMSR-E near-surface soil moisture product to 1 km using two recent surface wetness index approaches which employ thermal and visible AVHRR and MODIS imagery.

Introduction Knowledge of spatial and temporal distribution of soil moisture is required for a variety of environmental studies. The Scaling and Assimilation of Soil Moisture And Streamflow (SASMAS) project aims to develop new methodologies for meaningful estimation of spatial distribution and temporal variations of soil moisture content through a combination of modeling, observations and data assimilation [see *Rüdiger et al.*, 2003]. The recent development in microwave remote sensing techniques for near surface soil moisture monitoring [e.g., *Schmugge*, 1998; *Western et al.*, 2002] has been one of the triggers for the formation of the SASMAS project.

This paper addresses two SASMAS research objectives: (1) field validation of the Advanced Microwave Scanning Radiometer for the Earth observing systems (AMSR-E) soil moisture product; and (2) development of new methods for disaggregation of large area soil moisture estimates. Its broad aim is to assist in assessing the calibration reliability of AMSR-E and to increase its hydrological applicability by disaggregating the low resolution (25 km × 25 km) AMSR-E soil moisture data into moderate resolution (1 km × 1 km) soil moisture values. The paper describes preliminary results from recent intensive field validation campaigns and presents a soil moisture disaggregation methodology for AMSR-E footprints based on AVHRR and MODIS satellite data.

Theory Measurements in the microwave region of the electromagnetic spectrum can provide all-weather quantitative estimates of near-surface soil moisture under low-to-moderate vegetation cover. AMSR-E is a passive microwave sensor with a 6.9 GHz (C band) channel and footprint size of more than 25 km. Based on published results and supporting theory, AMSR-E holds great promise for estimating soil water content in the top 1 cm layer of soil for relatively low vegetation cover [*Choudhury and Golus*, 1988; *Ahmed*, 1995; *Njoku and Li*, 1999; *Schmugge et al.*, 2002].

Over the last two decades, substantial research has been dedicated to the development of new methods of using visible and thermal infrared observations for evaluating land surface wetness conditions [*Carlson et al.*, 1994; *Gillies et al.*, 1997; *Czajkowski et al.*, 2002; *Goward et al.*, 2002; *Weidong et al.*, 2002]. These studies have shown that surface temperature and the Normalised Difference Vegetation Index (NDVI) can together provide information on vegetation and surface

moisture conditions. Furthermore, these studies have introduced a range of moisture indices to better understand the regional distribution of soil moisture [e.g., *Moran et al.*, 1994; *Sandholt et al.*, 2002; *Wan et al.*, 2004].

Soil moisture (or wetness) index methods generally provide only a poor indication of *absolute* soil moisture content because they are based on measurements of the reflected shortwave and emitted thermal radiation, which are influenced by a wide range of other factors including organic matter, soil texture, surface roughness, angle of incidence, plant cover and colour. However, despite these limitations, such methods are potentially capable of providing an indication of *relative* variations of land surface wetness conditions. They can therefore provide a methodology to downscale 25 km × 25 km scale near surface soil moisture measurements based on the relative variations within the larger AMSR-E footprint. In this study such downscaling approaches are evaluated with ground based soil moisture measurements obtained during intensive AMSR-E validation campaigns.

The first disaggregation method used here employs the Water Deficit Index (WDI) proposed by *Moran et al.* [1996] with AVHRR and MODIS data. This index is based on the relationship between land surface-air temperature difference ($T_s - T_a$) and the soil adjusted vegetation index (SAVI). The hypothetical trapezoidal shape that results from plotting these data allows the wet and dry edges for each biome class to be defined. Once the boundary values are known, WDI may be computed as the ratio between difference of maximum and observed temperatures and the range of temperature for the particular SAVI class. Theoretically, this temperature ratio is equal to the ratio of actual to potential evapotranspiration and should be valid for partially-vegetated surfaces. The computed WDI values are then used as weighing factors to downscale the AMSR-E pixel value to 1 km resolution.

The second downscaling method used is based on the Vegetation Temperature Condition Index (VTCI) proposed by *Wan et al.* [2004]. The VTCI uses a relationship between land surface temperature (LST) and NDVI. The scatter plot shape between these data is normally triangular at a regional scale if the study area is large enough to provide a wide range of NDVI and surface moisture conditions. The VTCI gives an indication of LST changes of pixels with specific NDVI values and it can be physically explained as the ratio of temperature differences among pixels. The higher values of VTCI are associated with wetter areas and lower values are associated with dryer areas, thus giving weighing parameters for downscaling of large area near surface moisture measurements.

Data The SASMAS project area is located in the 7000 km^2 Goulburn River catchment in SE Australia. The northern part of the catchment is dominated by an undulating landscape with average elevation of approximately 400 m, and is mainly cleared for cropping and grazing purposes, making it an appropriate region for remote sensing studies. For the field validation of an AMSR-E footprint, a sampling area of 40 km × 50 km was selected to ensure that a full 25 km × 25 km satellite footprint lay within the sampling area. Due to the large footprint size, available resources, travel times and access issues, complete coverage was not possible within a single day. Therefore, the validation area was divided into four quarters and one quarter assigned to each of four groups. Each quarter was further subdivided into nine cells, three of which were sampled per day over the three-day campaign period. A three-day field campaign was justified on the basis that soil moisture content would not vary greatly during the course of a few days under typical drying conditions. This was confirmed by the actual field data. The campaigns were undertaken on 7–9 November 2003, 1–3 May 2004 and 7–9 July 2004. These capture seasonal variations in soil moisture and vegetation conditions, and were scheduled to coincide with AMSR-E overpasses so that there was at least 1 overpass each day with 2 overpasses (am and pm) on the central day.

Each campaign was aimed at collecting soil moisture measurements at approximately 220 GPS

Table 2.1: Comparison of AMSR-E near surface soil water content and field measurements.

Campaign		Surface soil water content ($cm^3\ cm^{-3}$)		
Number (dates)	Sample size	AMSR-E	0–6 cm	0–1 cm
1 (7–9 Nov, 2003)	230	15.0	14.1	10.9
2 (1–3 May, 2004)	216	17.0	16.6	18.9

located sites spread across the validation area. It was expected that this number of point measurements and their coverage should provide a sufficient basis for the validation of the satellite soil moisture product and for the development of a procedure for downscaling large area-average moisture measurements. Five 0–1 cm soil moisture samples were obtained at each site with a steel sampling ring of 82 mm diameter and 10 mm thickness. The five samples were combined and used to obtain volumetric soil moisture contents. In addition, five observations were made at each site with a Theta® probe which yielded volumetric soil moisture content values integrated over a 0–6 cm layer. Apart from soil moisture, soil and air temperatures, soil type, and surface conditions were also recorded, and vegetation samples collected for determining vegetation water content and dry biomass.

In addition to AMSR-E data, NOAA and MODIS satellite images were also obtained. In order to use the best images for analysis, all available day and night images from NOAA 15, 16 and 17 were obtained and after careful consideration final images selected for the derivation of moisture index values.

Results Results from the first two validation campaigns are shown in Table 2.1 where AMSR-E near surface soil moisture values are compared with footprint averages of the volumetric soil moisture content in the top 1 cm and top 6 cm. The table indicates that AMSR-E is capable of providing reasonable estimates of near soil moisture content when compared with point observation averages. It should be noted that on theoretical grounds the 6.9 Hz channel of AMSR-E is expected to yield integrated soil moisture values for the top 1 cm. The AMSR-E values have been obtained with the old algorithm and will be modified once the new algorithm is implemented by the NASA DAAC.

An important task in the validation was to determine the minimum number of sampling sites reasonably required to obtain a representative areal average for the 25 km × 25 km AMSR-E footprint area. Figure 2.2 shows the effect of the number of sampling sites on the computed area average soil moisture content for 0–1 and 0–6 cm as compared with the averages based on all available sites (i.e., 230 sites during campaign 1 and 216 sites during campaign 2). It is shown that for the 0–1 cm observations the regional average stabilizes at about 100 sites, whilst for the 0–6 cm observations at least 150 sites are required.

Figure 2.3a shows a map of volumetric soil moisture content for the top 6 cm layer for the second campaign. The grid cells in this map is 1.21 km^2 in area and has been chosen to enable comparisons with wetness index distribution patterns obtained from AVHRR data as discussed below. Reasonably coherent patterns emerge, with strong similarities between the maps particularly for the 6 cm observation depth. It is also noticeable that the southern half of the study area appears to be drier than the northern half. This is partly due to differences between the clayey soils in the north and the sandy soils in the south.

The WDI and VTCI methods have been used with AVHRR and MODIS data for the first two campaigns. In order to ensure that a significant range of vegetation and surface soil moisture

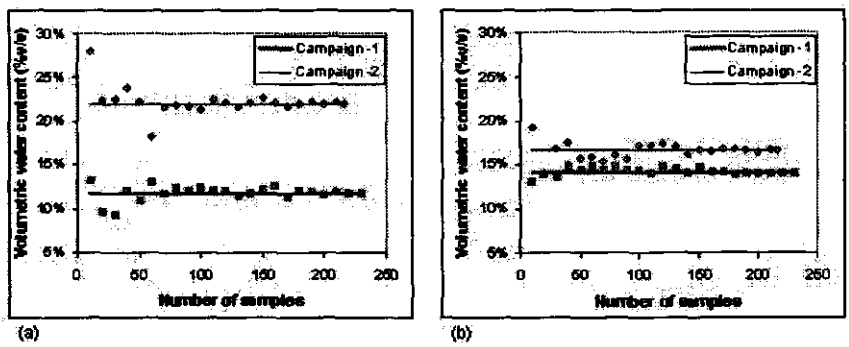

Figure 2.2: Spatial variation in field measured soil moisture for a) top 1 cm and b) top 6 cm soil layer in the first two intensive field campaigns (%).

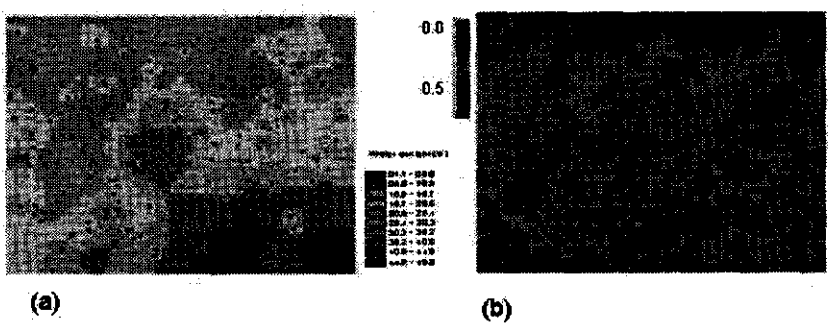

Figure 2.3: (a) Top 6 cm volumetric soil water content ($cm^3\ cm^{-3}$) distribution within the validation area for Campaign-2 (b) Disaggregated near surface water content ($cm^{-3}\ cm^{-3}$) for the validation area on 2 May 2004.

conditions were included in the computations, the entire Goulburn catchment (104 km × 124 km) was used in both methods.

A range of algorithms has been explored for using the index data in downscaling the AMSR-E near-surface soil moisture product and further work is continuing in this area. Preliminary results of one such downscaling approach using the WDI method with AVHRR data are shown for the 2 May 2004 campaign in Figure 2.3b. This downscaling approach involved calculating a weighting factor for each grid cell as the ratio between the index value for that cell and the sum of all index values across the AMSR-E footprint. Multiplying the AMSR-E value with this weighting factor yielded soil moisture content values across the study region. Reasonable agreement may be observed between the computed and observed near-surface soil moisture values. Particularly good agreement was found for areas with low to moderate vegetation.

Conclusions This paper has presented encouraging preliminary results for the validation and subsequent downscaling of low resolution AMSR-E passive microwave near-surface soil moisture data using soil moisture observations obtained in several large-scale field campaigns in south eastern Australia, and thermal and visible remote sensing imagery obtained with NOAA-AVHRR and

MODIS. The approach described here is part of an ongoing research project, which addresses various practical issues associated with the use of remote sensing for operational measurement of soil moisture. These include the role of vegetation and the relationship between near-surface soil moisture and total profile soil moisture. The soil moisture observations obtained in the field campaigns described here, as well as soil moisture data obtained at 26 monitoring sites with continuous soil moisture profile measurements, will also be analysed in greater detail to identify relationships with topography, soil properties and vegetation [e.g., *Western et al.*, 2002]. This involves the use of regionalisation techniques such as those outlined by *Sulebak et al.* [2000].

Acknowledgements This project is funded by Australian Research Council Discovery Project Grant DP0209724. MH is supported by a University of Newcastle Research Scholarship. The authors acknowledge the assistance of Barry Jacobs, Greg Hancock, Patricia Saco, Christina Martinez, Emily Barbour, Christoph Rüdiger, Ian Jeans and Makeena Kiugu for their assistance during the three field campaigns.

Inferring spatiotemporal soil moisture anisotropy at the catchment scale

T. Thierfelder[1], A. Western[2], R. Grayson[2], and G. Blöschl[3]

[1]*Department of Biometry & Engineering, Swedish University of Agricultural Sciences, Sweden*
[2]*Centre for Environmental Applied Hydrology, The University of Melbourne, Australia*
[3]*Department of Hydraulics, Hydrology and Water Resources Management, Vienna University of Technology, Austria*

The Tarrawarra (southeast Australia) dataset contains twenty time series of soil moisture data observed at spatially distributed locations within a 10 ha catchment. With every series containing fifty-three temporally distributed neutron moisture meter (NMM) measurements, the NMM data may be visualised as a set of spatially distributed series that progress simultaneously in time. The NMM data are complemented with thirteen spatially high-resolved time domain reflectory (TDR) surfaces distributed along the time-axis. Since these surfaces cover the complete catchment, they include the NMM sites and may be regarded as complete spatial realisations of the scenarios repeatedly sampled with NMM technique. In order to infer complete soil moisture surfaces at every NMM occasion, and to utilise the combined NMM/TDR dataset in such an inference, Kriging with external drift is methodologically suggested. This method offers quite robust estimates of the error associated with soil moisture inference at the Tarrawarra catchment, but requires a covariate that continuously compensates for spatiotemporally varying soil moisture anisotropy.

The resulting time series of Kriged (pixel-wise) soil moisture surfaces may again be considered as simultaneously progressing, spatially distributed (pixel-wise) time series. These series are analysed with ARMAX technique in order to identify the auto- and cross-covariance structures that define spatiotemporal soil moisture anisotropy at the catchment scale. Since the anisotropy information is required when Kriging parameters are estimated, ARMAX-conditioned Kriging is methodologically implied. The resulting inferential loop is implemented via the Kriging-ARMAX analogy, where respective residual statistics are compatible and, in fact, analogous.

As a result of the analysis performed, typically topography-dependent anisotropy structures are assessed at the landscape scale, together with auto- and cross-correlative characteristics of generic soil moisture. Based on this information, a distinction can be made between physically introduced observational effects and effects introduced by random processes. Such distinction is a necessary prerequisite for determining the location of Catchment Characteristic Soil Moisture Monitoring (CASMM) sites, i.e., non-redundant monitoring sites that together capture the characteristics of generic soil moisture variation at the catchment scale.

Scale dependent SVAT-model development towards assimilation of remotely sensed information using data-based methods

K. Schulz[1], I. Andrä[1], V. Stauch[2], and A.J. Jarvis[2]

[1]*Institute of Geoecology, TU Braunschweig, Braunschweig, Germany*
[2]*Environmental Science Department, Lancaster University, Lancaster, UK*

Recent studies have clearly demonstrated a miss-match can arise between the information content of SVAT calibration data and the information requirements of many components of current generation SVAT descriptions [*Franks and Beven*, 1997; *Franks et al.*, 1997; *Schulz and Beven*, 2003; *Schulz et al.*, 2001; *Wang et al.*, 2001]. As a result, much of the model functionality can remain unconstrained by the calibration process rendering any subsequent predictions from these schemes somewhat uncertain. One strategy for avoiding some of the difficulties associated with specifying SVAT models is to develop descriptions specifically at the scale of interest from the available observations at this scale in a top-down fashion [*Littlewood et al.*, 2003; *Schulz and Beven*, 2003; *Young*, 2003]. Such approaches rely not only on the availability of suitable data, but also on methodologies for identifying the dominant behavior being expressed in those data. In what follows we develop a model for the sum daily latent heat flux, λE, by including robust mechanistic information into environmental time series analysis to a degree that is supported by the available data. In particular we apply the Dynamic Linear Regression (DLR) estimation methodologies of Young [*Young*, 1999, 2000; *McKenna and Bruun*, 2001] to estimate the seasonal variations in Evaporative Fraction (EF) expressed within annual time series of eddy covariance measurements of latent heat fluxes above two forest sites each exhibiting significant seasonality. It will be shown that the time and state varying estimates of EF derived from DLR capture the seasonal variations in canopy behavior and can be related to vegetation characteristics (such as leaf area index, LAI) that might easily be detected by remote sensing thus allowing the prediction of surface fluxes to be extrapolated to the regional (GCM) scale.

Data and Site Description Two different FLUXNET [*Baldocchi et al.*, 2001] deciduous forest sites have been chosen for the illustration of the model development: Harvard Forest, Massachusetts (HF, 1998–1999, *Wofsy and Munger*, 2003) and University of Michigan Biological Station, Michigan (UMBS, 1999–2001, *Curtis*, 2003; *Curtis et al.*, 2002; *Schmid et al.*, 2004). The two sites differ especially in the mean annual precipitation (1066 mm at HF and 750 mm at UMBS) and the mean annual temperature (7.8°C at HF and 6.2°C at UMBS). The different climatic conditions are mirrored in the vegetation type. While HF is a temperate deciduous forest site, the vegetation at UMBS is characterised by an intermediate mix of temperate deciduous and boreal forest. Both forests are of similar age and stage of maturity (70 years at HF, 90 years at UMBS).

Half-hourly data sets comprising standard meteorological parameters as well as eddy flux measurements for latent heat and LAI measurements were available for periods from 1998–1999 for HF and from 1999–2001 for UMBS. As our research interest here lies in the prediction of cumulative latent heat fluxes as a water balance component, there is a need for gap free data sets. Therefore, gaps in the flux and micrometeorological time series data have been filled following the methodology described by *Jarvis et al.* [2004]. These data were then summed to give daily values on which the analysis is based.

λE Model identfication Here, we define EF as the proportion of incoming solar radiation, S_0, expressed as the daily latent heat, λE. Therefore, the EF models applied in this study assume the following form:

$$\lambda E = EF \cdot S_0 \tag{2.1}$$

The seasonal variations in EF expressed within the daily eddy covariance measurements are estimated using (2.1) within the DLR framework. The advantage of estimating EF as non-stationary parameters within a regression framework is that, unlike the estimates derived by simply inverting (2.1) which act to amplify noise effects, the DLR estimates minimized the effects of noise whilst at the same time retaining the systematic variations being expressed in the data. This greatly aids the identification of the sources of variation that need to be accounted for in any subsequent model description because the parameters are much more clearly defined.

DLR is based on recursive parameter estimation algorithms developed by Young and co-workers [see e.g., *Young*, 1999, 2000, 2001] which exploit Kalman filtering to estimate any parameter non-stationarity in linear models such as (2.1) directly from time series of data. The dynamic variations in EF are estimated by assuming they follow a random walk process driven by a zero mean, white noise sequence, $\eta(t)$, [*Young*, 2000]. This ensures that the recursive parameter estimation at the sample instant only depends on a window of data in the vicinity of this sample with the bandwidth of this window being characterized by the ratio of the variances of $\eta(t)$ to $\xi(t)$, known as the Noise Variance Ratio (*NVR*) [*Young*, 1999]. An *NVR* of zero results in all the observations contributing equally to the DLR parameter estimate and hence stationary parameters across the entire observation interval, whereas an *NVR* greater than zero implies an exponential decay in the weighting of data in the DLR estimation as one moves away from the t'th sample instant. Hence, the magnitude of the *NVR* determines the rate of decay of this weighting and is an implicit property of the recursive *DLR* estimation procedure that arises from optimizing the one step ahead predictions of (2.1) [for further details see *Young*, 1999].

The seasonal variations in DLR estimates for EF, derived from the data are presented in Figure 2.4 as an illustration. This reveals a strong seasonality of EF with low values in the winter and high values in the summer. EF like most simple parameterizations must be viewed as complex aggregates of multiple factors. Indeed, it is the perception of this complexity that provides the motivation for attempting to describe their various components explicitly in the form of more complex SVAT models. However, the motivation here is to attempt to account for the seasonal variations in as simple a way as possible.

It can be seen from Figure 2.4 that the temporal development of EF is closely related with the corresponding values for the leaf area index (LAI) at both sites. A statistical analysis reveals a cross-correlation between both parameters of 0.86 for HF and 0.91 for the UMBS site indicating a strong linear dependency. This suggests to express EF as a linear function of LAI:

$$EF = a + b \cdot LAI \tag{2.2}$$

where a and b are the offset and gain of the assumed relationship. Combining (2.1) and (2.2) leads to a relatively simple expression for the calculation of λE:

$$\lambda E = (a + b \cdot LAI) \cdot S_0 \tag{2.3}$$

that will be analyzed further in the following sections.

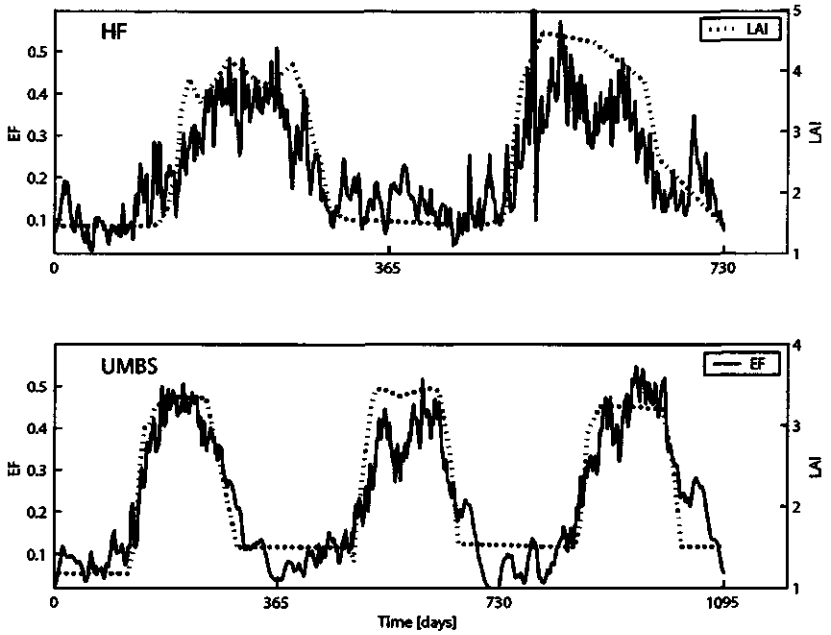

Figure 2.4: Temporal development of the evaporative fraction (EF) as derived from DLR analysis and associated leaf area index (LAI) measurements for both sites, HF and UMBS.

λE model calibration and evaluation Having identified a potential parametric model structure using the DLR parameter estimates, (2.3) can now be optimized using standard nonlinear least squares methods (Levenberg-Marquardt). The optimized parameter values as well as standard deviations for the estimates are given in Table 2.2. The goodness of fit is evaluated using two different measures: the standard deviation of the model residuals (RMSE) and the efficiency criteria (EC) [*Nash and Sutcliffe*, 1970], defined as $EC = 1 - \sigma^2_{res}/\sigma^2_{obs}$, where σ^2_{res} is the variance of the model residuals and σ^2_{obs} is the variance of the observed latent heat fluxes.

The results in Table 2.2 demonstrate that the derived model structure is able to explain much of the observed variations in λE (EC of 0.83 and 0.87 for HF and UMBS, respectively), whilst using relatively few (two) well defined parameters a and b.

While the model residuals for both data sets were found to be approximately zero mean they show some seasonality in the variance with higher values in the summer period and some autocorrelation suggesting that not all the system dynamic has yet been captured by the actual model structure. Statistical analysis however demonstrated no significant cross-correlation with either solar radiation, temperature, or evaporative demand indicating that these driving forces are well covered by the effective parameterizations. However, there was some significant cross-correlation with the cumulative differences between daily rainfall and actual evapotranspiration rates (max. cross-correlation coefficient of 0.21 and 0.26 at lags <30) highlighting some systematic impact of the local availability of water.

Discussion Despite its simplicity, (2.3) appears to capture the seasonal variations in the daily latent heat fluxes whilst also returning well defined parameter estimates. This is of particular importance when we are interested in comparing parameter values with site characteristics in order to infer

Table 2.2: Calibrated model parameters for the two sites, HF 1998–1999 and UMBS 1999–2001. Values in brackets represent standard deviation of the estimates. The goodness of fit is evaluated using the standard deviation of the model residuals (RMSE) and the efficiency criteria (EC).

Parameters	Units	HF 1998–1999	UMBS 1999–2001
a	-	$-2.07 \cdot 10^{-2}$ $(2.7 \cdot 10^{-3})$	-0.10 $(3.1 \cdot 10^{-3})$
b	-	$9.03 \cdot 10^{-2}$ $(9.2 \cdot 10^{-3})$	0.15 $(8.6 \cdot 10^{-3})$
RMSE	$MJ\,m^{-2}\,d^{-1}$	1.26	1.34
EC	$MJ\,m^{-2}\,d^{-1}$	0.83	0.87

more general rules which may allow for extrapolation to other locations and boundary conditions [see *Schulz and Beven*, 2003]. Especially the dependency on leaf area makes EF-type approaches as presented here very attractive in conjunction with the use of satellite imagery. This has so far been used to derive spatial distributed CO_2-fluxes [*Sellers et al.*, 1997] or to indirectly derive land surface characteristics (roughness lengths) in order to parameterize or drive more complex SVAT-schemes [e.g., *Braun et al.*, 2001; *Olioso et al.*, 1999] but has to our knowledge not been applied to derive areal information on EF and thus latent heat fluxes.

To what extent this approach can be successfully applied under different vegetation and climate conditions remains to be further investigated. Results presented here also demonstrate the need to explore the dependence (2.3) on the surface and sub-surface storage of water in more detail.

Links between river flow statistics and catchment characteristics: implications for land surface schemes

E. Blyth[1] and V. Bell[1]

[1]*Center of Ecology and Hydrology, Wallingford, UK*

The statistics of river flow depends, among other things, on the soil type in the catchment: permeable soils produce a more even spread of discharge through the year as the river is fed from groundwater, but the annual river flow is less. In addition, landscape characteristics (topography) that influence runoff generation also have an effect on the partitioning of runoff into surface and sub-surface flow. Finally, the river topology affects the attenuation of within-river flow. Each of these landscape characteristics affects a different aspect or statistic of the river flow. Using a standard land surface scheme with a runoff generation module and a grid-to-grid routing model, it is possible to quantify these links between the statistics of the river flow and the landscape, thus opening up the possibility of using river flow to calibrate the land surface scheme.

Introduction Land surface schemes in atmospheric models have been designed to reproduce the diurnal variation in fluxes of heat and water vapor to the atmosphere, to represent the meteorological forcing from the surface. Many land surface schemes have multi-layered soil models [see *Garratt*, 1993, for a review] which give good results in terms of the hourly fluctuations of surface conditions. However, as the atmospheric models aim at longer-term forecasts and at predicting future climates, land surface schemes now also need to model the longer timescale evolution of soil moisture [*Beljaars et al.*, 1996]. Soil moisture has a direct effect on the atmosphere via the soil evaporation and an indirect effect via plant water stress on the transpiration. In addition to the need for long term estimates of evaporation, more realistic representations of the surface water balance are needed to meet the goal of including runoff in atmospheric models.

However, it has been demonstrated that the water balance is still very inaccurate in atmospheric models [*Shao and Henderson-Sellers*, 1996]. Improvements to models have been made since this analysis, including the addition of runoff-generation schemes [*Blyth*, 2002; *Gedney and Cox*, 2003] and routing models [*Oki and Sud*, 1998]. However, the water balance is highly dependent on soil characteristics [*Blyth*, 2001] as well as the runoff generation and routing modules. The usual method of obtaining soil parameters for a meteorological land surface scheme (optimize the parameters against measured evaporation data, or to use the parameters given by a soil survey) are problematic on three accounts: Firstly, the soil parameters which control the long-term water balance are not sensitive to the traditional calibration exercise based on hourly surface flux data [*Harding et al.*, 2000]. Secondly, because soil is very heterogeneous, point evaporation measurements and soil samples may be unrepresentative of the area average soil type. Thirdly, the point where measurements were made may be unrepresentative of the area average in terms of hydrology e.g., groundwater level and drainage.

Atmospheric land surface schemes aim to reproduce mean fluxes over an area of 5 km $\times$ 5 km to 100 km $\times$ 100 km depending on the application and so require effective model parameters. The easiest way to obtain effective parameters is to calibrate them on area average data at the scale of interest. For the water balance this is readily available in the form of river flow data which aggregates the runoff from the catchment upstream of the gauging station. Using runoff is a very attractive prospect for the atmospheric land surface modeler: the data is extensive - river flow data

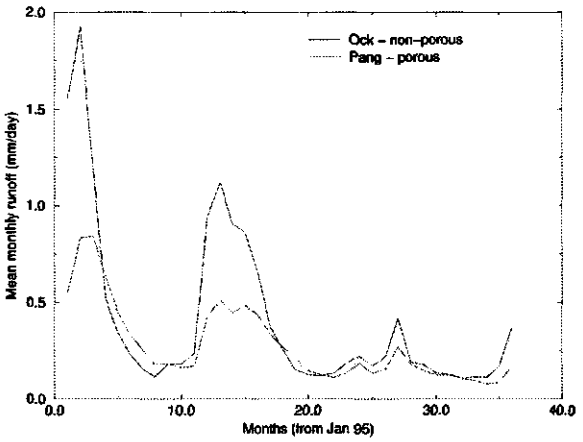

Figure 2.5: Observed monthly river flow for the Ock and Pang catchments in the Thames basin southern England.

are available in most parts of the world and because runoff represents an integrated response to a whole catchment it is appropriate to the problem.

It is the aim of this paper to show how river flow data can be used to calibrate a typical land surface scheme, to explore some of the pitfalls and to identify potential pathways to exploit this valuable data source. In this paper we will use the land surface scheme of the Unified Model of the UK Meteorological Office (referred to as MOSES, or Met Office Surface Energy Scheme) as described by *Cox et al.* [1998] with the PDM added to calculate runoff-generation [*Moore*, 1986] linked to a routing model developed for use with MOSES in Europe and the UK [*Bell and Moore*, 2004].

Observed relationship between riverflow and soil type In the UK the winter rainfall is high and the potential evaporation is low while in the summer the opposite is true. Some rivers reflect this seasonal pattern with high flows in winter compared to the summer. The soils in the catchment affect the seasonality of river flow as follows: Impermeable soils store the rainwater close to the surface and any excess water is routed quickly to the rivers so the seasonality of the river flow is closely linked to the seasonality of the rainfall. On the other hand, permeable soils allow the rainfall to drain into the deeper groundwater system. The river is then fed by the discharge of groundwater, thus smoothing out the river's response to the short term atmospheric forcing.

Examples of the two types of catchment response can be seen in the Ock (234 km^2) and the Pang (171 km^2). These two catchments are very similar in size and, being close together in the Upper Thames region, they experience similar rainfall and potential evaporation forcing. Both have similar land uses (rural, mainly grassland) and topography (they have the same altitude difference from the watershed to river gauge of the catchment over the same distance). However they have distinctly different soils; the Ock is 50% tertiary clays (non-permeable) and 50% chalk (permeable), while the Pang is principally permeable (chalk) and only 15% is non-permeable (Reading Beds, London Clay and Alluvium).

In Figure 2.5 the monthly river flow for the two catchments is plotted for 1995 to 1997. The data, measured by the UK Environment Agency, are held in the UK National River Flow Archive at the Institute of Hydrology. Firstly it can be seen that the total runoff as measured in the Ock river is greater than that measured in the Pang. Secondly, the link between the seasonality of the river flow and soil type is evident, with the Ock river flow, showing a more direct link to the forcing than the Pang river flow.

Effect of soil type on model water balance Driving the land surface model using locally observed driving data demonstrates the influence of soil type on the water balance. Table 2.3 shows the partition of rainfall into evaporation, surface runoff and drainage over the three years for the three soil types (coarse, medium and fine). Table 2.3 also shows that the fraction of rainfall that converts to evaporation is greater for coarse and medium soils than it is for fine soils. Evaporation accounts for 75% of the rainfall for coarse soils and the rest goes into the groundwater via drainage. For the fine soils, the evaporation accounts for about 50% of the rainfall, with the rest going to surface runoff. The medium soils convert about 70% of the rain to evaporation, and most of the rest is partitioned to surface runoff.

Table 2.3: Partition of rainfall into evaporation, surface runoff and drainage over the three years for the three soil types.

Process	Coarse	Medium	Fine	Ock	Pang
Evaporation	75	70	48	65	78
Surface runoff	5	27	53	35	22
Drainage	23	4	0	-	-

Table 2.3 confirms that the theory agrees with the observation: the Pang catchment contains coarser, more freely draining soils than the Ock.

Effect of runoff-generation and routing on river statistics An extended analysis will be carried over several more sub-catchments in the Thames basin. In this case, the catchments will be modeled with a 5 km gridded version of MOSES+PDM and the runoff routed grid-to-grid with the new routing model. The outputs will be compared to observed river flow. As an example of the model performance, Figure 2.6 shows initial results for some of the catchments. In this instance, a single value of the PDM parameter and no calibration of the routing parameters were used.

By analyzing how the model output changes the river-flow statistics as the soil, runoff and river flow parameters vary it will be possible to identify which parameters can be optimized by which river-flow statistic. Further analysis will be done to identify the uncertainty of such optimization. Case studies of contrasting catchments within the Thames region will be used.

Conclusions It is well established that catchments containing different soil types generate different monthly and annual river flow; catchments containing permeable soils generate a more even distribution of river flow but a lower annual total than catchments containing impermeable soils. This paper explores the potential of harnessing this information to calibrate land surface schemes for atmospheric models.

By driving the model with observed meteorological data from a point, it can be demonstrated that the representation of vertical soil water processes can significantly affect the water balance. The partition of rainfall into evaporation, surface runoff and drainage is strongly affected by the soil type chosen: fine soils have less evaporation than coarse soils and they have no drainage, while coarse soils have no surface runoff.

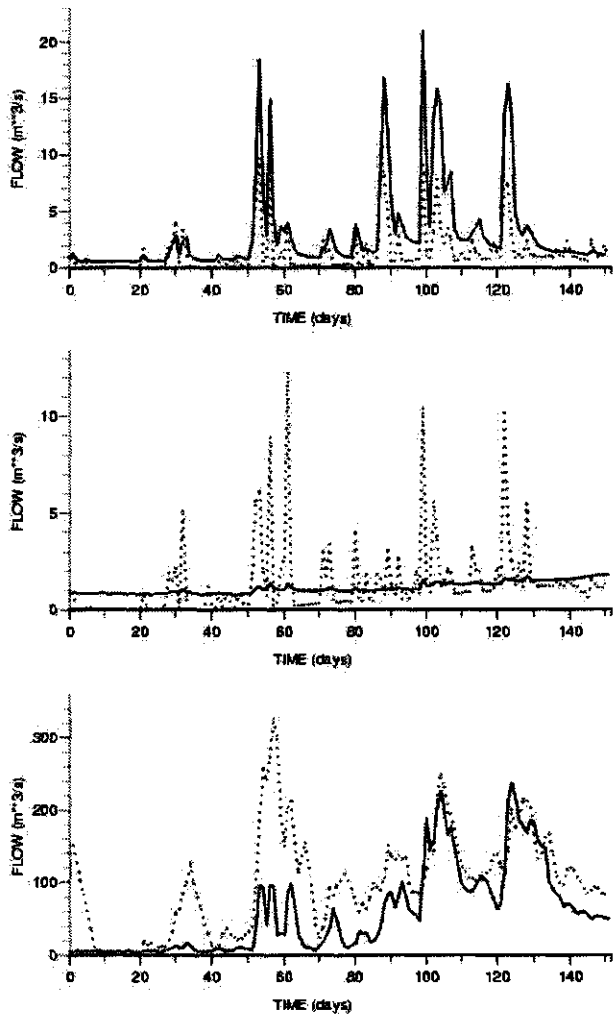

Figure 2.6: Observed and modeled river flow for several catchments (Mole, Lambourn and Thames) in the Thames Basin. The dotted lines are modeled flow.

This partitioning (evaporation/runoff and surface/subsurface runoff) affects different aspects of the water balance: The monthly river flow represents the runoff aspect of the model and the annual river flow represents the evaporation aspect. The routing of the model affects the flow at finer timescales - expressing the delay between runoff generation and catchment outlet. The actual timescale depends on the size of the catchment.

Finer scale modeling and accurate routing models allow for distinctions to be made between these various aspects of the model. Some statistical analysis will be used to unravel the signal of the landscape in the river flow.

Simulating soil moisture variability dynamics

Adriaan J. Teuling[1] **and Peter A. Troch**[1]

[1]*Hydrology and Quantitative Water Management Group, Wageningen University, Wageningen, The Netherlands*

During previous field experiments, different trends of soil moisture variability with mean moisture content have been reported. Here we explain these trends for three different data sets by showing how the different controls interact to either create or destroy spatial variance. Improved understanding of these processes is needed for the transformation of point-scale measurements and parameterizations to scales required for climate studies, operational weather forecasting, and large scale hydrological modeling.

Introduction Although the quantitative contribution of soil moisture to the global water budget is negligible, it plays a central role in the global water cycle by controlling the partitioning of water and energy fluxes at the earth's surface, and may control the continental water distribution through land-surface atmosphere feedback mechanisms [*Koster et al.*, 2003]. The ability of coupled models to reproduce these processes will strongly depend on the parameterization of soil moisture state-flux relationships at the regional scale. The lack of accurate observations of land surface states and fluxes at the regional scale, combined with the variability of soil moisture and the high non-linearity of land-surface processes at the small scale, requires aggregation of small scale processes to larger scales in order to prevent systematic biases in modeled water- and energy fluxes [*Crow and Wood*, 2002]. For successful aggregation, knowledge on soil moisture variability controls is indispensible.

Several scientists have reported soil moisture variability to increase with decreasing mean moisture content [e.g. *Famiglietti et al.*, 1999; *Hupet and Vanclooster*, 2002]. Other scientists reported opposite trends [e.g. *Western and Grayson*, 1998; *Famiglietti et al.*, 1998], were unable to detect a trend [e.g. *Hawley et al.*, 1983; *Charpentier and Groffman*, 1992], or found the trend to depend on the mean soil moisture state [e.g. *Owe et al.*, 1982; *Albertson and Montaldo*, 2003]. Although many scientists have speculated about the origin of soil moisture variability, only few have tried to quantitatively explain the apparent contradictions in observed soil moisture variability trends by looking at how the different controls interact.

Here we develop a simple model that is able to reproduce observed soil moisture variability trends for the three different data sets studied, and analyse the model results with an extension of the theoretical framework recently developed by *Albertson and Montaldo* [2003] to quantify soil, vegetation, and landscape controls on soil moisture variability. The results might lead to improved understanding of soil moisture variability observations and the aggregation problem.

Data Three datasets are used in this study, each with a different trend of variability with changing mean moisture content (Figure 2.7, upper panels).

Soil moisture (0–20 cm) variability was measured at an agricultural field in Louvain-la-Neuve (Belgium) at 60 days between 30 May 1999 and 13 September 1999 as part of a campaign with the objective to investigate the within-field spatial variability of transpiration [*Hupet and Vanclooster*, 2002]. The soils in the field are classified as well-drained silty-loam and there is little topography. During the campaign the field was cropped with maize. The climate is moderate humid. Meteorological observations are available from 1 January 1999 till 31 December 1999.

From 24 June 1998 to 26 Januari 1999, soil moisture (0–30 cm) was measured with 36 TDR sensors (spacing 1 m) at a gently sloping field transect at the Virginia Coastal Reserve Long Term Ecological Research (VCR-LTER) site on the eastern shore of Virginia [*Albertson and Montaldo*, 2003]. The soils were classified as sandy loam, with a vegetation of Johnson grass. Meteorological observations are available for the period 30 June 1998 till 27 September 1998.

The Australian Tarrawarra dataset results from an experiment that aimed at investigating the spatial pattern of soil moisture at the small catchment scale. Between 27 September 1995 and 29 November 1996 a total of 13 soil moisture (0–30 cm) patterns were measured [*Western and Grayson*, 1998]. Additional measurements are summarized in *Western et al.* [2004]. The soils in the catchment are silty-loam to clay, and the landscape is undulating with a maximum relief of 27 m. The climate is temperate. Land use is perennial pastures used for grazing. Meteorological observations are available for the period 10 August 1995 till 25 October 1997.

Modeling soil moisture variability Under most conditions, lateral flow in the upper part of the soil can be neglected, and the vertically integrated soil moisture balance over a depth L can be written as:

$$\frac{d\theta}{dt} = \frac{1}{L}(T - R - q - S) \tag{2.4}$$

where θ is the depth-averaged soil moisture content, T the throughfall, R the saturation excess runoff, q is the drainage at depth L, and S the root water uptake. Here, $L = 0.5$ m and $dt = 1$ d. Throughfall is the rainfall P that is not intercepted by vegetation, and the size of the interception reservoir is taken proportional to LAI. We assume bare soil evaporation to be small in comparison to the root uptake over the entire profile. Drainage is calculated using Darcy's law with the unit-gradient assumption, and applying the $k(\theta)$ parameterization proposed by *Campbell* [1974]. The vertically integrated root water uptake S is a function of the root fraction, a soil moisture stress function, LAI [following *Al-Kaisi et al.*, 1989], and potential evapotranspiration. For Louvain-la-Neuve, the positive relation between LAI and S was confirmed by *Hupet and Vanclooster* [2004]. LAI is modeled with a spatial and temporal component. The applied model sufficienty captures the non-linearities and dynamics of the soil moisture loss processes, and similar models have proven succesful in reproducing point scale soil moisture dynamics [e.g. *Albertson and Kiely*, 2001; *Laio et al.*, 2001].

We reproduce the first and second order spatial moments of θ ($\overline{\theta}$ and σ_m^2) by running a large ensemble of the model with variable parameters. Initial conditions of θ are set by taking $q = 1$ mm d^{-1}. We assume both the logarithm of the saturated hydraulic conductivity k_s and LAI to follow a normal distribution. Local soil parameters are related to k_s by linear regression with $\ln(k_s)$, fitted to the data provided by *Clapp and Hornberger* [1978]. Due to the positive effect of high k_s on canopy growth through better aeration, soil temperature and water transport to roots, we assume $\rho(\ln(k_s), \mathrm{LAI}_{max}) = 1$. Atmospheric forcing was calculated from available observations and assumed to be constant in space.

In order to account for spatial differences in the water balance caused by differences in exposure due to sloping of the landscape, we follow *Svetlitchnyi et al.* [2003] and write the effect of topography on the available moisture content $\theta^* = \theta - \theta_w$ in the top 0.5 m of the soil in terms of a wetness coefficient η:

$$\theta_i^* = \eta \cdot \theta^* \tag{2.5}$$

where θ_i^* is the "corrected" value of θ^*. η depends on slope profile shape, slope aspect, distance from the divide, and slope gradient, and can be derived from a digital elevation model. As a

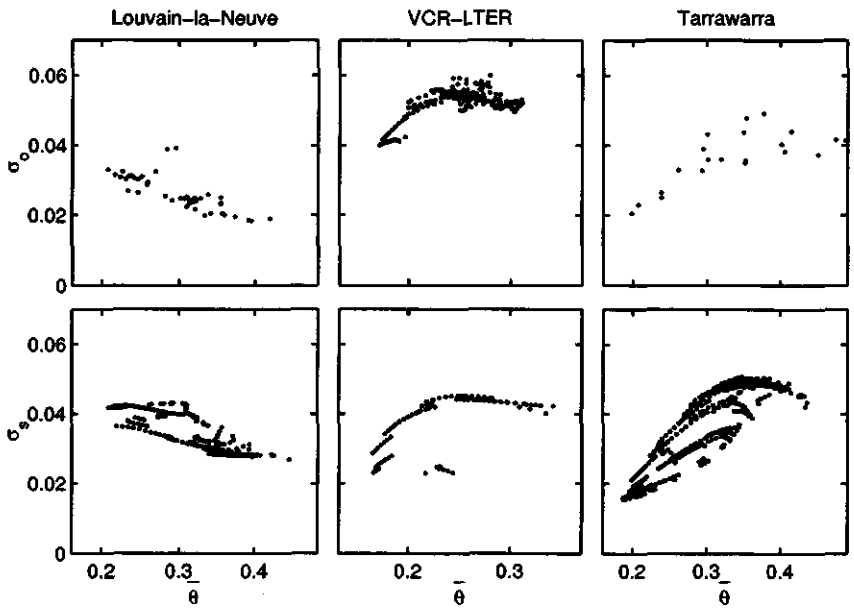

Figure 2.7: Observed (σ_o) and simulated (σ_s) soil moisture standard deviation as function of mean soil moisture content ($\bar{\theta}$).

first order approach, we add the variance caused by (2.5) to σ_m^2, assuming $\overline{\eta} = 1$. To allow direct comparison with observations, we also account for apparent variability due to a measurement error ε ($\bar{\varepsilon} = 0$). The total simulated soil moisture variance σ_s^2 can now be written as:

$$\sigma_s^2 = \sigma_m^2 + \sigma_\eta^2 \cdot \overline{\theta^*}^2 + \varepsilon^2 \tag{2.6}$$

Figure 2.7 shows that both the range of $\bar{\theta}$ as well as the magnitude, trend, and hysteresis effects of σ_s compare well to the observations.

Analysis In order to distinguish the contribution of different controls on the time evolution of σ_s, we first follow *Albertson and Montaldo* [2003]. Substracting the spatial average equivalent of (2.4) from (2.4) yields an expression for the time evolution of a local soil moisture anomaly:

$$\frac{d\theta'}{dt} = \frac{1}{L}(T' - R' - q' - S') \tag{2.7}$$

where $'$ denotes a deviation from the spatial average. Multiplying (2.7) by $2\theta'$, performing a chain rule operation to the left hand side, and averaging the result yields:

$$\frac{d\overline{\theta'^2}}{dt} = \frac{d\sigma_m^2}{dt} = \frac{2}{L}\left(\overline{\theta' T'} - \overline{\theta' R'} - \overline{\theta' q'} - \overline{\theta' S'}\right) \tag{2.8}$$

which is an expression for the time evolution of the spatial soil moisture variance. Since the right-hand side of (2.8) consists of covariance terms, their contribution depends on both the magnitude

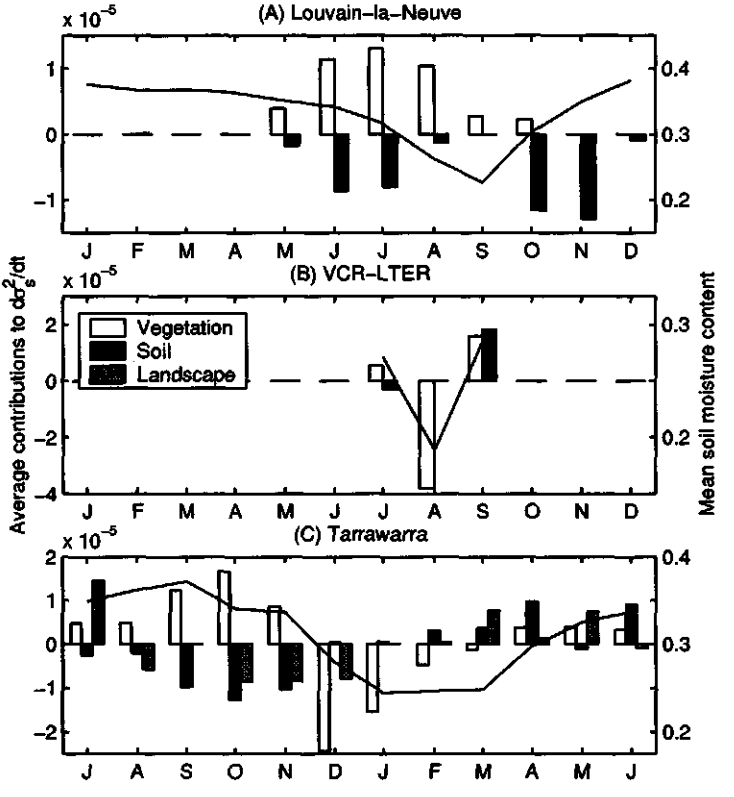

Figure 2.8: Monthly average vegetation, soil, and landscape contributions to $d\sigma_s^2/dt$, as in (2.9).

of soil moisture and flux anomalies as well as their mutual correlation. The sign of the correlation controls whether the different processes act to create or destroy spatial soil moisture variance [see *Albertson and Montaldo*, 2003, for synthetic examples]. Combining (2.8) with the time derivative of (2.6) yields:

$$\frac{d\sigma_s^2}{dt} = \underbrace{\frac{2}{L}\left(\overline{\theta' T'} - \overline{\theta' S'}\right)}_{\text{Vegetation}} \underbrace{-\frac{2}{L}\left(\overline{\theta' R'} + \overline{\theta' q'}\right)}_{\text{Soil}} \underbrace{+\sigma_\eta^2 \frac{d\overline{\theta^*}^2}{dt}}_{\text{Landscape}} \tag{2.9}$$

Rather than evaluating all terms seperately, we group the correlated terms as (local) vegetation and soil controls, and non-local landscape control. Figure 2.8 explains the different trends in Figure 2.7 by evaluating the contribution of the different groups in (2.9). For clarity the terms have been converted to monthly averages.

In the Louvain-la-Neuve dataset, soil moisture variability increases during the growing season. During winter and spring (December–April), precipitation surplus causes soil moisture to retain near field capacity, and the variance is fully adjusted to the soil footprint (Figure 2.8A). Untill July, increases in variance due to heterogeneous transpiration are effectively (although not entirely)

cancelled out by drainage. When drainage becomes neglectible (August–September), vegetation controls start to create additional variance. This increase is only destroyed during the first rainfall events in the late growing season (October–November), when the variance is "reset" to the soil footprint ($\overline{\theta' q'} > 0$). It should be noted that also during summer $\theta > \theta_c$ so that root water uptake is under atmospheric control, and ($\overline{\theta' S'} < 0$).

For the VCR-LTER data, this behavior is almost opposite (Figure 2.8B). The coarse soils in combination with high E_p limit root water uptake early during a drying cycle. The (small) initial increase in σ_s during July (Figure 2.7, not visible in monthly average value in Figure 2.8), is due to heterogeneous but unstressed transpiration ($\overline{\theta' S'} < 0$). During the second half of July this changes rapidly, and stressed transpiration causes a sharp decrease in variance ($\overline{\theta' S'} > 0$). Similar to the Louvain-la-Neuve case, rainfall events in September force σ_s to readjust to the soil footprint, only here $\overline{\theta' q'} < 0$.

Tarrawarra shows a more complex pattern (Figure 2.8C). In spring, vegetation controls act to create variance ($\overline{\theta' S'} < 0$), but this variance is initially destroyed by drainage of rainfall. In this period, drying of the soil ($\mathrm{d}\overline{\theta^*}^2/\mathrm{d}t < 0$) causes a transition from non-local to local controls on σ_s [*Grayson et al.*, 1997]. This can be seen by the negative landscape contributions. Later during summer (December–February), soil and landscape controls become effectively zero due to advanced drying. The strong soil controlled root water uptake ($\theta < \theta_c$) causes a transition of the sign of the correlation between S and θ ($\overline{\theta' S'} > 0$) resulting in a strong decrease in σ_s^2. The readjustment to the winter soil moisture state is accompanied by an increase in σ_s^2 caused by soil and (non-local) landscape controls.

Discussion Our simulations show that both soil and vegetation controls can act to either create or destroy spatial variance. The main discriminating factor between both behaviors is wether or not the soil dries below θ_c. This depends on the soil texture as well as on the depth of the drying phase. The fact that much of the observed soil moisture variability is actually created by vegetation anomalies (and thus $\rho(\theta, \xi) \neq 0$) calls for new approaches to the soil moisture aggregation problem. This suggests that future field campaigns can further contribute to our understanding of the soil-vegetation-atmosphere system not only by looking at soil moisture variability, but also at how this variability is related to anomalies in soil and vegetation characteristics.

Acknowledgments François Hupet and John Albertson are greatly acknowledged for providing access to their data sets.

Similarity analysis of subsurface flow response of hillslopes with complex geometry

A. Berne[1], R. Uijlenhoet[1], and P.A. Troch[1]

[1]*Hydrology and Quantitative Water Management Group, Wageningen University, Wageningen, The Netherlands*

Recently, *Troch et al.* [2003] introduced the hillslope-storage Boussinesq (hsB) equation to describe subsurface flow and saturation along complex hillslopes. The hsB equation can be linearized and further reduced to a diffusion-advection equation for hillslopes with constant bedrock slopes and exponential width functions. This paper presents a dimensional analysis of the latter equation in order to study the pure drainage flow response, which, once normalized by the flow volume, is defined as the characteristic response time distribution (CRTD). In the Laplace domain, an analytical expression for the discharge is obtained and used as moment generating function to derive the analytical expressions for the CRTD moments. These moments, in a dimensionless form, can be expressed as function of a subsurface flow similarity parameter, hereafter called the hillslope Peclet number, and a group of dimensionless numbers accounting for the initial condition effects. The analysis of their respective influences on the first four CRTD central moments shows that the first studied type of initial condition (uniform water table depth) has a strong impact on the dimensionless mean response time of the CRTD but negligible effect on the higher order moments, while the second studied type of initial condition (steady state water table profile) has a limited effect on all first four CRTD moments and hence, in this case, the hillslope Peclet number completely defines the subsurface flow similarity between hillslopes.

The relative effect of heterogeneities in rainfall and soil properties on soil moisture on a regional scale

H. Leijnse[1], A.J. Teuling[1], R. Uijlenhoet[1] and P.A. Troch[1]

[1] *Hydrology and Quantitative Water Management Group, Wageningen University, Wageningen, The Netherlands*

Accurate knowledge of spatial soil moisture fields is vital to correct modelling of land atmosphere interactions at different scales. It has been argued that soil moisture variability, when going to regional scales, increases to the extent that soil moisture-flux relationships are effecively linearized. This increase in variability should be due to variability in rainfall, since all sources of variability act on much smaller (soils, vegetation, topography, etc.) or much larger (radiation, climate, etc.) spatial scales. We investigate the effect of spatial heterogeneities in forcing and in model parameters on modelled soil moisture on scales ranging from ~ 1 km to $\sim 10^3$ km.

We use a point-scale soil moisture model (see contribution by Teuling and Troch, Page 81) with daily rainfall products as input. The 240 km $\times$ 240 km rainfall field is given on a 4 km $\times$ 4 km grid around the Little Washita SCAN site, and is a composite of several WSR-88D radars and with a raingauge network. This rainfall data, and soil moisture measured at Little Washita were collected as part of the SMEX03 campaign that took place between 20 May 2003 and 31 July 2003.

The effect of spatially aggregating rainfall and soil/vegetation properties on modelled soil moisture are investigated by means of a Monte Carlo simulation using soil and vegetation properties (saturated hydraulic conductivity and leaf area index) drawn from distributions that are representative of the area around Litte Washita. The model is compared to the measured soil moisture at the Little Washita SCAN site. The results of this study could be useful in determining the relative effect of heterogeneities in rainfall and soil/vegetation properties on soil moisture on a regional scale.

3 Hydrological modeling across scales

From catchment to continental scale: Issues in dealing with hydrological modeling across spatial and temporal scales

Dennis P. Lettenmaier[1]

[1]*Department of Civil and Environmental Engineering, University of Washington, Seattle, Washington, USA*

The traditional challenge charge to watershed hydrologic modelers has been to predict river discharge, given precipitation and other near-surface atmospheric variables that control evaporative demand. With the advent of the digital computer in the 1950s came spatially lumped hydrological models like the Stanford Watershed Model, and various more recent derivatives. These models attempted to represent runoff production using effective or spatially lumped parameters. These parameters represented the storage of water in the subsurface, and the rates of exchange among the storage compartments, including infiltration and surface runoff production, and subsurface drainage or baseflow. Evapotranspiration was typically represented as a fixed (seasonally varying) potential, with actual evapotranspiration determined by the potential modulated by resistance controlled by the relative storage in subsurface zones. These models represented a considerable advance over pre-computer methods that typically were event-based, rather than temporally continuous. The move to time-continuous modeling avoided the difficulty of specifying initial conditions (primarily moisture storage) at the onset of a storm, which has always plagued event models in hydrology.

Time-continuous spatially lumped catchment models remain widely used in practice. For instance, the Sacramento soil moisture accounting model is still at the heart of the National Weather Service River Forecast System, and the NWS Advanced Hydrologic Prediction System, which is intended to be the basis for hydrologic forecasts for purposes ranging from flood forecasting to seasonal water management. The issue of scale dependencies of model parameters in spatially lumped models is sidestepped by calibrating model parameters to match observed discharge at a specified set of locations. On the other hand, the need to calibrate has been a practical problem which has impeded the application of spatially lumped models, especially over large areas, notwithstanding some success in development of automated parameter estimation methods,

More recently, the evolution of surface hydrological modeling has been affected by two major developments. The first is the availability of spatially distributed land surface data sets from remote sensing and other sources, and GIS software that can easily manipulate these data. Of particular interest for hydrologic modeling and prediction are three general categories of land surface data: digital topography (including channel networks), soil characteristics, and vegetation. With the availability of such data has come demands for hydrologic prediction methods that not only provide information about hydrologic processes (runoff production, evapotranspiration, soil moisture) at spatial scales commensurate with the land surface data, but also that have the capability to reflect changes in land surface conditions, especially land cover. Interests in hydrologic consequences of land cover change ranges from effects on flooding of urbanization, logging, and fires, to the effects on groundwater recharge and water supply availability of urbanization. Spatially lumped models, parameters for which are estimated via calibration, are inherently unsuitable for such applications, since the calibrated parameters are specific to the land cover conditions that pertained over the historic period on which the calibration was based. However, the spatially distributed hydrologic

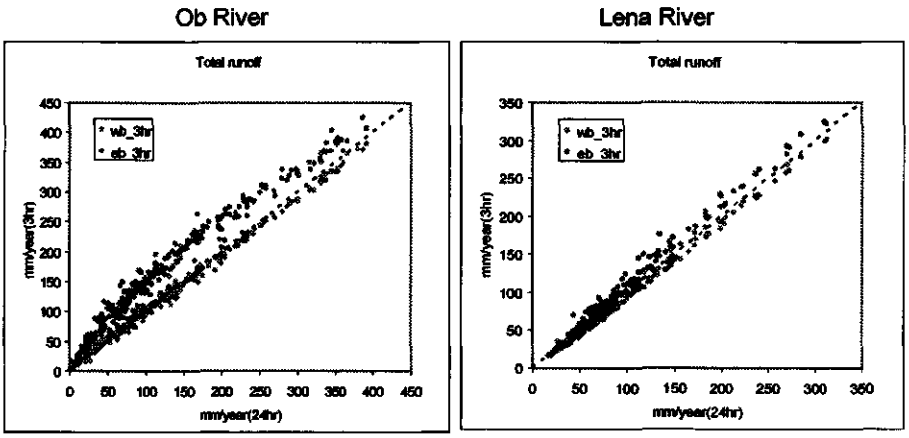

Figure 3.1: Simulated annual runoff for grid cells within the Ob River basin (left) and Lena River basin (right) by Variable Infiltration Capacity model, using full energy balance (purple) and water balance (green). Differences in sensitivity are apparently due primarily to differences in extent of permafrost in the two basins. Results courtesy of Fengge Su.

models that use spatial data explicitly must deal with the complications of spatial scale. As just one example, *Zhang and Montgomery* [1994] show how the topographic index at the heart of the widely used Topmodel [*Beven and Kirkby*, 1979], and in turn estimates of saturated area and runoff production, vary with the spatial resolution of the digital topographic data.

The second major development that has affected the development of surface hydrological models has been the demands for large scale representation of land surface processes, which has grown largely from the demands for better land surface representations in coupled land-atmosphere models used for numerical weather climate prediction. Whereas hydrological modelers typically had not gone much beyond watersheds very roughly in the 10^4 km^2 range, coupled land-atmosphere models must function at scales from subcontinental (for regional models) to global. Furthermore, the land surface representations used in these models must close both the surface water and energy budgets. While hydrologic models by construct close the surface water balance, most have not closed the surface energy balance, and instead either use prescribed potential evapotranspiration, thus avoiding representation of energy fluxes altogether, or explicitly or implicitly assume that the effective surface temperature is equal to the air temperature. Soil-Vegetation-Atmosphere Transfer Schemes (SVATS) used in coupled land-atmosphere models, on the other hand, iterate to solve for one or more effective surface temperatures such that the radiative, turbulent, and ground heat fluxes balance.

This discrepancy between traditional catchment models and land surface schemes leads to certain complications in the implementation of hydrological models at large scale. Figure 3.1, for instance, shows hydrographs for two large Arctic rivers simulated with the Variable Infiltration Capacity (VIC) model in water balance (surface air temperature assumed equal to effective surface temperature) and energy balance (effective surface temperature iterated to close the energy balance). As in more traditional spatially lumped models, macroscale models like VIC require some calibration to reproduce observed moisture and energy fluxes properly. Because water balance simulations are considerably less computationally intensive (by a factor of 10 or so), an

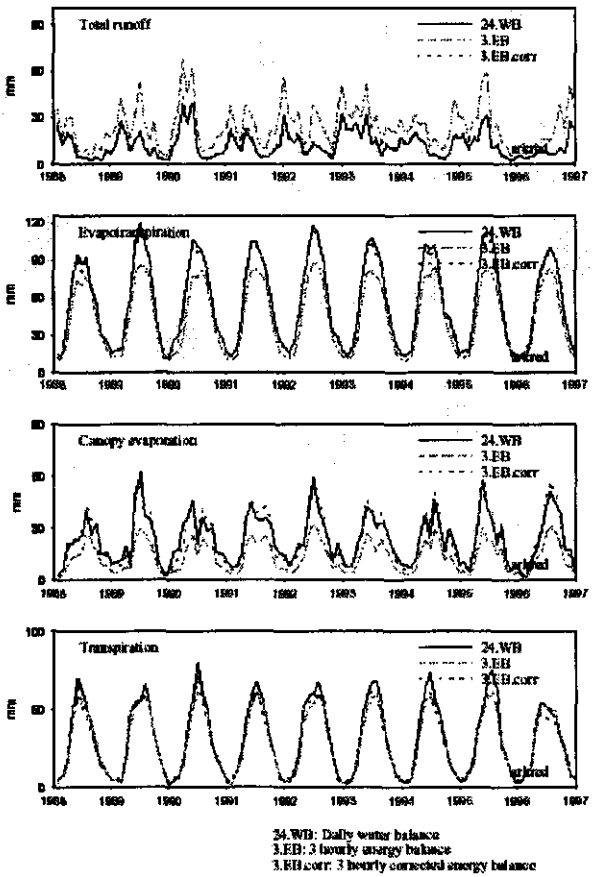

Figure 3.2: Simulated mean runoff, evapotranspiration, canopy evaporation, and transpiration from Variable Infiltration Capacity model over a transect from 80°W to 105°W at latitude 37°N. "Corrected" results are based on a scheme that adjusts the canopy interception capacity and minimum stomatal resistance to account for time step differences/ Preliminary results courtesy of Ingjerd Haddeland.

appealing approach is to estimate parameters in water balance mode, and transfer them to energy balance. As Figure 3.1 shows, however, this approach is complicated by the fact that the simulated fluxes can differ substantially in the two modes.

Another complication in the implementation of macroscale models is the role of temporal scale as it affects model parameters. Surface hydrological models typically are applied at scales dictated more by the time frequency of the data available for model calibration than by catchment dynamics. As a practical matter, this temporal scale often has been daily - in the U.S. because the U.S. Geological Survey archives of daily data are more readily obtainable, especially for long historical periods, than are the so-called unit values from which shorter time step data are derived. In the context of coupled modeling though, land surface models are applied at temporal scales that

are dictated by computational considerations, and are usually much shorter (e.g. fractions of an hour) than those used in off-line simulations. Figure 3.2 shows results of simulations performed for an east-west transect across the continental U.S. for a range of model time steps. Clearly, the results are quite sensitive to the model time step. The primary mechanism leading to this temporal dependence is the manner in which interception storage, and canopy evaporation, are computed in VIC (and most other land surface schemes). This sensitivity may be resolvable by an alternative formulation of the canopy evaporation process which is less scale dependent, important issues remain that are related to the temporal scale of the precipitation data, which in off-line simulations is, like streamflow, dictated by observational constraints.

Other issues related to spatial scale dependencies exist for macroscale models, as for spatially distributed models as discussed above. *Haddeland et al.* [2002] investigated some of these issues in an implementation of the VIC model for spatial scales ranging from 1/8 to 2 degrees over two large continental river basins (Arkansas-Red and Columbia). They found that for the VIC model, model predictions were relatively scale invariant, although others [e.g. *Koren et al.*, 1999] have found otherwise, suggesting that spatial scale model dependency is itself strongly model dependent.

Determining land use from satellite images using plant cover indices

Dilkushi De Alwis[1], Pierre Gérard Merchant[1], William D. Philpot[2], and Tammo S. Steenhuis[1]

[1]*Department of Biological and Environmental Engineering, Cornell University, Ithaca, New York, USA*
[2]*Department of Civil and Environmental Engineering, Cornell University, Ithaca, New York, USA*

Since the introduction of advanced and fast computers during the last 25 years, water cycle research has greatly benefited from the introduction of distributed and semi-distributed catchment-scale hydrological models. The parameterization of these distributed models is difficult and model predictability would greatly be enhanced by more advanced data assimilation methods. In this paper we will discuss a new data assimilation method for delineating land cover and use in a watershed.

Introduction The current methods used to observe changes in land cover over time are Spectral Mixture Analysis (SMA), Tasseled Cap Transformation (TCT) and Vegetation Indices. The detection of change over time of land cover from spectral signatures, despite its wide use, is affected to various degrees by the following factors: temporal changes in shading due to topography and sun angle, distortion caused by differences in viewing angles in temporal images, differences in plant cover during various times of the year, inaccuracies in georeferencing, and atmospheric scattering and absorption of light. Atmospheric correction of the radiation received at the satellite is by far the most difficult correction to make. Electromagnetic radiation collected by satellites is modified by scattering and absorption by gasses, water vapor, and particulate aerosols. A number of radiative transfer models based on ray tracing algorithms have been developed for correcting the atmospheric effects. Studies have shown that these models can accurately correct for the atmosphere. However, these corrections require accurate measurements of atmospheric optical properties. These measurements are often not available or are not exactly in the study area or coincident with the overpass. Since more light scatters at shorter wavelengths, the blue band is more sensitive to atmospheric effects than the red and infrared bands commonly used for vegetation indices. Thus, unless one uses data that have been atmospherically corrected, use of the blue band (c.f., the SMA, TCT) is less desirable than methods that use only the red and infrared bands as is the case for the standard vegetation indices.

There are a number of vegetation indexes that have been developed over the years primarily for the purpose of ecological assessment not directly for determining land use. The NDVI is the most commonly used index for ecological assessment [*Elmore et al.*, 2000]. NDVI has been shown to have a "reasonable correlation" [*Elmore et al.*, 2000] with vegetation abundance and other important ecological parameters such as leaf area index and the fraction of absorbed photosynthetically active radiation, CO_2 uptake, productivity rates, leaf biomass, leaf density and process rates (such as photosynthesis and transpiration).

The purpose of this paper is to employ a vegetation index in an unsupervised manner to delineate land cover types that are significantly different in terms of growth characteristics over time. The above can then be used directly in distributed models. Moreover, since growth characteristics are used for delineation, the method has hydrological significance. Our hypothesis is that by looking at the development of the vegetation in the watershed throughout the year, we can describe specific and unique patterns for the different land covers and uses

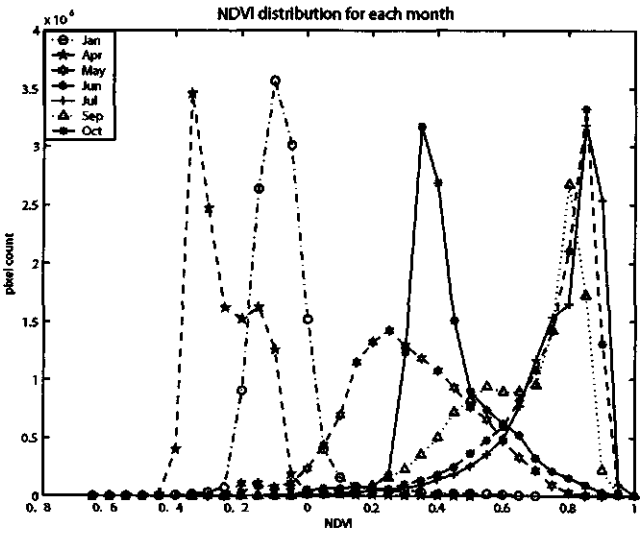

Figure 3.3: Distribution of NDVI values for the Town Brook watershed for different months.

For this study we will use the Town Book watershed which is located in the Catskill region of New York State. Town Brook is a 37 km^2 rural watershed with farms and forest. Summer homes are being built. It is chosen because Townbrook is one of the watersheds selected by the USDA and the New York City Department of Environmental Protection (NYCDEP) for detailed studies on watershed hydrology and NPS control. We have also developed a distributed watershed model for this area and in a subsequent paper we will test how satellite-derived landuse and the real landuse affect the hydrology

Material and Methods Seven cloud free, multi-spectral, Landsat ETM+ images that contained the Town Brook watershed were obtained for processing. The data were collected on 29 January 2000, and on 5 April, 7 May, 8 June, 10 July, 12 September and 30 October 2001. The Landsat ETM+ sensor data have 30 m resolution in six spectral bands ranging from Blue to Middle Infrared, an additional sensor that records data in a wide bandwidth (encompassing bands 2, 3, and 4) in a panchromatic mode (black and white) and a 120 m resolution in one Thermal Infrared band. Only the six 30 m bands were used for this study.

The NDVI was calculated by first correcting each of the images for atmospheric effects with Dark Object Subtraction (DOS). The red and infrared bands are generally corrected using dense vegetation. Since images are compared throughout the year, not all the images had dense vegetation and clear, deep water bodies were used as dark objects. After the correction, the NDVI was calculated as $(R_{ir} - R_{red})(R_{ir} + R_{red})$ where R refers to the reflectance of the target with the subscript defining the spectral region, *red* for the red band and *ir* for the infrared band. The NDVI, like any of the vegetation indices based on ratios, helps to compensate for many of the complicating factors, e.g., illumination effects, atmospheric effects. The NDVI has the additional advantage that the maximum value is 1.

The NDVI landuse images were compared with the 2001 land cover/use map produced by NYCDEP, is the agency in charge of the water supply. This map was generated using automated land cover classification based on Landsat ETM+ imagery, and enhanced it with impervious surface

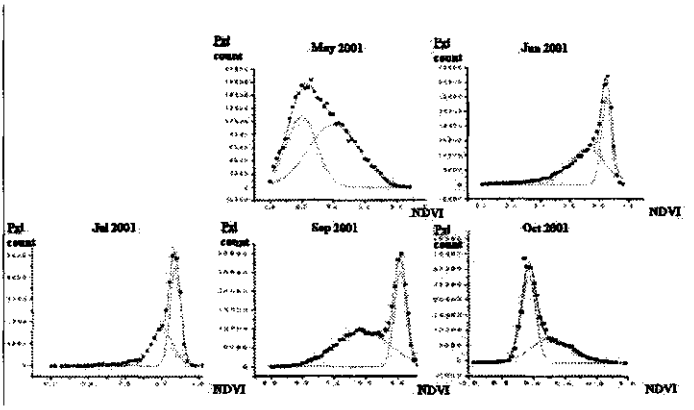

Figure 3.4: The pixel distribution can be approximated as the sum of with two normal distribution curves.

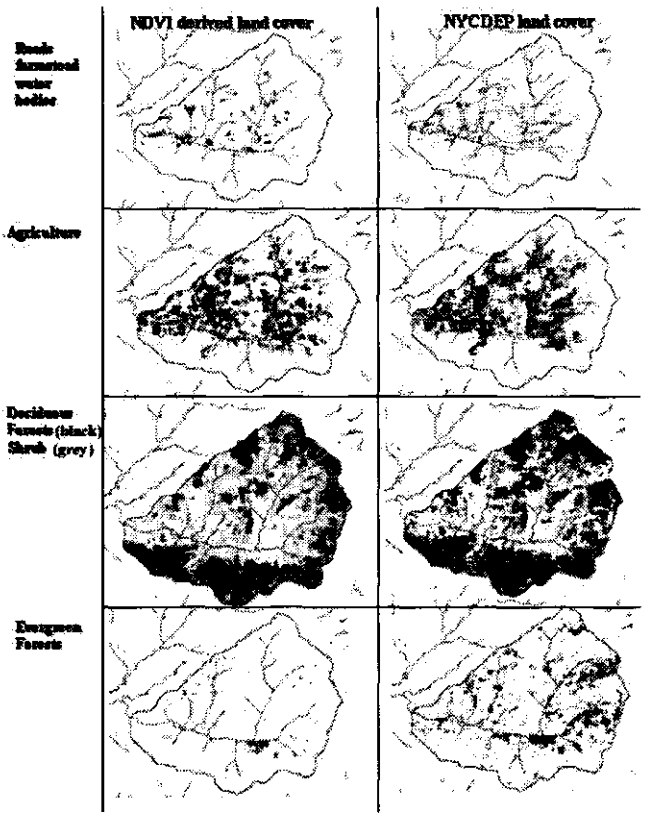

Figure 3.5: The NDVI landcover map (left) and the NYCDEP landcover map for Town Brook watershed.

feature extraction derived from 0.3 meter and 1 foot, color infrared digital ortho-imagery, with tax parcel and other inventory data employed to provide land use information where applicable.

Results and Discussion The distribution of the NDVI values for the 30 m $\times$ 30 m pixels for the seven Landsat ETM+ images are given in Figure 3.3. Most of the January and April NDVI values are negative due to the red colored soil which is brighter in the red than in the IR. In May, there is a wide distribution of NVDI values signaling a broad range in plant development stages. The highest NDVI values are found for June and July and the distributions of the two months are almost equal. The distribution of September NDVI values are almost the same as for the summer months with the exception of the deciduous forest that started to color and resulted in some pixel changing from a high NDVI to a much lower value. October NDVI values after several frosts have decreased from September. The grass and the conifers are the only green land cover in the landscape and have the highest NDVI values.

In order to derive land cover, we track the change of NDVI over the year for each pixel. Each land cover has a unique signature. The following land covers are distinguished: (1) Non vegetative surfaces consisting primarily of farms with barn yard, wide roads and lakes; (2) Forests - evergreens and deciduous trees are distinguished because they impact the hydrological balance differently; (3) Abandoned agricultural land consisting mostly of shrub and (4) Agriculture. Other agricultural land uses can be distinguished but that is beyond the scope of this abstract.

The best time to distinguish between the land covers is early in the growing season and late in the growing season. In the early growing season (May in Upstate New York) grasses and conifer forests are green and absorb the red energy (chlorophyll absorption). Deciduous trees do not have leaves and will not absorb in the red. During the growing season all plants are green. Forests grow more vigorously than grasses and, therefore, absorb more red light than shrub or grass. In the late growing season the trees have lost their leaves and grass and evergreens are absorbing the highest amounts of energy in the red band. In the abandoned farm land the grasses are not cut and are less vigorous throughout the growing season. The conifers are the only plants that will absorb some of the red light during the winter and the non growing season image can be used to differentiate them from other land uses. In addition lakes and non vegetative surfaces are distinguished by pixels that have NDVI values smaller than zero throughout the year.

To find the relative ranking of the "greenness" in the pixel, we divide the pixel NVDI values into four bins: High. Medium, Low and Negative. The boundaries between the bins are found by assuming that the high and low NDVI values can be represented by two normal distributions around their respective mean values. This is shown in Figure 3.4 where the plowed land pixels (NVDI values in May smaller than zero) and non vegetative surface pixels have been removed. Pixels with NDVI values greater than the highest mean are in the "high" bin for that particular image. Pixels with NDVI values lower than the lower mean but greater than zero are in the "low" bin. The remaining pixels with positive NDVI values are in the "medium" bin. Using this ranking system and the vegetative characteristics of each of the land covers discussed above, a scheme for identifying land covers shown in Table 3.1 were derived.

Based on the rules in Table 3.1, the NDVI based land cover for Town Brook watershed was made and shown on the left column of Figure 3.5. The NYCDEP 2001 landuse/landcover map (also derived from ETM+ data) is shown in the right column. The NYCDEP map had 16 land use categories that were lumped into 5 categories. Since the definition of abandoned agricultural land with shrub and forest is not obvious, we showed them together in the same map. The land cover maps are in general agreement with some differences in agricultural field boundaries. The NYCDEP map was corrected with tax parcel information while we did not use that information. The NYCDEP map had more forest than ours and this could have been caused by choosing the boundary between the high and medium bin that was too high in the NDVI method. Another

Table 3.1: Land cover NDVI signatures. The bold-printed entries are used for deciding the land cover type.

	Winter [January–April]	Early growing season [May]	Growing season [June–July]	Late growing season [October]
Non-vegetative	NDVI < 0	NDVI < 0	NDVI < 0	NDVI < 0
Forest (Evergreen)	**High**	*High*	*High*	*High*
Forest (Deciduous)	NDVI < 0	*Low*	**High**	**Low or medium**
Abandoned agricultural land	NDVI < 0	*Low*	**Low or medium**	**Low or medium**
Agriculture	Remaining pixels			

difference is the prediction of the area in conifers. The NYCDEP map showed that 10% of area was covered with conifers, while our NDVI map only indicated an area in the order of 1%. By using band 7 of the Landsat April image, which is particularly sensitive to leaf water content in dry weather, to estimate the areas with conifers, it appeared that the NDVI derived estimate was correct. Independent of what interpretation method is correct, the NDVI method is directly linked to plant growth characteristics (and evaporation rates) and is therefore desirable over the NYCDEP method for use in distributed hydrological models. In these models the ability to extract water from the ground is more important than the exact landuse.

Remotely sensed estimates of canopy stomatal conductance for regions around flux towers

D. Scott Mackay[1], Sudeep Samanta[2], Ramakrishna R. Nemani[3], and Brent E. Ewers[4]

[1]*Department of Geography, State University of New York, Buffalo, New York, USA*
[2]*Department of Forest Ecology and Management, Madison, Wisconsin, USA*
[3]*NASA Ames Research Center, Moffett Field, California, USA*
[4]*Department of Botany, University of Wyoming, Laramie, Wyoming, USA*

Terrestrial vegetation plays a central role in the response of the energy balance and composition of the atmospheric boundary layer to forcing, through evapotranspiration and controls on carbon sources/sinks. Plants, through the leaf stomata, regulate the rate of exchange of carbon and water between the land surface and the atmosphere. Canopy stomatal conductance, a measure of the rate of this gas exchange, is one of the most important variables needing to be simulated by land surface models, as it responds dynamically to the integrated effects of multiple stressors, forcing, and the local and regional consequences of global environmental change. Accurate representation of these dynamics and their prediction over seasonal, inter-annual, and decadal timescales at regional to global scales requires an ability to estimate canopy conductance over a large spatial extent at relatively short timescales (daily or more frequently). In this paper we develop a simple scheme for estimating canopy average stomatal conductance using remotely sensed land surface temperature to estimate vapor pressure deficit (D) over a regional extent, and flux tower data to estimate reference canopy conductance (G_{Sref}) derived from flux tower data. Slowly varying land use and land cover changes, climate changes, and environmental variables such as light, are associated with measurable adjustments to G_{Sref}, which will be updated using water flux data or MODIS land surface temperature (LST) data from a tower sites. A second timescale is associated with the periodic update (sub daily to daily) of MODIS land surface temperatures (LST) at a given tower site. A logic based on the complimentary relationship between potential and actual evaporation will be used to derive D at daily, and potentially down to 3-hourly timescales. The slowly varying G_{Sref} and rapidly varying D are then combined in a linear relationship based on plant hydraulic theory to obtain a mechanistic estimate of G_S. This assimilation logic will be evaluated using data from the WLEF AmeriFlux tower in northern Wisconsin, USA.

Theory It has been shown empirically [*Oren et al.*, 1999], explained mechanistically [*Ewers et al.*, 2000], and demonstrated in modeling studies [*Mackay et al.*, 2003a; *Katul et al.*, 2003] that plants that regulate leaf water potential to just prevent runaway cavitation obey the following relation:

$$G_S = G_{Sref} - m \ln D \tag{3.1}$$

where G_{Sref} is reference canopy stomatal conductance at vapor pressure deficit, $D = 1$ kPa and $m = dG_S/d\ln D \approx 0.6 G_{Sref}$ is the sensitivity of stomatal conductance to increasing D.

Vegetation indices are widely used to model regional and global vegetation dynamics. Similar remote sensing tools have yet to be developed for physiological parameters, such as canopy stomatal conductance. However, numerous studies have made strides towards this by relating foliage

temperature to transpiration [*Idso et al.*, 1978; *Nemani and Running*, 1989; *Carlson et al.*, 1995; *Norman et al.*, 2000]. *Mackay et al.* [2003b] showed that thermal remote sensing can detect vegetation responses that follow (3.1). *Hashimoto et al.* [2003] extended Granger's [1989] feedback link logic and demonstrated the feasibility of estimating daily average D by relating saturation vapor pressure determined at the surface temperature ($SVP(T_S)$) derived from MODIS or AQUA LST to ground-based estimates of D:

$$D = 0.32 \cdot SVP(T_S) \tag{3.2}$$

(3.1) and (3.2) are combined to estimate daily G_S. We first derived a set of optimized reference conductance parameters [*Mackay et al.*, 2003a] for a number of species using sapflux data from year 2000 as a basis for model evaluation. We then test the combined model using LST from MODIS during 2001 by evaluating the relationships between MODIS estimated G_S and sapflux estimated transpiration from 2001.

Methods The study was conducted in northern Wisconsin, near Park Falls (45.94°N, 90.27°W). The study area is a 12 km^2 region centered on a 447 m tall communications tower (WLEF tower). Sap flux was measured continuously in seven primary species [*Ewers et al.*, 2002]. These species represent over 85% of land surface area [*Mackay et al.*, 2002] around the WLEF tower. Four of the species, red pine, sugar maple, trembling aspen, and basswood, were selected for the present study to capture the full range of measured stomatal conductance at the site. We used the Terrestrial Regional Ecosystem Exchange Simulator (TREES; *Mackay et al.* [2003a]) and Adaptive Parameter Restriction and Selection (APRèS; *Samanta and Mackay* [2003]) to estimate reference conductance, G_{Sref}, for our tree species.

We acquired MODIS LST data for several days during 2001, as well as micrometeorological measurements of surface temperature and humidity from approximately 2.5 m above ground. MODIS data was acquired in a 5 km × 5 km window centered on the WLEF tower. For each date we screened for cloud cover in each of the 25 pixels within the window. Cloud pixels were removed. The cloud-free pixels were averaged to obtain LST estimates for the region. We determined $SVP(T_S)$ from MODIS LST and compared these estimates to the ground-based estimates of D. We then applied our site-specific relationship to estimate G_S.

Results The relation between measured D and $SVP(T_S)$ for WLEF (2001) was

$$D = 0.30 \cdot SVP(T_S) \tag{3.3}$$

Within the uncertainy of the data the slope of relationship 3.3 (0.30) is not significantly different from the slope (0.32) suggested by *Hashimoto et al.* [2003]. Furthermore, it is equivalent to results obtained at some of the AmeriFlux tower sites. We compared estimates of daily average canopy stomatal conductance from MODIS LST to sap flux estimates of transpiration for the four species. If the species are conforming to theory, and their stomata are regulating leaf water potential to just prevent runaway cavitation, then we should expect a decline in canopy stomatal conductance as the rate of transpiration increases. The results are shown in Figure 3.6. For each of the species there is a clear negative relationship between G_S and transpiration rate. We note that five data points per species is not sufficient to quantify the significance of the differences in slopes among the species, but it is sufficient to demonstrate the feasibility of deriving canopy stomatal conductance.

Conclusions A remote sensing logic for estimating daily canopy average stomatal conductance was presented. The logic combines MODIS land surface temperatures to obtain a daily estimate of vapor pressure deficit, and a simple model of canopy stomatal conductance that relies on a

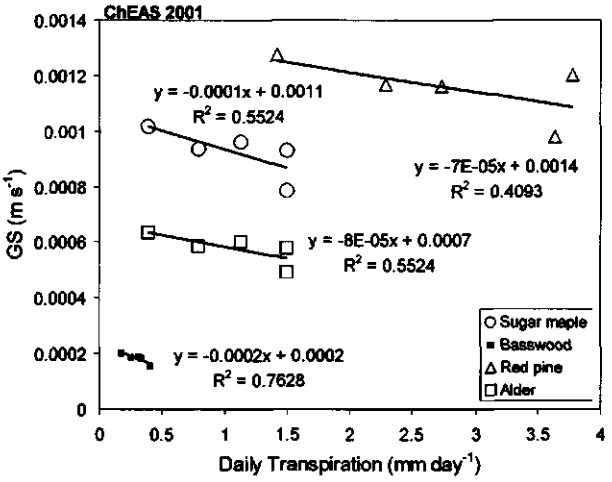

Figure 3.6: Canopy average stomatal conductance (G_S) versus daily transpiration measured with sap flux instrumentation.

single measurable parameter, reference stomatal conductance, and vapor pressure deficit. Based on the limited data used in this study we can conclude that MODIS-based estimates of canopy conductance can be consistent with hydraulic limitations that require stomata to regulate leaf water potential in response to increased rates of transpiration. This suggests that regional to global estimates of physiologically constrained canopy stomatal conductance on daily timescales is foreseeable. It is not clear based on the current data if MODIS can be used to resolve inter-species differences in the regulation of leaf water potential. A more extensive database is needed to address the question of how well we can identify species level responses, which would allow for estimates of transpiration and photosynthesis across species gradients without making extensive ground-based measurements.

Acknowledgements Support from NASA (NAG5-8554) and NSF (EAR-0405306) are gratefully acknowledged.

GEO_{TOP}: a distributed model of the hydrological cycle in the remote sensing era

R. Rigon[1], G. Bertoldi[1], T.M. Over[1], and D. Tamanini[1]

[1]*Dept. of Civil and Environmental Engineering - CUDAM, University of Trento, Trento, Italy*
[2]*Dept. of Geology/Geography, Eastern Illinois University, Charleston, Illinois, USA*

The study of the hydrologic cycle is physically focused on the analysis of the interactions between the soil surface (and specifically the soil water content, linked with precipitation) and the lower atmosphere, which occur mainly through the mediation of the soil itself, the vegetation, and the turbulent and radiative energy transfers which take place at the Earth's surface. In recent years, hydrologic research has evolved towards a comprehensive theory describing the exchanges of mass, energy and momentum between the land surface and the atmosphere over a range of spatial and temporal scales. The practical aims of this effort are: (1) to improve mid- and long-term hydrologic forecasts; (2) to increase our capability of describing the impacts resulting from changes in the soil use and climate on the hydrologic cycle and on the Earth's ecosystems.

In the last thirty years, several distributed hydrological models and, mostly independently, soil-atmosphere interaction models (also called land surface models, LSMs) have been developed. Event rainfall-runoff models, if data are available for calibration, are successful in modeling flood, but they are generally unable to simulate the baseflow afterwards and, obviously, to estimate evapotranspiration. Vice versa, LSMs represent soil-atmosphere interactions with different degrees of complexity and accuracy, but they are not endowed with a detailed representation of runoff and lateral fluxes, as they have been developed mainly to provide a land-surface interface in support atmospheric global circulation models (GCMs).

A new distributed hydrological model, GEO_{TOP}, which aims at estimating in an integrated way the runoff and energy fluxes in small basins is presented here. It can be seen both as a continuous-time rainfall and snowmelt-runoff model capable of simulating the hydrological cycle and as an attempt to incorporate in LSMs an adequate treatment of hydrological variability at small scales (in particular the effects due to different land uses, complex topography, and the structure of the channel network). The model, like a rainfall-runoff model, calculates the discharge of a watershed; moreover, it estimates the surface and subsurface water fluxes, the water table depth, and the value of the matric potential in both the saturated and the unsaturated soil. Like an LSM, it estimates the local values and the spatial distribution of numerous hydro-meteorological variables like soil moisture, surface temperature, radiative fluxes and heat fluxes into the soil. Furthermore, it computes the evolution of the snow cover distribution and the surface snow temperature following the methodology of *Tarboton and Luce* [1996].

GEO_{TOP} is a terrain-based model, i.e., it is based on the employment of Digital elevation models (DEMs); it is a distributed model, since all the simulated variables are returned for each grid cell in the basin; it is a model of the full hydrological cycle, in the sense that it simulates not only the mass balance but also the energy balance: in fact the two balance equations are coupled by the evapotranspiration terms and by the soil temperature, which controls the soil hydraulic conductivity and the evolution of the snow cover.

In modeling the soil-atmosphere interaction, GEO_{TOP} follows the treatment initially developed by *Deardorff* [1978], and then implemented, with numerous changes, in LSMs either at the global

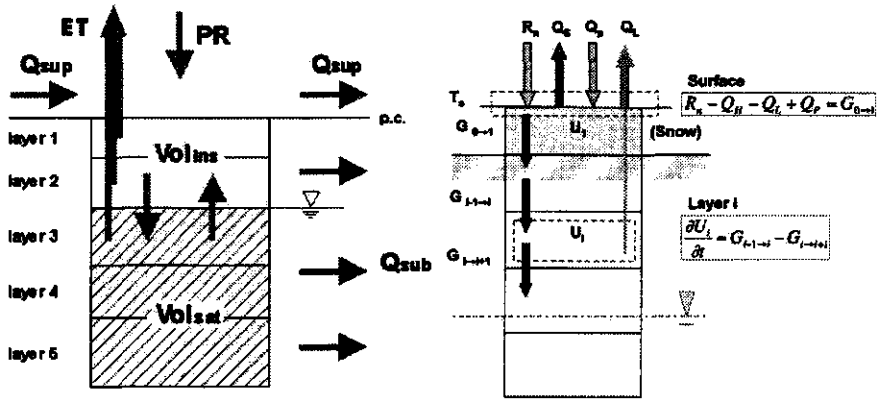

Figure 3.7: **Left:** Scheme of the water flows in the GEO_{TOP} model. For every cell precipitation (P) is partitioned in evapotraspiration (ET), sub-surface runoff (Q_{sub}) and overland flow (Q_{sup}). Both the saturated and unsaturated part contribute to the lateral flow. The dynamic balance between lateral and vertical flows determines the water table depth. **Right:** energy balance scheme in GEO_{TOP} (compare equations 3.4 and 3.5). U_i is the i-thlayer's specific energy , R_n the net radiation, Q_l the latent heat flux, Q_s the sensible heat flux, Q_p the precipitation heat influx, $G_{e,i\rightarrow i+1}$ the heat flux exchanged between soil layers, that includes also the snow melt heat flux Q_m (if snow is present).

scale - like BATS [*Dickinson et al.*, 1986] and NCAR-LSM [*Bonan*, 1996] - or at regional scale - like VIC [*Liang et al.*, 1994] or at basin scale - like DHSVM [*Wigmosta et al.*, 2002], to cite a few. However, GEO_{TOP} differs from most of these models because it integrates the whole energy balance equation and it is able to give directly in its output those optical features such as brightness temperatue, that are measured from remote sensors.

The model calculates the energy balance as a function of the soil (or snow layer) specific energy. The heat flux in the soil (or snow) is calculated through the integration of the heat conduction equation, with an implicit scheme on an arbitrary number of layers. The snowpack (if present) is represented by the first two layers, of which the upper one has infinitesimal thickness and is used only to calculate the snow surface temperature. For the generic i-*th* layer the energy balance equation is:

$$\frac{\Delta U_i}{\Delta t} = G_{e,i-1\rightarrow i} - G_{e,i\rightarrow i+1}, \tag{3.4}$$

where t is time as independent variable, U_i the internal energy of the i-*th* layer, $G_{e,i-1\rightarrow i}$ and $G_{e,i\rightarrow i+1}$ are respectively the heat fluxes exchanged between the i-1*th* and the *ith* layer (positive according to the arrow) and between the *ith* and the i+1*th* layer. The fluxes G_e include the heat flux exchanged by thermal conduction (due to temperature gradients) and the heat flux advected by mass transport (for example if snow on the surface is present, also the heat coming from snow melting Q_m is included). If i is equal to 1, $G_{e,0\rightarrow 1}$ is the heat flux from the atmosphere to the surface soil (or snow) layer, which is calculated solving the surface energy balance:

$$G_{e,0\rightarrow 1} = R_n - Q_s - Q_l + Q_p \tag{3.5}$$

where R_n is the net radiation, Q_s is the sensible heat flux and Q_l the latent heat flux (both positive towards the atmosphere) and Q_p is the heat flux advected by precipitation. All terms (except Q_p) are function of the soil surface temperature, which is unknown and is calculated solving the surface energy balance with an iterative scheme.

Radiation is separated into its long- and short-wave components, each of which have diffuse, direct and reflected sub-components, both emitted by land and shielded by cloud cover. Effects on radiation due to topography are also taken into account: shadowing, reduction of the sky view factor, and variation in net radiation as result of aspect and slope.

The vegetation is represented by a one-layer canopy model [*Garrat*, 1992]. The root fraction of each soil layer *i*is calculated decreasing linearly from the surface to a maximum root depth, depending on the cover type. The canopy resistance r_c depends on solar radiation, vapor pressure deficit, temperature as in *Best* [1998] and on water content in the root zone as in *Wigmosta et al.* [1994].

The flow of water in the unsaturated zone in GEO_{TOP} is computed solving numerically the Richards' equation, which makes it possible to describe also the transients of flow and infiltration generated by the dynamics of the suction potential gradient, not just the flow generated by the topographic gradient. The use of Richards' equation also does not make any assumption of stationary conditions in subsurface flows (as is assumed, for example, in *Beven and Kirkby* [1979]).

The numerical schematization of the model inherits the knowledge acquired starting from Freeze's studies [1978] and it is in some aspects similar to that implemented in the SHE model [*Abbott et al.*, 1986] and in the SHETRAN [*Ewen et al.*, 2000]. The basin surface is divided into cells that can be vertically divided in an arbitrary number of levels. As a boundary condition at the bottom, it is possible to impose a known value of the potential, a known gradient or an impermeable surface. All the basin properties can be defined in a completely distributed way; in particular, soils can be chosen to differ in profiles and depth in every cell . To calculate the soil hydraulic properties the *Van Genuchten* [1980] model is used, whose parameters can be derived from the soil texture by means of the pedotransfer functions proposed by *Vereecken et al.* [1989]. The hydraulic conductivity is expressed as a function of the water content as in *Mualem* [1976].

The vertical infiltration is described taking in account the surface fraction actually covered in water, supposing the presence of micro-relief in the terrain, parameterized by a surface roughness. The water redistribution is determined on the basis of the total head gradient according to the Darcy law. All the basin's cells are designated as either channel or hillslope cells. The surface runoff in the hillslope cells is described as a series of uniform motions following a kinematic scheme, according to the relation:

$$v_{sup} = C_m \, h^{\gamma} \, i^{0.5}, \tag{3.6}$$

where C_m is a resistance coefficient, R_H is the surface water thickness, i the local slope and γ is variable also as a function of the runoff phenomena geometry. The connectivity among the cells is described by a scheme with eight drainage directions, and water that runs off one cell and onto another, can it then infiltrate. The motion in the channels is described by the convolution of the incoming discharge with the solution of the de Saint-Venant parabolic equation found by *Rinaldo et al.* [1991].

The model has been applied and tested in various basins of Trento Province in Italy and in some experimental basins in USA [*Bertoldi et al.*, 2002; *Bertoldi*, 2004]. The models code is fully documented in *Bertoldi and Rigon* [2004], and it will be realesed as Open Source project by the end of 2004.

Towards understanding the spatial and temporal distribution and dynamics of soil organic carbon within a large temperate agricultural catchment

Barry Jacobs[1], Jetse Kalma[1], Greg Hancock[2], Manju Hemakumara[1], Jeffrey Walker[3], and Garry Willgoose[4]

[1]*School of Engineering, University of Newcastle, Callaghan, Australia*
[2]*School of Science and Information Technology, University of Newcastle, Callaghan, Australia*
[3]*Department of Civil and Environmental Engineering, University of Melbourne, Parkville, Australia*
[4]*School of Geography, University of Leeds, Leeds, UK*

Soil carbon has considerable temporal and spatial impacts on the ecohydrological state of all catchments. Total organic carbon, land use, climate, and soil physical and chemical properties are being monitored at 26 sites within a 7000 km^2 temperate agricultural catchment in south eastern Australia, to investigate total organic carbon dynamics. Preliminary results from multi-variable statistical analyses of data obtained during the first 6 months of an 18 month study are presented. The primary research goal is to understand and quantify point and catchment carbon stocks using relationships between remote sensing and other readily available data. This paper includes discussion of preliminary attempts to upscale point and hill slope data to the catchment scale.

Introduction Soil organic carbon (SOC; the entire organic fraction including undecomposed and decomposed plant and animal organic debris) is a major component of the global carbon store, containing nearly three times the carbon stored in the atmosphere and four times the carbon contained in terrestrial vegetation. Human activity has resulted in atmospheric CO_2 concentrations increasing at approximately 0.5 to 3 ppm annually [*Keeling and Whorf*, 2001], with increased levels being a known cause of global warming. Therefore management of soil carbon has significant potential to slow the build up of atmospheric CO_2. The global response to increasing atmospheric CO_2 concentrations is highlighted by the development of the Kyoto Protocol [*UNFCCC (United Nations Framework Convention on Climate Change)*, 1997], and the focus on CO_2 sequestration opportunities in an effort to mitigate emissions, particularly within the agricultural sector.

SOC has significant impacts and benefits on the physical, chemical and biological properties of soils. First, soil organic matter (SOM) retains up to 20 times its weight in water, and improves drainage and permeability [*Delgado and Follett*, 2002]. A catchment's SOM status therefore has significant hydrological impacts by affecting the soil moisture status, surface runoff, and subsurface flows; factors rarely (if ever) included in hydrology models. Second, SOM affects soil aggregation and the stability of aggregates [*Coffin and Herrick*, 1999]. It thus plays a critical role with regard to the susceptibility of soils to erosion [*Phillips et al.*, 1993], serves as a store for nitrogen, phosphorus and sulfur [*Delgado and Follett*, 2002], and plays a role in the cycling of essential nutrients [*Delgado and Follett*, 2002].

Despite current knowledge of the impacts and benefits of SOC, significant gaps remain in our knowledge of carbon cycle dynamics. The knowledge gaps most relevant to this study include: (1) The lack of a fundamental understanding of SOC dynamics at the molecular, landscape, regional, and global scales [*Metting et al.*, 1999; *Quideau et al.*, 2001]; (2) Uncertainty in the magnitude

and timing of the response of the soil carbon reservoir to changes in climate, land-use and land cover [*Wang and Hsieh*, 2002]; (3) The paucity of data documenting erosional SOC losses and the fate of eroded SOC [*Jacinthe and Lal*, 2001]; (4) Limited information about organic carbon export from agricultural catchments [*Jacinthe and Lal*, 2001]; and (5) The lack of data for specific runoff events of SOC losses to enable calibration of empirical models, including a need for more detailed analyses of particle size distributions and densities of SOC within nested catchments [*Starr et al.*, 2000].

This paper reports on research concerning total organic carbon (TOC; that fraction of SOC which passes through a 2 mm sieve excluding all fine roots) from hydrological and scaling perspectives, and addresses the above knowledge gaps to various degrees. The research investigates spatial and temporal dynamics of TOC based on an analysis of field based, remotely sensed, and GIS data. The aim is to identify relationships that allow quantification of TOC at any point within a catchment, from routinely measured parameters such as soil type (specifically the proportion of clay); long term climate (with soil moisture and temperature being driving forces of biomass decomposition); the position in the landscape (for erosional and depositional effects); vegetation and/or land use (biomass for the input of carbon); and anthropogenic site history (including cultivation). Any longer-term change in TOC, the dynamical perspective, is expected to be a function of antecedent TOC; land use change; and climatic change. Shorter-term changes will be influenced by environmental factors including recent rainfall and perhaps recent tillage operations. Specific research objectives include: (1) assessing temporal patterns in measured and predicted TOC at monitoring sites; (2) upscaling and integration of these TOC distributions to assess spatial patterns and to determine total catchment carbon stocks; and (3) analysis of soil carbon storage for various land use and climate change scenarios. Data from an intensive network of monitoring sites are used to develop and evaluate predictive relationships for hillslope and subcatchment TOC dynamics in the top 300 mm of the soil profile.

Field Data The 7000 km^2 Goulburn River Catchment is a mixed grazing and cropping region located 200 km west of Newcastle in south eastern Australia. Figure 3.8 shows the catchment, its 10 major subcatchments and the 26 permanent monitoring sites used in the present study.

The mean annual rainfall over the past 100 years was 660 mm $\pm$ 200 mm (Bureau of Meteorology data). The maximum and minimum annual rainfalls over the same period were 1318 and 334 mm respectively. As a result, most rivers and streams in the Goulburn River Catchment are ephemeral. The region has encountered severe drought conditions in recent years; a factor that will be considered in the evaluation of current TOC distributions.

From an agricultural perspective, land use in the Goulburn River Catchment becomes marginal if years with significantly lower than average rainfall become a regular occurrence, resulting in semi-arid conditions across the region. Recent trends towards lower rainfall may be associated with natural and/or human induced climate change and variability.

The catchment is dominated by sandy soils in the south and heavy basalt clay soils in the north. The southern half retains large tracts of native eucalypt forest, whereas the majority of the north of the Goulburn River Catchment has been extensively cleared of natural vegetation with the lower slopes and areas adjacent to riparian zones comprising native or improved pastures interspersed with eucalypts. These different soil, vegetation and climate conditions result in a wide range of ecophysiological diversity.

The research utilises the unique data set of the "Scaling and Assimilation of Soil Moisture and Streamflow" (SASMAS) project currently being conducted in the Goulburn River Catchment. Precipitation, soil and air temperatures, soil moisture, and stream flow are monitored continu-

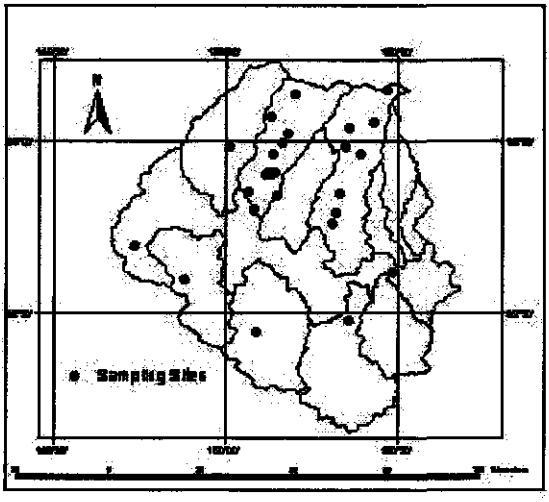

Figure 3.8: Major subcatchments and permanent monitoring sites within the Goulburn River Catchment.

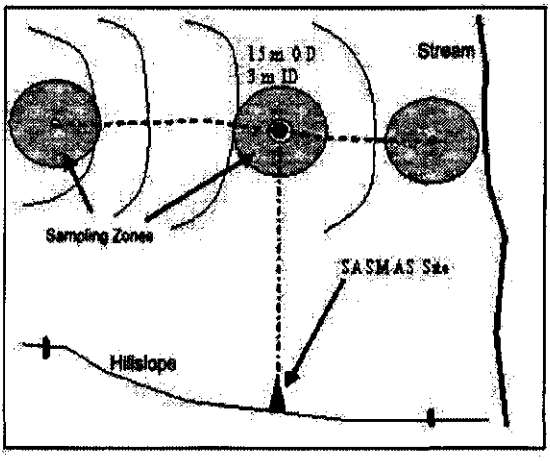

Figure 3.9: Schematic of hill slope transect studies.

ally across the network of monitoring sites*. Land form, land use, soil physical and chemical properties, and vegetation data (living and litter) have been obtained from GIS data sets, and are supplemented with data from a number of intensive field campaigns. Soil samples 50 mm in diameter and to a depth of 300 mm are collected at 6-weekly intervals over an 18 month period from each of the 26 monitoring sites. The sites have unique combinations of soil type, soil depth, biomass, soil moisture, soil temperature, and terrain characteristics. Samples are being collected each trip from 3 randomly generated vectors within a 15 m radius of each monitoring site. This

*see http://www.civenv.unimelb.edu.au/~jwalker/data/sasmas

allows investigations into local scale variability as well as assisting in bias removal. Additional samples are being collected quarterly from 3-point hill slope transects for 10 of the 26 sites. The data are being used for lateral transport studies. The transects are shown generically in Figure 3.9.

All samples are being analysed for TOC, nitrogen, pH, conductivity, and soil physical parameters (bulk density, field capacity, porosity, hydraulic conductivity). The combined data sets are analysed using multi-variable statistical techniques to determine and calibrate relationships for TOC prediction.

Results This paper presents preliminary results of the spatial and temporal variability of TOC within the Goulburn River Catchment from six temporal samples of TOC for all 26 monitoring sites, and two temporal samples of hill slope transect data. Preliminary multivariate statistical and graphical analyses of the data sets for each site will be presented including the dominant impacts of each of the parameters on TOC levels and distributions. Preliminary results will also be presented of biomass assessments based on remote sensing as well as initial erosion risk analyses for the selected hill slopes. We will report on the development of relationships between TOC and a range of static and dynamic site characteristics, and explore strategies for how these relationships may be used with remote sensing and GIS data to predict TOC levels at any point in space and time in the Goulburn River Catchment, without needing expensive field and laboratory data.

One complete set of TOC data for the 26 monitoring sites has been determined. These showed that minimum and maximum TOC levels within the Goulburn River Catchment were 0.39% and 5.7% respectively. The mean for all sites was $2.45\% \pm 1.42\%$. These values were within the range commonly reported in literature for similar climate and land use systems. Although one data set is insufficient for the identification of temporal patterns and trends there was an apparent correlation between soil texture and TOC. The sandy sites had lower TOC values and heavy clay sites had higher values. This is potentially due to the sandy soils having a lower sequestration capability due to a much smaller clay component, and the free draining nature of those soils. This was an expected result.

Acknowledgement This project is funded by ARC Discovery Grant DP 0209724.

Retrieval of model grid scale heat capacity using satellite land surface temperature tendencies

William M. Lapenta[1] **R.T. McNider**[2], **A.P. Biazar**[2], **G. Jedlovec**[1], **and J. Pleim**[3]

[1]*NASA Marshall Space Flight Center, USA*
[2]*University of Alabama, Huntsville, USA*
[3]*Air Resources Laboratory/NOAA, USA*

In both atmospheric and hydrologic model, the behavior of the surface energy budget can be critically dependent on the magnitude of the effective grid-scale bulk heat capacity. Yet, this parameter is uncertain both in its value and in its conceptual meaning for a model grid in heterogeneous conditions. Current methods for estimating the grid-scale heat capacity involve the areal/volume weighting of heat capacity (resistance) of various, often ill-defined, components. This can lead to errors in model performance in certain parameter spaces.

A technique suitable for recovering bulk heat capacity using time tendencies in satellite retrieved land surface temperature has been developed and tested. It is formulated based on previous studies that show that surface temperature is most sensitive to thermal inertia in the early evening hours. The retrievals are made within the context of a surface energy budget in a regional scale model (MM5). The paper will present results from two uniquely separate applications. The first is within the context of an operational model framework with emphasis on a 48 h simulation. The second is within the context of a week-long simulation conducted with continuous dynamic nudging in the free atmosphere for the purpose of conducting air quality simulations.

On the need to preserve hillslope form and processes within large-scale models

P.W. Bogaart[1], J. Boll[2], and P.A. Troch[1]

[1]*Hydrology and Quantitative Water Management Group, Wageningen University, Wageningen, The Netherlands*
[2]*Department of Biological and Agricultural Engineering, University of Idaho, Moscow, Idaho, USA*

Currently the role of lateral flow and structured spatial variability is underestimated within land surface schemes [*Wood*, 1999]. We study the impact of this hillslope scale variability in hydrologically relevant landscape parameters on large-scale hydrological behavior. Hillslope geometry (mainly slope gradient and soil depth) and soil hydraulic properties (hydraulic conductivity and drainable porosity) can be expected to vary in consistent ways along hillslopes (catenas) as the result of topography controlled soil formation and geomorphic processes.

Based on ongoing field investigations in the Troy (Idaho) catchment, we set up downhill gradients of input parameters of a catchment-scale semi-distributed hillslope-storage Boussinesq model, which is based on the hydraulic groundwater theory [*Troch et al.*, 2003]. By systematically varying the downhill trends in one, some, or all of these input parameters, we determine the effect of structured spatial variability on the shape of a characteristic (e.g. unit) hydrograph.

Although not explicitly modeled, the subsequent effect on land surface-atmosphere energy exchange is assessed by making assumptions on the relationship between hydrograph shape and/or statistics and the separation of rainfall into stream runoff and evapotranspiration. Other potential fields of application are ecology (e.g. soil moisture) and hydrogeology (e.g. aquifer recharge). Our presentation is intended to revive the discussion on the importance of hillslope form and subsurface lateral flow in large-scale models.

Role of bedrock heterogeneties and soil thickness on the saturation overland flow dynamics in headwater catchments: field observation and simulation using a distributed hydrological model

G. Bertoldi[1], W.E. Dietrich[2], N.L. Miller[3], and R. Rigon[1]

[1]*Dept. of Civil and Environmental Engineering - CUDAM, University of Trento, Trento, Italy*
[2]*Dept. of Earth and Planetary Science, University of California Berkeley, Berkeley, California, USA*
[3]*Earth Sciences Division, Lawrence Berkeley National Laboratory, California, USA*

Most of the models used to reproduce the runoff at hillslope scale and at small-catchment scale are based on the assumption that the sub-surface runoff flows following the bedrock topography, often considered impermeable and parallel to the surface. Another common hypothesis is that the motion can be described as a function of the only topographic gradient rather than of the total hydraulic head gradient. In this contribution, to understand the role of bedrock permeability and soil thickness on the saturation overland flow dynamics in headwater catchments, the distributed hydrological model GEO$_{TOP}$ [*Bertoldi and Rigon*, 2004; *Bertoldi*, 2004] has been applied to a small catchment (2.3 ha), located in the Mount Tamalpais State Park in Marin County, California, USA.

The basin is constituted by two hollows with deep colluvial sandy and gravelly silt soil (from 2 to 5.5 m) and by sideslopes with a thin soil thickness (from 0.2 up to 0.7 m). The bedrock is constituted by strongly fractured sandstone with some more solid blocks close to the channel beginning. The first 2 meters of rock are strongly weathered. The basin has been monitored and instrumented with over 100 piezometers, two raingages and a weir in the years 1985-1986 by *Wilson and Dietrich* [1987]. The soil thickness has been measured by means of seismic refraction [*Dengler and Lehre*, 1987]. Hydraulic conductivity has been measured into the piezometers holes, both in the soil and in the bedrock. Conductivity decreases with depth, but a clear distinction between soil and bedrock conductivity does not emerge. During the precipitation periods, data regarding rainfall, pressure, runoff and saturated area have been collected manually every 6 hours.

During the 1985–1986 wet season, there was an intense storm, on which the present study focuses, from 11 February to 21 February. The precipitation observed has been 440 mm in the basin. The peak discharge was 40 $l s^{-1}$ 6 days after the beginning of the precipitation with a 4-hour delay with respect to the greatest rainfall intensity. The saturated area expands during the event involving both hollows completely. The pressure in the piezometres starts increasing about 1 day after the beginning of the event: its peak is after 6 days and corresponds to the greatest superficial saturation, with a maximum exfiltration gradient in the hollows of 0.87 m. The study of *Wilson* [1988] has recognized a motion field where the fractured bedrock contribution appears significant. In the hollows the water table is close to the surface inside the colluvium also in the periods distant in time from precipitation. During most of the storm, local exfiltration gradients occur, associated with bedrock heterogeneities. In the hillslopes, on the contrary, the water table is deeper than the bedrock and during the precipitation a perched water table does not form at the soil-rock interface, but the water filters rapidly into the fractured rock, with a strongly transient response in pressure in the bedrock and in the colluvium.

Simulations with the GEO$_{TOP}$ model have been performed under different conditions, with a uniform soil thickness, with a measured soil thickness and with different degrees of bedrock perme-

ability. A 20 m-deep soil layer, divided in 8 levels, has been used, with *Van Genuchten* [1980]'s parameters for a silty-sandy terrain. The conductivity profile has been chosen on the basis of the data measured. The simulations show how the hollows are partly saturated while hillslopes are quite dry, at the beginning of the flood. This different behavior lasts during the whole event, when the saturated area in the hollows grows, but hillslopes remain unsaturated. The moisture profile in the hillslopes in fact shows that there is no formation of a perched water table between rock and soil, as supported by observations. In the hillslopes, the strong decrease in conductivity with depth allows little interaction between the water table and the surface runoff.

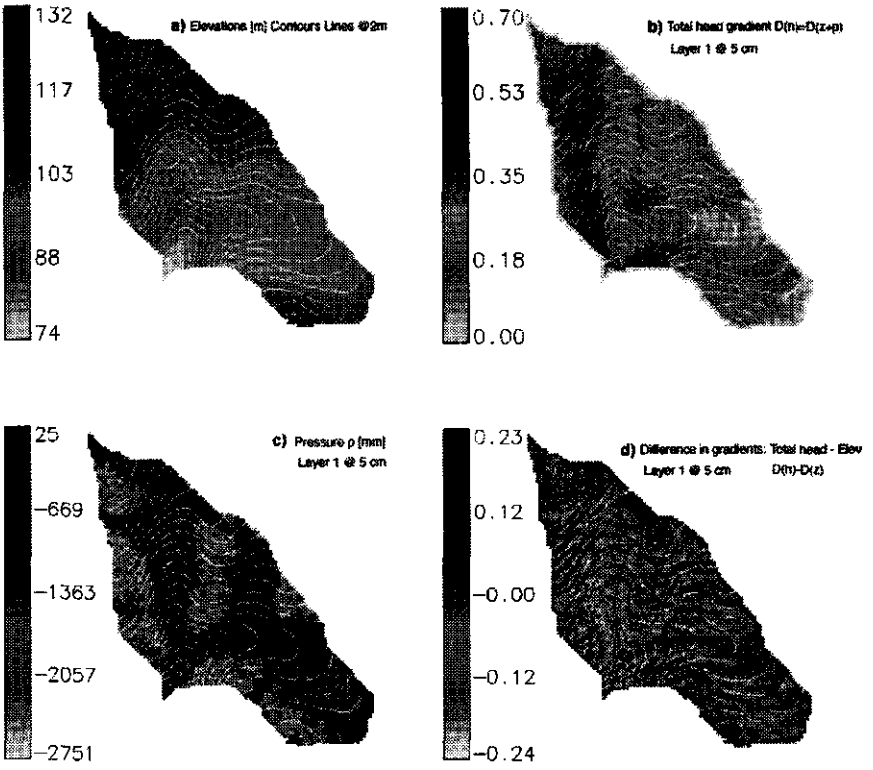

Figure 3.10: a) Map of basins elevation h [m]. b) Distribution, in the day before the maximum saturation, of the of the total gradient $\frac{\partial(\psi+z)}{\partial x}$, expressed as a fraction, in the first 5 cm soil. c) Distribution of the suction potential field ψ [mm], in the first 5 cm soil. d) Distribution of the contribution of the suction potential $\frac{\partial \psi}{\partial x}$ to the total gradient $\frac{\partial(\psi+z)}{\partial x}$, expressed as a fraction. The basin contour lines are superimposed. Green colors indicate negative contributions, which slow down the motion, violet colors indicate positive contributions, which accelerate the motion. There is a negative contribution along the hollow border (red line) and positive areas in the upper hillslope zone (black line).

If we impose in the model the measured soil thickness, with a permeability value in the bedrock far lesser than that of the soil ($K = 10^{-7}$ m s^{-1}), it is not possible to simulate the flood wave in a correct way. The small soil thickness present in the hillslopes indeed saturates quickly, with

the formation of too much surface runoff by saturation. The presence of a permeable bedrock then results determinant to obtain the delay observed in the hydrologic response. The degree of hillslope-hollow disconnection increases as the bedrock permeability increases.

The suction potential distribution ψ is probably the most interesting information provided by the model. Its distribution is connected to the water content distribution, with positive values in the saturated hollows and negative values in the unsaturated hillslopes, as shown in Figure 3.10c. Although the total load gradient along the drainage direction $\frac{\partial(\psi+z)}{\partial x}$ (Figure 3.10b) is strongly linked with the topographic gradient $\frac{\partial z}{\partial x}$, the potential gradient contribution $\frac{\partial \psi}{\partial x}$ to the total gradient is not negligible (Figure 3.10d), with increases and decreases up to 20% out of the total gradient. Along the border of the saturated area there is an uphill water contribution, thus contributing to the saturated area expansion. Moreover in Figure 3.10d one can notice that, in the convex zones in the upper part of the hillslopes, there is a contribution accelerating the downhill flow. Only once this wet band moves across the entire hillslope can the latter contribute to the basin response in terms of surface runoff.

To conclude, the model is able to reproduce the runoff mechanism observed, confirming the importance of considering the flow inside the bedrock in order to reproduce the basin response. The assumption of an impermeable bedrock determines an overestimate of the discharge. Hillslopes and hollows have a different behavior, with infiltration into the bedrock for the former, and surface water table in the latter. Although the surface runoff by saturation plays an important role in providing water to the channel along the hollow, probably this is not the mechanism responsible for the flowing of the water from the basin head and the hillslopes to the hollow axis.

The simulations suggest that the hypothesis that a perched water table forms in the hillslopes, with sub-surface runoff at the soil-bedrock interface, is valid only in the case of an actual contrast between rock and soil permeability. Lastly, the model shows that a significant contribution to the saturated area expansion is given by the potential suction gradient, which forms at the interface between unsaturated hillslopes and saturated hollows, and that this can influence the response times of small unchannelled basins.

Multiscale parameterization strategies for a spatially distributed hydrological model

N. Chahinian[1], R. Moussa[1], M. Voltz[1], and P. Andrieux[1]

[1]*Institut National de la Recherche Agronomique, Laboratoire d'étude des Interactions entre Sol, Agrosystème et Hydrosystème, Montpellier, France*

To predict the effects of land-use change on a heterogeneous catchments, one needs to use spatially distributed hydrological models. Although it was once sufficient to model only catchment outflow, growing concerns in pollution and water management require outputs at various points in a catchment, taking into account both surface and groundwater flow as these are the driving mechanisms of solute and sediment transport. These processes are very sensitive to the hydraulic properties of the soil surface and the channel network. The objective of the present study is to formulate and analyse a parameterisation strategy for the soil surface hydraulic properties used in infiltration-runoff models across scales on heterogeneous catchments. The methodology used herein is based on both experimental and modelling approaches at various scales. It consists first on identifying the main local features controlling infiltration and runoff at the local scale and suggesting a proper representation in the distributed model. The second step consists in the transfer of information from the local to the catchment scale through a spatial distribution scheme. The Roujan experimental catchment is used to illustrate our methodology. Three different scales are hence studied: the local scale of a single ring infiltration experiments (100 cm^2) used to identify soil hydrodynamic properties, the plot scale (1000 m^2) which is the management on farmed catchments and the small catchment scale (1 km^2) which represents the elementary scale of flood genesis. First, soil hydrodynamic properties are identified at the local scale of the ring infiltrometer. Then these values are used in infiltration-runoff models to simulate hydrographs at the plot and the catchment scales. Various physically-based infiltration-runoff models and various strategies of spatialization of the soil hydraulic properties are compared. Multiscale calibration and validation approaches are used. Finally, a comparison of the values of the soil hydraulic conductivity obtained for the various scales and for the various approaches of calibration is undertaken in order to analyse the results function of the scale of use of the models. In the following sections, we present the main characteristics of the studied site, the hydrological models, the parameterisation procedures and describe the main results.

The study site The study area is the farmed Roujan catchment (0.91 km^2) located in Southern France [*Andrieux et al.*, 1993; *Voltz et al.*, 1994]. The catchment is mainly covered by vineyards and is divided into 237 plots. The major runoff events are usually caused by high-intensity short-duration storms, and are well representative of the hydrology in the Mediterranean zone. The main hydrological processes are runoff and infiltration at the field scale and the ground- and surface-water exchange through the ditch network at the catchment scale. The drainage network is formed by man-made ditches and generally follows agricultural field limits. Two main runoff control features are identified: soil surface crusts that limit infiltration and tillage operations that increase infiltration.

The basic instrumental design of the catchment consists of rain gauges, stream flow recorders, piezometers and tensio-neutronic sites. Experiments were undertaken at the local scale of a simple ring infiltration in order to identify soil hydrodynamic properties. Then, in an attempt to describe

spatial variability of runoff, discharge is measured at three gauging stations at the outlets of the catchment (0.91 km^2), a crusted plot (1200 m^2) and a tilled plot (3240 m^2). The sensors are read every minute. A network of piezometers has also been installed to measure the spatial variation of the water table at 10 minutes intervals.

The hydrological models used across scales At the local ring infiltrometer, the HYDRUS 2D two-dimensional vertical infiltration model [*Šimunek and Van Genuchten*, 1996] was used in inverse mode to estimate the soil hydrodynamic properties.

Moving up at the plot scale (the non-tilled and tilled plots), a rainfall-runoff model coupling a production function to a unit hydrograph transfer function, was used to simulate overland flow hydrographs. Three physically based production function models are compared: Richards-1D [*Richards*, 1931], Morel-Seytoux [*Morel-Seytoux*, 1978] and Philip [*Philip*, 1957] model. These models differ by their mathematical structure while input hydrologic data and the soil hydraulic properties used are the same.

Finally at the catchment scale, the MHYDAS distributed model [*Moussa et al.*, 2002] was used. The model subdivides the basin into "hydrological units" taking into account the hydrological discontinuities of farmed catchments. Over each hydrological unit, MHYDAS simulates Hortonian mechanisms of overland flow using one of the three production functions studied above. Infiltrated water is assumed to flow vertically through an unsaturated layer from where it can flow to the groundwater. The flow exchange between the ditch network and the groundwater is calculated using a simple Darcian model. The unit hydrograph is used to route surface runoff at the scale of each hydrological unit, and the diffusive wave equation is used for flood routing through the ditch network. Evaporation is not represented since the purpose of the model is to simulate individual flood events. The model is most sensitive to the following parameters; the hydraulic conductivity at natural saturation K_s of the hydrological units, the exchange coefficients between the reaches and the groundwater, and the average value of the Manning coefficient in the ditch network.

The parameterisation procedure The calibration process was subdivided in three main steps corresponding to each spatial scale.

First, the soil hydrodynamic properties were identified at the local scale using a simple ring infiltration experiments (14 cm ∅). Two separate single ring infiltration experiments were undertaken [*Chahinian et al.*, 2004b]. The first was performed on the undisturbed soil whereas the second was done after removal of the soil surface crust. HYDRUS 2D was then used, in an inverse modeling approach, to estimate first the soil hydraulic properties of the crust and the subsoil, and then the effective hydraulic properties of the soil represented as a single uniform layer. The results showed that the crust hydraulic conductivity (6 $mm\,h^{-1}$) is five times lower than that of the subsoil (29 $mm\,h^{-1}$) thus illustrating the limiting role the crust has on infiltration.

The second step concerns the plot scales. Two cases were distinguished, the crusted plot characterised by invariable surface features all round the year and the tilled plot characterised by variable surface features function of rain occurrence. Fourteen flood events were used for calibration and fourteen for validation:

- On the crusted plot, the use of the Richards-1D production function coupled to a transfer function shows that the representation of the soil as a single uniform layer gives similar results as the representation of the soil in a double layer (crust and the subsoil). The hydraulic conductivity at natural saturation (K_s) of the crust and subsoil considered as a homogeneous layer is 10 $mm\,h^{-1}$. When calibrating K_s for Morel-Seytoux's and Philip's models, results show that the values range between 3 and 5 $mm\,h^{-1}$ depending on the calibration criteria (runoff volume, peakflow, or Nash and Sutcliffe criteria; *Chahinian et al.* [2004a]). The

calibrated values of K_s are 50 to 70% lower than the values identified at the local infiltrometer scales. Finally, the comparison of the three models (Richards-1D, Morel-Seytoux and Philip) performance at the plot scale shows that all three models give accurate results and that the calibration of soil hydrodynamic characteristics in Morel-Seytoux's model improves the quality of simulations and reduces the time of calculation in comparison to Richards' model.

- On the tilled plot, the transient nature of soil surface properties needs to be taken into account. The calibration procedure consists first in calibrating the K_s for each flood events, then in defining simple mathematical laws describing the evolution of K_s in time. Results show that the value of K_s decreases from a value of 25 mm h^{-1} just after tillage to a threshold value around 4 mm h^{-1} function of the total rainfall amount after tillage.

Finally at the catchment scale (1 km^2), three strategies for spatializing K_s over the 237 plots were compared [*Chahinian*, 2004]: (1) by calibrating a unique value of K_s for all hydrological units, (2) by spatializing K_s using the calibrated values at the plot scale and (3) by using values of K_s obtained from rainfall simulations. For each strategy, the other parameters of the model (the exchange coefficients between the groundwater and the ditches and the value of the Manning coefficient) were calibrated using the measured hydrograph at the outlet of the whole catchment. Results show that the spatialized strategies give better results than the global one. The K_s calibration for both crusted and tilled plots improves the quality of simulated hydrographs both on the eleven calibration events and on the six validation events. The calibrated K_s values at the catchment scale are 20% higher than those calibrated at the plot scales. When calibrating each flood event individually, the K_s values fluctuate between 0.5 to 12 mm h^{-1} on the crusted plot and vary by $\sim$ 70% on the tilled plot.

Conclusions The aim of this study is to suggest and compare various parameterization strategies for runoff-infiltration models across scales on heterogeneous catchments. The studied scales are the local ring infiltrometer, the plot and the small catchment scales. The sensitivity analysis shows that the rainfall-runoff models, used at both the plot and the catchment scales, are very sensitive to the soil surface hydraulic conductivity. At both the local and the plot scale, results show that a single layer representation of the soil gives accurate results compared to a double layer. At the plot scale, the use of the Morel-Seytoux model gives comparable results to the Richards-1D but reduces the time of calculation. These results are similar on both tilled and crusted plots. However, on the crusted plot, soil hydrodynamic properties are constant all year round while on the tilled plot they vary in time function of rainfall amount and intensity. The calibrated K_s values at the plot scale are 50% lower than those measured using the single infiltrometer ring and the calibrated values at the catchment scale are 20% higher than those calibrated at the plot scale. This multi-scale approach is well adapted to heterogeneous catchments characterized by different landuse types and runoff control mechanisms.

Real time forecasting of water table depth and soil moisture profiles

Ate Visser[1], Roelof Stuurman[1], and Marc F.P. Bierkens[1,2]

[1]*TNO-Institute of Applied Geoscience, Utrecht, The Netherlands*
[2]*Department of Physical Geography, Utrecht University, Utrecht, The Netherlands*

A method is presented for online forecasting of water table depth and soil moisture profiles. The method combines a simple form of data assimilation with a moving window calibration of a deterministic model describing flow in the unsaturated zone as well as regional drainage. Previous work with physically-deterministic models [*Knotters and Bierkens*, 2000; *Knotters and De Gooijer*, 1999] has focussed on offline calibration and validation. However, availability of online measurements makes online forecasting possible. Online forecasting can be used for both drought and flood warnings, enabling more timely and accurate operational water management. Also, online calibration provides substantially better forecasts than offline calibration.

Materials and methods The groundwater data were obtained from an observation well located on the main meteorological field of the Royal Netherlands Meteorological Office at De Bilt. The field lies at the edge of an ice-pushed ridge that is a remnant from the glaciers that covered the north of the Netherlands during the Saalien ice age. Because of its proximity, the ridge is expected to be a source of regional groundwater fluxes, influencing the phreatic surface [*Bierkens et al.*, 1999].

Besides a long series (15 years) of daily groundwater measurements, online measurements of water table depth and soil moisture (at 25, 50, 75 and 100 cm below surface) were available for a period of three months. Each day these measurements were sent to a central server by short message service (sms) over the consumer gsm network. From there, the data was retrieved over the internet, together with historical weather data and weather forecasts (for which the Royal Netherlands Meteorological Institute is acknowledged) to be used for calibration and forecasting.

The Soil Water Atmosphere Plant model (SWAP) [*van Dam*, 1997] was used, which applies the Richards equation in combination with the Mualem-Van Genuchten soil hydraulic parameters, to describe the flow of water in the unsaturated zone. A linear relationship between drainage flux and phreatic surface depth was assumed, parameterised by the drainage level of the nearest draining agent, h_s, and the drainage and infiltration resistance, γ. The bottom flux, q_b, was assumed to be constant in time here, although it might have a seasonal fluctuating component. A mobile fraction, f_m, was used to compensate for preferential flow of percolating water. In addition, to allow for a fast responding system, the saturated conductivity K_s, was calibrated. This left five parameters (h_s, γ, q_b, f_m and K_s) to be estimated on long series of groundwater data. The additional use of soil water content measurements also allowed for calibration of the Van Genuchten parameters α and n, strongly improving soil water profile predictions. To account for seasonal fluctuations and compensate for model error, a 31-day moving window calibration of the drainage level, h_s, was used, because this parameter is directly related to the absolute value of the water table depth.

For short lead-time forecasting with a dynamic model (here a maximum lead time of 5 days was used), two criteria are important: (1) adequate parameters and (2) a close approximation of the initial conditions. Using predictions from a 31-day moving window calibration often resulted in a large error when compared to the last available measurement, introducing an error in the initial condition for the forecast. To eliminate this error, the objective function (O) for the moving

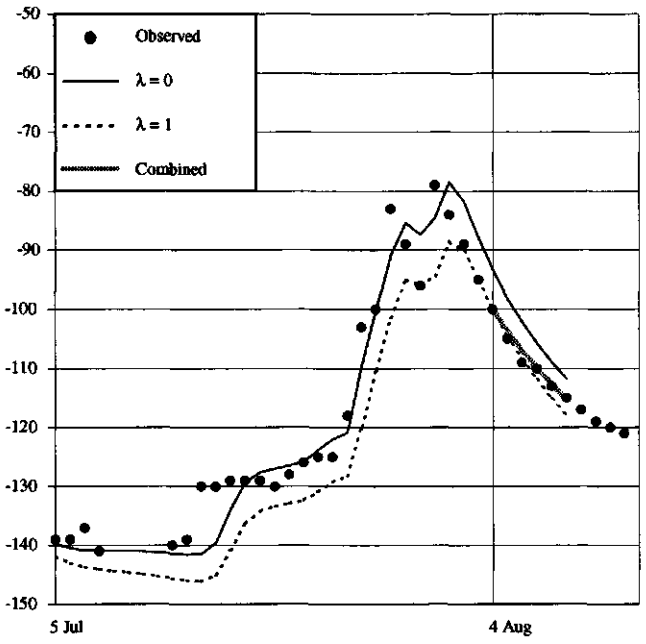

Figure 3.11: Illustration of the advantage of the combined method. Benefiting from the initial state from the $\lambda = 1$ calibration and the parameter value of the $\lambda = 0$ calibration, the combined method starts of well and stays in line with the observed values.

window calibration was changed and the last measurement of the calibration period was given extra weight.

$$O = (1-\lambda)\cdot\sum_{i=1}^{n} R(i) + \lambda \cdot R(n) \tag{3.7}$$

with $R(i)$ being the residual to the i-th measurement. This will force the calibration method to "work towards" the last measurement. We define λ as the measure for the extra weight (i.e., $\lambda = 0$ assigns equal weight to all measurements and $\lambda = 1$ assigns only weight to the last measurement). Note that this produces a form of model adaptation that is in between calibration and a form of data assimilation, similar to Newtonian Nudging [*Houser et al.*, 1998]. Assigning more weight to the last measurement (high λ) will reduce the initial error, but introduces a larger parameter error. Therefore we also combined the initial condition of $\lambda = 1$ and the estimated parameter of $\lambda = 0$, to further improve the forecast.

The forecast method was tested on a 15-year series of historical groundwater data, as well as on simulated series for a sensitivity analysis. Finally, the combined method was applied to a short period for which both groundwater and soil moisture content measurements were available.

Results We found an optimum λ of 0.25 when considering the overall RMSE of the forecast period (5-day lead time). Larger values of λ resulted in large errors in the model parameter, whereas smaller values of λ result in large errors in initial values. This is shown in Figure 3.11 where the prediction error is plotted against lead-time for several values for λ as well as the combined

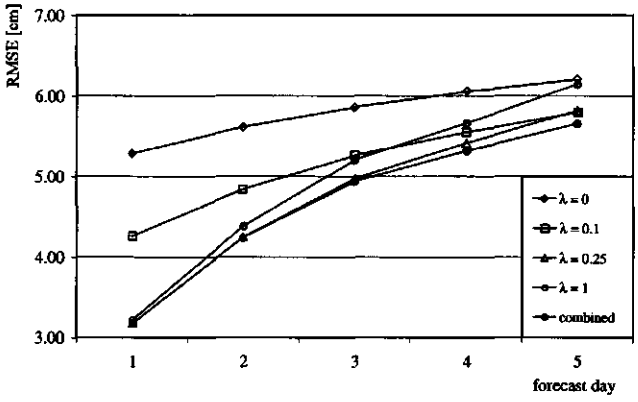

Figure 3.12: Evolution of prediction error over forecast period with several values for weighing λ and combined method.

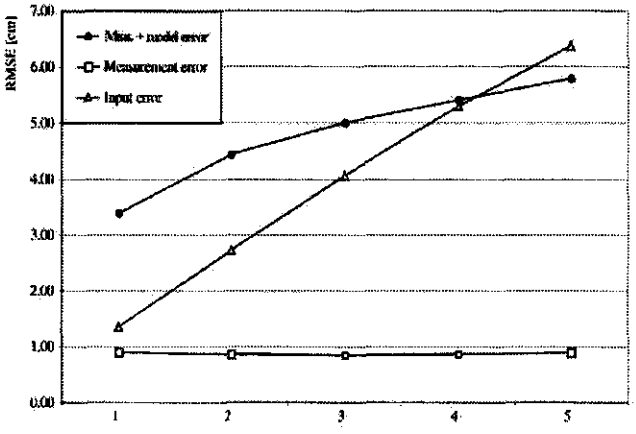

Figure 3.13: Evolution of the prediction error of the water table depth over the forecast period for three sources of error, model error in real data, and measurement error and input error from simulated time series.

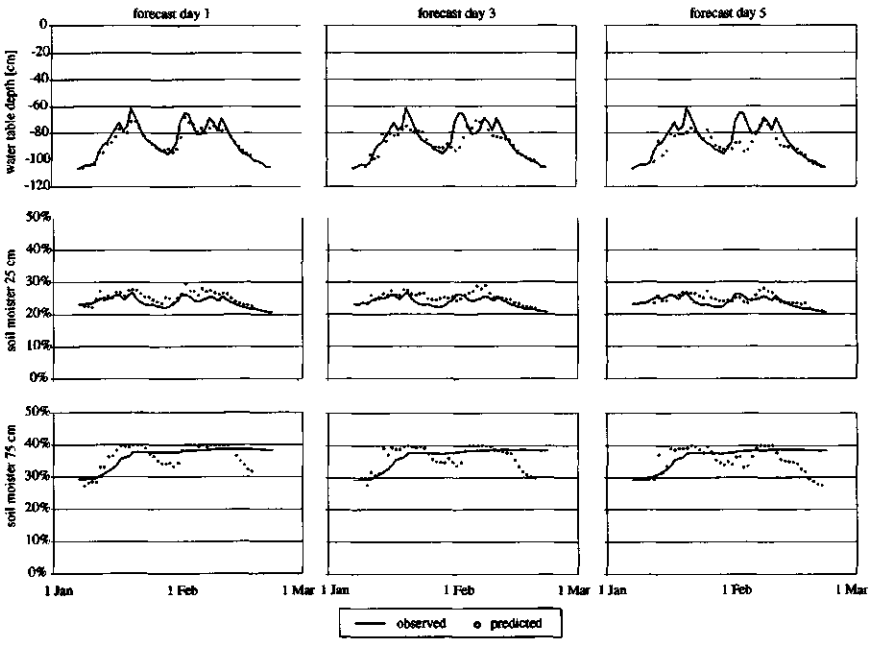

Figure 3.14: Time series of observed and predicted water table depths and soil moisture content of the 1st, 3rd and 5th forecast day.

method. The combination of $\lambda = 0$ and $\lambda = 1$ calibration benefits from both a very small initial error and a better parameter value, and gives the best overall forecast in terms of RMSE, better than using a λ of 0.25. This effect is further illustrated in Figure 3.12.

Three types of error can be distinguished: model error, measurement error and input error (errors in the weather forecast). The difference between historical groundwater data and forecasts using observed meteorological data provided an estimate of the combined model error and measurement error. Noise added to simulated time series (mimicking measurement error) or input variables (mimicking errors in weather forecast) gave insight into the other two sources of error. As shown by Figure 3.13, the model error is largest, up to the 4th forecast day, when the error from the weather forecast becomes as large.

Finally we applied the whole scheme for online forecasts of ground water level and soil moisture profiles (5 day maximum lead time), using weather forecasts and the combined moving window calibration of both groundwater and soil moisture data. Figure 3.14 shows some time series of observed and forecasted water table depth and soil moisture content. Differences in error statistics of soil water content hereby reflect differences in dynamics; see Figure 3.15. The 25 cm soil water content series remains the same in error during the forecast period, reflecting diffusion of soil moisture mitigating the error from the weather forecast. The 50 cm soil water content shows similar behaviour, whereas the 75 cm soil water content is more influenced by ground water level fluctuations and therefore follows the pattern of groundwater error statistics, deteriorating over the forecast period.

Conclusions We introduced a method for on-line forecasting of water table depth and soil moisture profiles. The method is based on a combination of a moving window calibration of the determinis-

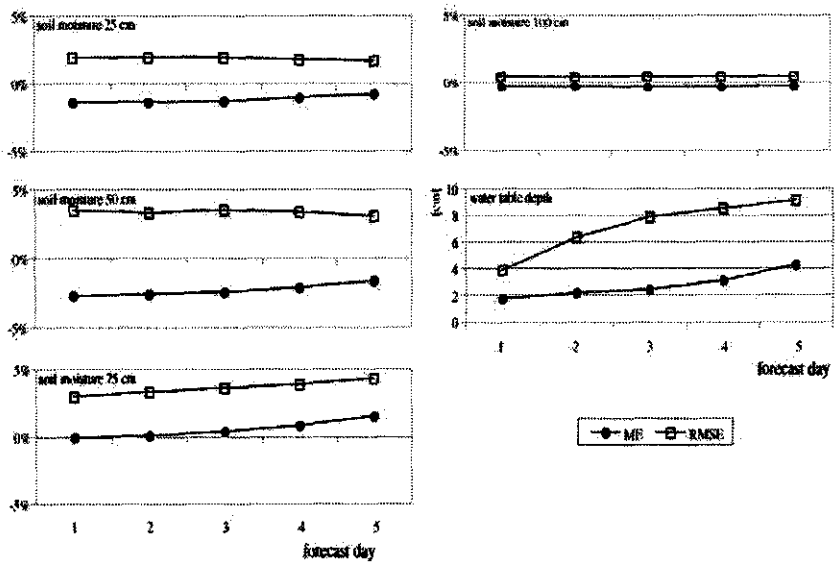

Figure 3.15: Evolution of prediction error over forecast period of groundwater level and soil moisture profile.

tic model of the unsaturated zone SWAP and a simple form of data assimilation. Moving window calibration improves the forecast compared to an offline model. Adding a simple form of data assimilation improved the forecast further.

The model error is the largest source of error, except for lead times larger than 4 days, when the error resulting from the error in weather forecast becomes as large. Forecasts of groundwater level and soil moisture content below the topsoil deteriorate over the forecast period. Diffusion processes in the topsoil mitigate the deteriorating prediction forecast, resulting in a constant accuracy of the predicted water content over the forecast period.

Use of estimation of surface energy fluxes for the calibration of a semidistributed rainfall-runoff model

G. Boni[1,4], S. Gabellani[1,2], R. Rudari[1,3], and F. Silvestro[1]

[1]*CIMA, Università di Genova, Savona, Italy*
[2]*DIAm, Università di Genova, Genova, Italy*
[3]*CNR-GNDCI, Gruppo Nazionale per la Difesa dalle Catastrofi Idrogeologiche, Italy*
[4]*DIST, Università di Genova, Genova, Italy*

A calibration method of a rainfall-runoff model able to reproduce the hydrological response in continuous is proposed. The rainfall runoff model uses a Pristley-Taylor scheme to simulate the evapotranspiration process. The aim of this method is to calibrate the Pristley-Taylor parameter using surface energy fluxes obtained from a data assimilation model. An appropriate objective function that take count both the errors between evapotraspiration, computed with rainfall-runoff model and assimilation model, and between simulated and observed discharge is defined. As test cases the model will be applied to a Southern Italian basin.

For further reading see *Giannoni et al.* [2000] and *Boni et al.* [2004].

The model GEO_{TOP}-SF to forecast the triggering of slopes and debris flow instability: distributed data requirements and remote sensing opportunities

S. Simoni[1], C. Tiso[1], G. Bertoldi[1], and R. Rigon[1]

[1]*Dept. of Civil and Environmental Engineering - CUDAM, University of Trento, Trento, Italy*

It is used a model of the hydrological cycle, GEO_{TOP}, apt to model the behavior of mountain catchments coupled to a module, called SF, which determines the terrain stability. SF uses an indefinite slope stability modelling to follow the dynamical evolution of a hillslope during a rainfall event. If surface runoff is present, the stability is inferred from the well known theory of Takahashi of debris flow triggering, otherwise, if only flow into the soil is present, it models soil slips. It is shown an application of the model to the Centa thorrent catchment (Trento-Italy) using hydrological and landslides data collected during some recent events. We discuss also the possible improvements deriving from the use of remote sensed data of cloud cover, soil cover, surface temperature, soil moisture to obtain the final forecasts.

Use of different hydrological variables and impacts of atmospheric forcing errors on optimization and uncertainty analysis of the CHASM surface model at a cold catchment

Youlong Xia[1], Zong-Liang Yang[2], Paul L. Stoffa[3], and Mrinal K. Sen[3]

[1]*Atmospheric and Oceanic Science Program, Princeton University, Princeton, New Jersey, USA*
[2]*Department of Geological Sciences, The John A. and Katherine G. Jackson School of Geosciences, University of Texas at Austin, Austin, Texas, USA*
[3]*Institute for Geophysics, The John A. and Katherine G. Jackson School of Geosciences, University of Texas at Austin, Austin, Texas, USA*

We used Bayesian stochastic inversion and 18-year forcing and calibration data as well as information about uncertainties in forcing variables at Valdai, Russia to study the impacts of forcing errors on selection of optimal model parameters and their uncertainty estimates when three different hydrological variables were used, respectively for calibration. The results show that forcing errors had few effects on selection of optimal model parameter sets when monthly evapotranspiration and runoff were calibrated. However, forcing errors had significant effects on selection of optimal model parameters when daily snow water equivalent was calibrated. Forcing errors also significantly affect uncertainty estimates of the land surface model parameters.

Introduction PILPS experiments (e.g., *Schlosser et al.* [2000]) have identified and documented two key atmospheric variables, precipitation (P) and downwelling longwave radiation (LWR), that are critical for accurately determining the snow mass balances, across different scales in cold regions. However, almost all these studies concerning the derivation of optimal land surface parameters assume that the forcing data are accurate and do not contain observational errors [*Xia et al.*, 2004]. In fact, significant systematic biases in precipitation measurement, obviously caused by wind, existed in all types of precipitation gauges, in particular for snowfalls. Besides precipitation errors, radiation errors also significantly affect simulations of water fluxes and energy fluxes both for a catchment simulation. In order to investigate how considering the errors in these forcing data impact the derivation of optimal parameters, and to study how the results depend on the calibration variable, we designed 2 experiments for each of three calibration variables. The first experiment is to use the fixed forcing data and varying model parameters, and the second experiment is to use both varying forcing data and varying model parameters. Therefore, we conducted a total of 6 experiments. For each experiment, Bayesian stochastic inversion selects 60,000–90,000 parameter sets. Therefore, we have almost 500,000 model runs. For all experiments, we used a one-year spin-up period to minimize impact of initial condition on simulations of monthly runoff, monthly evapotranspiration and daily snow water equivalent. This spin-up time is appropriate for the CHASM land surface model, according to *Schlosser et al.* [2000].

Impacts of atmospheric forcing errors Figure 3.16 shows a cross-validation test for optimal model parameters, that is, we pair five optimal model parameters derived with consideration of forcing errors, with original forcing data (Figure 3.16c), and pair five optimal model parameter derived using fixed forcing with optimal forcing data (Figure 3.16d) into two separate simulations. The validation results show that simulated evapotranspiration and runoff are consistent with observations. This is consistent with our optimal parameter analysis because two forcing data sets generate similar optimal model parameters when monthly evapotranspiration and runoff were used

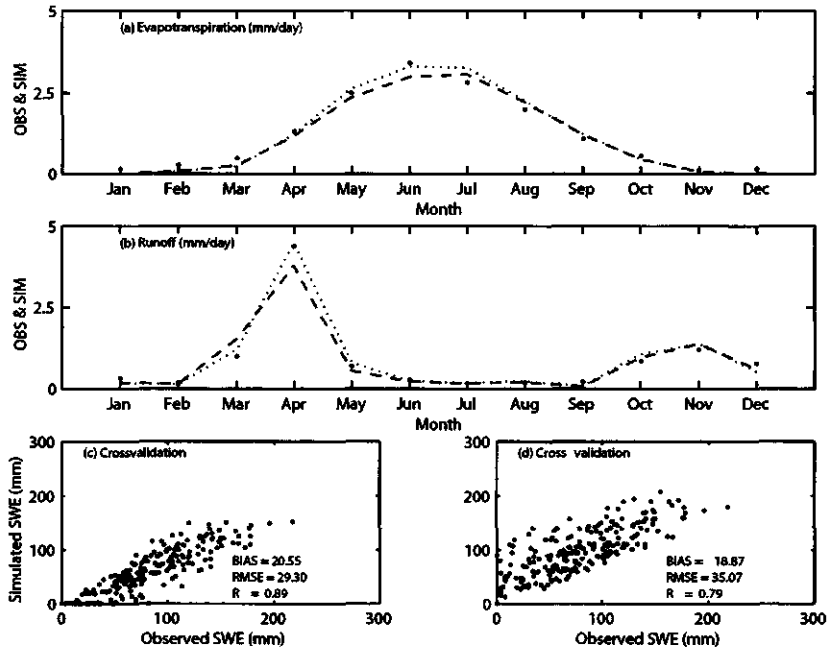

Figure 3.16: Observed and simulated (a) monthly evapotranspiration, (b) runoff, (c) cross-validation of daily snow water equivalent when optimal model parameters derived from fixed forcing and optimized forcing was used or when optimal model parameters derived from forcing error factors and fixed forcing was used, and (d) cross-validation of daily snow water equivalent when optimal model parameters derived from forcing errors and fixed forcing were used (dot = observations; dashed = simulations when optimal model parameters derived from fixed forcing and optimal forcing were used; dotted = simulations when optimal model parameters derived from forcing errors and fixed forcing were used).

as calibrated variables. However, when the optimal model parameters derived using forcing errors and fixed forcing were used to simulate snow water equivalent, its bias is changed from -1.7 mm to -18.9 mm, RMSE (root mean square error) is increased from 21.9 mm to 35.1 mm, and r (correlation coefficient) is reduced from 0.89 to 0.79. When optimal model parameters derived from fixed forcing and optimal forcing were used to simulate snow water equivalent, its bias is changed from 6.2 mm to 20.6 mm, RMSE is increased from 18.5 mm to 29.3 mm, and r is reduced from 0.93 to 0.89. This significant change is a result of different optimal parameter sets, particularly different snow albedo (ALBN). Therefore, forcing errors have significant impact on daily snow water equivalent simulations.

Figure 3.17 shows marginal posterior probability density distributions for three most sensitive parameters such as ALBN, fractional vegetation cover seasonality (VEGS) and minimum stomatal resistance (RCMIN). For evapotranspiration case, forcing errors (solid line) result in wider PPD's range which means larger uncertainty when compared to fixed forcing case (dashed line). For the runoff case, forcing errors not only influence uncertainty range of ALBN and RCMIN but also influence the shape of PPD's distribution for ALBN. The same conclusion can be drawn for ALBN

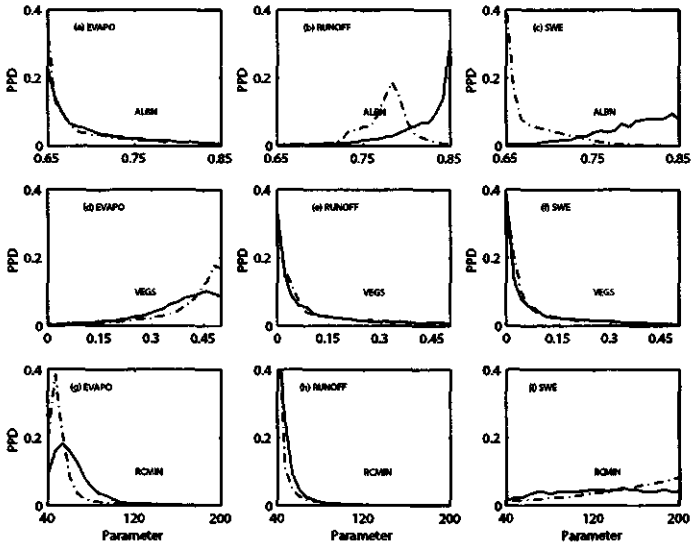

Figure 3.17: Calculated PPD's for three most sensitive model parameters when observed monthly evapotranspiration, monthly runoff, and daily snow water equivalent were used as calibration variables (solid = fixed forcing; dashed-dotted = forcing with errors; EVAPO = evapotranspiration; SWE = snow water equivalent).

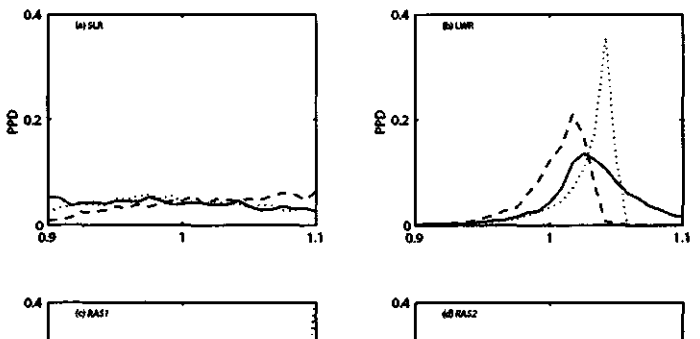

Figure 3.18: Calculated PPD's for four forcing error factors (a) SLR, (b) LWR, (c) RAS1, and (d) RAS2 when observed monthly evapotranspiration, monthly runoff, and daily snow water equivalent were used as calibration variables (solid = evpotranspiration; dashed = runoff; dotted = snow water equivalent).

for snow water equivalent case. Forcing errors result in quite different PPD's distribution, that is, ALBN favors small values for fixed forcing case, and it favors large values for the case of forcing with error. Therefore, forcing errors indeed influence width and shape of the PPD's distributions for the most important model parameters. This error effect was introduced by model parameters and forcing error interdependency (correlation of model parameters and forcing errors). This also includes interactions between model parameters and interactions between forcing errors. Large correlation coefficients show this interdependency. For example, 0.75 is for LWR and snowfalls and 0.65 is for LWR and ALBN when daily snow water equivalent was calibrated. 0.65 is for LWR and ALBN when monthly runoff was calibrated.

Forcing data can be optimized and their uncertainties can be estimated using Bayesian stochastic inversion. Figure 3.18 shows marginal posterior probability density (PPD) for downelling shortwave radiation (SLR), LWR, winter snowfalls (RAS1 for December, January, and February snowfalls, and RAS2 for November, March and April snowfalls) when different hydrological variables (i.e., evapotranspiration, runoff, snow water equivalent) were used to constrain errors between observations and simulations. The results show that all hydrological variables give good constraints for LWR although peaks of PPDs are different. Most likely values exist within 0.98 and 1.05, which is relatively consistent with the value of 1.0 used in PILPS 2d experiment. In addition, optimal values are very close to each other (i.e., 1.02, 1.03, 1.05) for the three calibrations. Snow water equivalent and runoff give strong constraints on winter snowfalls although constraints are much stronger on RAS1 than on RAS2. Evapotranspiration gives weak constraint on winter snowfalls. All hydrological variables give weak constraints on SLR because their PPD's are almost uniform, indicating largest uncertainties.

Potentialities of thermal infrared remote sensing for SVAT model calibration

B. Coudert[1], B. Boudevillain[1], C. Ottlé[1], and J. Demarty[2]

[1]*Centre d'étude des Environnements Terrestres et Planétaires (CETP/IPSL), Vélizy, France*
[2]*INRA, Unité CSE, Avignon, France*

Previous studies have demonstrated the use of Earth Observation satellite data to improve the initialization and the calibration of hydrological models. Indeed, they allow the assessment of several surface properties (surface temperature, soil water content, soil roughness, type of soil, dynamics of the vegetation...). Studies have recently shown that Soil Vegetation Atmosphere Transfers (SVAT) models can be corrected thanks to the brightness temperature estimated by thermal infrared satellite data. However the thermal infrared instruments resolution is rather coarse if a good repetitivity is required. Consequently, there is a need to explore the potentialities of low spatial resolution captors to inform higher resolution modelisations [*Boudevillain et al.*, 2004]. The purpose of this paper is to show the contribution and limits of thermal infrared brightness temperature to calibrate the surface parameters and initialization variables of a SVAT model at field scale.

The Alpilles-ReSeDA database [*Baret*, 2002; *Olioso and co-authors*, 2002a, b] has been used for this work. The two layers and two sources SVAT model used in this study and developed at CETP/IPSL calculates the surface energy and water transfers and include several soil and vegetation parameters and initialization variables (especially soil water content in the surface and root zone). This model was coupled with radiative transfer models in the solar and thermal infrared domains in order to simulate both spectral reflectance and brightness temperature of the surface. The Multiobjective Generalized Sensitivity Analysis (MOGSA) methodology [*Gupta et al.*, 1998; *Demarty et al.*, 2004] has first been used to analyse the sensitivity of the simulated variables (surface fluxes, soil moisture, brightness temperature) to model parameters and initialisation. Then, the potentialities of such a methodology have been investigated for model calibration. Different numerical experiments have been undertaken in order to show the impact of reduced available information. The analysis of these experiments permitted us to show the contribution and the limits of the use of thermal remote sensing data for SVAT model calibration according to the surface conditions (vegetation cover) and to quantify the uncertainty on the simulated variables [*Coudert et al.*, 2004].

Land-atmosphere exchanges of water and energy in space and time over a heterogeneous land surface

Z. (Bob) Su[1], L. Jia[2], X. Jin[2], J. Elbers[3], A. Gieske[1], W. Timmermans[1], H. van der Kwast[4], A. Olioso[5], J.A. Sobrino[6], J. Moreno[6], F. Nerry[8], D. Sabol[8]

[1]*International Institute for Geo-Information Science and Earth Observation (ITC), Enschede, The Netherlands*
[2]*Wageningen University, Wageningen, The Netherlands*
[3]*Alterra, Wageningen University and Research Centre, Wageningen, The Netherlands*
[4]*University of Utrecht, Utrecht, The Netherlands*
[5]*INRA, Avignon, France*
[6]*University of Valencia, Valencia, Spain*
[7]*TRIO/ULP, Strasbourg, France*
[8]*University of Washington, Seattle, U.S.A*

In order to advance our understanding of land-atmosphere exchanges of water and energy in space and time over heterogeneous land surfaces, an intensive field campaign was carried out at the Barrax agricultural test site in Spain in the period 12–21 July involving multiple field, satellite and airborne instruments for characterizing the state of the atmosphere, the vegetation and the soil from visible to microwave range of the spectrum. Part of the experimental area is a core site of a 25 km^2 area within which numerous crops are grown - on both irrigated and dry land - alongside fields of bare soil. This campaign formed part of the preparatory study for a proposed ESA Earth Explorer mission called SPECTRA (Surface Processes and Ecosystem Changes Through Response Analysis) of the European Space Agency, thus was named as SPARC-2004 (SPECTRA Barrax Campaign-2004) in combination with the EU 6FP EAGLE Project.

Used for the first time during SPARC-2004 was the new Airborne Hyperspectral System (AHS), operated by Spain's Instituto Nacional de Técnica Aeroespacial (INTA). The AHS has a total of 80 spectral channels available in the visible, short wave infrared and thermal infrared. A total of 16 multiangular acquisition flight lines were obtained over Barrax with spatial resolutions varying from 2.5 to 6.8 m. Several satellite sensors, including the Compact High Resolution Imaging Spectrometer (CHRIS) on the Proba spacecraft, with two days of consecutive multiangular acquisitions over the campaign site, as well as sensors from several other satellites (ENVISAT, TERRA, MSG) were deployed for image data acquisition.

A large number of ground based instruments were also deployed including lidars and balloon-based radio sondes to sample atmospheric variables, sun photometers to measure sky radiance and sensors mounted on mobile towers to record local vegetation characteristics. Several mobile instrument towers, including four eddy correlation devices and two scintillometers, were deployed in the field to monitor the individual components of the energy, water and carbon dioxide flux exchanged between land and the atmosphere. In addition to CHRIS data, two ENVISAT overpasses enabled acquisitions from that spacecraft's Medium Resolution Imaging Spectrometer (MERIS) and Advanced Along Track Scanning Radiometer (AATSR), as part of parallel ENVISAT data product validation activities. Data from the Spinning Enhanced Visible and InfraRed Imager (SEVIRI) instrument aboard MSG-1 (Meteosat Second Generation) were acquired during the campaign as part of the validation activities for MSG vegetation products, alongside data from Landsat and also

the Moderate Resolution Imaging Spectroradiometer (MODIS) and Advanced Spaceborne Thermal Emission and Reflection Radiometer (ASTER) on Terra, collected to complete the SPARC dataset.

In the CHRIS configuration available to the SPARC-2004 campaign, 62 spectral bands were available for five angular acquisitions with 34 m spectral resolution. The higher resolution data, in combination with data from other sensors (spatial resolution from 90 m of ASTER, 300 m of MERIS, to 1 km of AATSR and MODIS, and to over 3 km of MSG data) provide unprecedented opportunity for studying of the scaling behavior of the land-atmosphere exchanges of water and energy.

A total of 80 people from 21 different institutions in five different countries were involved in the SPARC-2004 activity, with around 50 people directly participating in the daily field measurements. Participants included Spanish teams from Universities in Valencia, Albacete and Castellon along with national research institutes (INTA, INM, CSIC, CIEMAT, CEDEX, ITAP and CECAF), French teams from LURE-Paris, INRA-Avignon and the University of Strasbourg, Italian teams from the University of Naples and the National Research Council and a large team from the Netherlands involving Alterra, Wageningen University, ITC and the University of Utrecht, plus ESA participants. A team from the University of Washington in Seattle also took part in the campaign, as part of a NASA project related to validation of Terra/ASTER data over the Barrax site. The SPARC-2004 activity has been funded by ESA and the European Commission with additional contributions from Eumetsat and national projects.

The in-situ data relevant to land-atmosphere exchanges included the following measurements:

- Turbulence, H_2O, CO_2 fluxes and CO_2 concentrations using an eddy correlation system (Gill 3D sonic + closed path Licor gasanalyser: CO_2 and H_2O + nitrogen reference gas +pneumatic mast + dataloggers);
- Soil heat flux, soil temperatures (two levels), air temperature and humidity
- Leaf temperatures (thermal couples);
- Radiation balance (shortwave and longwave incoming and outgoing radiation, wind, air temperature, radiometric surface temperature) and sensible heat flux (using two scintillometer systems);
- Photosynthesis, conductance and transpiration measurements at leaf level (using a CIRAS from PP systems);
- Radiometric surface temperature measurements using a hand-held radiometer (Everest);
- Roughness measurements using stereo photogrammetry with the NEar Sensing CAmera Field Equipment (NESCAFE);
- Emissivity measurements with the "two-lid box method";
- LAI measurements with hemispherical photographs, which will be processed with WinPhot[†].

Digital photos are taken to document the actual field situations. These data and part of the satellite data have undergone preliminary analysis in space and time, the results and findings will be presented at the workshop.

[†] http://www.bio.uu.nl/~herba/Guyana/winphot/wp_index.htm

Linked from below: The impact of shallow groundwater dynamics on the spatial variability of soil moisture along hillslopes

P.W. Bogaart[1], A.J. Teuling[1], and P.A. Troch[1]

[1]*Hydrology and Quantitative Water Management Group, Wageningen University, Wageningen, The Netherlands*

Soil moisture content is the single most important hydrological state variable with respect to land-surface-atmosphere interaction. Evapotranspiration and runoff are highly non-linear dependent on soil moisture. Because of this nonlinearity, information on large-area average soil moisture (as e.g. obtained from remote sensing) is insufficient to estimate large-area average surface fluxes. If, however, the spatial distribution of soil moisture can be conditioned on large-area average soil moisture using terrain features (such as land-surface curvature), then more reliable estimates of large-area average surface fluxes can be made.

Spatial variability of soil moisture stems from three distinct sources. First, spatial variability is caused by land use and soil types. This spatial variability is characterised by direct imprinting of soil properties and evironmental controls on soil moisture patterns, and will not be considered here. The second source of spatial variability of soil moisture is due to small-scale stochastic variability of soil and vegetation properties. The third source is due to redistribution of soil moisture. In this paper we consider these last two sources of variability.

The hypothesis is that in soil-mantled, bedrock underlain landscapes, shallow, perched, groundwater dynamics effectively "couples" soil moisture dynamics at different locations along a hillslope. The upper part of a hillslope is the recharge area [*Kim et al.*, 1999]. Any water that leaks from the root zone recharges the perched groundwater table, which is relatively deep here. In the lower part of the hillslope, the perched groundwater table is more shallow, and is likely to affect the root zone above it. In an extreme case this root zone will be saturated because of groundwater tables rising to the land surface. Because of this groundwater induced lateral coupling between upslope and downslope soils, along-slope differences in soil moisture are to be expected.

We present a simple model-based approach to test this hypothesis. A field of independent root-zone soil moisture models (having variable properties) is coupled to a hydraulic groundwater theory based, semi-distributed hillslope hydrological model [*Troch et al.*, 2003]. The advantages of this hillslope model is that it accounts in a simple way for hillslope geometric complexity (plan form and profile curvature), while preserving the physical behavior of the natural system. Drainage from the root-zone models acts as recharge to the groundwater model, and if the groundwater system becomes saturated somewhere along the hillslope, then drainage from the root-zone system is blocked, and this zone wets up as long as rainfall continues. Because we compare a "coupled" and an "uncoupled" case, the contribution of the groundwater system to (the evolution of) total soil moisture variability can be estimated.

Results for an idealized hillslope and synthetic climate series illustrate the concept. During the wet season, the shallow groundwater table rises to the surface at the lower end of the hillslope and root-zone soils here become saturated, in contrast to the soils in a more upslope position. During the following dry season, the groundwater table "disconnects" from the root zone, but the along-slope spatial differences in soil moisture persist. The modeling approach proposed here shows potential for large-scale hydrological applications, as it allows to link spatial variability of soil moisture fields to readily-available surface features, such as land-surface curvature.

4 Data assimilation: potential for advancement

Soil moisture assimilation for meteorological purposes: Observation synergy and data assimilation needs

Pedro Viterbo[1], Janneke Ettema[1], Gisela Seuffert[1], and Bart van den Hurk[2]

[1]*European Centre for Medium-Range Weather Forecasts, Reading, UK*
[2]*KNMI, De Bilt, The Netherlands*

Despite the well-documented impact of soil moisture initial conditions for weather forecast performance and monthly-to-seasonal prediction, the assimilation methods used so far in operational meteorological applications are relatively crude and make scant use of data, with no remote sensing information.

Because of its longer timescale, the relevant state variable to initialize in a model is root-zone soil moisture (RSM). There is no current wide coverage observation system of RSM, and there will not be one in the foreseeable future. The observations to assimilate will all contain some information on RSM, under certain caveats, and they can be broadly grouped in 3 classes: (1) In-situ air surface temperature and humidity or early morning rate of change in IR brightness temperature; (2) C- or L-band brightness temperatures; (3) The contrast between the visible and near-infrared reflectance, often expressed as a vegetation index. The first class will provide information on the surface evaporative fraction which, under spring and summer fair-weather conditions depends on RSM. The second class provides information on surface soil moisture and a model will be needed to transfer that information to deeper layers. Finally, the last class provides information on the state of vegetation which depends to a large extent on the water available in the root-zone.

The wide variety of observations listed above require a flexible assimilation system. Using an Extended Kalman Filter data assimilation system, examples will be given of the synergistic use of the observations to improve soil moisture and surface fluxes. In the presence of conflicting observations, the soil moisture analysis values depend on the application: The values obtained by a meteorologically driven system will emphasize the correct evaporative fraction at the surface, and might not be ideal for hydrological applications.

Finally, the emphasis is put on data assimilation as a tool to expose model errors and to focus research; improvements to the model physical realism will be necessary in order to have a more accurate background field and to effectively extract the information contents of the observations.

The Global Land Data Assimilation System (GLDAS)

P.R. Houser[1], M. Rodell[1], J. Gottschalck[2], C.-J. Meng[2], U. Jambor[2], K. Mitchell[3], and C.D. Peters-Lidard[1]

[1]*Hydrological Sciences Branch, NASA Goddard Space Flight Center, USA*
[2]*Goddard Earth Science Technology Center, University of Maryland, Maryland, USA*
[3]*NOAA National Centers for Environmental Prediction, USA*

The development of GLDAS has been motivated by three factors. First, we know that land surface states, including surface temperature, soil moisture, and snow, significantly influence Earth system processes and predictability at multiple scales. Second, improved knowledge of land surface conditions will promote better land resource management, natural hazard mitigation, and homeland security. Third, we now have sufficient understanding of land physical processes (in the form of sophisticated land surface models (LSMs)), global data from advanced satellite observing systems, and economical computing power, enabling us to merge understanding and observations using data assimilation strategies within an operational system. Therefore, the major goal of the GLDAS project is to produce high resolution, reliable fields of land surface states and fluxes by parameterizing, forcing, and constraining multiple, sophisticated land surface models with data from advanced observing systems, in order to improve Earth system prediction and critical applications.

GLDAS is unique in that it is an uncoupled land surface modeling system that drives multiple models, integrates a huge quantity of observation based data, runs globally at high resolution (0.25°), and produces results in near-real time (typically within 48 hours of the present). GLDAS is also a test bed for innovative modeling and assimilation capabilities. A vegetation-based "tiling" approach is used to simulate sub-grid scale variability, with a 1 km global vegetation dataset as its basis. Soil and elevation parameters are based on high resolution global datasets. Observation-based precipitation and downward radiation and output fields from the best available global coupled atmospheric data assimilation systems are employed as forcing data. The high-quality, global land surface fields provided by GLDAS will be used to initialize weather and climate prediction models and will promote various hydrometeorological studies and applications. The 2001-forward GLDAS archive of modeled and observed, global, surface meteorological data, parameter maps, and output is publicly available.

Several multiyear retrospective simulations at lower spatial resolutions have been executed. Forcing and output images are available for viewing through the GLDAS website*. Data have been provided to support research at GSFC and several other institutions, including studies relating to the GEWEX Coordinated Enhanced Observing Period (CEOP). In addition, specialized simulations were executed for testing the effects of improved model initialization on seasonal climate predictability as part of NASA's Seasonal to Interannual Prediction Project (NSIPP). Preparations are currently being made for short term and seasonal forecast model initialization testing in cooperation with NOAA's National Centers for Environmental Prediction (NCEP). Recent system enhancements include installation of the Noah land surface model, additional forcing options, a satellite based leaf area index updating scheme, and a MODIS snow data assimilation scheme.

*http://ldas.gsfc.nasa.gov

A report on the progress in ELDAS

Bart van den Hurk[1]

[1] *KNMI, De Bilt, The Netherlands*

The European Land Data Assimilation Project ELDAS† has entered its last year of formal support by the European Union. In ELDAS a European wide soil moisture data assimilation system is built, applied, validated and demonstrated. It is partially inspired on the US NLDAS/GLDAS systems, but uses different data assimilation techniques and forcing data. In particular, soil moisture corrections are applied as a result of model deviations from observed air temperature, air humidity, (synthetic) brightness temperatures and surface heating rates observed from a geostationary satellite platform.

The presentation will give a brief overview of past ELDAS activities (collection of forcing data bases, design and application of the data assimilation system, trial runs). In addition, case studies exploring the impact of assimilation of synthetic brightness temperatures and surface heating rates are described and discussed.

† http://www.knmi.nl/samenw/eldas

Land data assimilation at NOAA/NCEP/EMC

D. Lohmann[1], Pablo Grunman[1], and Kenneth Mitchell[1]

[1]*NOAA/NCEP/EMC, Suitland, Maryland, USA*

Improving weather and seasonal climate prediction by dynamical models requires multidisciplinary advances in providing reliable initial states for the atmosphere, land and ocean components of the earth system. For two decades, advances in providing atmospheric initial states via 4-dimensional data assimilation (4DDA) have paved the way for the development of counterpart 4DDA systems for the ocean and land. In 4DDA, a geophysical model provides temporally and spatially continuous background states into which temporally and spatially discontinuous observations are assimilated from various observing platforms (in situ, satellite, radar). The backbone then of any atmospheric, ocean or land 4DDA system is the geophysical model whose day-to-day execution provides the continuous timeline of background states. A land data assimilation system (LDAS) blends sparse land observations with the background fields of a reliable land surface model (LSM). The accuracy of the LSM background field (and the attendant surface and sub-surface water/energy fluxes that drive those background fields) is crucial to the viability of an LDAS. We present the progress within NOAA/NCEP/EMC to develop such a land surface data assimilation system. This progress includes the development of the adjoint model/tangent linear model for the Noah LSM [*Ek et al.*, 2003] and it's incorporation into the North American Land Data Assimilation System [*Mitchell et al.*, 2004], referred to as NLDAS. We demonstrate here the improvement achieved in Noah LSM 1-D column-model simulations of soil moisture by means of an "identical twin" experiment, which assimilates the land surface temperature (LST) produced by a Noah LSM control run. Later at the workshop, we will show results of the assimilation of hourly satellite-derived LST retrieved from NOAA GOES satellites.

Influence of soil moisture on LST in the Noah LSM Before embarking on LST assimilation to improve the Noah LSM simulation of soil moisture, it is important to quantify the impact of soil moisture changes on the LST simulations of the Noah LSM. To assess this impact, we performed Monte-Carlo simulations for the year 1998, preceded by one year of spin-up (1997). Herein the 1-D Noah LSM column model was forced with surface meteorological data observed at 30-minute intervals from a Champaign, Illinois flux station (40.01°N latitude, 88.37°W longitude) operated by NOAA/ARL (Tilden Meyers, personal communication). We executed an 8000-member ensemble of Noah LSM simulations, in which each simulation utilized a different random specification of model parameter values, wherein we constrained the parameters by our knowledge (belief) in reasonable parameter ranges.

The resulting ensemble-mean of the simulated LST and the LST standard deviation of the ensemble are shown in figures 4.1a and 4.1b. Additionally, the ensemble mean and standard deviation of the derivative of LST with respect to soil moisture - d(LST)/d(soil moisture) - in the Noah model are shown in figures 4.1c and 4.1d. During the warm season (April–October) this ensemble mean derivative is negative with values up to -0.4K per one percent volumetric soil moisture change (total column), while the ensemble shows a variance of up to 2K.

We therefore can expect to successfully assimilate LST into the Noah LSM if we can find parameters that yield unbiased estimates in the Noah LSM of LST and other state variables and fluxes, assuming that the LST measurements themselves are unbiased. This will be explored further in

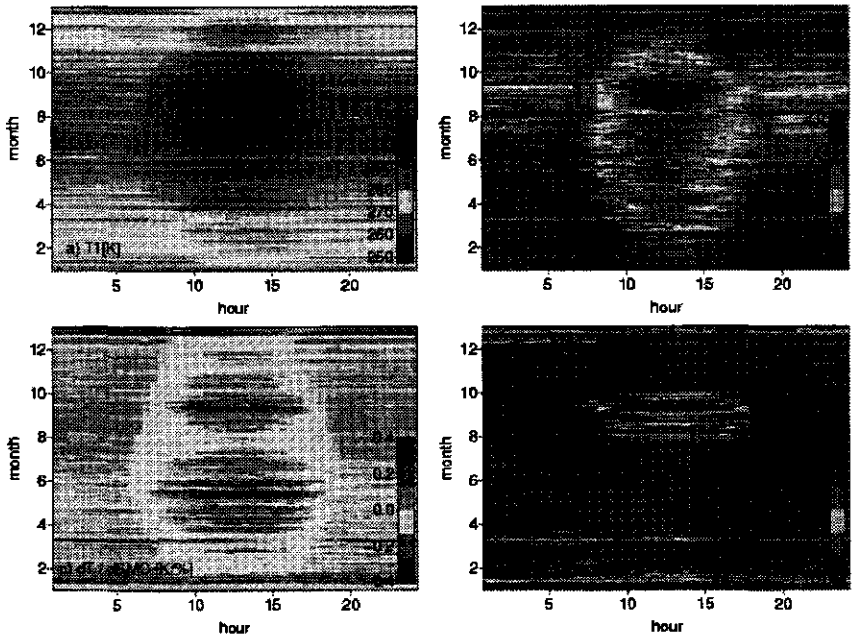

Figure 4.1: Results of the Monte Carlo Noah LSM simulations for 1998, showing ensemble mean of LST (upper left), standard deviation of the ensemble LST (upper right), ensemble mean of the derivative of LST with-respect-to soil moisture (lower left) and standard deviation of the latter (lower right). The x-axis is the hour of the day and the y-axis is the month of year.

our workshop presentation in the context of (1) parameter optimization (especially for NLDAS regions with limited available measurements) and (2) the assimilation of GOES-derived LST.

Identical-Twin Experiments To test our basic assimilation approach, we performed a 1-D identical-twin experiment with the Noah LSM column model. In this experiment, the control run used the Noah LSM default parameter values and the one-year spin-up initialization and forcing data of the Champaign, IL site as in the previous section. The companion data assimilation run was identical to the control run, with two exceptions. First, following the spin-up year (1997), we degraded the forcing throughout 1998 by imposing a 30% reduction to all moderate or greater amounts in the 30-minute precipitation forcing. Second, we assimilated the control-run LST during the $3\frac{1}{2}$-day period beginning 0000 UTC on 25 May.

Figure 4.2 shows the layer-1 and layer-2 soil moisture of the control run ("cntrl", green line) and the data assimilation run ("errDA", black line) for a nearly two-month interval (May–June) of 1998. The vertical blue lines in Figure 4.2 denote the beginning of the $3\frac{1}{2}$-day assimilation period. During this period, the assimilation routine calculates the cost function and the tangent linear of the Noah LSM and finds the optimal correction to the soil moisture content for 0000 UTC on 25 May that minimizes the difference between the "control" and simulated LST over the subsequent $3\frac{1}{2}$ days. No assimilation was performed after this $3\frac{1}{2}$-day period and therefore the two runs drift apart in June. Our presentation will include more examples and give more details of the setup. The numerical optimization was performed using a Truncated-Newton scheme, adapted

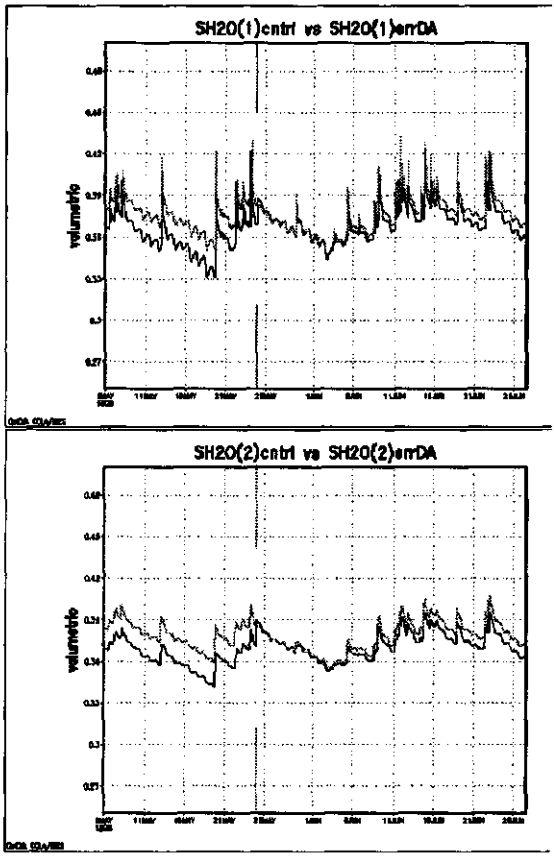

Figure 4.2: Volumetric soil moisture content for model soil layers of 0–10 cm depth (upper panel) and 10–40 cm depth (lower panel) for the control run (green) and data assimilation run (black).

from Nash, Stephen G., 1984: SIAM J. Num. Anal.770-788.

Intended application setting The NOAA operational partners in NLDAS include NCEP/EMC and OHD of the NWS and NESDIS/ORA, who have joined with the NLDAS research partners of NASA/GSFC, Princeton and Rutgers University, and the Universities of Maryland, Oklahoma and Washington. These partners have developed, executed, and evaluated a realtime and retrospective uncoupled NLDAS. The NLDAS generates hourly surface forcing (anchored by observation-based solar insolation and precipitation fields) and uses this forcing to drive four LSMs running in parallel to produce hourly output on a common $\frac{1}{8}^{\circ}$ grid over a CONUS domain. The paper of *Mitchell et al.* [2004] contains all the references of other papers published within this project that measure the quality of the forcing data and assess the model results.

Streamflow data assimilation: A study on nested catchments

C. Rüdiger[1], J.P. Walker[1], J.D. Kalma[2], G.R. Willgoose[3], and P.R. Houser[4]

[1]*Dept. of Civil and Environmental Engineering, University of Melbourne, Parkville, Australia*
[2]*School of Engineering, University of Newcastle, Callaghan, Australia*
[3]*School of Geography, University of Leeds, Leeds, UK*
[4]*Hydrological Sciences Branch, NASA Goddard Space Flight Center, Greenbelt, USA*

Soil moisture is an important variable in land surface modelling with a significant impact on climate prediction, but the areas shown to have the greatest potential impact are typically also the most densely vegetated. While much work has been concentrated on the assimilation of remotely sensed surface soil moisture observations to constrain land surface model predictions of soil moisture, the use of these measurements is limited to areas of low-to-moderate vegetation. This work proposes to contribute to soil moisture prediction in those densely vegetated areas through the assimilation of streamflow observations. The potential for this approach is demonstrated for a semiarid catchment in a synthetic twin experiment.

Introduction Climate model results are strongly dependent on the initial soil moisture conditions predicted by a land surface model. Moreover, it has been shown that correct initialisation of soil moisture content in areas with dense vegetation cover, such as the Sahel, the Amazon, and south-east Asia, has the greatest potential for positively influencing the predictability of precipitation [*Koster et al.*, 2000].

Previous work has shown that initial conditions on root zone soil moisture content can be accurately predicted when the near-surface soil moisture observations that are available from remote sensing are assimilated into a land surface model [e.g., *Walker and Houser*, 2001]. However, the approach is limited to areas with low-to-moderate vegetation cover, as dense vegetation masks the remotely sensed soil moisture signal. Thus, we seek to improve soil moisture prediction in densely vegetated catchments through the assimilation of observed streamflow. As streamflow is an integrated measure of soil moisture content and rainfall events hours, days, or even weeks in the past, implementation of an assimilation scheme to account for this time-lag requires careful consideration.

This paper uses a brute-force implementation of the variational assimilation approach in a synthetic study to demonstrate that this approach to soil moisture initial condition retrieval is feasible. This study is the first step towards a field-based multi-catchment study.

Models The assimilation of streamflow data for the retrieval of initial soil moisture content is addressed in this paper through a synthetic data assimilation study. First, a land surface model is used to generate a "true" data set that provides both the surface soil moisture "observations" and the evaluation data. The initial conditions and land surface forcing data are then degraded in two individual experiments in order to obtain control results.

The land surface model used in this study is the Catchment Land Surface Model (CLSM) of *Koster et al.* [2000]. Its framework includes an explicit treatment of sub-catchment soil moisture variability and its effect on runoff and evaporation. Consideration of both spatial distribution of the water table depth and non-equilibrium conditions in the root zone leads to the definition of three bulk moisture prognostic variables (catchment deficit, root zone excess and surface excess) and a special treatment of moisture transfer between them. Using these three prognostic variables, the

catchment may be divided into regions of stressed, unstressed and saturated soil moisture regimes, and the soil moisture profile calculated.

Model runoff is only produced when the current soil moisture content exceeds field capacity and is routed instantaneously to the catchment outlet. To counter this, an inter-catchment routing scheme has been introduced into the model to separately route the surface and subsurface runoff generation throughout the catchment. Surface and subsurface routing is undertaken using a digital elevation model of the catchment and an approximation to the Manning's equation; $V = cS^{0.5}$, where V is velocity, S is surface slope and c is a parameter fitted individually for surface, subsurface, and streamflow conditions to observed streamflow data for the specific catchment. While this parameter depends on the surface and flow conditions of the individual pixels, we assume a single uniform value for the hillslope and streamflow runoff routing components, respectively. Due to their size, travel time in most catchments is short, and losses due to evaporation were therefore considered negligible.

The variational data assimilation approach is based on minimising an objective function over an assimilation window, rather than sequentially using individual observations. In our application we use the Bayesian nonlinear regression suite (NLFIT) of *Kuczera* [1983], which is based on the shuffled complex evolution method of *Duan et al.* [1992], to perform this optimisation. The optimisation is achieved by changing the initial soil moisture state variables until the best fit between model predicted and observed streamflow for a given assimilation window is achieved.

The length of the assimilation window was kept to one month for the results presented in this paper, while the input parameters necessary for the calculations within NLFIT (Box-Cox λ, Box-Cox K, autoregressive parameter) were initially estimated and later manually adjusted. The initial assumption being that the data were normally distributed.

Synthetic Experiments To demonstrate the feasibility of the proposed approach, a set of synthetic experiments have been undertaken for a subcatchment of the Goulburn River experimental catchment in SE Australia [*Rüdiger et al.*, 2003]. Observed meteorological forcing data from five weather stations located within and surrounding the Goulburn River catchment were used as input to the model. In this application averages for the five weather stations were applied uniformly throughout the catchment for each forcing parameter. The data set used comprised a one-year period. Forcing data used by CLSM are temperature, wind speed, precipitation, specific humidity, and long and short wave downward solar radiation. While most of these forcing data are observed by the weather station, radiation observations were not available and radiation data were therefore obtained from the Global Data Acquisition System (GDAS) model.

Soil and vegetation properties in the subcatchment were assumed to be spatially uniform and estimated as the dominant value for each parameter. Vegetation data and greenness index were obtained from $0.25° \times 0.25°$ global vegetation maps, while soil type and properties were taken from the a digitised version of the Australian Soils Atlas [*Northcote et al.*, 1968]. Topographic data are incorporated in the model from compound topographic index calculated from a DEM with a resolution of 250 m.

Using the input data described above, CLSM was spun-up for a one-year period on the aforementioned forcing data, by repeated simulation until convergence of the initial conditions to an equilibrium state was achieved. The output from the subsequent simulation with these initial conditions was then assumed to be the "true" data. This was used to provide both the one-hourly streamflow observation data and the soil moisture time series evaluation data. The assimilation experiments were run for one month of this period during which two significant runoff events took place.

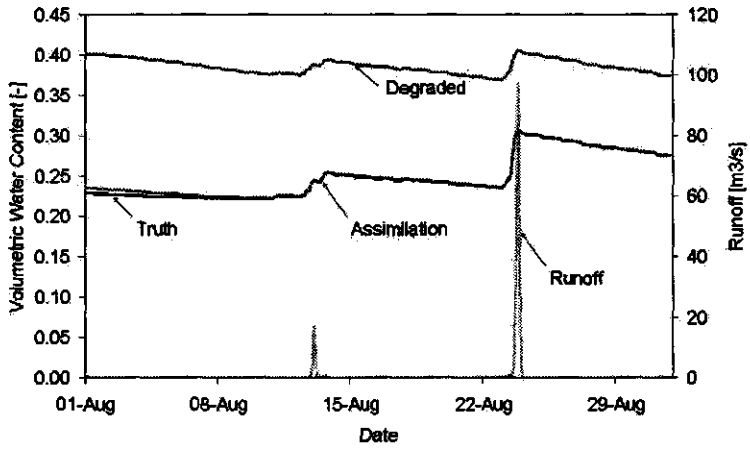

Figure 4.3: Results for experiment 1 assimilation run showing profile soil moisture content and observed streamflow.

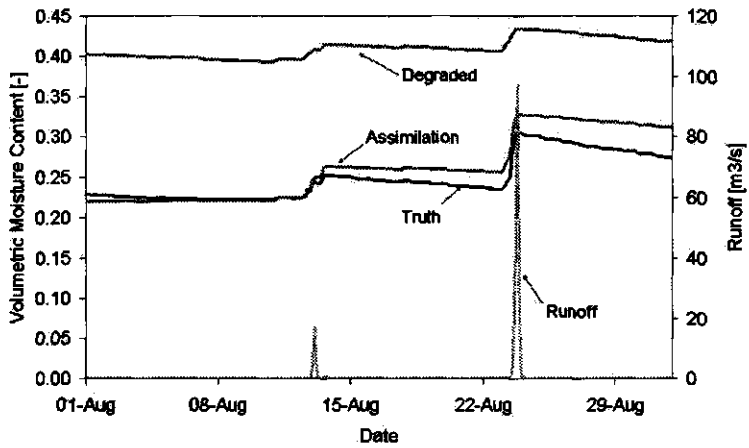

Figure 4.4: Results for experiment 2 assimilation run showing profile soil moisture content and observed streamflow.

Streamflow data output form the model is only available for the catchment outlet and is not available for ungauged tributaries within the catchment. Hence, streamflow output is only a lumped value for the whole upstream catchment. Similarly, soil moisture values are catchment averages of the surface, root zone and profile soil moisture content.

Two synthetic experiments were undertaken to demonstrate the assimilation of streamflow data for soil moisture retrieval. First, only the initial conditions of the three prognostic soil moisture states (catchment deficit, surface excess, and root zone excess) were arbitrarily degraded (experiment 1) while the forcing and observation data were perfect; initial conditions were degraded arbitrarily, so that an extreme wet condition was created. Second, both the soil moisture initial conditions and the forcing data were artificially degraded (experiment 2); the precipitation was increased by 20% and the incoming solar radiation was decreased by 33%. In this way we were able to explore the effect of erroneous forcing data on the assimilation results. The impact of this was to create an artificially wet catchment simulation.

Figures 4.3 and 4.4 show the catchment average profile soil moisture content for the assimilation and no assimilation runs compared to the "true" data and the "observed" streamflow, for experiment 1 and 2 respectively. In experiment 1 there is a good agreement between the retrieved and truth soil moisture data, while the results from no assimilation continue to overestimate the true soil moisture amount. While there is a small difference between the true and retrieved initial soil moisture states, this is quickly corrected when a streamflow runoff event takes place. Although these results were anticipated, given that we used a perfect model with perfect observations, it still demonstrates that there is a significantly strong relationship between the streamflow prediction and profile soil moisture content, even under semi-arid conditions.

Results from experiment 2 show a similar improvement in soil moisture prediction when streamflow observations are assimilated, compared with the no assimilation run. However, due to the dramatic increase in precipitation and decrease in radiation compared to the truth, the soil moisture prediction, even with assimilation, tends to predict a soil moisture content which is too wet towards the end of the assimilation window. To counter this, the assimilation attempts to make the initial conditions as dry as possible, but is constrained by the residual soil moisture content set in the model.

Both experiments showed good results for the retrieval of catchment average soil moisture profiles and adequate results for the root zone moisture content. However, retrieval of surface soil moisture was problematic for experiment 2. In this case, NLFIT was unable to find an optimum value for the initial surface excess prognostic variable. This is due to the small influence of the initial surface excess states on the total runoff, and the fact that only minor changes were produced in the objective function, even for major changes of the initial prognostic state value.

Conclusion This study has demonstrated using synthetic experiments that streamflow data assimilation has the potential to improve model prediction of soil moisture. Using a variational data assimilation approach, initial soil moisture states were retrieved by "calibrating" the model streamflow prediction to observed streamflow records. As residual soil moisture and porosity set upper and lower limits on the initial soil moisture storage, it was not possible to correctly predict the soil moisture time series over long time periods in the presence of large water balance errors. It is proposed that this problem may be resolved through shorter event based assimilation windows.

Acknowledgements This project is funded by an ARC Discovery Grant (DP 0209724). A visit by the principal author to NASA Goddard Space Flight Center was sponsored by a Postgraduate Overseas Research Exchange Scholarship from the University of Melbourne. The invaluable help and insight to the catchment land surface model provided by Randy Koster and Sarith Mahanama is greatly appreciated.

Assimilating AMSR-E observations into the NOAH land surface model to improve water cycle predictions

Xiwu Zhan[1], **Paul Houser**[2], **and Jiancheng Shi**[3]

[1]*UMBC-GEST/NASA-GSFC Hydrological Sciences Branch, Greenbelt, Maryland, USA*
[2]*NASA-GSFC Hydrological Sciences Branch, Greenbelt, Maryland, USA*
[3]*Institute for Computational Earth System Science, University of California, Santa Barbara, California, USA*

Soil moisture is a critical hydrosphere state variable that often limits the exchanges of water and energy between the atmosphere and land surface, controls the partitioning of rainfall among evaporation, infiltration and runoff, and impacts vegetation photosynthetic rate and soil microbiologic respiratory activities. Accurate initialization of this variable in water, energy and carbon cycle models is thus required for their reliable predictions. With real time or near real time global satellite observations of land surface soil moisture becoming readily available, how to effectively and efficiently assimilate these observations into weather or climate models becomes an urgent science question. This paper uses a Kalman Filter data assimilation method to evaluate several different approaches to assimilating the AMSR-E observations into the NOAH land surface model that is implemented in National Center for Environmental Predictions (NCEP) operational weather forecast models. Among these approaches are: (1) directly assimilate AMSR-E brightness temperatures into NOAH model using a simple microwave emission; (2) directly assimilate the brightness temperatures into NOAH model using a more detailed microwave emission; (3) assimilate surface soil moisture retrieved from the brightness temperature observations. The effectiveness and efficiency of these approaches are, several questions are evaluated against "true" soil moisture and water and energy fluxes observations collected during SMEX02 or SMEX03. Results of these soil moisture data assimilation approaches will be presented to the workshop for an in-depth discussion on various issues associated with soil moisture data assimilation.

The impact of incorrect model error assumptions on the assimilation of remotely sensed surface soil moisture

Wade T. Crow[1] and Rajat Bindlish[1]

[1]*USDA ARS Hydrology and Remote Sensing Laboratory, Beltsville, Maryland, USA*

Recent advances in the development of sequential land data assimilation techniques have demonstrated that remote sensing observations of surface soil moisture can improve the dynamic representation of root-zone soil moisture and streamflow in hydrologic models. However, much of the available evidence is based on identical twin experiments using synthetically generated, and artificially perturbed, measurements. These experiments, while extremely useful diagnostic tools for evaluating filter efficiency, typically simplify or avoid a number of key complexities facing operational efforts to assimilate spaceborne observations. One typical assumption in synthetic experiment is that the statistical nature of model errors is perfectly known. In reality, error in hydrologic model predictions comes from a wide variety of sources and manifests itself within multiple model state variables. Consequently, error information required by sequential data assimilation filter is almost never available in operational settings. The flexibility of approaches like the Ensemble Kalman filter with regards to model error is frequently cited to support its use in hydrologic data assimilation [e.g., *Crow*, 2003]. However, such flexibility cannot be properly exploited if the structure and source of model errors cannot be constrained in some way. Generally, little is known about the impact of poorly specified model error on the efficiency of assimilating remote observations into hydrologic models. This analysis describes a set of synthetic experiments where by model errors used to generate the Ensemble Kalman filter are statistically different from errors used to originally perturb the model.

The Ensemble Kalman Filter The Ensemble Kalman filter (EnKF) is based on the generation of an ensemble of model predictions to estimate the error/covariance information required by the standard Kalman filter (KF) for the updating of model predictions with observations [*Reichle et al.*, 2002; *Evensen*, 1994]. The EnKF can be generalized using a state space representation of prediction and observation operators. Take $\mathbf{Y}(t)$ to be a vector of land surface state variables at time t. The equation describing the evolution of these states, as determined by a potentially nonlinear land surface model $\mathbf{f}$, is given by:

$$\frac{d\mathbf{Y}}{dt} = \mathbf{f}(\mathbf{Y}, \mathbf{w}) \tag{4.1}$$

where $\mathbf{w}$ relates errors in model physics, parameterization, and/or forcing data and is taken to be mean zero with a covariance $\mathbf{C}_w$. The goal of the filtering problem is to constrain these predictions using a set of observations which are related to the model states contained in $\mathbf{Y}$. Let the operator $\mathbf{M}$ represent the observation process which relates $\mathbf{Y}$ to the actual measurements taken at time t_k:

$$\mathbf{Z}_k = \mathbf{M}(\mathbf{Y}(t_k), \mathbf{v}_k) \tag{4.2}$$

where $\mathbf{v}_k$ represents Gaussian measurement error with covariance $\mathbf{C}_{vk}$. The EnKF is initialized by the introduction of synthetic Gaussian error into initial conditions and generating an ensemble

of model predictions using (4.1). At the time of measurement predictions made by the ith model replicate are referred to as the state forecast $\mathbf{Y}^i_-$. If $\mathbf{f}$ is linear and all errors are additive, independent and Gaussian, the optimal updating of $\mathbf{Y}^i_-$ by the measurement $\mathbf{Z}_k$ is given by:

$$\mathbf{Y}^i_+ = \mathbf{Y}^i_- + \mathbf{K}_k[\mathbf{Z}_k + \mathbf{v}_k - \mathbf{M}_k(\mathbf{Y}^i_-)] \tag{4.3}$$

and:

$$\mathbf{K}_k = [\mathbf{C}_{YM}(\mathbf{C}_M + \mathbf{C}_v)^{-1}]_{t=t_k} \tag{4.4}$$

where $\mathbf{C}_M$ is the error covariance matrix of the measurement forecasts $\mathbf{M}_k(\mathbf{Y}^i_-)$ and $\mathbf{C}_{YM}$ is the cross-covariance matrix linking the predicted measurements with the state variables contained in $\mathbf{Y}^i_-$. All covariance values are statistically estimated around the ensemble mean. Here $\mathbf{Y}^i_+$ signifies the updated or analysis state representation. Of particular interest here are modeling errors represented by $\mathbf{w}$ and the impact of making inaccurate assumptions concerning $\mathbf{w}$. One potential diagnostic tool is the filter innovation ($\mathbf{v}$), defined as

$$\mathbf{v} = \mathbf{Z}_k - \mathbf{M}_k(\mathbf{Y}^i_-). \tag{4.5}$$

If $\mathbf{w}$ is perfectly represented (in a statistical sense) then the normalized innovations

$$\alpha = m^{-1}\mathbf{v}^T(\mathbf{C}_M + \mathbf{C}_v)^{-1}\mathbf{v} \tag{4.6}$$

should be mean one and temporally uncorrelated [*Dee*, 1995]. Normalized innovations have value as a diagnostic tool since various choices for $\mathbf{w}$ used to generate the model ensemble can be evaluated based on the observed statistical properties of α.

TOPLATS modeling framework Land surface modeling will be based on the TOPMODEL-based Land Atmosphere Transfer Scheme [*Famiglietti and Wood*, 1994; *Peters-Lidard et al.*, 1997]. TOPLATS surface zone soil moisture (θ) predictions are based on the linear combination of two dynamic model states variables: the fraction of the land surface saturated from below by the water table (f_w) and the surface soil water content in non-saturated portions of the basin:

$$\theta = \theta_{sat} f_w + \theta_{unsat}. \tag{4.7}$$

Saturated fraction is, in turn, is calculated by assuming spatial variability in local scale water table depth is driven solely by variations in the local soils topographic index (STI) defined as

$$STI = \ln(a\overline{T}/T\tan\beta) \tag{4.8}$$

where a is area drained, T soil transmissivity, and β local slope. Variations in STI are related to variations in local water table depth (z) via

$$z = \overline{z} - f^{-1}(STI - \overline{STI}) \tag{4.9}$$

where the overbar represents spatial averaging of quantities within the basin and f the vertical decay of saturated hydrologic conductivity. Areas where $z <= 0$ indicates surface saturation, therefore

$$f_w = 1 - F(zf + \overline{STI}) \tag{4.10}$$

where F is the cumulative density function for STI, typically determined from high-resolution soil and topographic maps. Runoff is modeled as a combination of saturation excess runoff (the product of rainfall intensity and f_w) and separate parameterizations of infiltration excess runoff and baseflow. Soil moisture in unsaturated portions of the basin is calculated using a finite difference numerical approximation to the richards equations and predicted infiltration.

Methodology The experimental methodology is based on designating a single, unperturbed model realization as truth. Some statistical representation of model errors, w, is assumed and used to generate an open loop simulation that represents the unconstrained impact of model error on hydrologic predictions. Errors present in the open loop simulations are then filtered via the implementation of the EnKF and soil moisture observations (plus some random noise) generated from the original truth simulation. The EnKF filtering methodology is based on the *a prior* specification of an estimate model error, w'. Assumed model error may or may not represent w accurately. The focus of the analysis will be on the impact of instances in which $\mathbf{w} \neq \mathbf{w}'$. As illustrated in (4.7), surface soil moisture predictions in TOPLATS are driven by two key state variables: θ_{unsat} and z via its impact on f_w. Model error is represented here by applying adding additive Gaussian noise to both states. The impact of incorrect model error assumptions on EnKF results is represented via the intentional misspecification of model error magnitude and/or location.

Results Solid lines in Figure 4.5 demonstrate results for the simplified case where model error is assumed to be limited to a single known model state variable (i.e. θ_{unsat} for figures 4.5ab and z for figures 4.5cd).

Normalized error results on the y-axis of figures 4.5ac convey the fraction of 40 cm soil moisture root-mean-square (RMS) error calculated in the open loop case that is corrected via the assimilation of surface soil moisture. Variations in assumed levels of model errors can have strong consequences for the ability of the EnKF to filter model error. The critical issue is whether optimal levels of assumed model error (i.e., minimums in figures 4.5ac) can be identified from study of normalized innovations. According to linear filtering theory, properly tuned normalized innovations (α) should be mean one and temporally uncorrelated. Too large (small) an estimate of model error should result in innovations with a mean less (greater) than one. This is the case is figures 4.5ab. Tuning of assumed error in θ_{unsat} to produce temporally uncorrelated normalized innovations with a mean of one (in Figure 4.5b) leads to efficient filter results (in Figure 4.5a). Prospects for tuning are less promising for the case of error in z. A broad range of error values in Figure 4.5d (solid line) are associated with a mean slightly greater than one. Consequently, it is difficult to identify errors associated with optimal filtering. The problem stems from drift in the filter caused by the nonlinear relationship assumed between f_w and z in (4.10). This drift produces temporally correlated innovations (solid line in Figure 4.5d) that prevent the filter's normalized innovations from falling below mean one - even when model error is overestimated. Difficulties are compounded for the case where both the source and magnitude of model errors are unknown. Dashed lines in figures 4.5ad describe the impact of representing model error via fluctuations in z when, in reality, model error is due to random perturbations in θ_{unsat}. This misspecification of error prevents the assimilation of observed soil moisture from improving model results beyond those observed in the uncorrected open loop case (i.e., unity on the y-axis in Figure 4.5a). More importantly, tuning of model error to force normalized innovations closer to unity (see dashed line in Figure 4.5b) will actually make filter results worse.

Conclusions Prospects for using innovations to operationally tune sequential data assimilation filters appear dependent on the type and location of model error which requires filtering. Furthermore, misspecified model error can lead to circumstances under which the tuning of assumed

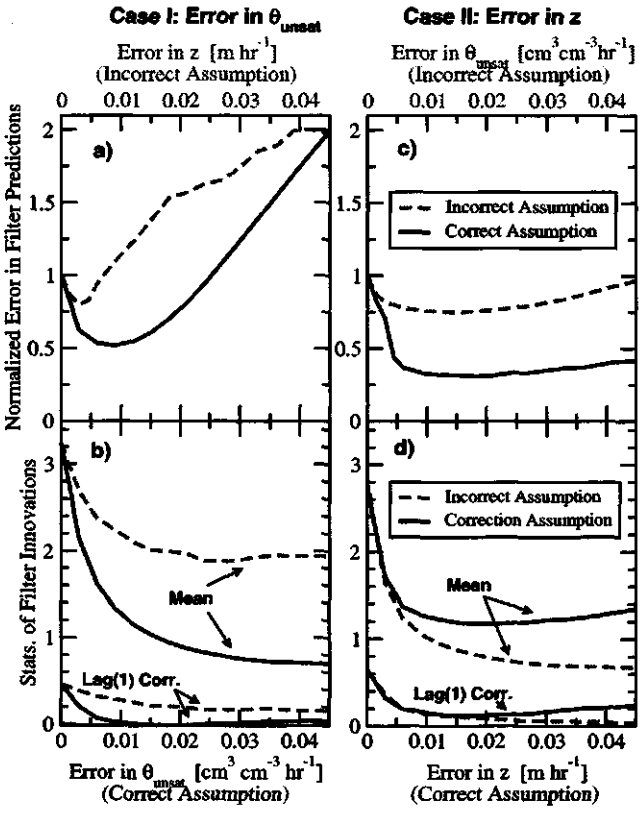

Figure 4.5: Impact of model error assumptions on the efficiency of filter predictions and the statistical properties of observed filter innovations.

model error via analysis of filter innovations will actually degrade the performance of the filter. Further study is required to determine the impact of poorly known model errors on the development of operational data assimilation systems to ingest remote sensing data into hydrologic models.

Bias correction of satellite soil moisture and assimilation into the NASA Catchment land surface model

R.H. Reichle[1,2], **R.D. Koster**[2], **and S.P.P. Mahanama**[1,2]

[1]*Goddard Earth Sciences and Technology Center, University of Maryland, Baltimore, Maryland, USA*
[2]*NASA-GSFC, Greenbelt, Maryland, USA*

Surface soil moisture data from different sources (satellite retrievals, ground measurements, and land model integrations of observed meteorological forcing data) have been shown to contain consistent and useful information in their seasonal cycle and anomaly signals even though they typically exhibit very different mean values and variability. At the global scale, in particular, it is currently impossible to determine which soil moisture climatology is more correct. The biases pose a severe obstacle to exploiting the useful information contained in satellite retrievals of soil moisture in a data assimilation algorithm. A simple method of bias removal is to match the cumulative distribution functions (cdf) of the satellite and model data. Cdf estimation typically requires a long data record. By using spatial averaging with a 2 degree moving window we can obtain statistics based on a one-year satellite record that are a good approximation of the desired local statistics of a long time series. This key property opens up the possibility for operational use of current and future soil moisture satellite data.

Introduction and Approach Accurate knowledge of the state of the land surface is important for many applications. For example, there is increasing evidence that accurate land initialization contributes to skill in subseasonal climate forecasts of summer mid-latitude precipitation and air temperature [*Koster et al.*, 2003, 2004]. Our ability to accurately characterize global soil moisture fields relies on (1) retrievals of surface soil moisture from satellite, and (2) land surface models that integrate meteorological forcing data (such as precipitation and radiation from observations or atmospheric data assimilation) and land surface parameters (such as soil hydraulic or vegetation properties). It has long been argued that a land data assimilation system that merges these two sources of information will improve our knowledge of the state of the land surface. Such a data assimilation system must, however, address severe biases that have been identified in surface soil moisture.

Reichle et al. [2004] show that the time series mean and variability of surface soil moisture from satellite retrievals and model integrations differ substantially, and neither agrees better with the sparse ground measurements that are available. It is in fact impossible at this time to determine a "correct" global surface soil moisture climatology towards which satellite and model data could be corrected in a data assimilation system. Rather, we are limited to removing biases between the satellite retrievals and model soil moisture by ensuring statistical consistency between the two data sources. An obvious method for doing so is to match the cumulative distribution functions (cdf's) of the satellite retrievals and model soil moisture. Similar cdf matching techniques have been used successfully for example to establish reflectivity-rainfall relationships for calibration of radar or satellite observations of precipitation [*Atlas et al.*, 1990; *Anagnostou et al.*, 1999]. Cdf matching is conceptually straightforward, but the need to estimate the cdf of satellite retrievals of soil moisture is difficult in practice because of the limited availability of such data.

The historic Scanning Multichannel Microwave Radiometer (SMMR) offers a unique record of almost nine consecutive years of passive C-band (6.63 GHz) observations. A record of such length

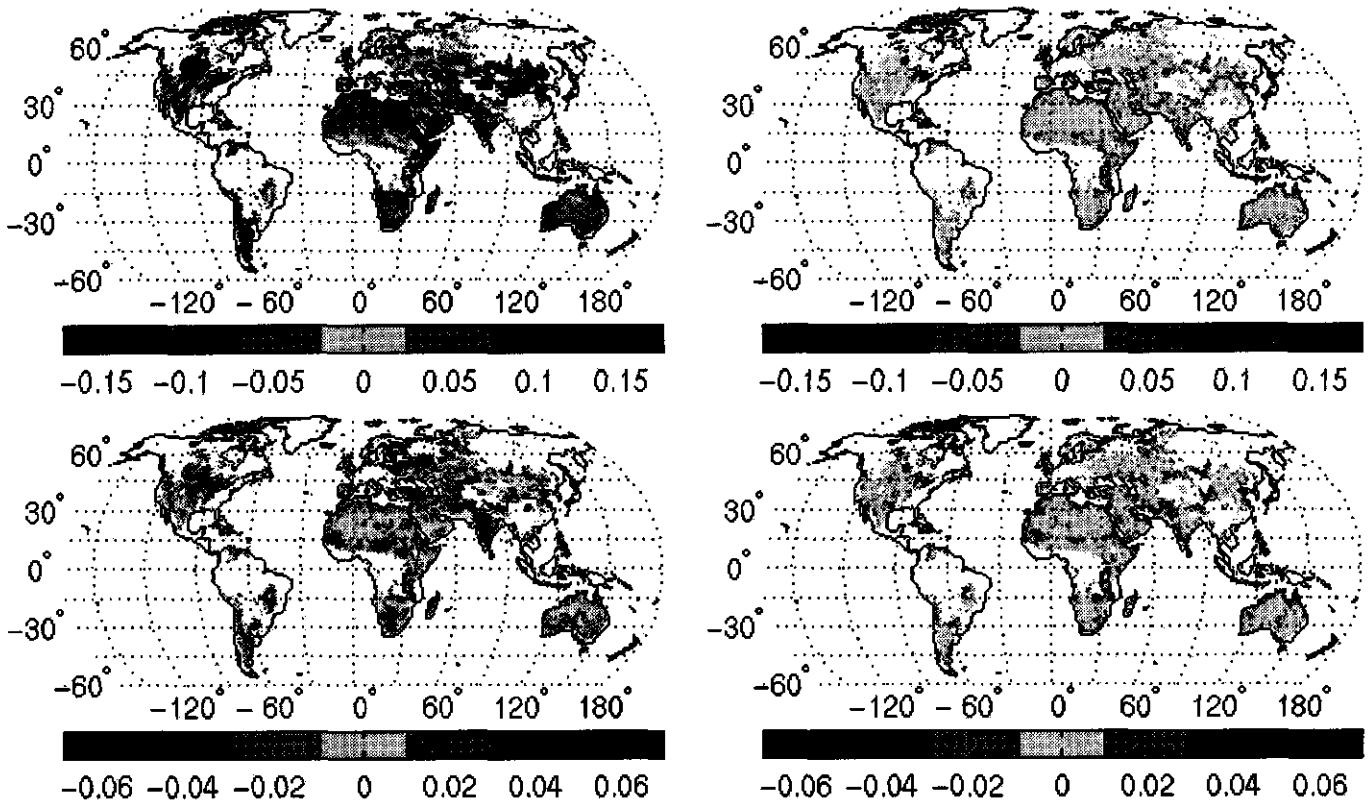

Figure 4.6: Difference in (Top) mean and (Bottom) standard deviation of SMMR soil moisture retrievals and model soil moisture time series (1979–1987) (Left) before and (Right) after cdf matching. Approximate cdf for scaling is estimated from 1979 SMMR data only with spatial aggregation at a scale of 2 degrees. Missing data are plotted white. Units are volumetric percent [$m^3\ m^{-3}$].

permits estimation of the statistics with reasonable accuracy. On the other hand, current and planned soil moisture sensors are designed for shorter observing periods of three to six years. These include the currently operational C-band Advanced Microwave Scanning Radiometer for the Earth Observing System (AMSR-E), and two planned L-band (1.4 GHz) sensors, the Soil Moisture and Ocean Salinity (SMOS) mission, and the Hydrosphere State (HYDROS) mission. Even more importantly, it is a primary goal of these missions to provide near-real time data for operational research applications. But operational applications would be impossible if the satellite retrievals became useful only after the lifetime of the satellite. In this paper we use the nine-year SMMR record to demonstrate that temporal aggregation of SMMR data can be traded off against spatial aggregation. Robust estimation of the statistics for bias removal is accomplished using only a one-year satellite record. With our method, current and future satellite retrievals of soil moisture can be processed in near-real time using only a one-year climatology.

Data and Method SMMR satellite retrievals of soil moisture are from October 1978 to August 1987 [*de Jeu*, 2003]. The sensor's configuration on a polar-orbiting platform allowed for a maximum repeat frequency of about three to four days in mid-latitudes. Despite global coverage of the satellite, soil moisture retrievals are not available everywhere. Areas for which surface soil moisture cannot be retrieved include areas with frozen soil, mixed pixels that contain a significant fraction of surface water, and highly vegetated areas. Our land modeling system uses the state-of-the-art NASA Catchment land surface model [*Ducharne et al.*, 2000] and surface meteorological data from [*Berg et al.*, 2003]. The surface meteorological forcing data are based on the European Centre for Medium-Range Weather Forecasting 15-year reanalysis (ERA-15) available from 1979 to 1993 and have been corrected to observed data as much as possible. Precipitation - arguably the most critical input for accurate soil moisture modeling - has been corrected primarily with a merged product of satellite and gauge data from the Global Precipitation Climatology Project (GPCP, Version 2) [*Huffman et al.*, 1997]. For further details on the SMMR retrievals and Catchment model soil moisture see [*Reichle et al.*, 2004].

Approach Our strategy for bias removal is to match the cdf of the satellite retrievals to the cdf of the model soil moisture by scaling the satellite retrievals. The scaled satellite retrieval x' is given implicitly by the solution to $cdf_m(x') = cdf_s(x)$, where cdf_s and cdf_m denote the cumulative distribution functions of the satellite and model soil moisture, respectively, and x is the unscaled satellite soil moisture. Note that cdf matching corrects all moments of the distribution function, subject to statistical errors that are due to a limited sample size. In practice, we can expect meaningful estimates only for the first few moments of the distribution function, and limit ourselves to analyzing the mean, standard deviation, and skewness. The key to successful bias removal via cdf matching is to identify the temporal and spatial scales at which the cdf is estimated and cdf matching is applied. Since an assimilation systems ingests instantaneous satellite retrievals at the local (or catchment) scale, statistics used for bias removal should be computed from and applied to local, instantaneous data. In fact, the complex heterogeneity of the land surface is only approximately described by the retrieval algorithm and the land model, and errors vary strongly in space. The ideal estimate of the local cdf for our purpose is thus based on the longest available data record and computed without spatial averaging.

Figure 4.6 shows global maps of the biases in the time series mean and standard deviation between model soil moisture and satellite retrievals. Across the globe, SMMR retrievals are typically wetter than model soil moisture, except in the eastern half of North America, northern Eurasia, and the Sahel. SMMR retrievals exhibit more variability than model soil moisture across North America, in northern Eurasia, southern Africa, and southern Australia. Elsewhere, particularly in India, SMMR retrievals are less variable in time than model soil moisture. Figure 4.6 demonstrates that there are severe biases between satellite retrievals and model soil moisture. Most importantly,

these biases are not uniform but spatially distributed in complex patterns and are on the order of the dynamic range of the signal.

Next, we estimated the cdf based on various subsets of the full dataset of SMMR retrievals. In order to control statistical noise in the cdf estimate, we spatially aggregate the data: At any given location, observations of neighboring catchments that are within a given distance are also used to compute the statistics at the given location. In other words, we apply a moving spatial window to the computation of the statistics and implicitly assume that some degree of ergodicity is present in the data. We then use this approximate estimate of the cdf to solve $cdf_m(x') = cdf_s(x)$ and obtain scaled SMMR retrievals whose statistics are again compared to those of the model soil moisture.

Results When the cdf that is used for scaling is estimated from a subset of the SMMR retrievals, some locations will inevitably have insufficient data for robust estimation of the statistics. Our cutoff criterion for estimating the cdf is that at least 100 measurements must be available. Without spatial aggregation, the cdf cannot be estimated from just one year of data anywhere. Coverage increases rapidly with increasing spatial aggregation scale, and for spatial aggregation scales of 2 degrees and larger virtually no extra data are lost. The loss of coverage must be traded off against the ergodicity error, that is the error resulting from spatially averaging when estimating the cdf. We computed relative bias reduction using various 1 and 2 year subsets of the SMMR data in combination with spatial aggregation scales ranging from 0 to 5 degrees. It is important to note that the bias is always computed for the full data set (1979–1987) after scaling all SMMR retrievals with a cdf that is based on a subset of the data.

Clearly, the smallest relative biases in the mean and standard deviation are typically achieved when the full SMMR dataset (1979–1987) is used to estimate the scaling cdf. Without spatial aggregation (ideal scenario), the bias in the mean (standard deviation; or skewness) is reduced to about 2% (10%; or 45%) of the bias before cdf matching. When the full set of data is used in combination with spatial aggregation at a scale of 5 degrees, the bias in the mean (standard deviation) is about 26% (65%) of the bias before cdf matching, while the bias in the skewness after cdf matching is worse than before cdf matching. If only a single year of SMMR retrievals is used to estimate the cdf in combination with spatial aggregation, scaling with such an approximate cdf does still considerably reduce the biases. We also find that the bias after cdf matching depends only weakly on the particular year that has been used for estimating the cdf. This is not surprising, given that the biases are much larger than the interannual variability.

Knowing the loss of spatial coverage and the increase in ergodicity error as a function of the spatial aggregation scale enables us to optimize for a particular spatial aggregation scale. Since the ergodicity error increases with increasing horizontal aggregation scale, a reasonable approach is to use the minimum spatial aggregation scale for which coverage is almost complete. In our case, this strategy suggests a spatial aggregation scale of 2 degrees. In other words, the best estimate of the cdf of all SMMR retrievals that is based only on 1979 data is obtained for a spatial aggregation scale of 2 degrees. We refer to this estimate as the approximate cdf. Finally, Figure 4.6 also shows global maps of the remaining biases relative to the model soil moisture after bias removal using the approximate cdf for SMMR retrievals. While there is some bias left after cdf matching, bias removal with the approximate cdf based on just one year of satellite data clearly removes most of the bias in the original data.

Conclusions We use the nine-year SMMR record to demonstrate that temporal aggregation of SMMR soil moisture retrievals can be traded off against spatial aggregation. Robust estimation of the statistics for bias removal via cdf matching was accomplished using only a one-year satellite record in combination with a spatial aggregation scale of 2 degrees. This approximate scenario yields almost the same coverage as the ideal scenario where the statistics are computed from a long data record without spatial aggregation. The global average bias is reduced by 98% in the ideal

scenario and by 80% in the approximate scenario when compared to the original bias between the SMMR retrievals and model soil moisture. For the standard deviation (skewness), the ideal scenario allows bias reduction by 90% (55%) and the approximate scenario permits bias reduction by 55% (25%). With our method, current and future satellite retrievals of soil moisture can be processed in near-real time using only a one-year climatology.

An obvious assumption of the applicability of our approach to current and future sensors is that biases for AMSR-E or HYDROS retrievals relative to model soil moisture are comparable to biases encountered with SMMR retrievals. While AMSR-E and future sensors are likely to yield improved measurements of brightness temperatures when compared to SMMR, the underlying errors in the retrieval algorithm, the land surface model, and the surface meteorological forcing data are unlikely to change significantly in the near future because the retrievals used here are based on a state-of-the-art algorithm, as is the modeling system. Therefore, our approach presents a valuable tool for the imminent operational use of AMSR-E soil moisture retrievals.

Multisensor and multiresolution variational assimilation of land surface temperature to estimate surface turbulent fluxes

Francesca Caparrini[1], Fabio Castelli[1], and Dara Entekhabi[2]

[1]*Dipartimento di Ingegneria Civile, Universita' degli Studi di Firenze, Firenze, Italy*
[2]*Massachusetts Institute of Technology, Cambridge, Massachusetts, USA*

A variational assimilation system for the estimation of two key parameters of surface turbulent heat flux (the non-dimensional turbulent heat transfer coefficient and the non-dimensional evaporative fraction) is implemented that uses land surface temperature sensed from a constellation of environmental satellites. The data relate to different times of day and apply at different and often overlapping resolutions. Thus the assimilation system has to be multiscale and capable of constraining the estimation at varying resolutions. It is shown that the separation of the surface source term into a bare soil and a vegetation component yields turbulent flux and parameters estimates that are consistent with the regional conditions over the study area. The system is applied to a large area within the U.S. Great Plains. Spatial patterns of the retrieved parameters and correspond to observed land use maps and show consistency with seasonal phenology across the Great Plains. The methodological innovations as well as physical insights gained as a result of the study are outlined. The advantages and limitations of the approach are listed. The information contained in sequences of land surface temperature from a constellation of satellites is shown to be valuable for the mapping of surface turbulent fluxes without reliance on empiricism or heavily-parameterized land surface models. Sensors capable of providing estimate of land surface temperature date back for decades. Thus multi-year maps of evaporation over land surfaces may now be possible.

Satellite data assimilation model with precipitation and micrometeorological forcing for the estimation of surface energy fluxes

F. Sini[1], G. Boni[1], and D. Entekhabi[2]

[1]*CIMA, Università di Genova e della Basilicata, Savona, Italy*
[2]*Ralph M. Parsons Laboratory, MIT, Cambridge, Massachusetts, USA*

The aim of this research is to estimate energy fluxes at the land surface, using satellite based Land Surface Temperature (LST) estimates. Ground based data of latent and sensible heat fluxes are available only for limited time periods and over very small areas. Satellite data are useful to obtain spatially distributed estimates of these variables. A variational assimilation scheme is used here to estimate energy fluxes at land surface over extended area. The model is based on surface energy balance, using bulk transfer formulation for sensible and latent heat fluxes. The dynamic equation of heat diffusion and Antecedent Precipitation Index (API) are used as constraints using the adjoint technique. LST, signature of dynamics energy balance, is the assimilated variable. LST, retrieved from sensors with different resolution is estimated using a split window algorithm. The model is tested and validated over Southern Great Plains 1997 hydrology field experiment data.

Land data assimilation scheme The starting point of this study is the assimilation scheme developed by *Boni et al.* [2001] and *Caparrini et al.* [2003]. Here no precipitation input or soil moisture related parameters were used. Soil moisture is the primary hydrological state variable that controls and it is controlled by land surface processes. Assessment of feedback mechanism between land surface and the atmosphere must involve soil moisture and thence precipitation. The model is modified in order to use precipitation information for a better simulation of soil moisture conditions [*Saxton and Lenz*, 1967].

The variational assimilation scheme is based on the definition of a penalty function that incorporates, as a physical constraint through Lagrange multipliers, a simple surface energy balance model for the "prediction" of the land surface temperature (LST) evolution (see *Caparrini et al.* [2003] for details). The first term of the penalty function is a quadratic measure of the misfit between model predictions and LST observations. This has to be minimized on the parameter space under the model's constraint. The physical constraint on the assimilation scheme is the dynamic equation of heat diffusion in the soil, in its simplified force restore approximation:

$$\frac{dT_s}{dt} = 2\sqrt{\pi\omega}\frac{R_n - H - LE}{P} - 2\pi\omega(T_s - T_{deep}) \tag{4.11}$$

where T_s is the LST, ω is the dominant (diurnal) frequency, P is the effective thermal inertia, R_n is the net radiation at the surface, H and LE are the turbulent sensible and latent heat fluxes and T_{deep} is a "restoring" deep-ground temperature.

For taking into account precipitation input, it was added, as simplified mass balance equation, the Antecedent Precipitation Index (API) relation:

$$\frac{dS}{dt} = -\gamma S + I \tag{4.12}$$

where γ is the decay API parameter and I the intensity of precipitation. The two equations have a number of parameters to be estimated: the bulk transfer coefficient C_B for heat, a soil moisture index α in the bulk transfer equation for latent heat and the API decay parameter γ.

The use of the evaporative fraction EF, defined as the ratio between the latent flux and the sum of turbulent fluxes, allows the elimination of the parameter α. The advantage of using EF instead of α to calculate latent heat fluxes, is that it can be assumed constant during daytime. The constraint equation can be written in terms of EF formulating LE as $LE = \frac{H \cdot EF}{1-EF}$. EF is the link between API and force restore equation. An empirical relation between API and EF is found using FIFE 87 field campaign data. EF is function of the mean daily API and of a parameter K, that takes into account physical constraints on EF other than soil moisture:

$$EF = a + b \cdot \frac{\arctan(K\overline{S})}{\pi} \tag{4.13}$$

K is assumed to be constant during the simulation period (see below), in accordance with vegetation cover changes time scale. In this way EF holds both daily "moisture" and monthly land use dependence. After all, K is the only estimated parameter into the assimilation scheme, whereas mean daily S is calculated from hourly precipitation data. The model doesn't require auxiliary data on soil texture and vegetation.

The model was thought and set to assimilate also the decay daily API parameter. After several experiment it was seen that its value is not very sensitive to the assimilation procedure. So, because of its almost insignificant influence over the final result, it is put constant, with a time decay value $\gamma = 0.07$ that corresponds to a period of more or less two days. In this way a faster convergence was obtained. Also the C_B coefficient is put constant, since model runs with all parameters assimilated did not show any significant improvement. Air temperature, wind speed at reference height (2 m), net radiation are the other forcing meteorological data, measured by ground micrometeorological stations.

Application The assimilation model has been applied on the US Southern Great Plains (SGP) site, a field measurement site established by US Department of Energy's Atmospheric Radiation Measurement (ARM) Program. The field experiment site, is located in north-eastern Oklahoma and its extension is about 16,000 km^2. The period of assimilation spans from 18 June to 18 July 1997 . A grid of 4 km over SGP field was set for the model.

The scheme is formulated using a multi-scale approach. Estimates of land surface temperature from AVHRR, SSM/I and GOES Imager sensors (see *Caparrini et al.* [2002] for details) are assimilated over the specified region every 30 minute, where data is available. The gridded (4 km $\times$ 4 km) precipitation field, created by the Hydrometeorological Analysis Support forecasters at the Arkansas-Red Basin River Forecast Center[‡], is used as precipitation input. This field is a combination of WSR-88D Nexrad radar precipitation estimates and raingauge reports. An important improvement on final result was obtained using this data instead of gauge data alone, interpolated with nearest neighbour method. Other forcing of data assimilation system is taken from micrometeorological stations and interpolated on field domain.

The application on the SGP site has shown consistent estimation of EF and turbulent fluxes with field measurement data and agreement with precipitation trend. In the following figure is plotted the evaporative fraction for El Reno site. Bars indicate the range of variability of daily EF data measured with different ground sensors and black dots are the model estimates of mean daily EF at the same place.

[‡]http://www.srh.noaa.gov/abrfc/cgi-bin/arc_search.php

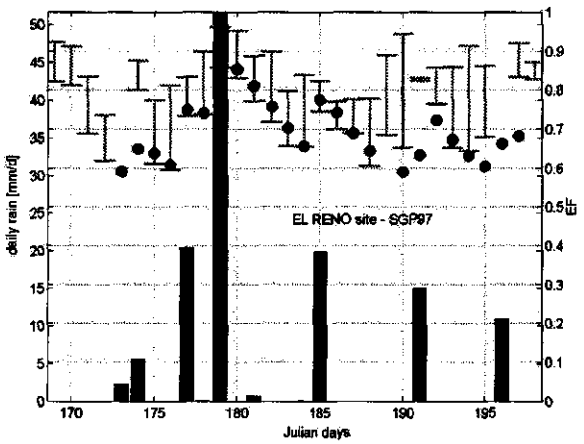

Figure 4.7: EL RENO SGP site. Right axis- Dot: model estimates of mean daily EF. Bars: range of variability of ground different sensors measurements. Left axis- histogram: daily cumulated precipitation.

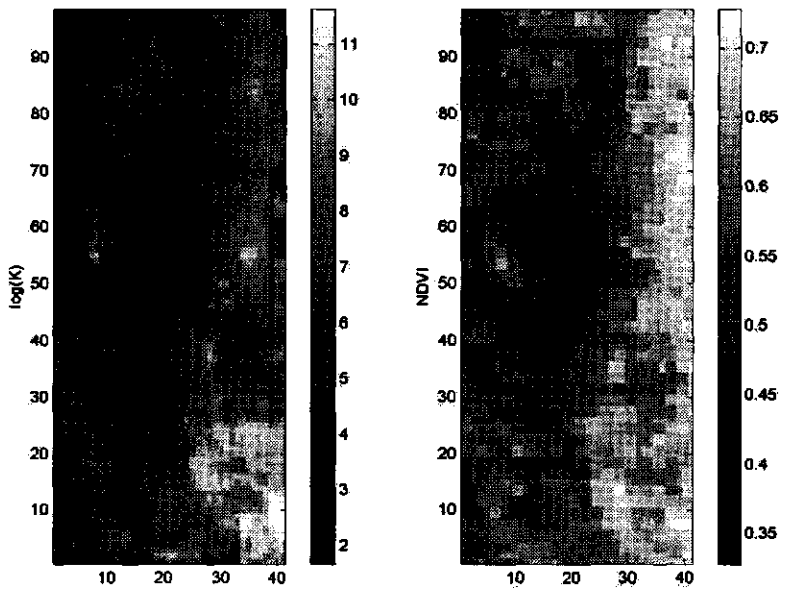

Figure 4.8: On the left $\log(K)$ pattern on SGP97 selected domain. On the right NDVI pattern field.

The pattern of K parameter was compared with the Normalized Difference Vegetation Index (NDVI) field, which is not used in the assimilation but only for posterior considerations. Figure 4.8 shows the good spatial agreement between the two parameters, with a correlation coefficient equal to 0.72 .

The following step is to apply the model to a Southern Italian basin with the aim of using the estimated evapotranspiration into a rainfall-runoff model. Usually hydrological models are calibrated using just integral measures such as discharge observations. The outputs of the assimilation scheme can be used for calibration and validation of hydrological models minimizing an objective function that minimizes the differences between observed and estimated discharges and energy fluxes. The output of present model could be used to validate the rainfall-runoff model or integrated as input field with Kalman filter technique. In particular the Basento river basin (southern Italy) is chosen, where validation measurement of LST and fluxes, and micrometeorological forcing data are available on some ground sites. The land surface temperature from SEVIRI data, on board of Meteosat Second Generation, will be used as observations within the assimilation scheme.

Assimilation of latent and sensible heat flux data into a land surface model

Robert Pipunic[1], Jeffrey P. Walker[1], Andrew W. Western[1], and Cressida Savige[1]

[1]*Department of Civil and Environmental Engineering, University of Melbourne, Parkville, Victoria, Australia*

In the science of numerical weather prediction, land surface models coupled with climate and weather forecast models are now commonplace. Sensible and latent heat flux predictions from land surface models provide valuable atmospheric feedback for climate and weather forecast models to achieve optimal predictions. This research will focus on the assimilation of sensible and latent heat flux data into a stand-alone land surface model to test how this might improve modelled sensible and latent heat fluxes compared with traditional approaches of assimilating soil moisture and/or screen level temperature and relative humidity data. Since soil moisture and screen level temperature and humidity states are weakly related to heat fluxes, this research is motivated by the assumption that assimilating sensible and latent heat flux data may yield better predictions. The investigation will be carried out using both synthetically generated sensible and latent heat flux and soil moisture data, in addition to measured sensible and latent heat flux and soil moisture data from three study sites in south eastern Australia. Of the measured data, ground based point measurements will be used, in addition to measurements from airborne sensors and derived from remotely sensed satellite estimates.

Introduction It has long been established that weather and climate forecast accuracy is improved when a coupled land surface model accurately represents the latent and sensible heat flux feedback to the atmosphere [*Pathmathevan et al.*, 2003; *Pitman*, 2003; *Entekhabi et al.*, 1996]. In this context, data assimilation research has focussed on improving land surface prediction of latent and sensible heat fluxes by improving soil moisture prediction through the assimilation of remotely sensed near surface soil moisture [e.g., *Walker and Houser*, 2001] or screen level humidity and temperature observations [e.g., *Margulis and Entekhabi*, 2003; *Seuffert et al.*, 2003; *Bouttier et al.*, 1993; *Mahfouf*, 1991]. However, screen level humidity and temperature are indirectly and sometimes weakly related to evapotranspiration [*Qu et al.*, 1998]. Moreover, most land surface models coupled to atmospheric models use soil moisture primarily as a tuning variable to achieve the correct latent and sensible heat flux prediction. Thus, there is no guarantee that assimilation of these variables (particularly a physical soil moisture content observation) into these models will improve the model prediction of latent and sensible heat flux [*Richter et al.*, 2004]. Therefore, this research aims to assimilate observed sensible and latent heat flux data into a land surface model, to correct the model's prediction of latent and sensible heat flux by modifying the model's prediction of soil moisture and temperature. The impact of assimilation on these states can then be compared with observations. This is an approach that has received little attention to date, with *Schuurmans et al.* [2003] representing one of the few published examples of this approach. In the study presented by *Schuurmans et al.* [2003], only remotely sensed latent heat flux estimates were used as observed data. These data were treated as truth and used to evaluate the values output from the land surface model. The latent heat flux data derived from remotely sensed data were assimilated into the land surface model to improve modelled latent heat flux values. However, no ground based validation of the remotely sensed fluxes was presented, or validation of the model

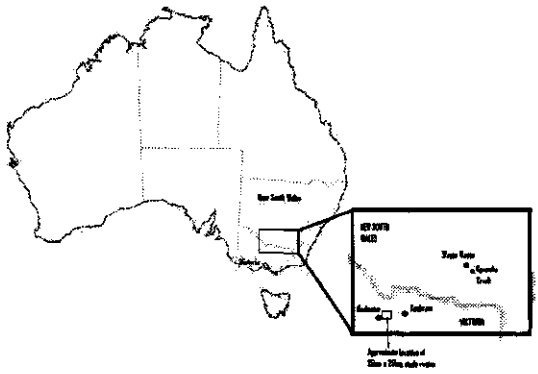

Figure 4.9: Map of Australia with close up showing approximate locations of study sites at Kyeamba Creek, Kyabram and the 25 km × 25 km study region near Rochester.

predictions after assimilation using ground based latent heat flux or soil moisture data in between assimilation time steps.

Method The assimilation will be performed using both synthetic and real datasets. The synthetic data assimilation approach will be similar to that of Walker and Houser (2001) for soil moisture assimilation. First, a one-dimensional soil column model will be spun-up for a fixed time period using forcing data that represents realistic meteorological conditions. Using the spin-up initial condition the model will be used to generate "true" land surface observation and evaluation data. Second, degraded simulations will be made representing the same period; one by setting the initial soil moisture variables to extreme wet values, and another by setting the soil moisture to extreme dry values. Typical errors in forcing data and model parameters will also be applied. Finally, simulations will be made whereby the "true" latent and sensible heat flux values from the original model simulation will be treated as observations and assimilated into each of the degraded simulations. The aim is to develop the assimilation algorithm and test the ability of the assimilation to improve the latent and sensible heat flux prediction from the degraded simulations as compared to the "true" values from the original simulation. At the same time, we aim to positively impact on the soil moisture and temperature profile predictions.

To test the performance of the assimilation approaches developed under real conditions, two one dimensional field sites will be investigated, each using latent and sensible heat flux data recorded via eddy correlation systems, along with soil moisture and temperature profiles. For these sites, the land surface model will be forced using measured meteorological and radiation data collected at the sites. The measured latent and sensible heat fluxes will be assimilated into the model. Measured values of soil temperature, soil moisture and latent and sensible heat flux between assimilation time steps will be used to test the assimilation performance. A 25 km × 25 km study region will also be investigated using spatial latent and sensible heat flux data from an airborne eddy correlation system, satellite remotely sensed data and ground based point measurements of soil moisture and of latent and sensible heat flux from eddy correlation systems. Forcing data for modelling in this region will be sourced from available point meteorological and radiation measurements, and from the nearest Australian Bureau of Meteorology station. A spatial study will first involve the assimilation of airborne eddy correlation data, using ground based point latent and sensible heat flux measurements, and soil moisture data to validate the modelled results. Then

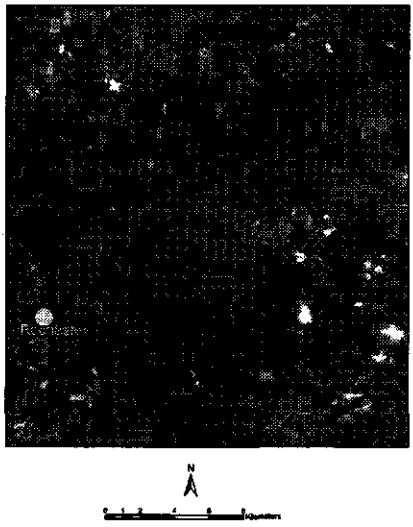

Figure 4.10: False colour (near infra red) Landsat image covering the 25 km × 25 km study region in Victoria. Blue dots represent soil moisture monitoring sites.

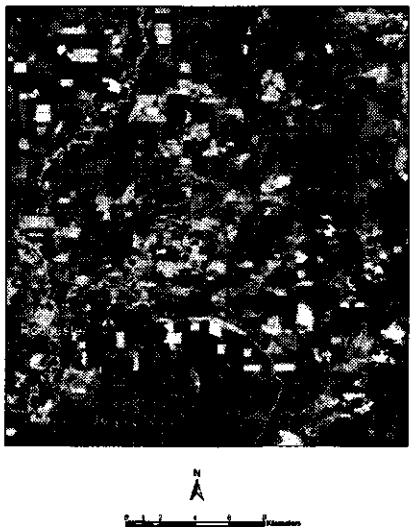

Figure 4.11: Remotely sensed thermal infra red image of the 25 km × 25 km study region shown above. Darker shades represent a higher thermal signature.

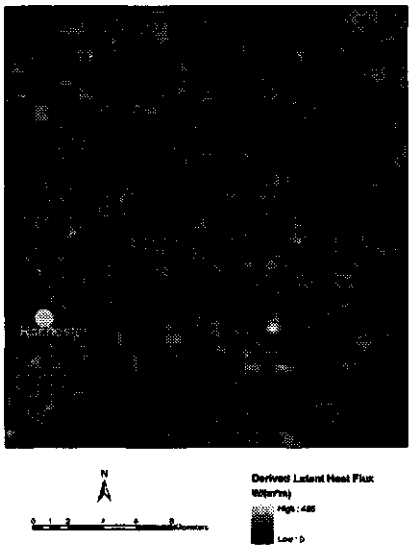

Figure 4.12: Image of latent heat flux values for the 25 km × 25 km study region, derived from satellite imagery shown above using the SEBAL algorithm.

using satellite remotely sensed data, assimilations will be made both with observed surface temperature data and with latent and sensible heat flux values derived using the SEBAL algorithm [*Bastiaanssen et al.*, 1998]. The performance of these two remote sensing based approaches will be compared, again with ground based latent and sensible heat flux and soil moisture measurements used as testing data sets.

Models A Kalman filtering approach will be used to assimilate the observed latent and sensible heat flux data into the European Center for Medium range Weather Forecasting land surface scheme used by the Australian Bureau of Meteorology. This land surface model was developed by *Viterbo and Beljaars* [1995], and is referred to herein as VB95. It consists of four prognostic layers for soil moisture and soil temperature, including a skin temperature and surface interception reservoir. The thickness of the four layers are 7 cm, 21 cm, 72 cm and 189 cm, from top to bottom respectively, with the penetration of roots from vegetation allowed in the three top layers. Vertical movement of water between the layers is governed by the diffusion form of Richard's equation, and vertical energy fluxes are governed by a soil heat diffusion equation. The lower boundary condition is characterised by a free drainage condition and zero heat flux. Net heat flux, computed from a surface energy balance calculation, and net water infiltration, which is the difference between incoming precipitation and a combination of interception, bare soil evaporation and surface runoff from the incoming precipitation, represent the upper boundary condition. Evapotranspiration in VB95 can occur from the interception reservoir, bare soil in the top soil layer and through transpiration from vegetation having roots in the top three soil layers (the root zone). Latent and sensible heat flux data and/or skin temperature data will be assimilated into the VB95 model using the Ensemble Kalman Filter, which is discussed in detail by *Evensen* [2003].

Data Sets The field data will be from three study sites in south eastern Australia (Figure 4.9).

These data consist of (1) two one dimensional sites measuring eddy correlation, soil temperature and soil moisture data in different landscapes, and (2) a 25 km $\times$ 25 km region with sixteen soil moisture monitoring sites, and remotely sensed (airborne and satellite) latent and sensible heat flux data.

At the one dimensional sites, continuous measurements of soil and atmospheric data are made over a 12 month period. One of the one dimensional sites is situated at Kyeamba Creek within the Murrumbidgee catchment, approximately 30km south east of the city of Wagga Wagga in New South Wales, and is located in a flat area of non irrigated grass pasture. The other is located near the town of Kyabram in Victoria on irrigated grass pasture land. The 25 km $\times$ 25 km monitoring region is located in northern Victoria near the town of Rochester and has one week of aircraft (January 2003) and nine months of satellite remote sensing measurements during periods from 2002 to 2004 that are being analysed for latent and sensible heat flux. Figure 4.10 is a false colour (near infra red) Landsat satellite image of the area which was used for analysis, with Figure 4.11 showing the thermal infra red image of the same area. Figure 4.12 illustrates latent heat flux coverage in the area that was derived from the Landsat data using the SEBAL algorithm [*Bastiaanssen et al.*, 1998]. In addition there are 16 ground point measurements of neutron probe soil moisture data collected at 4 depths (15 cm, 45 cm, 75 cm and 105 cm), these were collected fortnightly to coincide with the satellite overpass for the summer months of 2003 and 2004. The blue dots in figures 4.10 through 4.12 show their spatial distribution throughout the area. Also from the area are point measurements of atmospheric, radiation and latent and sensible heat flux data from 1D eddy correlation and Bowen ratio systems for the beginning of the irrigation season (October 2002) until January 2003. Continuous 3D eddy correlation, atmospheric and radiation data from the opening of the 2003 irrigation season (October 2003) until January 2004 are also available.

Summary This project aims to analyse the improvements in predictions of latent and sensible heat flux, together with soil moisture and temperature by a land surface model resulting from assimilating estimates of some or all of latent and sensible heat fluxes and surface temperature. Further, it aims to determine the best approaches to this assimilation problem. An assumption is made that assimilating latent and sensible heat flux into a land surface model, as opposed to soil moisture data, may lead to better model estimates of the surface energy balance as the process will bypass the dependency on soil parameterisation errors inherent in land surface models. These errors can lead to poor heat flux predictions when assimilating soil moisture.

Acknowledgements The senior author was supported by an Australian Postgraduate Award scholarship. This research was funded by the Australian Research Council Linkage Program Grant LP0211929 and the Shepparton Irrigation Region Implementation Committee. Landholders in the Nanneella and Kyeamba Creek areas are thanked for providing access to their farms for field measurements.

Assimilation of gravity data into a soil moisture and groundwater column model

A.B. Smith[1], **J.P. Walker**[1], **and A.W. Western**[1,2]

[1]*Department of Civil and Environmental Engineering, University of Melbourne, Australia*
[2]*Centre for Environmental Applied Hydrology and Cooperative Research Centre for Catchment Hydrology, Australia*

Gravity has the potential to become a new source of important remote sensing data for catchment-scale hydrological modelling. Monitoring of changes in the earths gravity field through time is expected to yield information on the change in terrestrial water storage (soil moisture, groundwater, etc) over that time period. However, the usefulness of this data has not yet been demonstrated. Specifically, the ability to accurately disaggregate the vertical (and spatial) distribution of terrestrial water storage change information contained in gravity measurements has not been explored. Through a series of synthetic twin studies, we seek to demonstrate the potential for gravity data to constrain a land surface model through data assimilation, and thus yield more accurate predictions of soil moisture profile distribution and groundwater storage. This pilot study uses a simple soil column model to describe the temporal variation of soil moisture and groundwater for a point in the landscape; we do not address the spatial disaggregation problem in this paper, which presents a methodology but no results.

Introduction Soil moisture is important for a number of applications, including global climate modelling, numerical weather prediction, rainfall-runoff modelling, and agriculture [*Western et al.*, 2002]. For meteorological applications it influences the energy balance by determining the partitioning of available energy at the land surface between latent and sensible heat fluxes. For hydrological applications it influences the water balance by partitioning precipitation between infiltration and runoff. For agriculture the amount and distribution of soil moisture heavily influences crop yield. However, the distribution of soil moisture is not well understood as it is highly variable in both space and time and there is a poor history of systematic monitoring. Hence there is a demonstrated need for improved prediction and monitoring of soil moisture. One potential way to improve predictions is from remotely sensed data assimilation.

With the recent launch of GRACE satellites in 2002, routinely collected gravity data has become a potential new source of remote sensing information for catchment-scale hydrological modelling. Monitoring changes in the earth's gravity field through time is expected to give information on the change in terrestrial water storage, which includes changes in soil moisture, groundwater, snow, lake and reservoir storage, etc, over that time period [*Wahr et al.*, 1998; *Rodell and Famiglietti*, 1999, 2001]. However, temporal gravity observations provide only a lumped measure of total terrestrial water storage change over large areas. For these data to be useful, methods need to be developed to (1) relate changes in terrestrial water storage to actual storage levels, (2) vertically disaggregate the terrestrial water storage signal into at least surface, root zone and groundwater components, and (3) spatially downscale from large basin averages to small sub-catchments.

We seek to demonstrate through a series of synthetic twin studies the potential to use gravity data to improve hydrologic prediction of the surface, root zone and groundwater stores; we do not address the spatial downscaling in the context of this paper. Our approach uses the gravity data to constrain a land surface model through data assimilation. This pilot study uses a simple soil

column model that describes the temporal variation of soil moisture (in three layers: near-surface, root zone and vadose zone) and groundwater. We present the methodology in this paper, but no results.

Model A simple column bucket model is used to predict the one-dimensional profile water storage in four different moisture stores. The first storage represents a shallow near-surface layer of 1 cm thickness (equivalent to the depth measured by passive microwave remote sensing satellites such as AMSR-E). The second storage represents the root zone, which we take to be approximately the top 1 m of soil. This is followed by vadose zone storage to approximately 4 m depth. Finally there is groundwater storage with an impermeable boundary assumed at 10 m depth.

The physics of the model are summarised as follows. Precipitation recharges the near-surface storage only. Bare soil evaporation (assumed to be 10% of the potential evapotranspiration multiplied by a moisture index for the near-surface store; the moisture index is the storage amount divided by storage capacity) is taken from the near-surface storage, and transpiration (assumed to be 90% of the potential evapotranspiration multiplied by the moisture index for the root zone store) is taken from the root zone storage. Water percolates down through the soil column to the underlying layer under gravity drainage. The gravity drainage is approximated as the saturated hydraulic conductivity multiplied by the moisture index of the origin store, constrained by the capacity of the receiving store. There is no possibility for water to move upward through the soil column or to be redistributed horizontally. Water is released from the groundwater store as baseflow, estimated as saturated hydraulic conductivity multiplied by the moisture index for the groundwater store. The model is run on a daily time step.

Data The observation and evaluation data to be used for this investigation are synthetically generated from the column bucket model described above. The only input data required by the model are saturated hydraulic conductivity (assumed as 5 mm h^{-1}), soil porosity (assumed as 50% v/v), initial moisture storage levels, precipitation, and potential evapotranspiration. Precipitation and evapotranspiration data are taken from 2-years of the Nerrigundah catchment data set [*Walker et al.*, 2001]. The catchment is located in temperate south eastern Australia.

Initial conditions for the moisture stores are obtained through repeated simulation of the model for 10 years using a single year of forcing data. The model is then run for the two years of forcing data to provide the "truth" evaluation data for vertical distribution of soil moisture and groundwater. The monthly synthetic gravity data "observations" are generated from the model output of soil moisture and groundwater at the start of each month.

Data Assimilation Two assimilation approaches are explored for the retrieval of soil moisture and groundwater from the monthly observations of gravity. These are the Kalman filter and variational approaches.

The Kalman filter is used to sequentially assimilate gravity observations as they become available [*Kalman*, 1960]. As temporal gravity data is only useful in terms of the change in gravity from one observation time to the next, rather than the absolute amount (the absolute gravity signal contains information on mass of the earth etc which is not part of a typical land surface model), the assimilation scheme either needs to include an additional state (change in total terrestrial water storage) or be used to estimate an additional parameter (the time invariant component of the gravity signal). In this way either changes in observed gravity, or the absolute gravity observation itself, may be sequentially assimilated. We have chosen the latter approach, with an added assumption that we actually know the time invariant component of the gravity signal. Further refinements to the algorithm will explore ways to determine this through the assimilation procedure.

The variational approach is used to assimilate the gravity data by considering the match between model predictions and observations over some time window. In this way the models predictions

of change in gravity (by difference between the two observation times) are optimised against the observed changes in gravity directly, by "calibrating" the model *initial conditions*. As such this is a conceptually more simple approach. Rather than derive an adjoint to perform the optimisation, we use a "brute-force" approach with standard optimisation software. We explore assimilation window lengths ranging from 1 month to 2 years.

Gravity Observations The Bouger slab approximation is obtained by calculating the gravitational attraction of a subterranean right vertical cylinder, and extending the radius of the cylinder to infinity [*Telford et al.*, 1990]. In this way the density of the slab multiplied by its thickness is directly proportional to the gravity. However, there is a change in gravity if the density is held constant but there is a change in height (useful for representing water table fluctuations), or if the height of the slab is maintained and its density is varied (useful for modelling gravity changes due to volumetric soil moisture variation). It should be noted however that the Bouger slab approximation is independent of depth to the source, so that large magnitude hydrological changes result in large magnitude modelled gravity even if the changes take place far underground (e.g., deep water table fluctuations).

Discussion Starting from poor initial conditions a number of simulations will be made for the 2 year time period. Both assimilation and non-assimilation predictions of soil moisture, groundwater and gravity will be compared with the truth and observation data. It is expected that the largest magnitude changes will be most accurately retrieved (usually groundwater table fluctuations) and that the assimilation will be ineffective for the smallest magnitude changes (near-surface soil moisture). This is particularly so if the Bouger slab model is used as it assumes independence of depth to source, contrary to the inverse distance square law of gravity. It is also hypothesised that maximum sensitivity will be obtained by having the water storages in terms of dimensionless volumetric water content rather than storage amounts. The longer assimilation windows are expected to give best results in the case of perfect model, forcing and observation data, but shorter assimilation windows are expected to give best results in the case of significant model and/or forcing error. This is because the initial conditions can be changed more often to account for mass imbalances. Finally, assimilation of daily near-surface soil moisture data (as available from the AMSR-E satellite) together with the monthly gravity data is expected to yield the greatest soil moisture retrieval accuracy. The accuracy requirements of temporal gravity will also be explored through the addition of white noise to gravity observations.

Acknowledgements This study is funded by Australian Research Council Discovery Project DP0343778 and a Faculty of Engineering Scholarship from the University of Melbourne.

Assimilation of GRACE-type observations to improve catchment-scale hydrological model prediction in the Murray-Darling Basin

Kevin M. Ellett[1], **Jeffrey P. Walker**[1], **Andrew W. Western**[1], **Rodger B. Grayson**[1], **and Matt Rodell**[2]

[1]*Department of Civil and Environmental Engineering, University of Melbourne, Australia*
[2]*Hydrological Sciences Branch, NASA Goddard Space Flight Center, Maryland, USA*

The GRACE (Gravity Recovery and Climate Experiment) mission of NASA and the German Aerospace Centre will provide global data sets of changes in earth's gravity field at unprecedented accuracy over the next several years. Hydrological processes occurring throughout the earth's surface lead to temporal changes in the distribution of mass which subsequently cause subtle changes in the earth's gravity field. Thus GRACE observations have the unique potential to provide the first-ever measurements of basin-scale changes in terrestrial water storage for monthly to annual time periods. Such observations show great promise in improving our understanding and simulation of the global hydrological cycle with clear implications for climate change prediction. This paper examines the potential utility of GRACE by assessing the improvement in catchment-scale hydrological model prediction from assimilation of basin-scale terrestrial water storage change observations. Using a conceptual rainfall-runoff model for the major catchments that comprise the Murray-Darling Basin (MDB) in Australia, synthetic twin studies are undertaken to explore the spatial disaggregation of GRACE-type observations. A variational data assimilation scheme enables us to downscale monthly synthetic GRACE observations to the catchment scale. Application of GRACE to specific hydrological basins depends on the size of the basin and the magnitude of the storage change signal. In the MDB, measurements from a ground-based monitoring network in one major catchment have an annual amplitude of total water storage change of approximately 80 mm, with average monthly changes of 13 mm. The estimated uncertainty in GRACE observations for the MDB is approximately 5 mm for monthly to annual water storage changes, suggesting that GRACE can improve catchment-scale modelling in the MDB through data assimilation.

Data assimilation of remotely sensed snow observations using an ensemble Kalman filter

Konstantinos M. Andreadis[1] **and Dennis P. Lettenmaier**[1]

[1]*Department of Civil and Environmental Engineering, University of Washington, Seattle, Washington, USA*

Snow is a major component of the hydrologic cycle and can play an important role in water resources management, especially in mountainous areas like the western United States. Current model-based approaches to hydrologic forecasting are limited by model biases and input data uncertainties, while ground based measurements have limited coverage and are unable to capture the spatial and temporal variability of snow properties. Remote sensing offers an opportunity for observation of snow properties, like areal extent and water equivalent, over large areas.

The Moderate Resolution Imaging Spectroradiometer (MODIS) on board the EOS Terra satellite has been operational since early 2000, and provides snow cover information at 500 m spatial resolution which is appropriate for regional applications. However, visible wavelength sensors like MODIS are inhibited by cloud cover which causes temporal discontinuities. Furthermore, MODIS provides no information about snow water content. Data assimilation offers a framework for optimally merging information from remotely sensed observations and hydrologic model predictions, and ideally overcoming limitations of both. A promising data assimilation technique that has found many applications in hydrology is the ensemble Kalman filter (enKF). The latter is a Monte Carlo variation of the traditional Kalman filter. Its most important advantage is the implicit propagation of error information through an ensemble of model states. This work describes the assimilation of MODIS snow areal extent data into a macroscale hydrologic model over the Snake River basin, where runoff is mainly snowmelt driven. The approach is built around the Variable Infiltration Capacity (VIC) macroscale hydrology model, which balances water and energy over each model grid cell at each timestep. The VIC model represents the effects of subgrid variability in soil moisture, vegetation, topography and precipitation. Model simulations were performed at a spatial resolution of $\frac{1}{8}^{\circ}$ with a daily timestep. The state variables included snow water equivalent at each model elevation band. A snow depletion curve parameterization was used as the nonlinear observation operator of the enKF. Results showed that the enKF is an effective and operationally feasible solution for the assimilation of remotely sensed observations. The filter successfully updated snow cover predictions by the model. Ground observation comparisons using SNOTEL and NCDC Cooperative Observer snow water equivalent and snow depth data, respectively, indicate that the filter estimates are an improvement over the "open-loop" VIC simulations. Additionally, the effect of the assimilation on streamflow and the potential of bias correction using data assimilation are investigated. Finally, specific limitations regarding filter sub-optimality and model simplifications are discussed.

Assimilating terrestrial hydrologic fluxes into land surface models using remote sensing data products

S. Chintalapati[1] **and P. Kumar**[1]

[1]*Dept. of Civil & Environmental Engineering, University of Illinois, Urbana-Champaign, USA*

The state of the land surface plays a critical role in the land-atmosphere interactions, through the dynamic evolution of moisture and energy fluxes at the land surface. The current crop of Land Surface Models (LSMs) estimating these fluxes, however sophistically parameterized they might be, are still constrained by the underlying approximate model physics. With the advent of a variety of land surface remote sensing (LSRS) data products, better estimations of the dynamic state can be obtained by integrating these LSRS products into the predictive models. However, some major challenges to such data integration lie in the discrepancies associated with the spatial and temporal scales of the LSRS products and those of model predictions and the unknown, yet dynamic, errors associated with them. We consider two approaches for LSRS data assimilation. In the first approach, we treat soil moisture state as the prognostic variable, enabling us to set up an assimilation framework to update the soil moisture profile and thus the associated energy fluxes, using remotely sensed near-surface soil moisture. While in the second approach, we use several LSRS products as surrogate data to provide an index to the energy fluxes, which is then used to update the soil moisture profile.

Numerous assimilation techniques of various levels of sophistication have been developed to assimilate remotely sense near-surface soil moisture to predict the soil moisture profile through deeper layers. But some of the major issues to address while using LSRS and their derived products for assimilation are related to the propagation of errors in these products into the estimates of the fluxes at the model's scales, especially when both the scales are different. We have developed a multi-scale system [*Kumar*, 1999; *Chintalapati and Kumar*, 2004; *Kumar and Chintalapati*, 2004] for assimilation of ESTAR-derived (Electronically Scanned Thinned Array Radiometer) near-surface soil moisture footprints into a land surface model at various spatial scales, run over a rectangular domain in the sub-humid environment of Southern Great Plains (SGP), Oklahoma. This system has a two step approach. In the first step, we use a multi-scale Kalman filter (MKF) to estimate near surface soil moisture and associated errors at a range of spatial scales (1 km to 32 km) using remotely sensed near surface soil moisture footprints at 1 km scale, obtained from SGP97 hydrology experiment conducted from 16 June to 17 July 1997 [*Jackson et al.*, 1999]. Figure 4.13 compares the ESTAR footprint soil-moisture and the multiscale estimates for the resolutions 1, 2, 4, 8, 16 and 32 km, represented with scale indices 7 to 2 (7 being the finest), obtained using the above procedure, for 20 June 1997. Since the multiscale Kalman filter is a least squares estimation procedure, the estimated fields are smoother than the original. However, they capture the spatial variability of the soil-moisture in the domain, although the representation within the footprint region is significantly better across scales.

In the second step, these estimates are assimilated into a land surface model using extended Kalman filter (EKF) algorithm to provide predictions of the entire soil moisture profile and energy fluxes at several scales. The simulation at each scale is run independently. Figure 4.14 shows the time series of daily average volumetric soil moisture of layers 1,2 and 3 (of LSM), to a total depth of 70 cm, at different spatial scales for a single station in the study domain referred to as

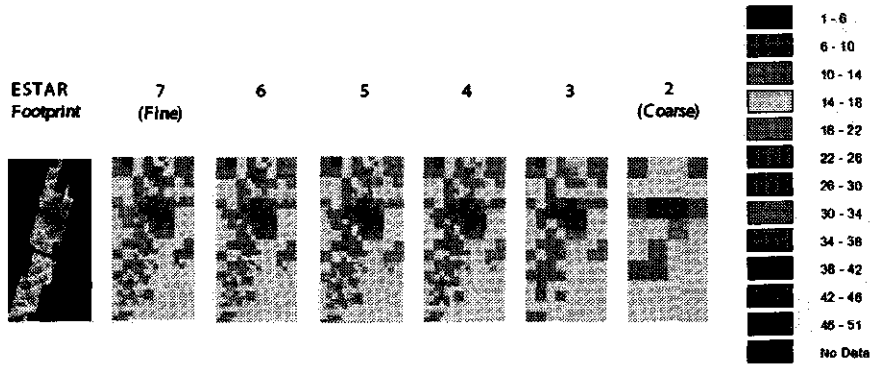

Figure 4.13: Soil Moisture estimates using multiscale Kalman filter with fractal model on 20th June (Julian day 171) at scale 7 (1 km) to scale 2 (32 km) for the whole study domain. Also shown at the left end is the ESTAR soil moisture footprint image covering nearly one-third of the domain. The legend shows percentage soil moisture.

ER05 (35.784°N latitude and 98.088°W longitude, grass and weeds over a rolling terrain). The *in situ* measurements at the station on two days (6 July and 15 July) are also shown. The 6 July (Julian day 187) measurement falls in a period with no assimilation for 2 days prior, while the 15 July (Julian day 196) measurement is preceeded by assimilation for 4 consecutive days. Figure 4.14(a) compares the daily average predictions of the first layer at different scales. The EKF predictions at most of the scales agree well with the validation measurements on 15 July, while showing deviations from the validation data on 6 July. The predictions at the finest scale show deviation from both the validation data and predictions at other scales during the period of Julian days 182–185 and Julian days 193–197. These periods are characterized by a preceeding rainfall event in an assimilation period. Similar trends can be noticed in Figure 4.14(b), which compares the EKF predictions at different scales for the soil moisture in the second layer (10 cm to 30 cm). The EKF predictions agree with the validation data on 15 July in the presence of assimilation at most of the scales. For the third layer (30 cm to 70 cm) in Figure 4.15, the EKF predictions do not show the consistency observed across scales in the first two layers during the early periods, but the consistency improves during the later part of the study period, especially during the last week. Although these validation results are a little disconcerting in that the predictions do not match the observations closely, they are an indicator of the inherent challenge in the prediction of soil moisture profile.

Though lot of research is being done to obtain remotely sensed near surface soil moisture as a reliable data product, the current coverage and spatial and temporal scales of the same have limited applications in land surface modeling. However, several other LSRS products are available as reliable global coverage data at desired spatial and temporal scales, which can be incorporated either directly or indirectly into LSMs to obtain reliable estimates of moisture and energy fluxes. As a second approach, we use LSRS products derived from radiation measurements by MODIS (MODerate-resolution Imaging Spectrometer) instrument flying on Terra and Aqua satellite platforms. These LSRS products are: Land Surface Temperature (LST), Vegetation Indices (NDVI/EVI), Fractional Vegetation Cover and Leaf Area Index (LAI). These data products, along with various Atmospheric Boundary Layer (ABL) variables (such as layer depth, pressure, humidity, wind speed, potential temperature, LW and SW radiation) obtained either as an output from an

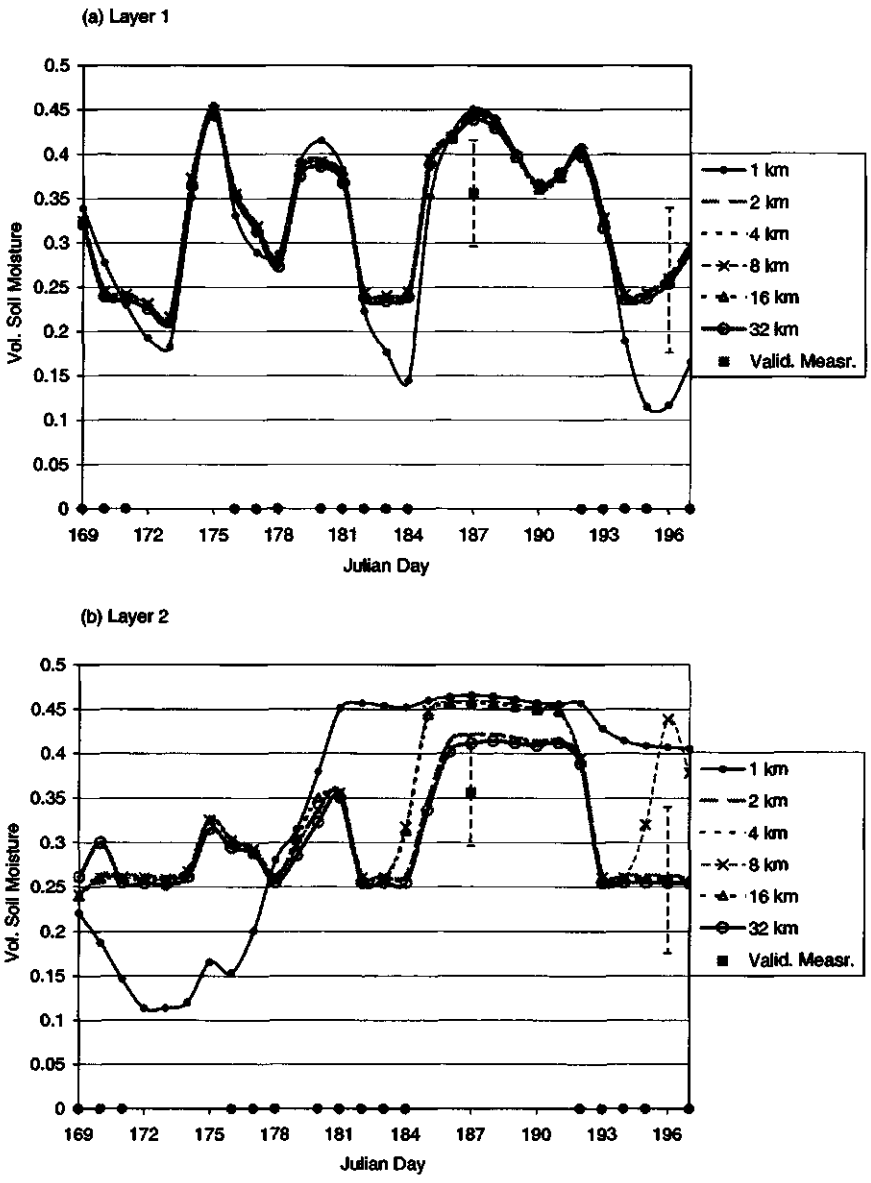

Figure 4.14: The time series of volumetric soil moisture at station ER05 shown at different scales. (a) 1st layer and (b) 2nd layer. Also shown are validaiton measurement values at 2 time points with their standard deviations. The days on which the assimilation is performed are marked as dots on the time axis.

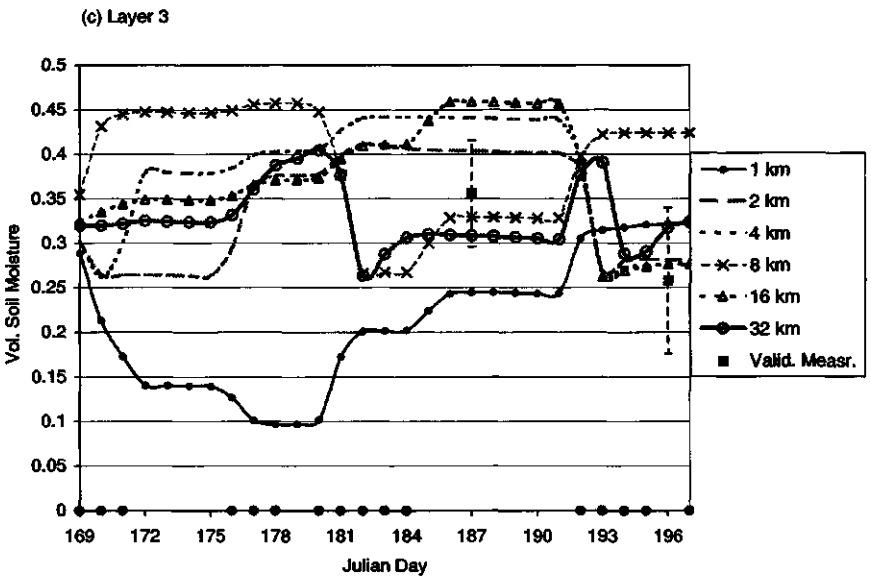

Figure 4.15: The time series of volumetric soil moisture at station ER05 shown at different scales. (c) 3rd layer. Also shown are validaiton measurement values at 2 time points with their standard deviations. The days on which the assimilation is performed are marked as dots on the time axis.

atmospheric model or measured, are used in the Surface Energy Balance System (SEBS) framework [*Su*, 2002; *Li et al.*, 2002] to obtain estimates of energy fluxes. These fluxes will then be assimilated into LSM at relevant spatial and temporal scales to update the soil moisture profile and associated fluxes at various spatial scales. The SEBS framework will be used in conjunction with LSM, so as to take advantage of more accurate parameterization from SEBS and the underlying physics representation in LSM, thus developing a blended system.

Adjoint sensitivity analysis and variational data assimilation for flash flood forecasting

W. Castaings[1], F.X. LeDimet[1], and D. Dartus[2]

[1]*French National Institute for Research in Computer Science and Control (INRIA), IDOPT Project, Grenoble, France*
[2]*Institute of Fluid Mechanics (IMFT), HYDRE Group, Toulouse, France*

Flooding is the result of complex interactions between the components of water cycle. Forecasting of a such catastrophic events requires a completely integrated approach (models and data) for the hydro-meteorological prediction chain. Actually, model components only lead to an approximation of the geophysical reality because models formulation, computational approach, inputs are all sources of uncertainty. Flash flood events are usually generated by heavy convective precipitations over a relatively small area but catchment hydrology plays a major in their occurrence. Thus, the transformation of rainfall into runoff is one of the most critical components for flash flood analysis. Recently, distributed hydrological models became an attractive alternative for the modelling of watershed hydrology but limited knowledge of all model inputs, initial conditions and observation of the hydrological response make the underlying problems of calibration, sensitivity analysis and uncertainty analysis very challenging. Variational methods provide a framework to carry out both sensitivity analysis and data assimilation. Sensitivity analysis is a key issue for providing physical insight into the model dynamics, ranking the sources of uncertainty and variational data assimilation is a good alternative to solve the key estimation problems. The potential of this technique will be discussed and illustrated for a flash flood model. Perspectives will be raised on the potential of a "continuous" monitoring and forecasting of land surface and atmospheric variables at larger scales.

Forward and Adjoint Models The underlying physics is of the model (MARINE) developed by *Estupina-Borrell et al.* [2000] is adapted to events for which infiltration excess dominates the generation of the flood. Therefore, for the temporal and spatial scales of interest rainfall abstractions by infiltration are evaluated by the Green Ampt model and the resulting surface runoff (hillslope flow) is distributed using the kinematic wave approximation. Lastly, river flow is routed with the full Saint-Venant equations, 1D or 2D depending on the valley configuration. The river hydraulics component will not be discussed in this paper. Event and physically based models like MARINE focus only on the physical processes of interest for the transformation of rainfall into runoff. Therefore, they are easier to set up, have lower computational cost and require less parameters to be calibrated. However, they have short term memory (antecedent conditions should be provided) and the prescription of consistent parameters associated with the model formulation is a challenging task. An adjoint model developed using automatic differentiation techniques is a flexible tool for sensitivity analysis and parameter estimation trough data assimilation. For the theoretical point of vue, the homogenous part of the adjoint model does not depend on the chosen objective function, from the algorithmic point of vue, only the part of the adjoint code gradient of the model response should be updated. MARINE adjoint model was developed using TAPENADE, a tool developed by *Hascoët et al.* [2003]. Then, extensive verification and validation were carried out, sensitivity and data assimilation experiments were carried out in order to illustrate the potential of this technique for catchment scale hydrology. They will be detailled in the following

sections of the paper.

Adjoint sensitivity analysis Catchment scale models sensitivity to spatial and temporal variations in precipitations received significant attention but the effect of runoff controlling factors (slope, soil infiltration capacity and land use) spatial variability is often completely underestimated. The rainfall-runoff relation is the typical case where dimension of the system response to be analysed is small compare the number of input parameters to be prescribed. In this case, the adjoint model is a very efficient alternative to compute the gradient of a response w.r.t the all parameters [see *Cacuci*, 2003, for a recent theoretical basis]. Appropriate measures of the model response were chosen and the adjoint model yields to the sensitivity of the model to input parameters. Spatial and temporal patterns of sensitivities can be obtained and a normalisation of the sensitivity fields allows analysis of the relative parameters contribution to the hydrological response. However, adjoint sensitivity analysis study the behavior of the system locally around a chosen point (local sensitivity analysis) given by a set of input parameters and forcing conditions. The influence of the chosen point on the analysis will be demonstrated and perspectives will be raised on global sensitivity analysis.

Variational data assimilation After extensive understanding and ranking of the sources of uncertainty for the given model structure, model calibration and/or updating which is very difficult problem for distributed catchment scale models is studied. Following the original idea suggested by *Le Dimet and Talagrand* [1986] for meteorology, the adjoint model is used in the variational data assimilation framework to compute the gradient of a misfit cost function between model results and observations. This gradient is used in an optimization algorithm to find the control vector (parameters to be estimated) leading to the lower value for the cost function. However, the parameter estimation issue for the rainfall-runoff transformation seem to be a pathological case of inverse problems. In fact, the component driving the partition of rainfall into infiltration and runoff is below the ground surface and observations of the catchment response to rainfall forcing is often only available at the basin outlet. In order to validate the algorithm synthetic observations were used for illustrative examples of the estimation problem for which the control space was arbitrarily simplified. A discussion on the possible methods to reduce the control space (parameterization) using identified spatial trends and correlations in the fields to be estimated using remote sensing data will conclude this part.

Conclusions and perspectives Sensitivity analysis and improvement of flash flood prediction by the assimilation of remote and in situ measurements and its relation to other components of the hydrologic cycle will be discussed for an event based flash flood model. During inter storms periods, understanding of the hydrological processes should be improved using more complex hydrological models which can benefit from the increasing sources of information at larger scales. The adjoint technique with the advent of powerful automatic differentiation tools for its practical implementation seem to be a very interesting alternative to solve numerous problems related to catchment scale modelling and data assimilation (sensitivity and uncertainty analysis, data assimilation, error propagation, error control, model coupling ...). In the future, the prediction of flash flood events will require interactive meteorological, hydrological and hydraulics models to be used in combination and include the use of all available data sources for the forecasting of the time and space distribution of both the rainfall and the resultant flooding.

Assimilation of observed discharge records into a lumped land-surface scheme using an extended Kalman smoother

Valentijn R.N. Pauwels[1] and Niko E.C. Verhoest[1]

[1] *Laboratory of Hydrology and Water Management, Ghent University, Ghent, Belgium*

The study of the relationship between precipitation and catchment discharge has always been one of the major interests in hydrology. The study of the processes which describe the partitioning of the incoming solar and atmospheric radiation into latent, sensible, and ground heat fluxes, and the partitioning of the precipitation into surface runoff, infiltration, and evapotranspiration, has lead to the development of Soil-Vegetation-Atmosphere Transfer Schemes (SVATS). It is well known that results from SVATS are prone to errors due to a variety of reasons, which can be errors or oversimplifications in the formulations of the model physics, and errors in the meteorological forcing data. Other reasons are the lack of soil, vegetation, and topographic data at a sufficiently high resolution and/or errors in these datasets. If observations of the model state variables or fluxes are available, these observations can be combined with the model results to reduce the errors in the model results. The updating of the model state with externally measured variables is commonly referred to as data assimilation. A wide variety of studies have put data assimilation in practice. These studies usually focus on the assimilation of observations of the surface soil moisture content and/or temperature. Due to the large spatial scales at which these models frequently need to be applied, one has to rely on remote sensing data for the observation of these variables. Although it has been proven that the assimilation of remotely sensed data can lead to an overall increase in model performance, remote sensing data usually have a larger uncertainty than in-situ observations, and are usually available at a coarse spatial and temporal resolution (e.g., weekly or monthly products). Because of these drawbacks, an alternative to using remote sensing observations is the use of catchment discharge observations in order to update the modeled soil moisture state. Although the assimilation of discharge observations into empirical models for the purpose of flood forecasting has been studied for three decades [*Wood*, 1980], the possibility to improve results of physically-based models through the assimilation of discharge observations has up to this data remained unexamined. The objective of this presentation is the demonstration of the possibility to improve SVATS results (in this case modeled latent heat fluxes and soil moisture content) through the continuous assimilation of discharge observations.

Test site and Data used The study is conducted entirely in the Zwalm catchment in Belgium. Figure 4.16 shows the location of the Zwalm catchment. The total drainage area of the catchment is 114 km^2 and the total length of the perennial channels is 177 km. The maximal elevation difference is 150 m. The average year temperature is 10°C, with January the coldest month (mean temperature 3°C) and July the warmest month (mean temperature 18^{o}C). The average yearly rainfall is 775 mm and is distributed evenly throughout the year. The annual evaporation is approximately 450 mm. For a further description of the Zwalm catchment, we refer to *Troch et al.* [1993].

Meteorological forcing data with an hourly resolution from 1994 through 1998 are used in this study. These data were prepared based on daily observations of air temperature and humidity, solar radiation, wind speed, and precipitation, from the climatological station located in Kruishoutem, approximately 5 km outside the catchment. Except for precipitation, the daily data were resam-

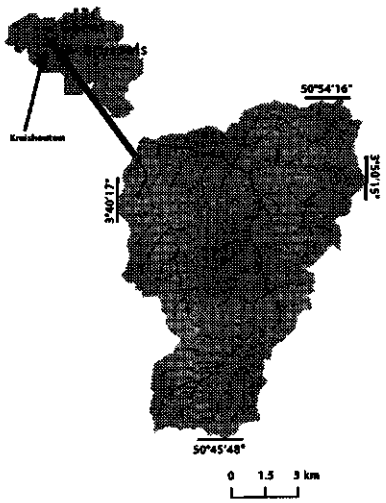

Figure 4.16: The location of the Zwalm catchment.

pled into hourly time-steps using the average diurnal cycle from discontinuous observations of these variables inside the catchment from 1991 through 1993. The daily precipitation was resampled into hourly time steps by rescaling hourly observations from the weather station of Uccle (located approximately 10 km outside Brussels) to the weekly totals of the Kruishoutem weather station. *Pauwels et al.* [2002] give a detailed description of this rescaling algorithm. Discharge observations at the outlet of the catchment are available at an hourly time step. Finally, a Digital Elevation Model (DEM), a digital soil texture map from the Belgian National Geographic Institute, and a SPOT-derived land cover classification map from 3 August 1998, are available at a 30 m resolution.

Model description The model used in the study is the TOPMODEL [*Beven and Kirkby*, 1979] based Land-Atmosphere Transfer Scheme (TOPLATS). The model was originally developed to simulate the surface water and energy balance for warm seasons [*Famiglietti and Wood*, 1994; *Peters-Lidard et al.*, 1997]. The hydrologic dynamics of the model has as its foundation the concept that shallow groundwater gradients set up spatial patterns of soil moisture that influence infiltration and runoff during storm events and evaporation and drainage between storm events. The assumption is made that these gradients can be estimated from local topography (through a soil-topographic index, *Sivapalan et al.*, 1987). From this foundation, the model was expanded to include infiltration and resistance-based evaporation processes, a surface vegetation layer and a surface energy balance equation with an improved ground heat flux parameterization, and the effect of atmospheric stability on energy fluxes [*Famiglietti and Wood*, 1994; *Peters-Lidard et al.*, 1997]. More recently, winter processes (frozen ground and a snow pack), an improved water and energy balance scheme for open water bodies, and a two-layer vegetation parameterization were added [*Pauwels and Wood*, 1999a]. Application to the Zwalm catchment [*Pauwels et al.*, 2001, 2002] and to field experiments such as FIFE [*Peters-Lidard et al.*, 1997] and BOREAS [*Pauwels and Wood*, 1999b, 2000] have proven that the model can adequately simulate surface energy fluxes, soil temperatures, and soil moisture. For a detailed description of the model, we refer to *Famiglietti and Wood* [1994], *Peters-Lidard et al.* [1997], and *Pauwels and Wood* [1999a].

The lumped version of TOPLATS is used in this study.

Methodology Model simulations are performed at an hourly time step, using a six-interval distrubution of topographic indexes, and seven land cover classes. The assimilation algorithm used in this study is based on the Fixed-Lag Extended Kalman Smoother (EKS), which is a extension to the Fixed-Lag Kalman Smoother (for linear systems) from *Cohn et al.* [1994]. The state vector consists of the modeled soil moisture for every interval in the land cover and topographic index distributions, for both the current time step, and the previous time steps, up to the concentration time ($n_c \triangle t$) of the catchment:

$$\begin{cases} x_k &= \left[\begin{array}{cccccccc} \mathcal{S}^{k\triangle t} & \bar{z}^{k\triangle t} & \mathcal{S}^{(k-1)\triangle t} & \bar{z}^{(k-1)\triangle t} & \ldots & \mathcal{S}^{(k-n_c)\triangle t} & \bar{z}^{(k-n_c)\triangle t} \end{array} \right]^{\mathrm{T}} \\ \mathcal{S} &= [O_u O_l] \\ O &= \left[\begin{array}{ccccccccc} \theta_{1,1} & \ldots & \theta_{1,n_v} & \theta_{2,1} & \ldots & \theta_{2,n_v} & \ldots & \theta_{n_l,1} & \ldots & \theta_{n_l,n_v} \end{array} \right] \end{cases} \tag{4.14}$$

with θ the soil moisture content, the subscript u referring to the upper soil layer, the subscript l referring to the lower soil layer, n_v the number of land cover classes, n_l the number of intervals in the distribution of the topographic index, n_c the number of time steps at which surface runoff generated at the furthers point in the catchment reaches the outlet, $\bar{z}$ the catchment averaged water table depth (m), T the transpose operator, and $\triangle t$ the time step (s). The vector with the observations consists of the observed discharge at time step $k\triangle t$:

$$z_k = [Q_k] \tag{4.15}$$

with Q_i the observed discharge at time step $i\triangle t$. The fundamental difference between the EKS and the traditional Extended Kalman Filter (EKF) is that in the latter the observations are a function of the current state only, while in the EKS the observations are a function of the model state at the current time step through the current time step minus the concentration time of the catchment:

$$z_k = h\left(\begin{array}{cccc} x_k, & x_{k-1}, & \ldots, & x_{k-n_c} \end{array} \right) \tag{4.16}$$

The modeled discharge at each time step is routed to the outlet of the basin using the unit hydrograph approach of *Troch et al.* [1994]. Using this approach, the catchment wetness conditions are updated for all time steps prior to the current time step which have an influence on the modeled discharge at the current time step.

A baseline run will first be established in order to check the model performance without data assimilation. The routed modeled discharge data will then be used as observed discharge values in a twin experiment. The model initial conditions and meteorological forcings will be disturbed to varying degrees, and the improvement in the model results caused by the assimilation of the observed discharge data will be quantified. The discharge observations will also be disturbed in order to assess the required accuracy of the discharge data for the purpose of data assimilation. Finally, the in-situ observed discharge data at the Zwalm catchment will be assimilated in the model run using the non-disturbed observed meteorological forcings, and the change in the model results will be quantified.

Anticipated results The expected results from this study are an understanding of the possibility to improve model results through the assimilation of observed discharge data, and the required accuracy and temporal resolution of these data in order to be useful for data assimilation.

Acknowledgement The lead author was, during the course of this work, funded by the Foundation for Scientific Research of the Flemish Community (FWO-Vlaanderen).

Snow data assimilation via ensemble Kalman methods

A.G. Slater[1] and M.P. Clark[1]

[1] *CIRES, University of Colorado, Boulder, Colorado, USA*

A snow data assimilation study was undertaken in which real data was used to update a conceptual snow model, SNOW-17 [*Slater and Clark*, 2004].

Within this model we implemented the Ensemble Kalman Filter (EnKF) and direct insertion assimilation methods. The research is based on the philosophy that calibration of the model allows it to capture the mean characteristics (or low frequency) of the system, while the assimilation process aids in capturing the high frequency events, thus model parameters remain constant across the ensemble. The study is based on use of individual stations in which ensembles of model forcing (temperature and precipitation) were stochastically generated by modeling the errors of regression based interpolation equations [*Clark and Slater*, 2004]. In each case, data from surrounding stations was used to produce the estimate at a given station, while measurements taken at the particular station were excluded from the procedure and provide an observed truth. Generating appropriate forcing data for use in the EnKF is an important step as it should encompass the forcing uncertainty. Figure 4.17a shows the results of the precipitation estimation at a sample point, indicating a large spread. The data to be assimilated into the models, that is, our interpolated estimates of snow water equivalent, were generated in the same fashion as the forcing data using the surrounding SNOTEL stations and error estimates are gained via cross validation. SNOTEL stations provide point measurements whereas the model operates over an area, thus as part of the assimilation process we transformed our observations into model (i.e., areal) space.

Figure 4.17b shows control simulation results by SNOW-17 in which the models were simply forced with all the different ensembles. Of note is that sometimes the true observations don't fall within the model results. This suggests that we are not accounting for all uncertainty within the system through just the forcing ensemble. The model structure and parameter choices also contribute to the total uncertainty of any one simulation. Results from a 20-day assimilation cycle using the EnKF and simple direct insertion are shown in Figures 4.17c and 4.17d respectively. These results indicate that different assimilation methods can present both advantages and disadvantages for any particular situation, hence it is desirable to examine various methods. The spread of the ensemble is clearly reduced in both cases but the zero error dependence of observations under direct insertion can lead to spurious situations such as in February 1990. The error of such a situation could be further amplified if a forecast was to be projected from these estimated initial conditions. An additional advantage of the EnKF is the simultaneous updating and information propagation to other state variables of the model; a matter that becomes more important as complexity increases in the model.

Future work includes coupling the current model to a soil moisture and streamflow model as well as a rigorous assessment of assimilation against observed gauge flows.

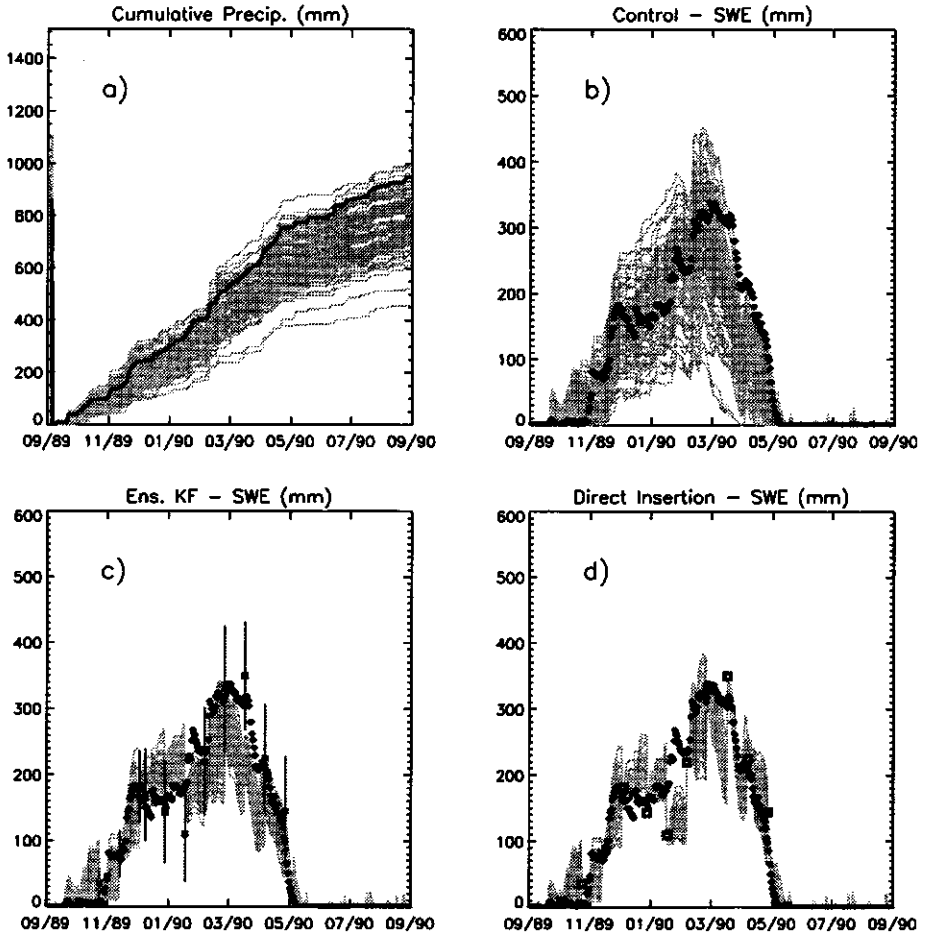

Figure 4.17: Results for Willow Park, Colorado (40.43°N, −105.73°E, 3261 m) for the water year 1989/1990. Ensemble results are given in light gray, while truth is plotted in the black, showing: a) the ensemble of cumulative precipitation forcing; b) control simulations performed by SNOW-17; c) results from using an Ensemble Kalman Filter where mid-gray boxes are our estimated observations, complete with error estimates; and d) results using direct insertion where the mid-gray boxes are the same estimated observations as in (c).

Soil moisture initialization for climate prediction: Assimilating SMMR into a land surface model

W. Ni-Meister[1], J.P. Walker[2], P.R. Houser[3], and R.H. Reichle[4]

[1]*Dept. of Geography, Hunter College of City University of New York, New York, USA*
[2]*Dept. of Civil and Environmental Engineering, University of Melbourne, Parkville, Australia*
[3]*Hydrological Sciences Branch, NASA Goddard Space Flight Center, Greenbelt, USA*
[4]*UMBC-GEST/NASA-GSFC Hydrological Sciences Branch, Greenbelt, Maryland, USA*

Current climate models for seasonal prediction or water resource management are limited due to poor initialization of land surface soil moisture states. Passive microwave remote sensing provides quantitative information on soil moisture in a very thin near-surface soil layer at large scale. This information can be assimilated into a land surface model to retrieve better estimates of the soil moisture states. A Kalman filter-based data assimilation strategy has been implemented in the catchment-based land surface model (CLSM) used by the NASA Seasonal-to-Interannual Prediction Project (NSIPP). In our previous study, we have characterized the model error and the remote sensing measurement error. In this study we assimilated Scanning Multifrequency Microwave Radiometer (SMMR) data for the period of 1979–1987 and compared the resulting soil moisture with in-situ measurements collected in Russia, Mongolia and China. Two data assimilation methods are used, one is to adjust the data assimilation parameters so that the model error and measurement error is consistent with the true values from our previous study, the other is to use one consistent data assimilation parameters. Our comparison results indicate that the first approach improves our soil moisture estimation over either by model or remote sensing alone and the second approach improves at least the rootzone soil moisture estimation. We discuss the possible reasons for the above results and investigate an operational approach to apply the ensemble Kalman filter to initialize soil moisture content for seasonal climate prediction.

5 Computational approaches for large-scale hydrologic problems

Computational approaches for large-scale hydrologic problems

Dennis McLaughlin[1]

[1]*Parsons Laboratory, Department of Civil and Environmental Engineering, Massachusetts Institute of Technology, USA*

Many of the data assimilation challenges encountered in hydrology are similar to those in other earth sciences. Particularly important are (1) nonlinearity, (2) high dimensionality, and (3) measurement and model uncertainty. The practical implications for hydrologic applications depend significantly on the distinctive aspects of land surface systems. These systems are quite heterogeneous, exhibiting significant spatial variations in topography, soil properties, and vegetation over a wide range of scales. Meteorological inputs to land surface systems (e.g., precipitation, air temperature, wind speed, etc.) vary over both time and space, also over a wide range of scales. A number of land surface states are constrained by thresholds (e.g., potential evapotranspiration) which themselves depend on the states. Finally, the relationships between land surface states and measurements can be nonlinear and are often influenced by state-dependent errors. All of these effects combine to create complex behavior that can be difficult to capture with traditional data assimilation methods. Alternatives to traditional methods are conceptually attractive but also tend to be more computationally demanding. This paper considers some computationally efficient techniques for dealing with large nonlinear hydrologic data assimilation problems. The methods of interest are developed from a Bayesian perspective that relies on ensemble statistics. Particular emphasis is given to multi-scale extensions of ensemble Kalman filtering. These techniques exploit changing space-time correlations in land surface states by introducing continually changing low-dimensional approximations for the update step of the filter. Other potentially promising methods for dealing with large nonlinear problems are also considered, with an emphasis on the tradeoffs implied whenever approximations are introduced to improve efficiency.

Data assimilation for estimating regional water balance using constrained ensemble Kalman filtering

Ming Pan[1], Eric Wood[1], and Matthew McCabe[1]

[1]*Department of Civil and Environmental Engineering, Princeton University, Princeton, New Jersey, USA*

The assimilation of observational data into a regional water balance model often results in non-closure of the balance equation. This non-closure can be avoided through the implementation of the Constrained Kalman Filter in which the balance equation is preserved. When the balance equation is parameterized through a non-linear land surface scheme, an ensemble data assimilation approach allows for a computationally efficient approach. The presentation develops the assimilation approach underlying the constrained ensemble Kalman filter (CEnKF) and applies the approach to estimating the regional water balance.

The constrained ensemble Kalman filter (CEnKF) approach for regional water budget estimation has the following advantages, which are: (1) allows the state dynamics to be represented by a complex, non-linear terrestrial land surface model; (2) assimilates various sources of observations and measurements, like streamflow, mean areal precipitation, tower estimates of evapotranspiration, etc.; (3) provides optimal updated terrestrial states and fluxes given the uncertainties in the modeled and observed values; and (4) obtain closure of the water budget with the updated states and fluxes.

The constrained ensemble Kalman filter is applied to estimate the water budget over the Southern Great Plain region of the U.S. using data collected from a variety of station and gauge data are available.

Ensemble land surface modeling using satellite-based precipitation forcing

Steven A. Margulis[1], **Dara Entekhabi**[2], **and Dennis McLaughlin**[2]

[1]*UCLA, Los Angeles, California, USA*
[2]*Ralph M. Parsons Lab, MIT, Cambridge, Massachusetts, USA*

Precipitation is the key forcing variable for land surface hydrologic processes and is largely responsible for variability in soil moisture and surface flux fields. The measurement of precipitation over large scales is difficult due to its inherent spatial and temporal intermittency and the lack of sufficiently dense ground-based monitoring networks in many regions of the globe. Methods for remotely sensing precipitation are now generally available, but provide estimates that are spatially coarse (e.g., tens to hundreds of kilometers), aggregated in time (daily to monthly), and have complex error structures (positive non-detection probability, non-zero false alarm rate, large uncertainty, etc.). Due to the nonlinearity of surface hydrologic processes, these products cannot be directly used in modeling studies. Furthermore, for accurate hydrologic state and flux predictions it is crucial that uncertainty in these estimates must be properly incorporated into modeling frameworks. In this paper we present a unified ensemble data assimilation framework that contains a spatio-temporal disaggregation scheme for remotely sensed Global Precipitation Climatology Project-1 degree daily (GPCP-1DD) precipitation product. A detailed study of the error characteristics of the GPCP 1DD precipitation forcing is undertaken and then incorporated in the framework. The spatio-temporal disaggregation scheme takes advantage of the ensemble nature of the Ensemble Kalman Filter (EnKF) by introducing precipitation realizations that are conditioned on the remote sensing data. The ability to use coarse precipitation observations is tested in experiments using data from the SGP97 field experiment. This approach not only captures the large scale spatial variability in precipitation contained in the remote sensing observations, but introduces a more realistic error structure in the precipitation forcing that accounts for errors in storm magnitudes, arrivals, and spatial structure. Results from tests using the remotely sensed precipitation show improvement in both soil moisture and land surface flux estimates over those using sparse ground-based precipitation. Furthermore the general ensemble framework is easily adapted to assimilate other observations (e.g., microwave radiobrightness).

Using ensemble smoothing techniques to obtain dynamically consistent soil moisture and surface energy fluxes from radiative brightness temperatures

Susan Dunne[1] **and Dara Entekhabi**[1]

[1]*Department of Civil and Environmental Engineering, Massachusetts Institute of Technology, Cambridge, Massachusetts, USA*

A reanalysis data assimilation framework in which remote sensing measurements are merged with a conventional land surface model to estimate soil moisture (surface and profile) and associated surface fluxes is presented. Land data assimilation using filters, such as extended or ensemble Kalman filters, ingests the data sequentially as they become available. The filtering approach is ideally suited to forecasting problems where the observations up to the current time are used to update the initial conditions for forecasts into the future. In land data assimilation, the problem is often reanalysis rather than forecasting: the objective is to obtain estimates of soil moisture or some state from data which has been collected using remote-sensing or in-situ techniques. The reanalysis data assimilation framework presented here uses smoothing rather than filtering, combining data from prior to and after an estimation time to form an estimate. Through use of additional information on how the system evolves, the smoothing approach yields improved estimates of the state at the present time. This is especially relevant for estimating profile soil moisture below the penetration depth of observations. The correct estimation of the profile will significantly impact the surface evaporation estimates where vegetation is present. Traditional smoothers such as the Rauch-Tung-Striebel (RTS) smoothers are optimal batch estimators, just as Kalman filters are optimal sequential estimators. In their traditional form both are limited to linear systems. Linearization of the system equation in either the Kalman filter or the RTS smoother is seriously prone to unstable growth of the covariance matrices. Artificial limits on the propagation of the covariance matrix can result in suboptimal filters and poor estimation. Ensemble techniques offer an alternative which avoids linearizing or having to find the adjoint of the model. This is particularly valuable in land data assimilation as it allows us to use a mainstream land surface model such as the NOAH LSM. Furthermore, ensemble techniques allow great flexibility in the specification of model and observation error. The framework presented here builds an ensemble smoother from a successful ensemble Kalman filter. Following initial testing using a linear model, the reanalysis framework was applied to the land data assimilation problem. Results will be presented which demonstrate the improvement in soil moisture estimates at the surface and at depth.

A smoothing approach to soil moisture estimation Various filtering techniques have been used to estimate soil moisture. The extended Kalman filter was used by *Entekhabi et al.* [1994], *Galantowicz et al.* [1999], *Walker and Houser* [2001], and *Crosson et al.* [2002]. Using this approach requires that the forward model be differentiable so that it may be linearized. There is also potential for divergence or bias in estimates in non-linear systems. The ensemble Kalman filter has been used in soil moisture estimation by *Reichle et al.* [2002], *Margulis et al.* [2002], and *Crow and Wood* [2003]. In both the extended Kalman filter and the ensemble Kalman filter, the filter proceeds sequentially through the study interval, updating the state estimate when an observation becomes available. Filtering is most suited to control-type or forecasting problems, where obser-

vations are available in real-time. Smoothing, on the other hand, involves using all measurements in an interval $\mathbf{T} = [0, T]$, to estimate the state of the system at some time t where $0 \leq t \leq T$. Therefore, the state estimate at a given time is determined by including information from subsequent observations. Smoothing is ideal for analyzing historic data or data which is not available in real-time, as is the case with data from field experiments (e.g., SGP97, SMEX02) and exploratory missions such as HYDROS and SMOS. As observations beyond the estimation time are available, using a smoothing approach rather than filtering includes additional information, thereby improving the estimate.

Ensemble techniques Variational schemes such as 4DVAR use all observations in a given window to yield the best estimate of the state. However the variational approach requires that the tangent linear model and adjoint of the forward model be obtained. This limits the choice of land surface model that can be used. In an ensemble approach, an ensemble of states are propagated forward in time using the non-linear forward model. There is no need for a tangent linear model or adjoint, facilitating the use of conventional land surface models such as the NOAH LSM or NCAR LSM. At any time, the statistics of the ensemble can be calculated which provides a useful measure of certainty in the estimate. Through the use of a conventional land surface model, other states such as soil temperature and latent heat flux are produced along with soil moisture. In fact, other quantities such as latent heat flux could be estimated directly by including them in the state vector. Model error is not limited to additive gaussian noise. Noise may be included as appropriate, for example if uncertainty arises due to uncertain parameters the value of the parameter can be made random. Noise may be multiplicative and non-gaussian.

Ensemble smoother algorithm This research focuses on the so-called batch estimation approach, in which all available observations are used together at one time. An augmented state vector is constructed by gathering the states of interest at each estimation time in some smoother window. All observations in the same smoother window are gathered into the augmented measurement vector. The augmented state vector is updated using the equations from the ensemble Kalman filter. The covariance matrices relate the soil moisture in each of six soil layers at any estimation time to all of the observations in the same smoother window. The length of the smoother window should be long enough to include all observations which are related to the current state without incurring excessive computational expense.

Data assimilation framework The NOAH land surface model [*Chen et al.*, 1996] was used as the forward model to propagate the states forward through the smoother window. It is a 1-D model of the soil column which outputs the soil moisture and temperature profiles as well as the surface water and energy fluxes. It was used in *Margulis et al.* [2002] with the ensemble Kalman filter, and is used in the NASA Land Data Assimilation System [*Lohmann et al.*, 2004]. The model is forced with hourly data from the Oklahoma Mesonet. Temperature, humidity, wind, relative humidity and radiation data was available beyond the duration of SGP97 so it was used to generate a synthetic experiment from 1 May to 1 September 1997. The radiative transfer model used in *Margulis et al.* [2002] was used here to generate synthetic L-band microwave measurements every 3 days for the experiment duration, and to transform the states into the observation space for the update. Additive Gaussian observation error with standard deviation of 3 K was included. Model error was included by allowing four key parameters to vary within an expected range. Uncertainty was imposed on the porosity, saturated hydraulic conductivity, minimum canopy resistance and wilting point. Uncertainty was also included in the initial soil moisture profile, and in the amount and timing of precipitation forcing.

Results Figure 5.1 demonstrates that the ensemble moving batch smoother, on average, yields an improved estimate over the ensemble Kalman filter, which in turn improves on the ensemble open loop. The greatest improvement due to smoothing is when the soil column is drying down

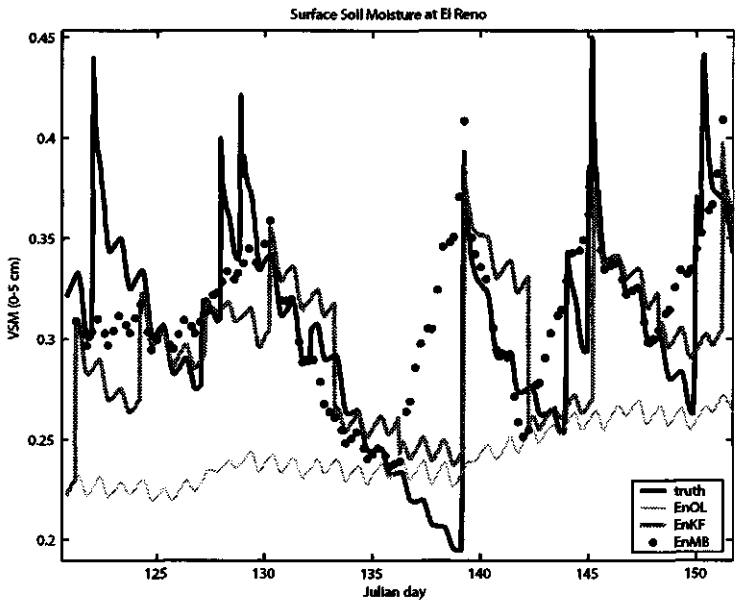

Figure 5.1: Ensemble mean volumetric soil moisture in the top 5 cm of the soil column at El Reno is compared to the truth. The results are the first 30 days of a 4 month experiment.

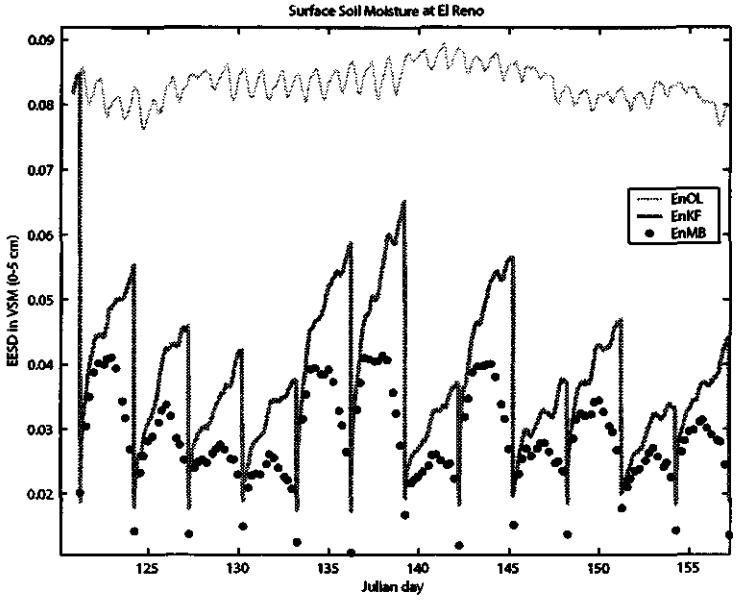

Figure 5.2: Estimation Error Standard Deviation in the estimate of surface (0–5 cm) volumetric soil moisture at El Reno. Results demonstrate reduction in uncertainty after smoothing compared to filtering and the ensemble open loop.

following a precipitation event. The smoother can result in an estimate worse than the filtered estimate if information from beyond a subsequent precipitation event is propagated back in time. Figure 5.2 shows the Estimation Error Standard Deviation (EESD) in surface soil moisture at El Reno. The standard deviation across the ensemble is a measure of the uncertainty in the estimate. Clearly, the ensemble open loop is the least certain as it does not include any information from the observations. The filtered estimate is more certain than the open loop as observations are available every three days. Certainty is greatest in the smoothed estimate as the state estimate includes information from subsequent as well as prior observations. The filtered EESD reflects the error growth as the state is propagated between observations. The more symmetric pattern in the smoother EESD reflects the fact that information is travelling back in time through the interval, so subsequent observations are improving the estimate of the current state.

Improvement in the soil moisture estimate and the improved confidence in the estimate was found in the surface soil moisture as well as the soil moisture at depth. In particular, the smoother was more effective than the filter in correcting for spurious initial conditions at depth.

The GSFC Land Information System as a multiscale ensemble hydrological modeling testbed

C.D. Peters-Lidard[1], S.V. Kumar[2], Y. Tian[2], J. Geiger[3], P.R. Houser[1], J. Sheffield[4], E.F. Wood[4], K. Mitchell[5], and P. Dirmeyer[6]

[1]*NASA, Goddard Space Flight Center, Hydrological Sciences Branch, Greenbelt, Maryland, USA*
[2]*UMBC/GEST, NASA, Goddard Space Flight Center, Hydrological Sciences Branch, Greenbelt, Maryland, USA*
[3]*NASA, Goddard Space Flight Center, Information Systems Division, Greenbelt, Maryland, USA*
[4]*Department of Civil and Environmental Engineering, Princeton University, Princeton, New Jersey, USA*
[5]*NCEP Environmental Modeling Center, NOAA/NWS, Camp Springs, Maryland, USA*
[6]*Center for Ocean-Land-Atmosphere Studies, Calverton, Maryland, USA*

NASA Goddard Space Flight Center has developed a Land Information System (LIS*) based on the Land Data Assimilation Systems (LDAS†) capable of global, distributed hydrometeorological modeling at spatial resolutions down to 1 km. The LIS framework is resolution independent, and is also being tested for catchment-scale applications on grids O(10m). LIS consists of an ensemble of land surface models (e.g., CLM, Noah, VIC, Mosaic) run offline using satellite-based precipitation, radiation and surface parameters, in addition to model-derived surface meteorology. Satellite-based surface parameters include AVHRR-based or MODIS-based land cover and Leaf Area Index (LAI), and MODIS-based albedo and emissivity. The high spatial resolution of LIS–enabled by the use of high performance computing and communications technologies–in addition to the extensible and interoperable design of LIS, make it ideal as a multiscale hydrological ensemble modeling testbed. We will present results demonstrating LIS applied globally at $\frac{1}{4}^{\circ}$, 5 km and 1 km resolutions, as well as on a 40 m grid for the Walnut Gulch Experimental Watershed (WGEW) in Arizona, USA. Several validation case studies conducted with LIS, including the Southern Great Plains, and the Coordinated Enhanced Observing Period (CEOP) reference sites, and the WGEW demonstrate the impacts of appropriately downscaling meteorological data, and the value of the ensemble approach to hydrological modeling.

*http://lis.gsfc.nasa.gov
†http://ldas.gsfc.nasa.gov

A Bayesian data assimilation approach to update states, parameters and structure of environmental models

Hoshin Gupta[1] and Thorsten Wagener[1]

[1]*SAHRA, University of Arizona, Tucson, Arizona, USA*

The use of data assimilation techniques to update model states is becoming increasingly popular. The short term bias in the model predictions can be largely reduced if adequate data is available. However, the temporal persistence of this bias reduction can be rather short and it is less helpful if long term predictions are required. It is likely that updating model parameters and maybe even model structural elements has a smaller effect on bias reduction, but that the temporal persistence will be much higher. A combination of both, the updating of states, and model parameters and structure is therefore highly desirable.

A new Bayesian approach that allows for the assimilation of data into model states, parameter and even model structure will be presented. This approach enables the merging of data and models with few constraints stemming from underlying assumptions.

Sequential data assimilation framework for hydrologic state-parameter estimation and ensemble forecasting

Hamid Moradkhani[1], Soroosh Sorooshian[1], Hoshin V. Gupta[2], Paul R. Houser[3], Kuo-lin Hsu[1]

[1]*Civil and environmental Engineering Department, University of California, Irvine, California, USA*
[2]*Hydrology and Water Resources Department, University of Arizona, Tucson, Arizona, USA*
[3]*Hydrological Sciences Branch, NASA-GSFC, Greenbelt, Maryland, USA*

One of the primary purposes of hydrologic models is to perform prediction using physical relationships bounded by parameters and state variables. Much of the efforts in simulation-based hydrologic-systems analysis have been primarily focused on (1) improved parameter estimation methods that do not include state variables or (2) improved time-varying state estimation with predetermined parameters. Although the parameters of a hydrologic model can be estimated in a batch-processing scheme, there is no guarantee that model behavior does not change over time; therefore model adjustment over time may be required. Additionally, due to the multiplicative nature of errors in forcing data and observation, it is prudent to assemble the parameter adaption in the state evolution and forecasting system. The need for the real time state-parameter estimation of hydrological models has been reported in several studies [*Todini et al.*, 1976; *Kitanidis and Bras*, 1980; *Bras and Rodriguez-Iturbe*, 1985; *Young*, 2002; *Moradkhani et al.*, 2004]. In this paper we extend the applicability of ensemble Kalman filter (EnKF), a recursive Data Assimilation (DA) technique, with Monte Carlo parameter smoothing to sequentially estimate model parameters and state variables. The applicability and usefulness of the current algorithm is demonstrated for the streamflow forecasting in Leaf River Watershed located north of Colins, Mississippi, using a conceptual hydrologic model, HyMOD [*Boyle*, 2000]. This methodology offers two additional features: (1) the various sources of uncertainties can be properly addressed, including input, output and parameter uncertainties, (2) unlike the batch calibration procedures; the algorithm is recursive and therefore does not require storage of all past information.

Recursive state-parameter estimation using EnKF Data assimilation techniques have garnered hydrologist's attention with the potential to use real time observations to produce more accurate hydrological forecasts. The basic objective of data assimilation is to characterize the system state at some future time given initial state knowledge. EnKF, a Monte Carlo approach of Kalman filter proposed by *Evensen* [1994] and later clarified by *Burgers et al.* [1998], is a DA algorithm suitable for nonlinear dynamic systems which uses a forecast model to integrate an ensemble of model states from one update time to the next and employs ensemble-based covariances in the update step to address the uncertainty in state estimation. To extend the applicability of the EnKF to simultaneous state-parameter estimation, we need to treat the parameters similar to state variables. Combined estimation can be provided by joint estimation where state and parameter vectors are concatenated into a single joint state vector (state augmentation). An alternative approach to joint estimation is dual estimation; designed as two interactive filters motivated either by the need to estimate state from the model (parameters) or by the need to estimate the model from state [*Moradkhani et al.*, 2004]. In combined estimation, parameter evolution needs to be set up artificially, i.e., it is assumed that the parameters follow a random walk. The drawback of such parameter sampling

is the loss of information between time points resulting in posterior distribution of parameters that are too diffuse comparing to the posteriors of fixed parameters [*Liu*, 2000]. One remedy to this problem is to use the Kernel smoothing of parameter samples introduced by *West* [1993] wherein the conditional evolution density of parameters is written as follows:

$$P(\theta_{t+1}|\theta_t) \sim N\left(\theta_{t+1}^{i-}|a\theta_t^{i+} + (1-a)\overline{\theta}^{i+}, h^2 V_t\right) \tag{5.1}$$

Where, θ_t^{i+} and θ_{t+1}^{i-} are respectively the updated and forecasted parameter vectors of i^{th} kernel at time t and $t+1$, a is a factor ranging in $0.95 \sim 0.99$, V_t is the variance of normal kernels, and h is the smoothing parameter.

The generic discrete-time nonlinear stochastic dynamic system and predictions in the EnKF framework can be respectively expressed in the form of

$$x_{t+1}^{i-} = f\left(x_t^{i+}, u_t^i, \theta_{t+1}^{i-}\right) \tag{5.2}$$

$$\hat{y}_{t+1}^i = h\left(x_{t+1}^{i-}, \theta_{t+1}^{i-}\right) \tag{5.3}$$

Where x_t^{i+} and x_{t+1}^{i-} are updated and forecasted state ensemble members at time t and $t+1$ respectively. u_t^i is the perturbed forcing data according to $u_t^i = u_t + \zeta_t^i$, $\zeta_t^i \sim N(0, \sum_t^u)$.

In the updating step, observation y_{t+1} needs to be perturbed in the amount of η_{t+1}^i, therefore parameters are updated as follows:

$$\theta_{t+1}^{i+} = \theta_{t+1}^{i-} + K_{t+1}^{\theta}\left(y_{t+1} + \eta_{t+1}^i - \hat{y}_{t+1}^i\right), \qquad \eta_{t+1}^i \sim N\left(0, \sigma_{t+1}^y\right) \tag{5.4}$$

Where, K_{t+1}^{θ} is the Kalman gain associated with the parameters [*Moradkhani et al.*, 2004]. Now using the updated parameters, we regenerate the model state and prediction trajectories as follows:

$$x_{t+1}^{i-} = f\left(x_t^{i+}, u_t^i, \theta_{t+1}^{i+}\right) \tag{5.5}$$

$$\hat{y}_{t+1}^i = h\left(x_{t+1}^{i-}, \theta_{t+1}^{i+}\right) \tag{5.6}$$

Model states ensemble is similarly updated as follows:

$$x_{t+1}^{i+} = x_{t+1}^{i-} + \Sigma_{t+1}^{xy}\left[\Sigma_{t+1}^{yy} + \Sigma_{t+1}^{y}\right]^{-1}\left(y_{t+1}^i + \eta_{t+1}^i - \hat{y}_{t+1}^i\right) \tag{5.7}$$

Where K_{t+1}^x is the Kalman gain associated with the state variables. The flowchart of dual state-parameter estimation using EnKF with kernel smoothing of parameters is demonstrated in Figure 5.3.

Results and Discussion The applicability and usefulness of the dual EnKF on state-parameter estimation of the conceptual Hydrologic MODel (HyMOD) described by *Boyle* [2000] was investigated (Figure 5.4). State variables in this system are S: storage in the nonlinear tank representing the watershed soil moisture content, x_1, x_2 and x_3: the quick-flow tank storages representing the temporary (short-time) detentions, e.g., depression storages, and x_4 as the slow-flow tank storage (subsurface storage). Correspondingly parameters of this model are C_{max}, as the maximum storage capacity within the watershed, b_{exp} the degree of spatial variability of the soil moisture

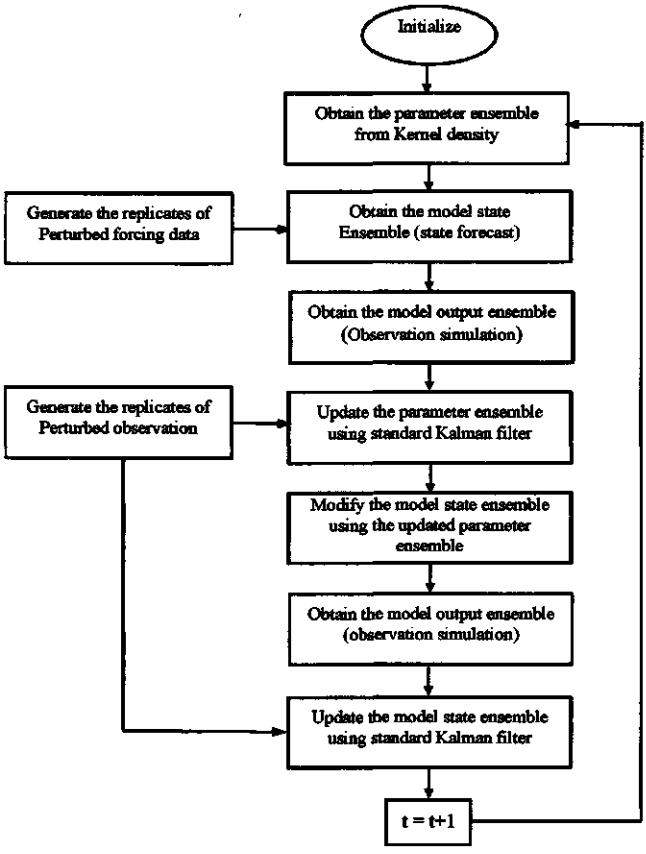

Figure 5.3: Dual state-parameter estimation flowchart using ensemble Kalman filter and kernel smoothing of parameters.

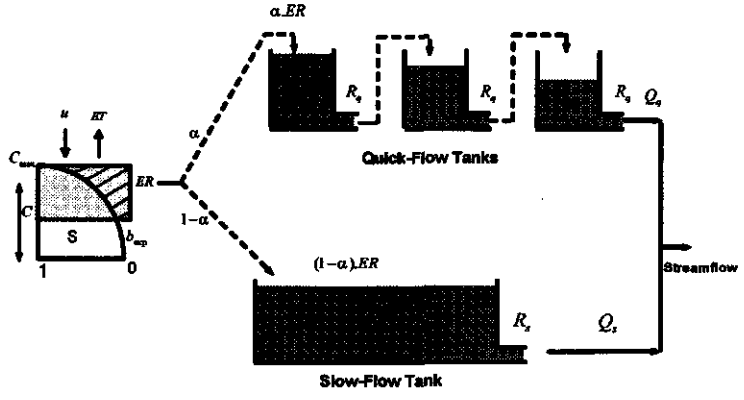

Figure 5.4: Hydrologic MODel (HyMOD) conceptualization.

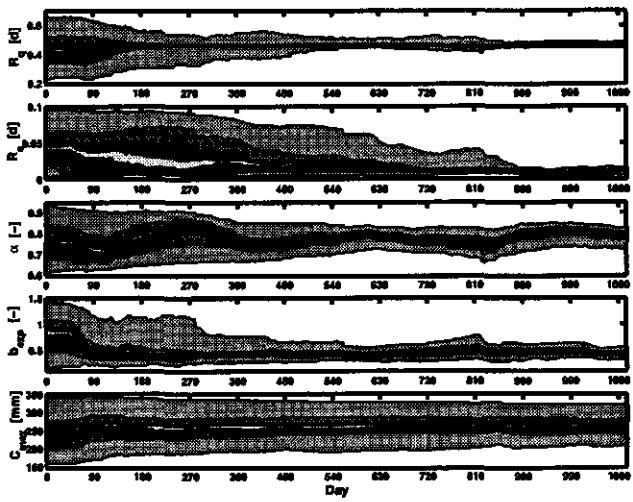

Figure 5.5: Time evolution of HyMOD model parameters for 3 years of dual ensemble filtering in Leaf River Watershed. Shaded areas correspond to 95, 75, 66 and 10 percentile confidence intervals.

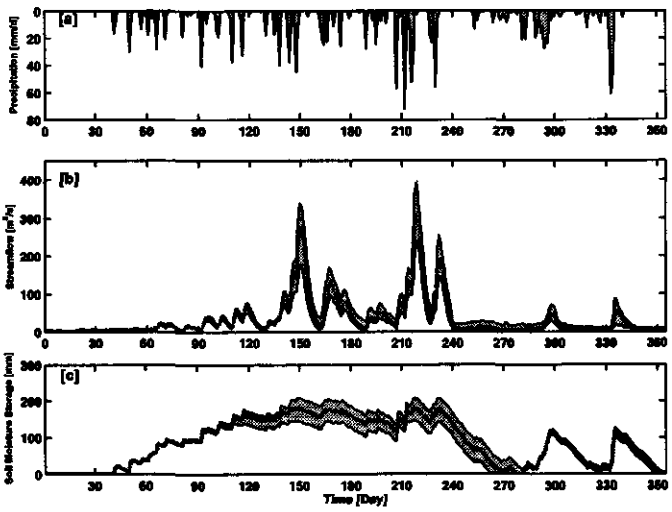

Figure 5.6: Results of the dual EnKF by application to the HyMOD, [a] Precipitation (forcing data); [b] streamflow forecasting with 95% uncertainty range; [c] Soil moisture storage variation (storage in the nonlinear tank of the HyMOD model). The solid line denotes the mean ensemble prediction.

capacity within the watershed, α, a factor for partitioning the flow between two series of tanks, R_q and R_s as the residence time parameters of quick-flow and slow-flow tanks respectively. The system is initialized by defining the prior uncertainty range associated with the parameters and state variables. Figure 5.5 displays the time evolution of HyMOD model parameters after dual filtering for the water years of 1950–1953. As seen, quick flow tank parameter R_q is the most identifiable parameter by showing the fastest convergence with minimum degree of uncertainty comparing to the others. In contrast, the maximum storage capacity of the watershed displayed by C_{max}, is less identifiable than the others and shows the slowest convergence. Ensemble time variation of the key state variable, S, representing the watershed soil moisture content, along with streamflow forecasting as predictive variable in the system are demonstrated in Figure 5.6. The streamflow forecasting result is very consistent with the observation; as a result state estimation as non-observable quantity shown in Figure 5.6 could be a reliable estimate.

In summary, the current algorithm introduces a number of novel features against the traditional calibration schemes: (1) both model states and parameters can be estimated simultaneously, (2) the algorithm is recursive and therefore does not require storage of all past information, as is the case in the batch calibration procedures, (3) the various sources of uncertainties can be properly addressed, including input, output and parameter uncertainties.

Study on parameter auto-calibration for large and complex distributed hydrologic model

Shugong Wang[1] and Xin Li[1]

[1]*Cold and Arid Regions Environmental and Engineering Research Institute, Chinese Academy of Sciences, Lanzhou Gansu, China*

Sponsored by CAREERI, large and complex distributed hydrologic models are playing more and more important roles in the systematic research on the interaction of hydrology, soil, atmosphere and ecology in Heihe river basin, which is a very typical inland river basin in Northwest China. Several successful distributed and semi-distributed hydrologic models, such as TOPMODEL, Variable Infiltration Capacity Model (VIC) and Distributed Hydrology Soil Vegetation Model (DHSVM) have been or will be used in this region. In comparison with conceptual model, distributed hydrologic model has much more parameters to be calibrated before application. Because of the large study area, lots of parameters can't be identified through field experiment or manual calibration. The high nonlinearity and discontinuity of distributed hydrologic model hinder the practical operation of traditional gradient based optimization approaches. Heuristics optimization algorithms, such as genetic algorithm and simulated annealing, without depending on the derivative of model, have been introduced to the calibration of distributed hydrologic model.

Aimed at the parameter calibration of TOPMODEL and VIC, a set of genetic algorithms and simulated annealing algorithms have been designed. Nash-Sutcliffe coefficient has been as the objective function in these algorithms. Numeric experiments in serial computing environment show those two series of algorithms all have good capability in model parameter calibration, and genetic algorithms have better performance. Different coding scheme of genetic algorithm and the selection of annealing schedule and state generating function of simulated annealing algorithm impact the performance and computing time in varying degrees.

As mentioned in many literatures, heuristic optimization algorithms spend much computing time and in some case, the computing time can not be stand. In order to shorten the computing time and improve the calibration performance, a MPI based master-slave parallel program for genetic algorithm has been designed. MPI is shortage of Message-Passing interface, which is the industrial standard about parallel computing and is supported by Windows, UNIX and Linux operating system. In the program, the master process controls the selection operation, crossover operation and mutation operation; the slave process only performs the fitness calculation. Numeric experiments on parallel computing environment (Dawning 1700 cluster server with four XRON 2.4GHz CPUs at each node) show that the parallel genetic algorithms are more capable in performance than the serial ones.

Automatic calibration approaches provide a big opportunity to use large and complex distributed hydrologic model in river basins without good data availability. But like other inverse problem, there are still some uncertainties about the parameters identified through automatic calibration. In most cases, there are always several sets of parameters that they can maximize the Nash-Sutcliffe coefficient. Because of poor data availability, lots of parameters can't be verified by observed data. To determine which set is the best and most proper to distributed hydrologic model is our work in following steps.

Improved treatment of uncertainty in hydrologic modeling

Jasper A. Vrugt[1], Cees G.H. Diks[2], Hoshin V. Gupta[3], Willem Bouten[1], and Jacobus M. Verstraten[1]

[1]*Universiteit van Amsterdam, Institute for Biodiversity and Ecosystem Dynamics, Department of Physical Geography, Faculty of Science, Amsterdam, The Netherlands*
[2]*Universiteit van Amsterdam, CenDEF, Department of Quantitative Finance, Faculty of Economics and Econometrics, Amsterdam, The Netherlands*
[3]*Department of Hydrology and Water Resources, University of Arizona, Tucson, Arizona, USA*

Hydrologic models use relatively simple mathematical equations to conceptualize and aggregate the complex, spatially distributed and highly interrelated water, energy, and vegetation processes in a watershed. A consequence of process aggregation is that the model parameters often do not represent directly measurable entities, and must therefore be estimated using measurements of the system inputs and outputs. During this process, known as model calibration, the parameters are adjusted so that the behavior of the model approximates, as closely and consistently as possible, the observed response of the hydrologic system over some historical period of time. In practice, however, because of errors in the model structure and the input (forcing) and output data, this has proven to be difficult, leading to considerable uncertainty in the model predictions. This paper surveys the limitations of current model calibration methodologies, which treat the uncertainty in the input - output relationship as being primarily attributable to uncertainty in the parameters, and presents a Simultaneous Optimization and particle filter Data Assimilation method, entitled SODA, which improves the treatment of uncertainty in hydrologic modeling. The usefulness and applicability of SODA is demonstrated by means of a pilot study using data from the Leaf River Watershed in Mississippi and a simple hydrologic model with typical conceptual components.

Bibliography

Abbott, M. B., J. C. Bathurst, J. A. Cunge, P. E. OConnell, and J. Rasmussen, An introduction to the European hydrological system-systeme hydrologique European,'she', 1: history and philosophy of a physically-based distributed modelling system, *J. Hydrol.*, *87*, 45–59, 1986.

Ahmed, N., Estimating soil moisture from 6.6 GHz dual polarization, and/or satellite derived vegetation index, *Int. J. Remote Sens.*, *16*, 687–708, 1995.

Al-Kaisi, M., L. Brun, and J. Enz, Transpiration and evapotranspiration from maize as related to leaf area index, *Agr. Forest Meteorol.*, *48*, 111–116, 1989.

Albertson, J., and G. Kiely, On the structure of soil moisture time series in the context of land surface models, *J. Hydrol.*, *243*, 101–119, 2001.

Albertson, J., and N. Montaldo, Temporal dynamics of soil moisture variability: 1. Theoretical basis, *Water Resour. Res.*, *39*(10), 1274, doi:10.1029/2002WR001616, 2003.

Alestalo, M., The atmospheric water vapour budget over Europe, in *Variations in the global water budget*, edited by A. Street-Perrott, pp. 67–79, D. Reidel Publishing Company, 1983.

Anagnostou, E., A. Negri, and R. Adler, Statistical adjustment of satellite microwave monthly rainfall estimates over Amazonia, *J. Appl. Meteorol.*, *38*(11), 1590–1598, 1999.

Anderson, J., and S. Anderson, A Monte Carlo implementation of the nonlinear filtering problem to produce ensemble assimilations and forecasts., *Mon. Weather Rev.*, *128*, 1971–1981, 1999.

Andrieux, P., R. Bouzigues, C. Joseph, M. Voltz, P. Lagacherie, and M. Bourlet, Le bassin versant de roujan: caratéristiques générales du milieu, *Tech. rep.*, French National Institute for agricultural research (INRA), Montpellier, 1993.

Atlas, D., D. Rosenfeld, and D. Wolff, Climatologically tuned reflectivity-rain rate relations and links to area-time integrals, *J. Appl. Meteorol.*, *29*(11), 1120–1135, 1990.

Baatz, M., and A. Schäpe, Multiresolution segmentation: an optimization approach for high quality multiscale image segmentation, in *Angewandte Geogr. Informationsverarbeitung*, edited by J. Strobl and T. Blaschke, pp. 12–23, Herbert Wichmann Verlag, Heidelberg, 2000.

Baldocchi, D., et al., FLUXNET: A new tool to study the temporal and spatial variability of ecosystem-scale carbon dioxide, water vapor, and energy flux densities, *Bull. Am. Meteorol. Soc.*, *82*(11), 2415–2434, 2001.

Baret, F., Preface: Special issue on "multi-sensor and multi-temporal remote sensing observations to characterize canopy functioning. The ReSeDA project", *Agronomie*, *22*, 529, 2002.

Bastiaanssen, W., M. Menenti, R. Feddes, and A. Holtslag, A remote sensing surface energy balance algorithm for land (SEBAL) 1. Formulation, *J. Hydrol.*, *212–213*, 198–212, 1998.

Beljaars, A., P. Viterbo, M. Miller, and A. Betts, The anomalous rainfall over the United States during July 1993 - sensitivity to land surface parameterizations and soil moisture, *Mon. Weather Rev.*, *124*, 362–383, 1996.

Bell, V., and R. Moore, A flow routing and flood inundation facility for Nimrod/CMetS, *Tech. rep.*, Met Office, 2004.

Berg, A., J. Famiglietti, J. Walker, and P. Houser, The impact of bias correction to reanalysis products on simulations of North American soil moisture and hydrological fluxes, *J. Geophys. Res.*, *108*, 4490, doi:10.1029/2002JD003334, 2003.

Bertoldi, G., The water and energy balance at basin scale: a distributed modeling approach, Ph.D. thesis, Università di Trento, 2004.

Bertoldi, G., and R. Rigon, Geotop: A hydrological balance model. technical description and programs guide, *Technical report dica-04-001*, University of Trento E-Prints, `http://eprints.biblio.unitn.it/archive/00000551/`, 2004.

Bertoldi, G., R. Rigon, and T. Over, Un'indagine sugli effetti della topografia con il modello geotop, *Atti del XXVIII Convegno Nazionale di Idraulica e Costruzioni Idrauliche*, *1*, 313–324, 2002.

Best, M., A model to predict suface temperatures, *Bound.-Lay. Meteorol.*, *88*(2), 279–306, 1998.

Beven, K., and M. Kirkby, A physically based, variable contributing area model of basin hydrology, *Hydrol. Sci. Bull.*, *24*(1), 43–69, 1979.

Bierkens, M., M. Knotters, and F. Van Geer, Calibration of transfer function-noise models to sparsely or irregularly observed time series, *Water Resour. Res.*, *35*, 1741–1750, 1999.

Blyth, E., Relative influence of vertical and horizontal processes in large-scale water and energy balance modelling, *Tech. Rep. 270*, IAHS, 2001.

Blyth, E., Modelling soil moisture for a grassland and a woodland site in south-east England, *Hydrol. Earth Syst. Sci.*, *6*, 39–47, 2002.

Boll, J., E. Brooks, C. Campbell, C. Stockle, S. Young, J. Hammel, and P. McDaniel, Progress toward development of a gis based water quality management tool for small rural watersheds: modification and application of a distributed model, paper presented at the 1998 ASAE Annual International Meeting in Orlando, Florida, July 12–16, 1998.

Bonan, G., A land surface model for ecological, hydrological, and atmospheric studies: technical description and user's guide., *Tech. Rep. NCAR/TN-417+STR*, NCAR, 1996.

Boni, G., D. Entekhabi, and F. Castelli, Land data assimilation with satellite measurements for the estimation of surface energy balance components and surface control on evaporation, *Water Resour. Res.*, *37*, 1713–1722, 2001.

Boni, G., S. Gabellani, R. Rudari, and F. Silvestro, Taratura e applicazione di un metode per il calcolo dell'infiltrazione derivato dall'equazione di Horton, in *Proceedings of XXIX Convegno di Idraulica e Costruzioni Idrauliche*, 2004.

Bosilovich, M., On the vertical distribution of local and remote sources of water for precipitation, *Meteorol. Atmos. Phys.*, *80*, 31–41, 2002.

Bosilovich, M., and S. Schubert, Water vapor tracers as diagnostics of the regional hydrologic cycle, *J. Hydrometeorol.*, *3*, 149–165, 2002.

Bosilovich, M., Y. Sud, S. Schubert, and G. Walker, Numerical simulation of the North American monsoon water sources, *J. Geophys. Res.*, *108*(D16), 8614, doi:10.1029/2002JD003095, 2003.

Bosilovich, M., S. Schubert, and G. Walker, Global changes of the water cycle intensity, *J. Climate*, conditionally accepted, 2004.

Boudevillain, B., C. Ottlé, and B. Coudert, Potentialities of thermal infrared remote sensing to improve SVAT model soil moisture simulation, in preparation, 2004.

Bouttier, F., J. Mahfouf, and J. Noilhan, Sequential assimilation of soil moisture from atmospheric low-level parameters. Part I: Sensitivity and calibration studies, *J. Appl. Meteorol.*, *32*(8), 1335–1351, 1993.

Box, G., and G. Jenkins, *Time Series Analysis: forecasting and control*, Holden-Day, San Francisco, USA, 1976.

Boyle, D., Multicriteria calibration of hydrological models, Ph.D. thesis, Univ. of Arizona, Tucson, 2000.

Boyle, D., H. V. Gupta, and S. Sorooshian, Toward improved calibration of hydrologic models: Combining the strengths of manual and automatic methods, *Water Resour. Res.*, *36*(12), 3663–3674, 2000.

Bras, R., and I. Rodriguez-Iturbe, *Random functions in hydrology*, Addison Wesley, Reading, Massachusetts, USA, 1985.

Braun, P., B. Maurer, G. Muller, P. Gross, G. Heinemann, and C. Simmer, An integrated approach for the determination of regional evapotranspiration using mesoscale modelling, remote sensing and boundary layer measurements, *Meteorol. Atmos. Phys.*, *76*(1–2), 83–105, 2001.

Brooks, E., and J. Boll, Distributed and integrated response of a gis-based distributed hydrologic model, submitted to Hydrol. Process., 2004.

Brubaker, K., D. Entekhabi, and P. Eagleson, Estimation of precipitation recycling, *J. Climate*, *6*, 1077–1089, 1993.

Burgers, G., P. van Leeuwen, and G. Evensen, Analysis scheme in the ensemble Kalman filter, *Mon. Weather Rev.*, *126*, 1719–1724, 1998.

Cacuci, D., *Sensitivity and Uncertainty Anlysis, Vol. I Theory*, Chapman and Hall/CRC, 2003.

Campbell, G., A simple method for determining unsaturated conductivity from moisture retention data, *Soil Science*, *117*(6), 311–314, 1974.

Caparrini, F., F. Castelli, and D. Entekhabi, Overcoming data starvation in hydrology: estimation of surface fluxes with dynamical assimilation of remote sensing measurements, in *New frontiers in hydrology, Proceedings of the 1st CNR-Princeton workshop held at Princeton University, U.S.A., October 23–25, 2002*, 2002.

Caparrini, F., F. Castelli, and D. Entekhabi, Mapping of land-atmosphere heat fluxes and surface parameters with remote sensing data, *Bound.-Lay. Meteorol.*, *107*, 605–633, 2003.

Carlson, T., R. Gillies, and E. Perry, A method to make use of thermal infrared temperature and ndvi measurements to infer surface soil water content and fractional vegetation cover, *Remote Sensing Reviews*, *9*, 161–173, 1994.

Carlson, T., W. Capehart, and R. Gillies, A new look at the simplified method for remote sensing of daily evapotranspiration, *Remote Sens. Environ.*, *54*, 161–167, 1995.

Chahinian, N., Paramétrisation multi-critère et multi-échelle d'un modèle hydrologique spatialisé de crue en milieu agricole, Ph.D. thesis, University of Montpellier, 2004.

Chahinian, N., R. Moussa, P. Andrieux, and M. Voltz, Comparison of infiltration models to simulate flood events at the field scale, *J. Hydrol.*, *accepted*, 2004a.

Chahinian, N., M. Voltz, R. Moussa, and G. Trotoux, Assessing the impact of hydraulic properties of a crusted soil on overland flow modelling at the field scale, *Hydrol. Proc.*, *accepted*, 2004b.

Charpentier, M., and P. Groffman, Soil moisture variability within remote sensing pixels, *J. Geophys. Res.*, *97*(D17), 18,987–18,995, 1992.

Chen, F., K. Mitchell, J. Schaake, Y. Xue, H. Pan, V. Koren, Q. Duan, M. Ek, and A. Betts, Modeling of land surface evaporation by four schemes and comparison with FIFE observations, *J. Geophys. Res.*, *101*(D3), 7251–7268, 1996.

Chintalapati, S., and P. Kumar, Assimilated soil moisture fields: Part i - spatial variability, *J. Geophys. Res.*, under revision, 2004.

Choudhurry, B., T. Schmugge, A. Chang, and R. Newton, Effect of surface roughness on the microwave emission for soils, *J. Geophys. Res.*, *84*, 5699–5706, 1979.

Choudhury, B., and R. Golus, Estimating soil wetness using satellite data, *Int. J. Remote Sens.*, *9*, 1251–1257, 1988.

Clapp, R., and G. Hornberger, Empirical equations for some soil hydraulic properties, *Water Resour. Res.*, *14*(4), 601–604, 1978.

Clark, M., and A. Slater, A method for generating high-resolution ensemble grids of surface climate fields, *J. Appl. Meteorol.*, in preparation, 2004.

Coffin, D., and J. Herrick, Vegetation-soil feedbacks and sensitivity of Chihuahuan desert ecosystems to climate change, *Bull. Ecol. Soc. Am.*, *80*, 69, 1999.

Cohn, S., N. S. Sivakumaran, and R. Todling, A fixed-lag Kalman smoother for retrospective data assimilation, *Mon. Weather Rev.*, *122*(12), 2838–2867, 1994.

Collins, W., et al., Describtion of the NCAR Community Atmosphere Model (CAM2), *Tech. rep.*, NCAR/TN, in preparation, 2003.

Coudert, B., B. Boudevillain, C. Ottlé, and J. Demarty, Contribution of thermal infrared remote sensing to SVAT model calibration, in preperation, 2004.

Cox, P., R. Betts, C. Bunton, R. Essery, P. Rowntree, and J. Smith, The impact of new land surface physics on the GCM simulation of climate and climate sensitivity, *Clim. Dynam.*, *15*, 183–203, 1998.

Crosson, W., C. Laymon, R. Inguva, and M. Schamschula, Assimilating remote sensing data in a surface flux-soil moisture model, *Hydrol. Proc.*, *16*, 1645–1662, 2002.

Crow, W., Correcting land surface model predictions for the impact of temporally sparse rainfall rate measurements using an Ensemble Kalman filter and surface brightness temperature observations, *J. Hydrometeorol.*, *4*, 960–973, 2003.

Crow, W., and E. Wood, Impact of soil moisture aggregation on surface energy flux prediction during SGP'97, *Geophys. Res. Lett.*, *29*(1), doi:10.1029/2001GL013796, 2002.

Crow, W., and E. Wood, The assimilation of remotely sensed soil brightness temperature imagery into a land surface model using Ensemble Kalman filtering: a case study based on ESTAR measurements during SGP97, *Adv. Water Resour.*, *26*, 137–149, 2003.

Curtis, P., UMBS Forest Carbon Cycle Research, UMBS Research, Ameriflux network, `http://cdiac.esd.ornl.gov/ftp/ameriflux/data/us-sites/preliminary-data/%UMBS`, data accessed on 14 February 2003, 2003.

Curtis, P., P. Hanson, P. Bolstad, C. Barford, J. Randolph, H. Schmid, and K. Wilson, Biometric and eddy-covariance based estimates of annual carbon storage in five eastern North American deciduous forests, *Agr. Forest Meteorol.*, *113*(1–4), 3–19, 2002.

Czajkowski, K., S. Goward, D. Shirey, and A. Walz, Thermal remote sensing of near-surface water vapor, *Remote Sens. Environ.*, *79*(2–3), 253–265, 2002.

Dai, A., K. Trenberth, and T. Qian, A global data set of Palmer Drought Severity Index for 1870–2002: Relationship with soil moisture and effects of surface warming, *J. Hydrometeorol.*, submitted.

Dai, Y., et al., The common land model, *Bull. Am. Meteorol. Soc.*, *84*(8), 1013–1023, 2003.

de Jeu, R., Retrieval of land surface parameters using passive microwave remote sensing, Ph.D. thesis, Vrije Universiteit Amsterdam, 2003.

Deardorff, J., Efficient prediction of ground surface temperature and moisture with inclusion of a layer of vegetation, *J. Geophys. Res.*, *83*(C4), 1889–1903, 1978.

Dee, D., On-line estimation of error covariance parameters for atmospheric data assimilation, *Mon. Weather Rev.*, *123*, 1128–1145, 1995.

Delgado, J., and R. Follett, Carbon and nutrient cycles, *J. Soil Water Conserv.*, *57*(6), 455–464, 2002.

Demarty, J., C. Ottlé, I. Braud, A. Olioso, J. Frangi, L. Bastidas, and H. Gupta, Using a multiobjective approach to retrieve information on surface properties used in a SVAT model, *J. Hydrol.*, *287*, 214–236, 2004.

Dengler, L., and A. Lehre, Bedrock geometry of unchannelized valleys, in *Erosion and sedimentation in the Pacific Rim*, Intl. Assoc. Hydrol. Sci., Pub. 165, pp. 81–90, 1987.

Dickinson, R., A. Heanderson-Sellers, P. Kennedy, and M. Wilson, Biosphere Atmosphere Transfer Scheme (BATS) for the NCAR Community Climate Model, *Tech. Rep. NCAR/TN-275+STR*, NCAR, 1986.

Duan, Q., S. Sooroosbin, and V. Gupta, Effective and efficient global optimisation for conceptual rainfall-runoff models, *Water Resour. Res.*, *28*, 1015–1031, 1992.

Ducharne, A., R. Koster, M. Suarez, M. Stieglitz, and P. Kumar, A catchment-based approach to modeling land surface processes in a general circulation model 2. Parameter estimation and model demonstration, *J. Geophys. Res.*, *105*(D20), 24,823–24,838, 2000.

Ek, M., K. Mitchell, Y. Lin, E. Rogers, P. Grunmann, V. Koren, G. Gayno, and J. Tarpley, Implementation of Noah land surface model advances in the National Centers for Environmental Prediction operational mesoscale Eta model, *J. Geophys. Res.*, *108*(D22), 8851, doi: 10.1029/2002JD003296, 2003.

Elmore, A., J. Mustard, S. Manning, and D. Lobell, Quantifying vegetation change in semiarid environments: Precision and accuracy of spectral mixture analysis and Normalized Difference Vegetation Index, *Remote Sens. Environ.*, *73*, 87–102, 2000.

Entekhabi, D., H. Nakamura, and E. Njoku, Solving the inverse problem for soil moisture and temperature profiles by sequential assimilation of multifrequency remotely sensed observations, *IEEE T. Geosci. Remote Sens.*, *32*(2), 438–447, 1994.

Entekhabi, D., I. Rodríguez-Iturbe, and F. Castelli, Mutual interaction of soil moisture state and atmospheric processes, *J. Hydrol.*, *184*, 3–17, 1996.

Estupina-Borrell, V., M. Maubourguet, J. Chorda, M. Alquier, and D. Dartus, Use of direct simulation whith space technology for flash flood events analysis, *Ecosystems and Floods, Hanoï*, pp. 72–87, 2000.

Evensen, G., Sequential data assimilation with a nonlinear quasi-geostrophic model using Monte Carlo methods to forecast error statistics, *J. Geophys. Res.*, *99*, 10,143–10,162, 1994.

Evensen, G., The ensemble Kalman filter: theoretical formulation and practical implementation, *Ocean Dynamics*, *53*, 343–367, 2003.

Ewen, J., G. Parkin, and P. O'Connell, SHETRAN: distributed river basin flow and transport modeling system, *J. Hydraul. Eng. ASCE*, *5*(3), 250–258, 2000.

Ewers, B., R. Oren, and J. Sperry, Influence of nutrient versus water supply on hydraulic architecture and water balance in *Pinus taeda*, *Plant Cell Environ.*, *23*, 1055–1066, 2000.

Ewers, B., D. Mackay, S. Gower, D. Ahl, S. Burrows, and S. Samanta, Tree species effects on stand transpiration in northern Wisconsin, *Water Resour. Res.*, *38*(7), doi:10.1029/2001WR000830, 2002.

Famiglietti, J., and E. Wood, Multiscale modeling of spatially variable water and energy balance processes, *Water Resour. Res.*, *30*(11), 3061–3078, 1994.

Famiglietti, J., J. Rudnicki, and M. Rodell, Variability in surface moisture content along a hillslope transect: Rattlesnake Hill, Texas, *J. Hydrol.*, *210*, 259–281, 1998.

Famiglietti, J., J. Devereaux, C. Laymon, T. Tsegaye, P. Houser, T. Jackson, S. Graham, M. Rodell, and P. Oevelen, Ground-based investigation of soil moisture variability within remote sensing footprints during the Southern Great Plains 1997 (SGP97) Hydrology Experiment, *Water Resour. Res.*, *35*(6), 1839–1851, 1999.

Figueiredo, M., and A. Jain, Unsupervised learning of finite mixture models, *IEEE T. Pattern Anal.*, *24*(3), 381–396, 2002.

Frankenberger, J., E. Brooks, M. Walter, M. Walter, and T. Steenhuis, A GIS-based variable source area hydrology model, *Hydrol. Proc.*, *13*, 805–822, 1999.

Franks, S., and K. Beven, Bayesian estimation of uncertainty in land surface-atmosphere flux predictions, *J. Geophys. Res.*, *102*(D20), 23,991–23,999, 1997.

Franks, S., K. Beven, P. Quinn, and I. Wright, On the sensitivity of soil-vegetation-atmosphere transfer (SVAT) schemes: equifinality and the problem of robust calibration, *Agr. Forest Meteorol.*, *86*, 63–75, 1997.

Freeze, R., Mathematical models of hillslope hydrol., in *Hillslope Hydrology, M.J. Kirkby, eds.*, John Wiley & Sons ed., pp. 177–225, 1978.

Galantowicz, J., D. Entekhabi, and E. Njoku, Tests of sequential data assimilation for retrieving profile soil moisture and temperature from observed L-band radiobrightness, *IEEE T. Geosci. Remote Sens.*, *37*(4), 1860–1870, 1999.

Garrat, J., *The Atmospheric Boundary Layer*, Cambridge University Press, 1992.

Garratt, J., Sensitivity of climate simulations to land and atmospheric boundary layer treatments - a review, *J. Climate*, *6*, 419–449, 1993.

Gedney, N., and P. Cox, The sensitivity of global climate model simulations to the representation of soil moisture heterogeneity, *J. Hydrometeorol.*, *4*, 1265–1275, 2003.

Giannoni, F., G. Roth, and R. Rudari, A semi-distributed rainfall-runoff model based on a geomorphologic approach, *Phys. Chem. Earth*, *25*(7-8), 665–671, 2000.

Gillies, R., T. Carlson, J. Gui, W. Kustas, and K. Humes, A verification of the "triangle" method for obtaining surface soil water content and energy fluxes from remote measurements of the Normalized Difference Vegetation Index (NDVI) and surface radiant temperature, *Int. J. Remote Sens.*, *18*(15), 3145–3166, 1997.

Goward, S., Y. Xue, and K. Czajkowski, Evaluating land surface moisture conditions from the remotely sensed temperature/vegetation index measurements, *Remote Sens. Environ.*, *79*(2–3), 225–242, 2002.

Granger, R., A complementary relationship approach for evaporation from nonsaturated surfaces, *J. Hydrol.*, *111*, 31–38, 1989.

Grayson, R., A. Western, F. Chiew, and G. Blöschl, Preffered states in spatial soil moisture patterns: Local and nonlocal controls, *Water Resour. Res.*, *33*(12), 2897–2908, 1997.

Grayson, R., G. Blöschl, A. Western, and T. McMahon, Advances in the use of observed spatial patterns of catchment hydrological response, *Adv. Water Resour.*, *25*(8–12), 1313–1334, 2002.

Gupta, H., S. Sorooshian, and P. Yapo, Toward improved calibration of hydrologic models: multiple and non-commensurable measures of information, *Water Resour. Res.*, *34*(4), 751–763, 1998.

Hack, J., Parameterization of moist convection in the National Center for Atmospheric Research Community Climate Model (CCM2), *J. Geophys. Res.*, *99*, 5551–5568, 1994.

Haddeland, I., B. Matheussen, and D. Lettenmaier, Influence of spatial resolution on simulated streamflow in a macroscale hydrologic model, *Water Resour. Res.*, *38*, 1124–1133, doi:10.1029/2001WR000854, 2002.

Hagen, A., Fuzzy set approach to assesing similarity of categorical maps, *Int. J. Geogr. Inf. Sci.*, *17*(3), 235–249, 2003.

Harding, R., C. Huntingford, and P. Cox, Modelling long-term transpiration measurements from grassland in southern England, *Agr. Forest Meteorol.*, *100*, 309–322, 2000.

Hascoët, L., V. Pascual, and R. Greborio, *The Tapenade AD tool,* TROPICS *Project, INRIA Sophia-Antipolis*, AD Workshop, Cranfield, June 5–6, 2003.

Hashimoto, H., R. Nemani, F. Yang, R. Granger, and S. Running, VPD estimation from land surface temperature (MOD11) for global map of evapotranspiration and NPP, *EOS T. Am. Geophys. Un.*, *84*(46), fall meeting supplement, Abstract H31F-07, 2003.

Hawley, M., T. Jackson, and R. McCuen, Surface soil moisture variation on small agricultural watersheds, *J. Hydrol.*, *62*, 179–200, 1983.

Hay, G., T. Blaschke, D. Marceau, and A. Bouchard, A comparison of three image-object methods for the multiscale analysis of landscape structure, *ISPRS J. Photogramm.*, *57*(5–6), 327–345, 2003.

Hirschi, M., S. Seneviratne, P. Viterbo, and C. Schär, Water-balance estimates of seasonal changes in terrestrial water storage for major river basins of the northern mid-latitudes, this issue, 2004.

Hobbins, M., J. Ramírez, and T. Brown, Trends in pan evaporation and actual evapotranspiration across the conterminous U.S.: Paradoxical or complementary?, *Geophys. Res. Lett.*, *31*, L13503, doi:10.1029/2004GL019846, 2004.

Hollinger, S., and S. Isard, A soil moisture climatology of Illinois, *J. Climate*, *7*, 822–833, 1994.

Houser, P., W. Shuttleworth, J. Famiglietti, H. Gupta, K. Syed, and D. Goodrich, Integration of soil moisture remote sensing and hydrologic modeling using data assimilation, *Water Resour. Res.*, *34*(12), 3405–3420, 1998.

HRSL, Soil Moisture Experiments in 2002 (SMEX02), Experiment Plan, 2002.

Huffman, G., et al., The Global Precipitation Climatology Project (GPCP) combined precipitation dataset, *Bull. Am. Meteorol. Soc.*, *78*(1), 5–20, 1997.

Hupet, F., and M. Vanclooster, Intraseasonal dynamics of soil moisture variability within a small agricultural maize cropped field, *J. Hydrol.*, *261*, 86–101, 2002.

Hupet, F., and M. Vanclooster, Sampling strategies to estimate field areal evapotranspiration fluxes with a soil water balance approach, *J. Hydrol.*, *292*, 262–280, doi:10.1016/j.jhydrol.2004.01.006, 2004.

Idso, S., R. Reginato, and R. Jackson, An equation for potential evaporation from soil, water and crop surfaces adaptable to use by remote sensing, *Geophys. Res. Lett.*, *4*, 187–188, 1978.

Jacinthe, P., and R. Lal, A mass balance approach to assess carbon dioxide evolution during erosional events, *Land Degrad. Dev.*, *12*, 329–339, 2001.

Jackson, T., Measuring large scale surface soil moisture using passive microwave remote sensing, *Hydrol. Proc.*, *7*, 139–152, 1993.

Jackson, T., D. Vine, A. Hsu, A. Oldak, P. Starks, C. Swift, J. Isham, and M. Haken, Soil moisture mapping at regional scales using microwave radiometry: the Southern Great Plains Hydrology Experiment, *IEEE T. Geosci. Remote Sens.*, *37*(5), 2136–2151, 1999.

Jarvis, A., V. Stauch, K. Schulz, and P. Young, The seasonal temperature dependency of light use efficiency and respiration in two deciduous forests, *Glob. Change Biol.*, *10*, 939–950, 2004.

Kaihatsu, I., Match-up data for AMSR/Soil moisture, *Tech. rep.*, Hiroshima University, 2003.

Kalman, R., A new approach to linear filtering and prediction problems, *J. Basic Eng.-T. ASME*, *82*, 35–45, 1960.

Katul, G., R. Leuning, and R. Oren, Relationship between plant hydraulic and biochemical properties derived from a steady-state coupled water and carbon model, *Plant Cell Environ.*, *26*, 339–350, 2003.

Kawanishi, T., et al., The Advanced Microwave Scanning Radiometer for the Earth Observing System (AMSR-E), NASDA's contribution to the EOS for global energy and water cycle studies, *IEEE T. Geosci. Remote Sens.*, *41*(2), 184–193, 2003.

Keeling, C., and T. Whorf, *Atmospheric CO_2 records from sites in the SIO air sampling network*, Carbon Dioxide Information Analysis Center, Oak Ridge National Laboratory, US Department of energy, Oak Ridge, Tenn., 2001.

Kiehl, J., J. Hack, G. Bonan, B. Boville, D. Williamson, and P. Rasch, The National Center for Atmospheric Research Community Climate Model (CCM3), *J. Climate*, *11*, 1131–1149, 1998.

Kim, C., G. Salvucci, and D. Entekhabi, Groundwater-surface water interaction and the climatic spatial patterns of hillslope hydrological response, *Hydrol. Earth Syst. Sci.*, *3*(3), 375–384, 1999.

Kitanidis, P., and R. Bras, Adaptive filtering through detection of isolated transient errors in rainfall-runoff models, *Water Resour. Res.*, *16*(4), 740–748, 1980.

Knotters, M., and M. Bierkens, Physical basis of time series models for water table depths, *Water Resour. Res.*, *36*, 181–188, 2000.

Knotters, M., and J. De Gooijer, TARSO modeling of water table depths, *Water Resour. Res.*, *35*, 695–705, 1999.

Koike, T., E. G. Njoku, T. J. Jackson, and S. Paloscia, Soil moisture algorithm development and validation for the ADEOS-II/AMSR, *IEEE special issue IGARSS 2000*, pp. 1253–1255, 2000.

Koren, V., B. Finnerty, J. Schaake, M. Smith, D. Seo, and Q. Duan, Scale dependencies of hydrologic models to spatial variability of precipitation, *J. Hydrol.*, *217*, 285–302, 1999.

Koster, R., M. Suarez, A. Ducharne, M. Stieglitz, and P. Kumar, A catchment-based approach to modeling land surface processes in a general circulation model, 1. Model structure, *J. Geophys. Res.*, *105*(D20), 24,809–24,822, 2000.

Koster, R., M. Suarez, R. Higgins, and H. V. den Dool, Observational evidence that soil moisture variations affect precipitation, *Geophys. Res. Lett.*, *30*(5), 1241, doi:doi:10.1029/2002GL016571, 2003.

Koster, R., M. Suarez, P. Liu, U. Jambor, A. Berg, M. Kistler, R. Reichle, M. Rodell, and J. Famiglietti, Realistic initialization of land surface states: Impacts on subseasonal forecast skill, *J. Hydrometeorol.*, submitted, 2004.

Kuczera, G., Improved parameter inference in catchment models, *Water Resour. Res.*, *19*(5), 1151–1162, 1983.

Kumar, P., A multiple scale state-space model for characterizing subgrid scale variability of near-surface soil moisture, *IEEE T. Geosci. Remote Sens.*, *37*(1), 182–197, 1999.

Kumar, P., Layer averaged Richard's equation with lateral flow, *Adv. Water Resour.*, *27*, 521–531, doi:10.1016/j.advwatres.2004.02.007, 2004.

Kumar, P., and S. Chintalapati, Assimilated soil moisture fields: Part ii - multiscale error propagation, *J. Geophys. Res.*, under revision, 2004.

Laio, F., A. Porporato, L. Ridolfi, and I. Rodriguez-Iturbe, Plants in water-controlled ecosystems: active role in hydrologic processes and response to water stress ii. Probabilistic soil moisture dynamics, *Adv. Water Resour.*, *24*, 707–723, 2001.

Le Dimet, F.-X., and O. Talagrand, Variational algorithms for analysis and assimilation of meteorogical observations, *Tellus*, *38A*, 97–110, 1986.

Legates, D., and G. McCabe, Evaluating the use of "goodness-of-fit" measures in hydrologic and hydroclimatic model validation, *Water Resour. Res.*, *35*, 233–242, 1999.

Li, J., Z. Su, B. van den Hurk, M. Menenti, A. Moene, H. D. Bruin, J. Yrisarry, M. Ibanez, and A. Cuesta, Estimation of sensible heat flux using the Surface Energy Balance System (SEBS) and ATSR measurements, *Phys. Chem. Earth*, *6*(1), 85–99, 2002.

Li, L., E. Njoku, E. Im, P. Chang, and K. St.Germain, A preliminary survey of Radio-Frequency Interference over the U.S. in Aqua AMSR-E data, *IEEE T. Geosci. Remote Sens.*, *42*(2), 380–390, 2004.

Liang, X., D. Lettenmaier, E. Wood, and S. Burges, A simple hydrologically based model of land surface water and energy fluxes for general circulation models, *J. Geophys. Res.*, *99*(D7), 14,415–14,428, 1994.

Lin, S., A "vertically Lagrangian" finite-volume dynamical core for global models, *Mon. Weather Rev.*, submitted, 2003.

Lin, S., and R. Rood, An explicit flux-form semi-Lagrangian shallow-water model of the sphere, *Q. J. Roy. Meteor. Soc.*, *123*, 2477–2498, 1997.

Littlewood, I., B. Croke, A. Jakeman, and A. Sivapalan, The role of "top-down" modelling for prediction in ungauged basins (PUB), *Hydrol. Proc.*, *17*(8), 1673–1679, 2003.

Liu, F., Bayesian time series: analysis methods using simulation based computations, Ph.D. thesis, Duke University, 2000.

Lohmann, D., et al., Streamflow and water balance intercomparisons of four land surface models in the North Americal Land Data Assimilation System project, *J. Geophys. Res.*, *109*(D7), doi: 10.1029/2003JD003517, 2004.

Mackay, D., D. Ahl, B. Ewers, S. Gower, S. Burrows, S. Samanta, and K. Davis, Effects of aggregated classifications of forest composition on estimates of evapotranspiration in a northern Wisconsin forest, *Glob. Change Biol.*, *8*(12), 1253–1265, 2002.

Mackay, D., D. Ahl, B. Ewers, S. Samanta, S. Gower, and S. Burrows, Physiological tradeoffs in the parameterization of a model of canopy transpiration, *Adv. Water Resour.*, *26*, 179–194, 2003a.

Mackay, D., S. Samanta, R. Nemani, and L. Band, Multi-objective parameter estimation for simulating canopy transpiration in forested watersheds, *J. Hydrol.*, *277*, 230–247, 2003b.

Mahfouf, J., Analysis of soil moisture from near-surface parameters: A feasibility study., *J. Appl. Meteorol.*, *30*, 1534–1547, 1991.

Margulis, S., and D. Entekhabi, Variational assimilation of radiometric surface temperature and reference-level micrometeorology into a model of the atmospheric boundary layer and land surface, *Mon. Weather Rev.*, *131*, 1272–1288, 2003.

Margulis, S., D. McLaughlin, D. Entekhabi, and S. Dunne, Land data assimilation and estimation of soil moisture using measurements from the Southern Great Plains 1997 Field Experiment, *Water Resour. Res.*, *38*(12), 1299, doi:10.1029/2001WR001114, 2002.

McKenna, P. Y. P., and J. Bruun, Data-based mechanistic modelling and validation of rainfall-flow proces, *Int. J. Control*, *74*(18), 1837–1857, 2001.

McLachlan, G., and D. Peel, *Finite Mixture Models*, Wiley Iterscience, New York, 2000.

Metting, F., J. Smith, and J. Amthor, Science needs and new technology for soil carbon sequestration, in *Carbon Sequestration in Soils-Science, Monitoring, and Beyond*, pp. 1–34, St. Michaels Workshop, 1999.

Mitchell, K., et al., The multi-institution North American Land Data Assimilation System N-LDAS: Leveraging multiple GCIP products in a real-time and reprospective distributed hydrological modeling system at continental scale, *J. Geophys. Res.*, in print, 2004.

Moore, R., Advances in real-time flood forecasting practice, in *Symposium on flood warning systems, Winter meeting of the River Engineering Section*, Inst. Water Engineers and Scientists, 1986.

Moradkhani, H., S. Sorooshian, H. Gupta, and P. Houser, Dual state-parameter estimation of hydrological models using ensemble Kalman filter, *Adv. Water Resour.*, in review, 2004.

Moran, M., T. Clarke, Y. Inoue, and A. Vidal, Estimating crop water deficit using the relation between surface-air temperature and spectral vegetation index, *Remote Sens. Environ.*, *49*, 246–263, 1994.

Moran, M., A. Rahman, J. Washburne, D. Goodrich, M. Weltz, and W. Kustas, Combining the Penman-Monteith equation with measurements of surface temperature and reflectance to estimate evaporation rates of semiarid grassland, *Agr. Forest Meteorol.*, *80*, 87–109, 1996.

Morel-Seytoux, H., Derivation of equations for variable rainfall infiltration, *Water Resour. Res.*, *14*(4), 561–568, 1978.

Moussa, R., M. Voltz, and P. Andrieux, Effects of the spatial organization of agricultural management on the hydrological behaviour of a farmed catchment during flood events, *Hydrol. Proc.*, *16*, 393–412, 2002.

Mualem, Y., A new model for predicting the hydraulic conductivity of unsaturated porous media, *Water Resour. Res.*, *12*, 513–522, 1976.

Nash, J., and J. Sutcliffe, River flow forecasting through conceptual models, 1. A discussion of principles, *J. Hydrol.*, *10*, 282–290, 1970.

Nemani, R., and S. Running, Estimation of regional surface resistance to evapotranspiration from NDVI and thermal-IR AVHRR data, *J. Appl. Meteorol.*, *28*(4), 276–284, 1989.

Njoku, E., and L. Li, Retrieval of land surface parameters using passive microwave measurements at 6 to 18 GHz, *IEEE T. Geosci. Remote Sens.*, *37*, 79–93, 1999.

Njoku, E., T. Jackson, V. Lakshmi, T. Chan, and S. Nghiem, Soil moisture retrieval from AMSR-E, *IEEE T. Geosci. Remote Sens.*, *41*(2), 215–229, 2003.

Norman, J., W. Kustas, J. Prueger, and G. Diak, Surface flux estimation using radiometric temperature: a dual-temperature-difference method to minimize measurement errors, *Water Resour. Res.*, *36*(8), 2263–2274, 2000.

Northcote, K., et al., Atlas of Australian soils, sheets 1 to 10. with explanatory data, CSIRO Aust. and Melbourne University Press, Melbourne, 1968.

Oki, T., and Y. Sud, Design of total runoff integrating pathways (TRIP) - A global river channel network, Earth interactions: 2, 1998.

Oki, T., T. Nishimura, and P. Dirmeyer, Assessment of annual runoff from land surface models using total runoff integrating pathways (TRIP), *J. Met. Soc. Japan*, *77*, 235–255, 1999.

Olioso, A., and co-authors, Monitoring energy and mass transfers during the Alpilles-ReSeDa experiment, *Agronomie*, *22*, 597–610, 2002a.

Olioso, A., and co-authors, SVAT modelling over the Alpilles-ReSeDA experiment: comparing SVAT models over wheat fields, *Agronomie*, *22*, 651–668, 2002b.

Olioso, A., H. Chauki, D. Courault, and J. Wigneron, Estimation of evapotranspiration and photosynthesis by assimilation of remote sensing data into SVAT models, *Remote Sens. Environ.*, *68*, 341–356, 1999.

Oren, R., J. Sperry, G. Katul, D. Pataki, B. Ewers, N. Phillips, and K. Schafer, Survey and synthesis of intra- and interspecific variation in stomatal sensitivity to vapour pressure deficit, *Plant Cell Environ.*, *22*, 1515–1526, 1999.

Owe, M., E. Jones, and T. Schmugge, Soil moisture variation patterns observed in Hand County, South Dakota, *Water Resour. Bull.*, *18*(6), 949–954, 1982.

Pathmathevan, M., T. Koike, X. Li, and H. Fujii, A simplified land data assimilation scheme and its application to soil moisture experiments in 2002 (smex02), *Water Resour. Res.*, *39*(12), 1341, doi:10.1029/2003WR002124, 2003.

Pauwels, V., and E. Wood, A soil-vegetation-atmosphere transfer scheme for the modeling of water and energy balance processes in high latitudes, 1. Model improvements, *J. Geophys. Res.*, *104*(D22), 27,811–27,822, 1999a.

Pauwels, V., and E. Wood, A soil-vegetation-atmosphere transfer scheme for the modeling of water and energy balance processes in high latitudes, 2. Application and validation, *J. Geophys. Res.*, *104*(D22), 27,823–27,839, 1999b.

Pauwels, V., and E. Wood, The importance of misclassifications and spatial resolution of land cover data in the uncertainty in model results over boreal ecosystems, *J. Hydrometeorol.*, *1*(3), 255–266, 2000.

Pauwels, V., R. Hoeben, N. Verhoest, and F. De Troch, The importance of the spatial patterns of remotely sensed soil moisture in the improvement of discharge predictions for small-scale basins through data assimilation, *J. Hydrol.*, *251*(1-2), 88–102, 2001.

Pauwels, V., R. Hoeben, N. Verhoest, F. De Troch, and P. Troch, Improvement of TOPLATS-based discharge predictions through assimilation of ERS-based remotely sensed soil moisture values, *Hydrol. Proc.*, *16*(5), 995–1013, 2002.

Peixoto, J., and A. Oort, *Physics of climate*, Am. Inst. of Phys. Press, Woodbury, New York, 1992.

Peters-Lidard, C., M. Zion, and E. Wood, A soil-vegetation-atmosphere transfer scheme for modeling spatially variable water and energy balance processes, *J. Geophys. Res.*, *102*(D4), 4303–4324, 1997.

Philip, J., The theory of infiltration: 4. Sorptivity and albegraic infiltration equations, *Soil Science*, *84*(3), 257–264, 1957.

Phillips, D., D. White, and C. Johnson, Implications of climate change scenarios for soil erosion in the USA, *Land Degrad. Rehabil.*, *4*, 61–72, 1993.

Pitman, A., The evolution of, and revolution in, land surface schemes designed for climate models, *Int. J. Climatol.*, *23*, 479–510, 2003.

Priestley, M., *Spectral Analysis and Time Series*, Academic Press, London, UK, 1981.

Qu, W., et al., Sensitivity of latent heat flux from PILPS land-surface schemes to pertubations of surface air temperature, *J. Atmos. Sci.*, *55*(11), 1909–1927, 1998.

Quideau, S., O. Chadwick, S. Trumbore, J. Johnson-Maynard, R. Graham, and M. Anderson, Vegetation control on soil organic matter dynamics, *Org. Geochem.*, *32*, 247–252, 2001.

Rasmusson, E., Atmospheric water vapor transport and the water balance of North America. II. large-scale water balance investigations, *Mon. Weather Rev.*, *96*, 720–734, 1968.

Reichle, R., D. McLaughlin, and D. Entekhabi, Hydrologic data assimilation with the ensemble Kalman filter, *Mon. Weather Rev.*, *130*(1), 103–114, 2002.

Reichle, R., R. Koster, J. Dong, and A. Berg, Global soil moisture from satellite observations, land surface models, and ground data: Implications for data assimilation, *J. Hydrometeorol.*, *5*(3), 430–442, 2004.

Richards, A., Capillary conduction of liquids through porous mediums, *Physics*, *1*, 318–333, 1931.

Richter, H., A. Western, and F. Chiew, The effect of soil and vegetation parameters in the ECMWF land surface scheme, *J. Hydrometeorol.*, in press, 2004.

Rinaldo, A., A. Marani, and R. Rigon, Geomorphological dispersion, *Water Resour. Res.*, *27*(4), 513–525, 1991.

Robock, A., K. Vinnikov, G. Srinivasan, J. Entin, S. Hollinger, N. Speranskaya, S. Liu, and A. Namkhai, The global soil moisture data bank, *Bull. Am. Meteorol. Soc.*, pp. 1281–1299, 2000.

Rodell, M., and J. Famiglietti, Detectability of variations in continental water storage from satellite observations of the time dependent gravity field, *Water Resour. Res.*, *35*, 2705–2723, 1999.

Rodell, M., and J. Famiglietti, An analysis of terrestial water storage variations in Illinois with implications for the Gravity Recovery and Climate Experiment (GRACE), *Water Resour. Res.*, *37*, 1327–1339, 2001.

Rüdiger, C., R. Davidson, H. Hemakumara, J. Walker, J. Kalma, G. Willgoose, and P. Houser, Catchment monitoring for scaling and assimilation of soil moisture and streamflow, in *Proceedings of the international congress on modelling and simulation (MODSIM), 14–17 July, 2003*, pp. 386–391, Modelling and Simulation Society of Australia and New Zealand, Townsville, Australia, 2003.

Samanta, S., and D. Mackay, Flexible automated parameterization of hydrologic models using fuzzy logic, *Water Resour. Res.*, *39*(1), 1009, doi:10.1029/2002WR001349, 2003.

Sandholt, I., K. Rasmussen, and J. Andersen, A simple interpretation of the surface temperature / vegetation index space for assessment of surface moisture status, *Remote Sens. Environ.*, *79*(2–3), 213–224, 2002.

Saxton, K., and A. Lenz, Antecedent retention indexes predict soil moisture, *J. Hydraul. Div.*, *4*, 223–241, 1967.

Scheibe, T., Characterization of the spatial structuring of natural porous media and its impacts on subsurface flow and transport, Ph.D. thesis, Stanford University, 1993.

Schlosser, C., A. Slater, A. Pitman, A. Robock, K. Vinnikov, A. Henderson-Sellers, N. Speranskaya, K. Mitchell, and The PILPS 2(D) Contributors, Simulation of a boreal grassland hydrology at Valdai, Russia: PILPS Phase 2(D), *Mon. Weather Rev.*, *128*(2), 301–321, doi: 10.1175/1520-0493(2000)128⟨0301:SOABGH⟩2.0.CO;2, 2000.

Schmid, H., H. Su, C. Vogel, and P. Curtis, Ecosystem-atmosphere exchange of carbon dioxide over a mixed hardwood forest in northern lower Michigan, *J. Geophys. Res.*, in press, 2004.

Schmugge, T., Applications of passive microwave observations of surface soil moisture, *J. Hydrol.*, *212-213*, 188–197, 1998.

Schmugge, T., W. Kustas, J. Ritchie, T. Jackson, and A. Rango, Remote sensing in hydrology, *Adv. Water Resour.*, *25*(8-12), 1367–1385, 2002.

Schulz, K., and K. Beven, Data-supported robust parameterisations in land surface-atmosphere flux predictions: towards a top-down approach, *Hydrol. Proc.*, *17*, 2259–2277, 2003.

Schulz, K., A. Jarvis, K. Beven, and H. Soegaard, The predictive uncertainty of land surface fluxes in response to increasing ambient carbon dioxide, *J. Climate*, *14*(12), 2551–2562, 2001.

Schuurmans, J., P. Troch, A. Veldhuizen, W. Bastiaanssen, and M. Bierkens, Assimilation of remotely sensed latent heat flux in a distributed hydrological model, *Adv. Water Resour.*, *26*, 151–159, 2003.

Scott, D., and W. Szewczyk, From kernels to mixtures, *Technometrics*, *43*, 323–335, 2001.

Sellers, P., et al., Modeling the exchanges of energy, water, and carbon between continents and the atmosphere, *Science*, *275*, 502–509, 1997.

Seneviratne, S., P. Viterbo, D. Lüthi, and C. Schär, Inferring changes in terrestrial water storage using ERA-40 reanalysis data: The Mississippi River basin, *J. Climate*, *17*(11), 2039–2057, 2004.

Seuffert, G., H. Wilker, P. Viterbo, J. Mahfouf, M. Drusch, and J. Calvet, Soil moisture analysis combining screen-level parameters and microwave brightness temperature: A test with field data, *Geophys. Res. Lett.*, *30*(10), 1498–1501, 2003.

Shao, Y., and A. Henderson-Sellers, Modeling soil moisture: A Project for Intercomparison of Land Surface Parameterization Schemes Phase 2(b), *J. Geophys. Res.*, *101*(D3), 7227–7250, 1996.

Šimunek, . J., and M. Van Genuchten, Estimating unsaturated soil hydraulic properties from tension disc infiltrometer data by numerical inversion, *Water Resour. Res.*, *32*(9), 2683–2696, 1996.

Sivapalan, M., K. Beven, and E. Wood, On hydrologic similarity, 2. A scaled model for runoff prediction, *Water Resour. Res.*, *23*(12), 2266–2278, 1987.

Slater, A., and M. Clark, Snow data assimilation via ensemble kalman methods, *J. Hydrometeorol.*, in preparation, 2004.

Starr, G., R. Lal, R. Malone, D. Hothem, L. Owens, and J. Kimble, Modeling soil carbon transported by water erosion processes, *Land Degrad. Dev.*, *11*, 83–91, 2000.

Su, Z., The surface energy balance system (SEBS) for estimation of turbulent heat fluxes, *Hydrol. Earth Syst. Sci.*, *6*(1), 85–99, 2002.

Sulebak, J., L. Tallaksen, and B. Erichsen, Estimation of areal soil moisture by use of terrain data, *Geografiska Annaler*, *82A*, 89–105, 2000.

Svetlitchnyi, A., S. Plotnitskiy, and O. Stepovaya, Spatial distribution of soil moisture content within catchments and its modelling on the basis of topographic data, *J. Hydrol.*, *277*, 50–60, 2003.

Tarboton, D. G., and C. H. Luce, Utah energy balance snow accumulation and melt model (ueb), 1996, computer model technical description and users guide, *Coupled atmosphere-biophysics-hydrology models for environmental modeling 20*, Utah Water Research Laboratory and USDA Forest Service Intermountain Research Station, 1996.

Telford, W., L. Geldart, and R. Sheriff, *Applied geophysics*, Cambridge University Press, Cambridge, 1990.

Todini, E., A. Szollosi-Nagy, and E. Wood, Adaptive state-parameter estimation algorithm for real time hydrologic forecasting; a case study, in *IISA/WMO workshop on the recent developments in real time forecasting/control of water resources systems; Laxemburg (Austria)*, 1976.

Tompa, D., J. Morton, and E. Jernigan, Perceptually based image comparison, in *International conference on image processing*, pp. 489–492, Vancouver, BC, Canada, 2000.

Torfs, P., E. van Loon, R. Wójcik, and P. Troch, Data assimilation by non-parametric local density estimation, in *Computational Methods in Water Resources*, edited by S. Hassanizadeh, R. Schotting, W. Gray, and G. Pinder, pp. 1355–1362, Elsevier, Amsterdam, 2002.

Torge, W., *Gravimetry*, de Gruyter, Berlin, Germany, 1989.

Trenberth, K., Atmospheric moisture residence times and cycling: Implications for rainfall rates with climate change, *Climatic Change*, *39*, 667–694, 1998.

Trenberth, K., Conceptual framework for changes of extremes of the hydrological cycle with climate change, *Climatic Change*, *42*, 327–339, 1999.

Trenberth, K., A. Dai, R. Rasmussen, and D. Parsons, The changing character of precipitation, *Bull. Am. Meteorol. Soc.*, *84*, 1205–1217, 2003.

Troch, P., F. De Troch, and W. Brutsaert, Effective water table depth to describe initial conditions prior to storm rainfall in humid regions, *Water Resour. Res.*, *29*(2), 427–434, 1993.

Troch, P., C. Paniconi, and E. van Loon, Hillslope-storage Boussinesq model for subsurface flow and variable source areas along complex hillslopes: 1. Formulation and characteristic response, *Water Resour. Res.*, *39*(11), 1316, doi:10.1029/2002WR001728, 2003.

Troch, P. A., J. A. Smith, E. F. Wood, and F. P. De Troch, Hydrologic controls of large floods in a small basin: Central Appalachian case study, *J. Hydrol.*, *156*(1-4), 285–309, 1994.

UNFCCC (United Nations Framework Convention on Climate Change), Kyoto protocol to the United Nations Framework Convention on Climate Change, Kyoto, 1997.

van Dam, J., Theory of SWAP version 2.0: simulation of water flow, solute transport and plant growth in the Soil-Water-Atmosphere-Plant environment, *Tech. rep.*, DLO Winand Staring Centre, Wageningen, 1997.

Van Genuchten, M., A closed-form equation for predicting the hydraulic conductivity of unsaturated soils, *Soil Sci. Soc. Am. J.*, *44*, 892–898, 1980.

Vereecken, H., J. Maes, J. Feyen, and P. Darius, Estimating the soil moisture retention characteristic from texture, bulk density and carbon content, *Soil Science*, *148*, 389–403, 1989.

Viterbo, P., and A. Beljaars, An improved land surface parameterization scheme in the ECMWF model and its validation, *J. Climate*, *8*, 2716–2748, 1995.

Voltz, M., P. Andrieux, C. Bocquillon, and S. Rambal, Le site atelier Allegro, Languedoc, in *Actes du séminaire hydrosystèmes*, pp. 121–129, CEMAGREF, Paris, 1994.

Wahr, J., M. Molenaar, and F. Bryan, Time variability of the Earth's gravity field: Hydrological and oceanic effects and their possible detection using GRACE, *J. Geophys. Res.*, *30*, 30,205–30,229, 1998.

Walker, J., and P. Houser, A methodology for initializing soil moisture in a global climate model: Assimilation of near-surface soil moisture observations, *J. Geophys. Res.*, *106*(D11), 11,761–11,774, 2001.

Walker, J., and P. Houser, Requirements of a global near-surface soil moisture satellite mission: accuracy, repeat time, and spatial resolution, *Adv. Water Resour.*, *27*, 785–801, doi:10.1016/j.advwatres.2004.05.006, 2004.

Walker, J., G. Willgoose, and J. Kalma, The Nerrigundah data set: soil moisture patterns, soil characteristics, and hydrological flux measurements, *Water Resour. Res.*, *37*(11), 2653–2658, 2001.

Walter, M., D. Wilks, J. Parlange, and R. Schneider, Increasing evapotranspiration from the conterminous United States, *J. Hydrometeorol.*, *5*, 405–408, 2004.

Wan, Z., P. Wang, and X. Li, Using MODIS land surface temperature and normalized difference vegetation index products for monitoring drought in the southern Great Plains USA, *Int. J. Remote Sens.*, *25*(1), 61–72, 2004.

Wang, J., and T. Schmugge, An empirical model for the complex dielectric permittivity of soil as a function of water content, *IEEE T. Geosci. Remote Sens.*, *18*, 288–295, 1980.

Wang, Y., and Y. Hsieh, Uncertainties and novel prospects in the study of soil carbon dynamics, *Chemosphere*, *49*, 791–804, 2002.

Wang, Y., R. Leuning, H. Cleugh, and P. Coppin, Parameter estimation in surface exchange models using nonlinear inversion: how many parameters can we estimate and which measurements are most useful?, *Glob. Change Biol.*, *7*(5), 495–510, 2001.

Wealands, S., R. Grayson, and J. Walker, Quantitative comparison of spatial patterns for hydrological model assessment, *Adv. Water Resour.*, submitted, 2004.

Weidong, L., F. Baret, G. Xingfa, T. Qingxi, Z. Lanfen, and Z. Bing, Relating soil surface moisture to reflectance, *Remote Sens. Environ.*, *81*(2–3), 238–246, 2002.

Wen, J., Z. Su, and Y. Ma, Determination of land surface temperature and soil moisture from Tropical Rainfall Measuring Mission/Microwave Imager remote sensing data, *J. Geophys. Res.*, *108*(D2), 2003.

West, M., Mixture models, Monte Carlo, Bayesian updating and dynamic models, *Comp. Sci & Stat.*, *24*, 325–333, 1993.

Western, A., and R. Grayson, The Tarrawarra data set: soil moisture patterns, soil characteristics, and hydrological flux measurements, *Water Resour. Res.*, *34*(10), 2765–2768, 1998.

Western, A., R. Grayson, and G. Blöschl, Scaling of soil moisture: A hydrologic perspective, *Annu. Rev. Earth Planet. Sci.*, *30*, 149–180, doi:10.1146/annurev.earth.30.091201.140434, 2002.

Western, A., S. Zhou, R. Grayson, T. McMahon, G. Blöschl, and D. Wilson, Spatial correlation of soil moisture in small catchments and its relationship to dominant spatial hydrological processes, *J. Hydrol.*, *286*, 113–134, 2004.

Wigmosta, M., L. Vail, and D. Lettenmaier, A distributed hydrology-vegetation model for complex terrain, *Water Resour. Res.*, *30*(6), 1665–1679, 1994.

Wigmosta, M., B. Nijssen, P. Storck, and D. Lettenmaier, The distributed hydrol. soil vegetation model, in *In Mathematical Models of Small Watershed Hydrol. and Applications*, Wat. Resource Publications, Littleton, CO, V.P. Singh, D.K. Frevert, eds., pp. 7–42, 2002.

Wild, M., A. Ohmura, and H. Gilgen, On the consistency of trends in radiation and temperature records and implications for the global hydrological cycle, *Geophys. Res. Lett.*, *31*, L11201, doi:10.1029/2004GL019188, 2004.

Wilson, C., and W. Dietrich, The contribution of bedrock groundwater flow to storm runoff and high pore pressure development in hollows, in *Erosion and sedimentation in the Pacific Rim*, Intl. Assoc. Hydrol. Sci., Pub. 165, pp. 49–59, 1987.

Wilson, C. J., Runoff and pore pressure development in hollows, Ph.D. thesis, University of California, Berkeley, 1988.

Wofsy, S., and J. Munger, Harvard university, atmospheric sciences, forest and atmospheric measurements, data exchange, NIGEC archive, `http://www-as.harvard.edu/data/nigec-data.html`, accessed on 23 June 2003, 2003.

Wood, E., *Real-time forecasting/control of water resource systems, selected papers from an IIASA workshop, October 18–21, 1976*, Pergamon, Oxford, 1980.

Wood, E., The role of lateral flow: over- or underrated?, in *Integrating hydrology, ecosystem dynamics, and biogeochemistry in complex landscapes*, edited by J. Tenhunen and P. Kabat, pp. 197–216, JohnWiley & Sons, Chichester, 1999.

Xia, Y., M. Sen, C. Jackson, and P. Stoffa, Multi-dataset study of optimal parameter and uncertainty estimation of a land surface model with Bayesian stochastic inversion and multicriteria method, *J. Appl. Meteorol.*, in press, 2004.

Yeh, P., M. Irizarry, and E. Eltahir, Hydroclimatology of Illinois: A comparison of monthly evaporation estimates based on atmospheric water balance and soil water balance, *J. Geophys. Res.*, *103*(D16), 19,823–19,837, 1998.

Young, P., Nonstationary time series analysis and forecasting, *Progr. Environm. Sci.*, *1*(1), 3–48, 1999.

Young, P., Stochastic, dynamic modeling and signal processing: time variable and state dependent parameter estimation, in *Nonlinear and nonstationary signal processing*, edited by W. Fitzgerald, R. Smith, A. Walden, and P. Young, pp. 74–114, 2000.

Young, P., Data-based mechanistic modelling and validation of rainfall-flow processes, in *Model validation - Perspectives in hydrological sciences*, edited by M. Anderson and P. Bates, pp. 117–161, 2001.

Young, P., Advances in real-time flood forecasting, *Philos. Tr. Roy. Soc.*, *360*, 1433–1450, 2002.

Young, P., Top-down and data-based mechanistic modelling of rainfall-flow dynamics at the catchment scale, *Hydrol. Proc.*, *17*(11), 2195–2217, 2003.

Zhang, G., and N. McFarlane, Sensitivity of climate simulation to the parameterization of cumulus convection in the Canadian Climate Centre general circulation model, *Atmos.-Ocean*, *33*, 407–446, 1995.

Zhang, W., and D. Montgomery, Digital elevation model grid size, landscape representation, and hydrologic simulations, *Water Resour. Res.*, *30*, 1019–1028, 1994.

Index

E-mail adresses

Ajami, Newsha	nkhodata@uci.edu
Albertson, John D.	john.albertson@duke.edu
Alsdorf, Doug	alsdorf@geog.ucla.edu
Andreadis, Konstantinos M.	kostas@hydro.washington.edu
Berne, Alexis	alexis.berne@wur.nl
Bertoldi, G.	giacomo.bertoldi@ing.unitn.it
Bierkens, Marc F.P.	m.bierkens@geog.uu.nl
Blyth, E.	emb@ceh.ac.uk
Bogaart, P.W.	patrick.bogaart@wur.nl
Boll, J.	jboll@uidaho.edu
Bosilovich, Michael G.	michael.bosilovich@nasa.gov
Castaings, W.	william.castaings@inrialpes.fr
Chern, Jiundar	jchern@agnes.gsfc.nasa.gov
Chintalapati, S.	chintala@uiuc.edu
Coudert, Benoit	benoit.coudert@cetp.ipsl.fr
Crow, Wade T.	wcrow@hydrolab.arsusda.gov
De Alwis, Dilkushi	dd88@cornell.edu
Drusch, Matthias	dar@ecmwf.int
Dunne, Susan	susan@mit.edu
Ellett, Kevin M.	ellettk@civenv.unimelb.edu.au
Entekhabi, Dara	darae@mit.edu
Famiglietti, James S.	jfamigli@uci.edu
Gabellani, S.	simone.g@cima.unige.it
Gao, Huilin	huiling@princeton.edu
van de Giesen, Nick	nick@uni-bonn.de
Grayson, Rodger	rodger@civenv.unimelb.edu.au
Gupta, Hoshin	hoshin.gupta@hwr.arizona.edu
Hasan, Shaakeel	shaakeel.hasan@wur.nl
Hemakumara, Manju	h.hemakumara@studentmail.newcastle.edu.au
Hirschi, M.	martin.hirschi@env.ethz.ch
Houser, Paul R.	houser@hsbserv.gsfc.nasa.gov
van den Hurk, Bart	hurkvd@knmi.nl
Hurkmans, Ruud	ruud.hurkmans@wur.nl

Jacobs, Barry	barry.jacobs@studentmail.newcastle.edu.au
Lakshmi, Venkat	vlakshmi@geol.sc.edu
Lapenta, William M.	bill.lapenta@nasa.gov
Leijnse, Hidde	hidde.leijnse@wur.nl
Lettenmaier, Dennis	dennisl@u.washington.edu
Li, Haibin	hli@envsci.rutgers.edu
Lohmann, D.	dag.lohmann@noaa.gov
van Loon, E.E.	vanloon@science.uva.nl
Luo, Lifeng	lluo@princeton.edu
Mackay, D. Scott	dsmackay@buffalo.edu
Margulis, Steven A.	margulis@seas.ucla.edu
McLaughlin, Dennis	dennism@mit.edu
Milly, Christopher	cmilly@usgs.gov
Moradkhani, Hamid	moradkha@uci.edu
Moussa, Roger	moussa@ensam.inri.fr
Mu, Qiaozhen	qiaozhen@ntsg.umt.edu
Ni-Meister, Wenge	wenge.ni-meister@hunter.cuny.edu
Ottlé, Catherine	catherine.ottle@cetp.ipsl.fr
Over, Thomas	cftmo@uxl.cts.eiu.edu
Oyapidan, Rasheed O.	newhopefoundation@hormail.com
Pan, Ming	mpan@princeton.edu
Pauwels, Valentijn R.N.	valentijn.pauwels@ugent.be
Peters-Lidard, C.D.	christa.peters@nasa.gov
Pipunic, Robert	r.pipunic@civenv.unimelb.edu.au
Reichle, Rolf H.	reichle@janus.gsfc.nasa.gov
Rigon, R.	riccardo.rigon@ing.unitn.it
Roads, John	jroads@ucsd.edu
Rüdiger, C.	c.ruediger@civenv.unimelb.edu.au
Ryu, Dongryeol	dryu@uci.edu
Salvucci, Guido D.	gdsalvuc@bu.edu
Sheffield, Justin	justin@princeton.edu
Schulz, K.	k2.schulz@tu-bs.de
Seneviratne, Sonia I.	senevira@janus.gsfc.nasa.gov
Sharif, H.	hosharif@lbl.gov
Simoni, S.	silvia.simoni@ing.unitn.it
Sini, F.	fsini@katamail.com
Slater, Andrew	aslater@cires.colorado.edu
Smith, A.B.	a.smith@civenv.unimelb.edu.au
Steenhuis, Tammo	tss1@cornell.edu
Su, Bob	b_su@itc.nl
Su, Hongbo	hongbosu@princeton.edu

Teuling, Adriaan J.	ryan.teuling@wur.nl
Thierfelder, T.	tomas.thierfelder@bt.slu.se
Trenberth, K.E.	trenbert@ucar.edu
Troch, Peter A.	peter.troch@wur.nl
Uijlenhoet, Remko	remko.uijlenhoet@wur.nl
Viterbo, Pedro	pedro.viterbo@ecmwf.int
Vrugt, Jasper A.	jvrugt@science.uva.nl
Wagener, Thorsten	thorsten@hwr.arizona.edu
Walker, Jeffrey P.	j.walker@unimelb.edu.au
Wang, Shugong	wangsg@ns.lzb.ac.cn
Wealands, Stephen R.	srweal@civenv.unimelb.edu.au
Wójcik, Raf	raf.wojcik@wur.nl
Wood, Eric F.	efwood@runoff.princeton.edu
Xia, Youlong	youlong.xia@noaa.gov
Yuhua, Zhou	zhyh@mit.edu
Zhan, Xiwu	xiwuzhan@verizon.net